CIVIL ENGINEERING STUDIES
Illinois Center for Transportation Series No. 18-016
UILU-ENG-2018-2016
ISSN: 0197-9191

MATERIAL CONSTITUENTS AND PROPORTIONING FOR ROLLER-COMPACTED CONCRETE MECHANICAL PROPERTIES

Prepared By
Jeffrey R. LaHucik
Jeffery R. Roesler
University of Illinois at Urbana-Champaign

Research Report No. FHWA-ICT-18-014

A report of the findings of

ICT PROJECT R27-149-2
Mechanistic-Empirical Design Implementation and Monitoring for Rigid Pavements

Illinois Center for Transportation

August 2018

TECHNICAL REPORT DOCUMENTATION PAGE

1. Report No.	2. Government Accession No.	3. Recipient's Catalog No.
FHWA-ICT-18-014	N/A	N/A

4. Title and Subtitle	5. Report Date
Material Constituents and Proportioning for Roller-Compacted Concrete Mechanical Properties	August 2018
	6. Performing Organization Code N/A

7. Author(s)	8. Performing Organization Report No.
Jeffrey R. LaHucik and Jeffery R. Roesler	ICT-18-016 UILU-ENG-2018-2016

9. Performing Organization Name and Address	10. Work Unit No.
Illinois Center for Transportation Department of Civil and Environmental Engineering University of Illinois at Urbana-Champaign 205 North Mathews Avenue, MC-250 Urbana, IL 61801	N/A
	11. Contract or Grant No. R27-149-2

12. Sponsoring Agency Name and Address	13. Type of Report and Period Covered
Illinois Department of Transportation (SPR) Bureau of Research 126 East Ash Street Springfield, IL 62704	Final Report 7/1/2014 – 8/31/2018
	14. Sponsoring Agency Code FHWA

15. Supplementary Notes

Conducted in cooperation with the U.S. Department of Transportation, Federal Highway Administration.

16. Abstract

Roller-compacted concrete (RCC) is increasingly becoming an alternative pavement type because of its construction expediency, reductions in material and construction costs, sustainability benefits, and overall structural capacity. Current RCC pavement mix design procedures select mix constituents and proportions based on strength requirements, workability, and field density. Discrepancies in mechanical properties are known to exist between field and laboratory compacted specimens. In order to move toward designing and constructing performance-based RCC mixtures—the effects of various mixture constituents, proportions, and compaction methods must be quantified. The gap between laboratory and field properties must be minimized as well.

A wide range of RCC aggregate gradations were batched, tested, and found to impact RCC properties—especially compressive strength. The coarse-fine aggregate ratio was the parameter linked most directly to RCC compressive strength. Aggregate type (recycled aggregates, siliceous rounded sand and gravel, manufactured sand, and crushed aggregates) was also shown to affect aggregate packing density and RCC properties. Fly ash or ground granulated blast furnace slag replacement of cement statistically reduced the early-age RCC strength and likely would delay opening the RCC pavement to traffic. In general, fracture properties of RCC with virgin and recycled aggregates were similar or greater than fracture properties of conventional Portland cement concrete (PCC) pavements—which suggests similar or greater slab capacities and fatigue lives for RCC relative to PCC for the same slab thickness. Several types of macro-fibers incorporated into RCC were shown to statistically improve the RCC compressive strength as well as provide residual strength comparable to conventional fiber reinforced concrete.

Past researchers have demonstrated that the gyratory compactor has the potential to be an alternative RCC mix design tool to the modified Proctor procedure. The gyratory compactor provides similar compaction mechanisms and energies relative to construction equipment for RCC (and asphalt) pavements. It also significantly reduces operator error in specimen preparation. The gyratory compactor was employed in this research to evaluate several laboratory mixture proportions and constituents focusing on aggregate gradations and cementitious content. It was also used to compare companion gyratory results to already constructed RCC pavements. The gyratory compactor was verified to be more sensitive to changes in aggregate gradation and cementitious content compared to the modified Proctor and vibratory hammer—which are commonly used methods for RCC mix design and specimen fabrication, respectively. It was also useful in evaluating the potential for delayed compaction on RCC mixtures with different admixtures, delay times, and mixture temperatures.

17. Key Words	18. Distribution Statement
Roller-compacted concrete, mix design, compaction, concrete pavement	No restrictions. This document is available through the National Technical Information Service, Springfield, VA 22161.

19. Security Classif. (of this report)	20. Security Classif. (of this page)	21. No. of Pages	22. Price
Unclassified.	Unclassifed.	98 pp + appendices	N/A

Form DOT F 1700.7 (8-72) **Reproduction of completed page authorized**

ACKNOWLEDGMENT, DISCLAIMER, MANUFACTURERS' NAMES

This publication is based on the results of **ICT-R27-149-2, Mechanistic-Empirical Design Implementation and Monitoring for Rigid Pavements**. ICT-R27-149-2 was conducted in cooperation with the Illinois Center for Transportation, the Illinois Department of Transportation, and the U.S. Department of Transportation, Federal Highway Administration.

The authors would like to thank those whom have contributed to this project including Josh Cheung, who contributed extensively to the delayed compaction chapter, and many other students helping in the lab: Armen Amirkhanian, Sachindra Dahal, Aaron Dunton, Juan Pablo Ricardo Mendez Ruiz Fernandez, Omar Jadallah, Marvin Lim, Douglas De Andrade Neves, Sushobhan Sen, and Quang Tran.

Members of the Technical Review panel were the following:

- Wienrank, Charles (TRP Chair) Charles.Wienrank@illinois.gov
- Brand, Mike Michael.Brand@illinois.gov
- Krstulovich, James James.Krstulovich@illinois.gov
- Peters, Tim Tim.Peters@illinois.gov
- Riley, Randy pccman@ilacpa.com
- Rowden, LaDonna LaDonna.Rowden@illinois.gov
- Senger, John John.Senger@Illinois.gov
- Vespa, Joe Joseph.Vespa@illinois.gov
- Winkelman, Thomas Tom.Winkelman@illinois.gov
- Lippert, David DLippert@illinois.edu
- Mentjes, Dean dean.mentjes@dot.gov
- Niedernhofer, Paul Paul.niedernhofer@illinois.gov
- Pfeifer, Brian Brian.Pfeifer@illinois.gov
- Schutzbach, Amy Amy.Schutzbach@illinois.gov

EXECUTIVE SUMMARY

Roller-compacted concrete (RCC) is increasingly becoming an alternative pavement type because of its construction expediency, reductions in material and construction costs, sustainability benefits, and overall structural capacity. Current RCC pavement mix design procedures select mix constituents and proportions based on strength requirements, workability, and field density. Discrepancies in mechanical properties are known to exist between field and laboratory compacted specimens. In order to move toward designing and constructing performance-based RCC mixtures—the effects of various mixture constituents, proportions, and compaction methods must be quantified. The gap between laboratory and field properties must be minimized as well.

A wide range of RCC aggregate gradations were batched, tested, and found to impact RCC properties—especially compressive strength. The coarse-fine aggregate ratio was the parameter linked most directly to RCC compressive strength. Aggregate type (recycled aggregates, siliceous rounded sand and gravel, manufactured sand, and crushed aggregates) was also shown to affect aggregate packing density and RCC properties. Fly ash or ground granulated blast furnace slag replacement of cement statistically reduced the early-age RCC strength and likely would delay opening the RCC pavement to traffic. In general, fracture properties of RCC with virgin and recycled aggregates were similar or greater than fracture properties of conventional Portland cement concrete (PCC) pavements—which suggests similar or greater slab capacities and fatigue lives for RCC relative to PCC for the same slab thickness. Several types of macro-fibers incorporated into RCC were shown to statistically improve the RCC compressive strength as well as provide residual strength comparable to conventional fiber reinforced concrete.

Past researchers have demonstrated that the gyratory compactor has the potential to be an alternative RCC mix design tool to the modified Proctor procedure. The gyratory compactor provides similar compaction mechanisms and energies relative to construction equipment for RCC (and asphalt) pavements. It also significantly reduces operator error in specimen preparation. The gyratory compactor was employed in this research to evaluate several laboratory mixture proportions and constituents focusing on aggregate gradations and cementitious content. It was also used to compare companion gyratory results to already constructed RCC pavements. The gyratory compactor was verified to be more sensitive to changes in aggregate gradation and cementitious content compared to the modified Proctor and vibratory hammer—which are commonly used methods for RCC mix design and specimen fabrication, respectively. It was also useful in evaluating the potential for delayed compaction on RCC mixtures with different admixtures, delay times, and mixture temperatures.

CONTENTS

CHAPTER 1: INTRODUCTION

Roller-compacted concrete (RCC) pavements are becoming an increasingly viable pavement alternative because of their construction expediency, earlier opening to traffic, reduced material and construction cost, structural capacity per unit thickness, and sustainability rating. RCC is a type of concrete pavement that is constructed similarly to asphalt pavements. RCC differs from conventional Portland cement concrete (PCC) in the proportions of the constituents. RCC typically contains less cementitious materials, higher aggregate contents, no air entrainment, and less water than PCC– which results in a no-slump concrete. Construction of RCC involves paving with either a conventional asphalt or high-density paver (Figure 1) followed by rolling with a vibratory/static roller combination in order to compact the no-slump RCC material. The construction process results in a dense concrete layer that can be opened to traffic earlier than most PCC pavements. Previous guides to use and specification of RCC pavements have been published (ACI, 1995; PCA, 2004; Harrington et al. 2010; ACPA, 2014).

Figure 1. High-density paver placing RCC pavement from Prusinski (2016).

RCC has been applied to pavements since the mid-1970's. There has been a recent resurgence in the past decade (Figure 2) because of the sustainability and initial cost benefits that RCC has relative to PCC and asphalt pavements—as well as new paving equipment technology (Figure 1). Compared to PCC and asphalt pavements, there has been relatively little research into the mix design process and resulting material property requirements for RCC. It is well known that RCC can easily produce strengths that are more than sufficient for paving concrete. However, there are many factors that affect RCC fresh and hardened properties that have not been fully studied and documented. Such factors include aggregate gradation variations, aggregate type, cementitious content and type of cementitious materials, and method of RCC laboratory compaction. The fact that RCC mix design is completely different from PCC mix design only adds to the potential complications that can arise when engineers apply RCC technology for the first time. The mix design, lab compaction method, and fresh/hardened properties ideally should reflect the final RCC product from field construction. Therefore, lab methods that can account for varying aggregate gradations and types, cementitious

materials, and other mix design parameters (fibers, recycled materials, admixtures) is required to improve the state-of-the-art with respect to RCC pavement mix design and construction.

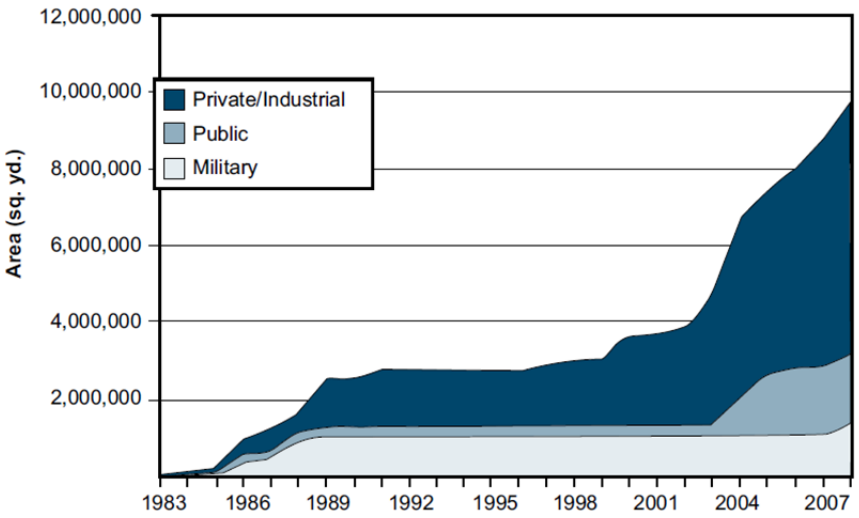

Figure 2. Increasing use of RCC pavements over time from Harrington et al. (2010).

A research study was conducted in order to systematically investigate the main parameters that affect RCC mix design and the resultant properties as well as the relationship between field and laboratory properties of RCC. The effect of aggregates, which comprises up to 85% of RCC, was investigated in terms of combined aggregate gradation, aggregate packing efficiency, and aggregate type (recycled and virgin). Cementitious materials were investigated in terms of cement contents as well as the utilization of different supplementary cementitious materials. Such materials included fly ash, silica fume, and ground-granulated blast furnace slag. The addition of fibers to RCC and lightly cement-treated bases were investigated to determine their impact on strength, flexural toughness, and fracture properties of RCC. Various RCC compaction methods (modified Proctor, vibrating hammer, vibrating table with surcharge weight, and gyratory compactor) were investigated to better define appropriate laboratory procedures to define RCC mix designs that produce the corresponding field properties. The RCC mixes were evaluated for various fresh, strength, durability, shrinkage, creep, and fracture properties. To meet these objectives, this report has been broken up into the following chapters:

Chapter 2: Effects of Aggregate Gradation on Roller-Compacted Concrete Properties: Sixteen RCC mix designs were developed—each with a different gradation—to characterize the effects of aggregate gradation on fresh and hardened properties.

Chapter 3: Mechanical Properties of Roller-Compacted Concrete Pavements from Field and Laboratory Samples: Mechanical properties of cores from RCC pavements were measured and compared with companion specimens fabricated using compaction methods in the laboratory.

Chapter 4: Influence of Mixture Proportions on Roller-Compacted Concrete Properties: A statistically rigorous experimental design was created to develop predictive models to determine the impact of cementitious content, fly ash dosage, and sand percentage on RCC properties.

CHAPTER 2: EFFECTS OF AGGREGATE GRADATION ON ROLLER-COMPACTED CONCRETE PROPERTIES

This chapter investigates the impact of a broad range of aggregate gradations from fixed aggregate sources on fresh and hardened properties of roller-compacted concrete (RCC). Fresh properties measured include moisture-density relationship from the modified Proctor test and compactibility by the Vebe test. The hardened properties quantified were strength (compressive, split tensile, and flexural), fracture properties (disk-shaped compact tension geometry), and drying shrinkage.

2.1 REVIEW OF PREVIOUS RESEARCH

The aggregate gradation for RCC is typically specified to be near the 0.45-power (i.e. maximum density) curve (ACI, 1995; Harrington et al., 2010; ACPA, 2014). However, little research was found validating that this gradation band is optimal for RCC. Due to the large volume fraction that aggregate occupies in RCC, the type and gradation of aggregates is anticipated to impact fresh and hardened properties (ACI, 1995). Previous research has shown that coarse to fine aggregate ratio and strength are positively correlated (Qasrawi et al., 2005; LaHucik and Roesler, 2015). Combined gradations that follow the maximum density curve have been shown to yield higher densities than gradations that simply fall within the recommended gradation band (Williams, 2013). Despite minimal research on optimizing aggregate gradations for RCC, there has been significant work on this topic for Portland cement concrete (PCC) pavements (Shilstone et al., 1990; Richardson, 2005; Cook et al., 2013; Ley and Cook, 2014; Lindquist et al., 2015; Taylor, 2015) as well as many more for asphalt concrete pavements.

2.2 MIX DESIGNS AND FRESH PROPERTIES

Three aggregate stockpiles were used to generate the engineered gradations: coarse dolomite, intermediate dolomite, and natural sand. In order to achieve these gradations, each aggregate was sieved into individual sieve sizes and recombined based on the desired combined gradation. A total of 16 aggregate gradations were created: 9 gradations (1-9) had a nominal maximum aggregate size (NMAS) of 19 mm (3/4 in.) and low aggregate fines contents (i.e., less than 1% passing the 0.075 mm (#200) sieve), 3 gradations (10-12) had a NMAS of 19 mm (3/4 in.) and high aggregate fines contents (3, 6, and 8.2% passing the 0.075 mm (#200) sieve), and 4 gradations (13-16) had a NMAS of 25.4 mm (1 in.) and low aggregate fines contents (i.e. less than 1% passing the 0.075 mm (#200) sieve). The low aggregate fines—19 mm (3/4 in.) NMAS gradations—are the same RCC mixes presented in LaHucik and Roesler (2015). The 3 gradations with the high aggregate fines content (along with mix 1) are all near the 0.45-power curve until the 0.075 mm (#200) sieve. Mixture 12 with 8.2% fines is equivalent to the 0.45-power curve for all sieve sizes. Mix 10 has 3% passing the 0.075 mm (#200) sieve and mix 11 has 6% passing the 0.075 mm (#200) sieve. Mixes 13, 14, and 15 from the 25.4 mm (1 in.) NMAS gradation group have increasing percentages of sand: 50, 55, and 60% respectively. Mix 16 represents a ternary blend of coarse (25%), intermediate (30%), and fine aggregate (45%). Table 1 provides a summary of the three groups of gradations.

Table 2 and Table 3 show the aggregate gradations for mixes 1-9 and 10-16, respectively. The gradations are shown in Figure 3 as a function of gradation group (i.e. gradations 1-9, 10-12, and 13-16). The cement content for all RCC mix designs was fixed at 282 kg/m^3 (475 lb/yd^3) which equates to approximately 11.6-12.1% of the total weight of aggregate and cement, depending on maximum dry density. The cement content can be considered as adding to the fines content of the total aggregate gradation.

Table 1. Description of Gradation Groups *(1 in = 25.4 mm)*

Mix Group	NMAS (mm)	% Passing 0.075 mm Sieve		% Passing 4.76 mm Sieve
1-9	19	< 1%		37.6 – 55.6%
10-12	19	3, 6, and 8.2%, respectively		53.6%
13-16	25.4	< 1%		49.1 – 58.4%

Table 2. Aggregate Gradations for Mixes 1 to 9 *(1 in = 25.4 mm)*

Sieve Size (mm)	Mix 1	Mix 2	Mix 3	Mix 4	Mix 5	Mix 6	Mix 7	Mix 8	Mix 9
25.4	100.0	100.0	100.0	100.0	100.0	100.0	100.0	100.0	100.0
19	100.0	100.0	100.0	100.0	100.0	100.0	100.0	100.0	100.0
12.7	84.6	81.8	80.9	83.4	83.6	81.6	86.3	80.0	96.7
9.51	73.2	68.6	69.2	73.3	73.2	69.2	76.7	62.0	70.6
4.76	51.7	45.0	46.7	55.6	51.9	37.6	48.5	42.0	38.8
2.38	41.2	34.1	30.2	44.3	39.3	21.9	34.3	28.0	32.9
1.19	28.7	22.5	18.1	36.0	34.5	18.1	30.8	20.0	23.5
0.595	19.9	14.1	9.2	25.0	29.3	15.4	28.0	14.0	14.8
0.297	15.4	10.0	2.7	10.6	8.1	4.3	16.8	7.0	4.5
0.149	0.8	0.5	0.0	1.0	0.3	0.2	1.3	1.0	0.9
0.074	0.2	0.1	0.0	0.3	0.2	0.1	0.2	0.0	0.2

Table 3. Aggregate Gradations for Mixes 10 to 16 *(1 in = 25.4 mm)*

Sieve Size (mm)	Mix 10	Mix 11	Mix 12	Mix 13	Mix 14	Mix 15	Mix 16
25.4	100.0	100.0	100.0	100.0	100.0	100.0	100.0
19	100.0	100.0	100.0	88.4	89.6	90.7	94.2
12.7	83.4	83.4	83.4	65.5	68.9	72.4	82.8
9.51	73.2	73.2	73.2	56.7	61.1	65.4	76.6
4.76	53.6	53.6	53.6	49.1	53.8	58.4	53.6
2.38	39.3	39.3	39.3	41.8	46.0	50.1	38.3
1.19	28.7	28.7	28.7	33.5	36.8	40.1	30.2
0.595	21.0	21.0	21.0	23.4	25.6	27.9	21.0
0.297	15.4	15.4	15.4	6.4	7.0	7.6	5.9
0.149	11.3	11.3	11.3	0.8	0.8	0.9	0.9
0.074	3.0	6.0	8.2	0.3	0.3	0.3	0.4

Based on previous work assessing the impact of aggregate gradation on PCC properties, the 16 gradations of these studies were compared in three ways: typical sieve analysis (i.e. cumulative percent passing vs. sieve size), the Tarantula curve (Ley and Cook, 2014), and the coarseness factor chart (Shilstone et al., 1990). Equations 1 and 2 define the coarseness factor (CF) and workability factor (WF), respectively, that were used to plot the gradations on the coarseness factor chart (Figure 3). The sixteen gradations were plotted against the Tarantula curve and coarseness factor chart to provide a comparison of these gradations relative to those recommended for lean and slip-formed concrete pavements. The high aggregate fines gradations (i.e., the gradations that follow the 0.45-power curve) generally meet the Tarantula curve boundaries. The tarantula curve was developed for lean concrete pavements with the objective of identifying aggregate gradations that would provide sufficient workability, reducing potential for honeycombing, and minimizing edge slumping. However, the gradations do not fall in the optimal zone for slip-formed concrete pavements (zone II) of the coarseness factor chart. The gradations were not necessarily designed to avoid zone II of the coarseness factor chart or to generally agree with the Tarantula curve—but rather was a result of the individual aggregate gradations that were sieved out and available to re-combine.

$$CF = \frac{Cumulative\ \%\ Retained\ on\ 9.51\ mm\ sieve}{Cumulative\ \%\ Retained\ on\ 2.36\ mm\ sieve} \cdot 100 \quad \text{(Eq. 1)}$$

$$WF = \%\ Passing\ 2.36\ mm\ sieve + \frac{2.5[cementitious\ content\ (kg/m^3) - 334.5]}{55.7} \quad \text{(Eq. 2)}$$

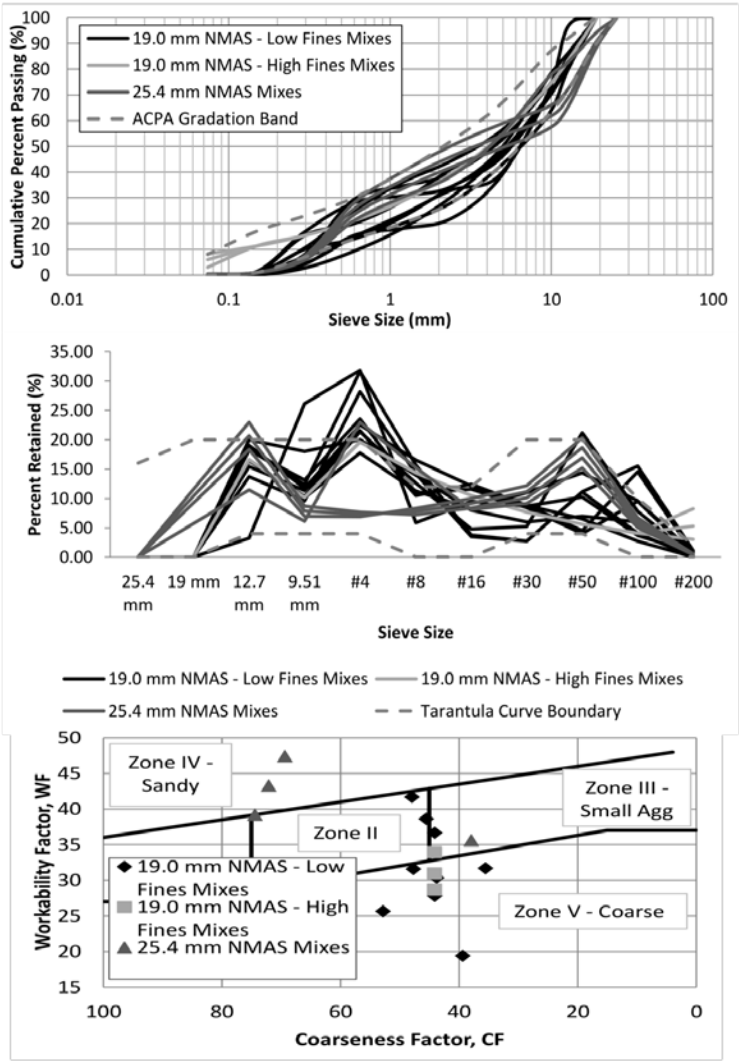

Figure 3. Aggregate gradation curves (top), tarantula curve (middle), and coarseness factor chart (bottom); *(1 inch = 25.4 mm; 1 kg/m³ = 1.686 lb/yd³).*

For each RCC mix, Modified Proctor testing was performed according to ASTM D1557 (ASTM, 2012) to determine the moisture-density relationship. The modified Proctor testing, optimum moisture content (OMC), and maximum dry density (MDD) results were used to determine the final mixture proportions (Table 4). In Table 4, the OMC values ranged from 6.1% to 7.1% for the 16 mixes while MDD values ranged from 2,328 kg/m^3 (145 lb/ft^3) to 2,435 kg/m^3 (152 lb/ft^3). Neither OMC nor MDD were significantly affected by aggregate fines content or NMAS based on the modified Proctor procedure. Modified Vebe testing, a subjective measure of RCC compactibility, was performed according to ASTM C1170 procedure A (ASTM, 2008). The Vebe test measures the amount of time required for an RCC mixture to form a mortar ring around the perimeter of a cylindrical mold (Figure 4) while on a vibrating table with a surcharge weight compacting the mixture. Therefore, greater modified Vebe times correspond to reduced compactibility of the RCC mixture but also suggest that the mix will has less roll down (reduction in thickness before and after roller pass) and an increased resistance to edge slumping. In general, all gradations that had low aggregate fines contents had Vebe times of 25 seconds or less while the high aggregate fines mixes had Vebe times in the range of 30-40 seconds. ACI (1995) recommends Vebe times in the range of 30-40 seconds which suggests that the high aggregate fines mixes might produce the optimal combination of compactibility, minimal roll down, and ability to hold an edge without slumping. Increasing the sand percentage (comparing mixes 13-15) increased the OMC and reduced the Vebe time.

Figure 4. Compacted vebe specimen with mortar ring around plate (left) and RCC surface appearance after testing (right).

Table 4. RCC Mix Designs and Fresh Properties *(1 inch = 25.4 mm; 1 kg/m³ = 1.686 lb/yd³)*

Mix Group	Mix #	OMC (%)	MDD (kg/m³)	Cement (kg/m³)	Oven-Dry Aggregate (kg/m³)	Water (kg/m³)	Vebe Time (sec)
19 mm NMAS – Low Aggregate Fines	1	6.4	2350.4	281.7	2068.7	151.1	6.5
	2	6.1	2385.6	281.7	2104.0	145.3	16.7
	3	6.7	2366.4	281.7	2084.8	159.3	16
	4	6.7	2328.0	281.7	2046.3	156.4	15.2
	5	6.4	2371.2	281.7	2089.6	152.0	19.6
	6	7.2	2435.3	281.7	2153.6	174.1	25.3
	7	6.7	2364.8	281.7	2083.1	158.2	22.9
	8	6.6	2393.6	281.7	2112.0	156.8	15.2
	9	6.7	2400.0	281.7	2118.4	161.3	13.3
19 mm NMAS – High Aggregate Fines	10	6.6	2382.4	281.7	2100.8	158.0	31.6
	11	6.7	2382.4	281.7	2100.8	160.6	38.1
	12	6.2	2384.0	281.7	2102.4	148.8	38.7
25.4 mm NMAS – Low Aggregate Fines	13	6.3	2371.2	281.7	2089.6	149.4	21.2
	14	7.0	2345.6	281.7	2063.9	163.3	15.3
	15	7.1	2356.8	281.7	2075.1	167.1	9.3
	16	6.5	2388.8	281.7	2107.2	155.8	10.9

All moisture-density test points from each mix are plotted in Figure 5. The typical parabolic relationship between dry density and moisture content for each mix is shown. However, the same behavior cannot be said of the wet density vs. moisture content relationships. For those mixes that do not have a significant decrease in dry density after their OMC, the corresponding wet densities reach a maximum (typically around the OMC of the mix) and then remain relatively constant (Figure 6). For those mixes that do have relatively significant and sharp reductions in dry density after the OMC (mixes 7, 9, and 12-16) a similar trend was seen in wet density (i.e. wet density reaches a

maximum and then begins to decrease). Since field compaction requirements for RCC pavements are typically specified in terms of wet density (Chapter 3), Figure 5 would indicate that certain mixes would be more forgiving in terms of moisture contents than others. Comparing two mixes that had different wet density vs. moisture content relationships (i.e. one that had constant wet density after OMC and another with decreasing wet density after OMC) in Figure 6—the mix with constant wet density after OMC shows less moisture sensitivity and therefore would likely be more forgiving with regards to slight changes in moisture content of the mix.

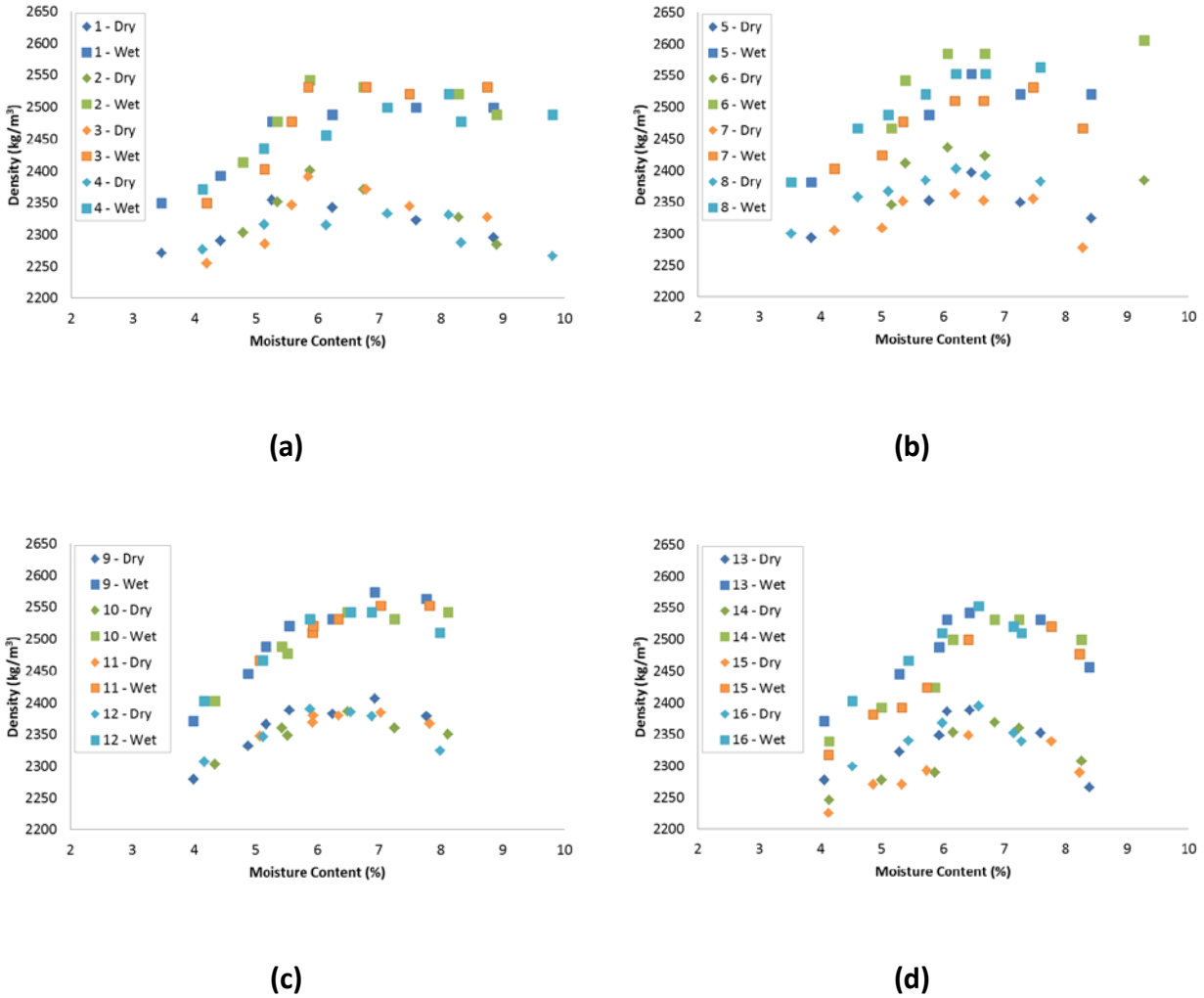

Figure 5. Comparison of dry and wet densities from modified proctor testing. Mixes 1-4 (a), 5-8 (b), 9-12 (c), 13-16 (d); *(1 kg/m³ = 1.686 lb/yd³).*

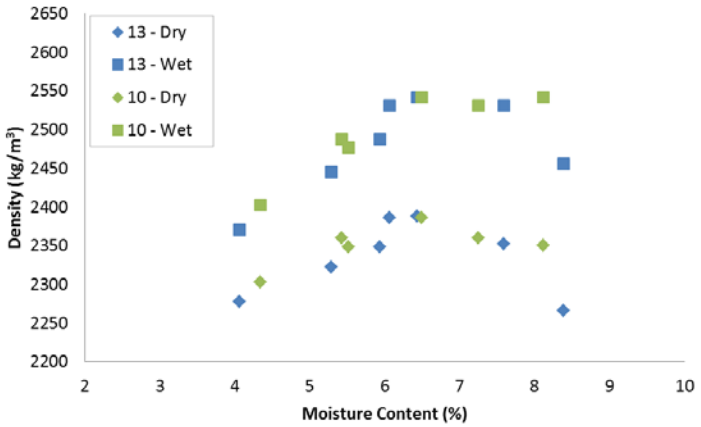

Figure 6. Comparison of wet and dry densities to check moisture sensitivity; *(1 kg/m³ = 1.686 lb/yd³)*.

2.3 STRENGTH PROPERTIES

Compressive strength was determined on 100x200 mm (4x8 in) cylinders at 7, 14, and 28 days with each mix having three replicates at each testing age. Compressive strength testing was performed according to ASTM C39 (ASTM, 2012). The 100x200 mm (4x8 in) cylinders were fabricated similarly to ASTM C1435 (ASTM, 2008) with the differences being the number of lifts (3 compared to 4) and the specimen size (100x200 mm (4x8 in) compared to 150x300 mm (6x12 in)). All 100x200 mm (4x8 in) RCC cylinders were fabricated with this procedure. While there have been many RCC studies in the literature (Haque and Ward, 1986; Nanni and Johari, 1989; Albuquerque et al. 2011; Bilodeau et al. 2011; Modarres and Hosseini, 2014; Olubanwo and Karadelis, 2015) that employed 100x200 mm (4x8 in) cylinders for strength testing, none of them discussed the validity of using this specimen size. A study on cementitious stabilized aggregates showed no significant difference in compressive strength between 100x200 mm (4x8 in) and 150x300 mm (6x12 in) cylinders (Symons, 1970).

A comparison of 16 different RCC mix designs with different gradations, aggregate types (virgin and recycled aggregates), and aggregate NMAS (19 or 25.4 mm (3/4 or 1 in) was performed in order to determine the validity of compacting—with the same vibratory hammer—different specimen geometries with respect to their respective strength results. The vibratory hammer, tamping plates, and steel molds that encased the plastic cylinder molds during compaction of the two cylindrical specimen sizes are shown in Figure 7. Three replicates of both specimen sizes were fabricated and tested at the same age. From Figure 8, both specimen sizes produce similar compressive strengths. The use of 100x200 mm (4x8 in) cylindrical specimens for strength testing is preferable because of reduced RCC material requirements. In addition, smaller specimens are easier to transport/store/cure. Lastly, similar to field core sizes, most RCC pavements are too thin for a 150x300 mm (6x12 in) core.

Figure 7. Compaction equipment for RCC cylinders.

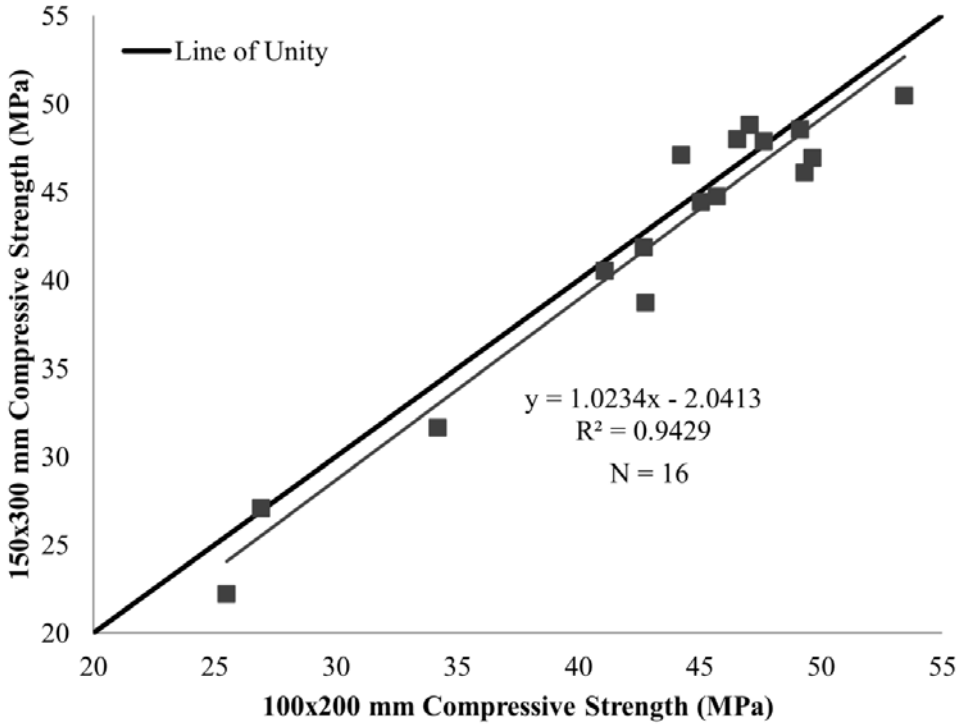

Figure 8. Comparison of 150x300 mm (6x12 in) and 100x200 mm (4x8 in) compressive strength; *(1 ksi = 6.89 MPa)*.

For all the RCC mixtures mixed and fabricated, the results of compressive strength testing (100x200 mm (4x8 in) cylinders) are shown in Figure 9. According to the RCC guide specification published by the American Concrete Pavement Association (ACPA, 2014), recommended 28-day compressive strengths are 28 MPa (4 ksi) and 31 MPa (4.5 ksi) for non-freeze and freeze-thaw climates, respectively. All mixes meet the recommended 31 MPa (4.5 ksi) at 28 days as seen in Figure 9. Some RCC specifications also call for 7-day compressive strengths of 24.0 MPa (3.5 ksi) (IDOT, 2014). All RCC mixes (all gradations) also meet a 7-day compressive strength requirement of 24.0 MPa (3.5 ksi).

The 28-day strengths of all mixes were statistically compared using the Tukey test (Mason et al. 2003). The Tukey test is a piecewise t-test (95% confidence) analyzing all possible pairs with the result being the statistical similarity or dissimilarity of each mix with respect to all other mixes. In general, from Table 5, the 19 mm (3/4 in) NMAS high fines mixes produced some of the lowest compressive strengths, statistically. While all mix designs met the specified 28-day compressive strength of 31 MPa (4.5 ksi), there were statistical differences between the mixes as noted in Table 5. There was not a significant effect of NMAS on 28-day compressive strength.

For mixes 1 through 9, triplicate 150x300 mm (6x12 in) cylinders were cast and tested for compressive strength at 14 days. The compressive strengths were highly correlated (R^2 = 0.999) with the following gradation parameters: FA_C ratio (percent passing the 1.18 mm (#16) sieve divided by percent passing the 4.75 mm (#4) sieve), coarse-fine aggregate (CA/FA) ratio (cumulative percent retained on 4.75 mm (#4) sieve divided by percent passing 4.75 mm (#4) sieve), and the individual percent retained on the 12.7 mm (1/2 in) and 2.36 mm (#6) sieves. For these gradations (mixes 1-9) and a fixed cement content of 282 kg/m^3 (475 lb/yd^3), LaHucik and Roesler (2015) proposed the following regression equation (Equation 3) for 14-day compressive strength, $\sigma_{c,14}$ (MPa), where all regression coefficients are statistically significant at 95% confidence:

$$\sigma_{c,14} = 41.39FA_c + 10.58\frac{CA}{FA} + 1.35(12.7\ mm) - 1.02(2.36\ mm) \qquad \text{(Eq. 3)}$$

In order to determine the effects of aggregate segregation, mixes 13-16 were batched using two methods: 1) the aggregates were separated into individual sieve sizes and re-combined to match their gradations from the initial sieve analysis; or 2) the aggregates were used in their "as-is" condition, i.e., no sieving. Two cylinder sizes (100x200 and 150x300 mm, 4x8 and 6x12 in) were cast with triplicate specimens of each specimen size for each mix. Generally, the sieved aggregate RCC mixes had higher mean compressive strengths than the unsieved. For the 150x300 mm (6x12 in) cylinders, 3 of the 4 mixes had statistically lower compressive strengths while only 1 mix was statistically different for the 100x200 mm (4x8 in) cylinders (Table 6) when comparing the sieved to un-sieved of the same cylinder size. The results of these tests suggest that 100x200 mm (4x8 in) cylinder strengths would be less likely to differentiate between a segregated batch and a non-segregated batch of RCC whereas 150x300 mm (6x12 in) cylinder strengths would be more likely. This behavior could be caused by the fact that more energy is input into the smaller cylinder sizes given the same mix and vibratory hammer. One general outcome of this comparison is that properly maintaining aggregate stockpiles and avoiding aggregate segregation will limit variability in RCC properties and performance.

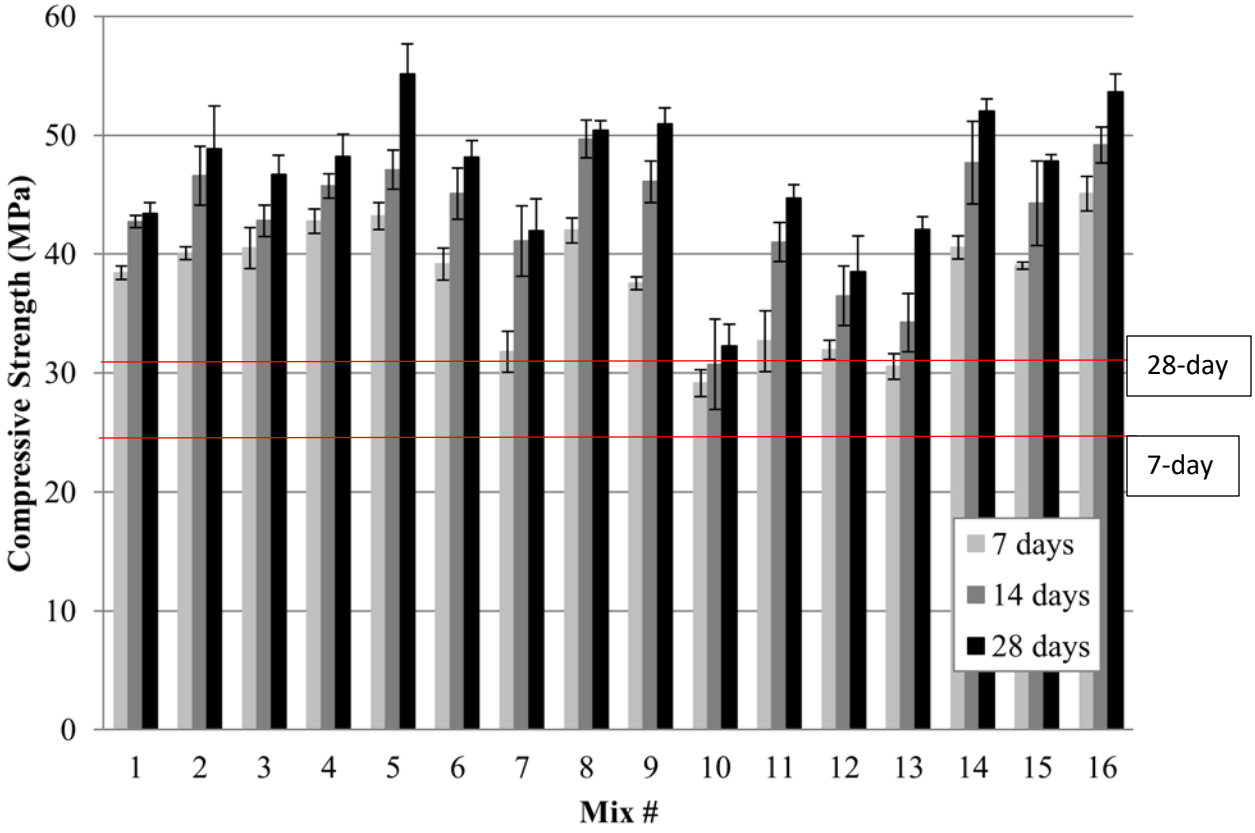

Figure 9. RCC compressive strength with 100x200mm (4x8 in) specimens (error bars indicate +/- one standard deviation). 7 and 28 day strength requires 3.5 and 4.5 ksi, respectively; *(1 ksi = 6.89 MPa)*.

Table 5. Statistical Analysis of 28-Day Compressive Strength *(1 ksi = 6.89 MPa)*

Mix #	Compressive Strength (MPa)	Statistical Grouping					
5	55.1	A					
16	53.6	A	B				
14	52.0	A	B				
9	50.9	A	B	C			
8	50.4	A	B	C			
2	48.8	A	B	C	D		
4	48.2	A	B	C	D		
6	48.2		B	C	D		
15	47.8		B	C	D		
3	46.7		B	C	D		
11	44.7			C	D	E	
1	43.4				D	E	
13	42.0				D	E	
7	41.9				D	E	
12	38.5					E	F
10	32.2						F

*Mixes that do not share the same statistical group(s) are statistically different.

Table 6. Statistical Comparison of Compressive Strength between Sieved and Unsieved RCC Mixes; *(1 ksi = 6.89 MPa; 1 in = 25.4 mm)*.

	100x200 mm Cylinder			150x300 mm Cylinder		
Mix #	Sieved Compressive Strength (MPa)	Unsieved Compressive Strength (MPa)	p-value	Sieved Compressive Strength (MPa)	Unsieved Compressive Strength (MPa)	p-value
13	34.2	41.6	0.070	31.6	29.5	0.273
14	47.7	41.8	0.196	**47.9**	**34.1**	**0.006**
15	44.3	39.2	0.182	**47.1**	**28.4**	**0.039**
16	**49.2**	**41.5**	**0.007**	**48.5**	**39.4**	**0.039**

*Bolded cells indicate statistical difference (p-value < 0.05) in compressive strength between sieved and unsieved mixes for a particular cylinder size.

Split tensile strength was determined on 100x200 mm (4x8 in) cylinders at 7, 14, and 28 days with each mix having three replicates at each testing age. Split tensile strength testing was performed according to ASTM C496 (ASTM, 2011). Results of split tensile strength testing (along with standard deviation) are shown in Figure 10. Statistical analysis was performed only on 28-day strengths using the Tukey test and results are shown in Table 7. While the high aggregate fines mixes (#10 to #12) yielded 3 of the 4 lowest split tensile strengths, they are not statistically different from the vast majority of the RCC mixes. This is due to the relatively large variability of split tensile strength testing in relation to compressive strength testing and less influence of aggregate gradation on tensile strength. For mixes 1-9, triplicate 150x300 mm (6x12 in) cylinders were cast and tested for 14-day split tensile strength testing. However there was no statistically significant correlation with gradation parameters (LaHucik and Roesler, 2015).

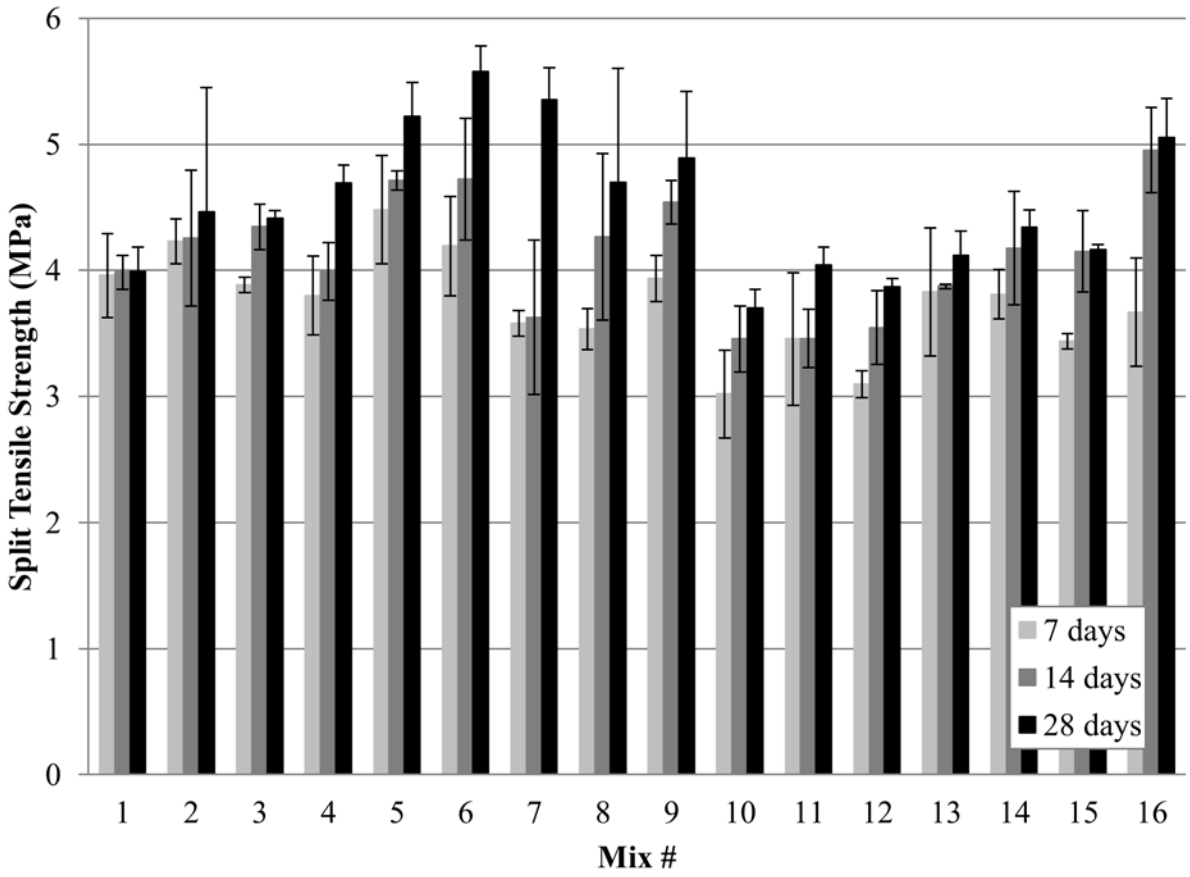

Figure 10. RCC split tensile strength with 100x200 mm (4x8 in) specimens (error bars indicate +/- one standard deviation); *(1 ksi = 6.89 MPa)*.

Table 7. Statistical Analysis of 28-Day RCC Split Tensile Strength *(1 ksi = 6.89 MPa)*

Mix #	Split Tensile Strength (MPa)	Statistical Grouping			
6	5.58	A			
7	5.35	A	B		
5	5.22	A	B	C	
16	5.05	A	B	C	D
9	4.89	A	B	C	D
8	4.70	A	B	C	D
4	4.69	A	B	C	D
2	4.46	A	B	C	D
3	4.41	A	B	C	D
14	4.34	A	B	C	D
15	4.16	A	B	C	D
13	4.11	A	B	C	D
11	4.04		B	C	D
1	3.99		B	C	D
12	3.87			C	D
10	3.70				D

*Mixes that do not share the same statistical group(s) are statistically different.

Flexural Strength (MOR) was determined on 100x100x400 mm (4x4x16 in) beams under third point (or four point) loading according to ASTM C78 (ASTM, 2010). Flexural strength was tested at 28 days with each mix having three replicates. Beam specimens (Figure 11) were fabricated in steel beam molds using an 88x88 mm (3.5x3.5 in) steel tamping plate affixed to a vibratory hammer (Figure 12). The beams were cast in two lifts with each lift receiving a total of 25 seconds of vibration (5 seconds at each end, 5 seconds in the middle, and 5 seconds between each end and the middle).

Figure 11. 100x100x400 mm (4x4x16 in) MOR beam specimen being tested in four-point bending.

Figure 12. Tamping plate for shrinkage prisms (left) and tamping plate for MOR beams (right).

According to Tanesi et al. (2013), there is a good correlation (R^2 = 0.933) between MOR results of 100x100x400 mm (4x4x16 in) and 150x150x525 mm (6x6x21 in) beams for conventional paving concrete and is given by Equation 3, where both MOR values are in units of MPa. It is not clear if this correlation equation would be valid for RCC mixes. Figure 13 shows results of 28-day flexural strength testing with the smaller specimen along with the predicted flexural strength for a 150x150x525 mm (6x6x21 in) specimen size, computed using Equation 4. Results of the Tukey test for 28-day flexural strength are shown in Table 8. Similar to split tensile strength, a large majority of the mixes yielded statistically similar flexural strengths. In general, the 28-day flexural strengths were greater than 6 MPa (with the exception of two high aggregate fines mixes) which is significantly greater than typical 28-day flexural design strengths utilized for concrete pavement, e.g., approximately 5.2 MPa (0.75 ksi). Mixes 1 and 12 have statistically different flexural strengths; however, they have very similar gradations until the 0.297 mm (#50) sieve after which mix 12 has a much higher fines content than mix 1. As stated earlier, the gradation for mix 12 is equal to that of the 0.45-power (maximum density) curve but it produced the lowest mean flexural strength. The combination of the cement content and the higher aggregate fines content (8.2%) in mix 12 served to increase the spacing between coarse aggregates by pushing them apart and also reduce the strength of the mortar fraction (i.e. fine aggregate and paste) because of the high content of inert aggregate fines.

$$MOR_{150x150x525mm} = 1.1099 \cdot MOR_{100x100x400mm} - 0.756 \quad \text{(Eq. 4)}$$

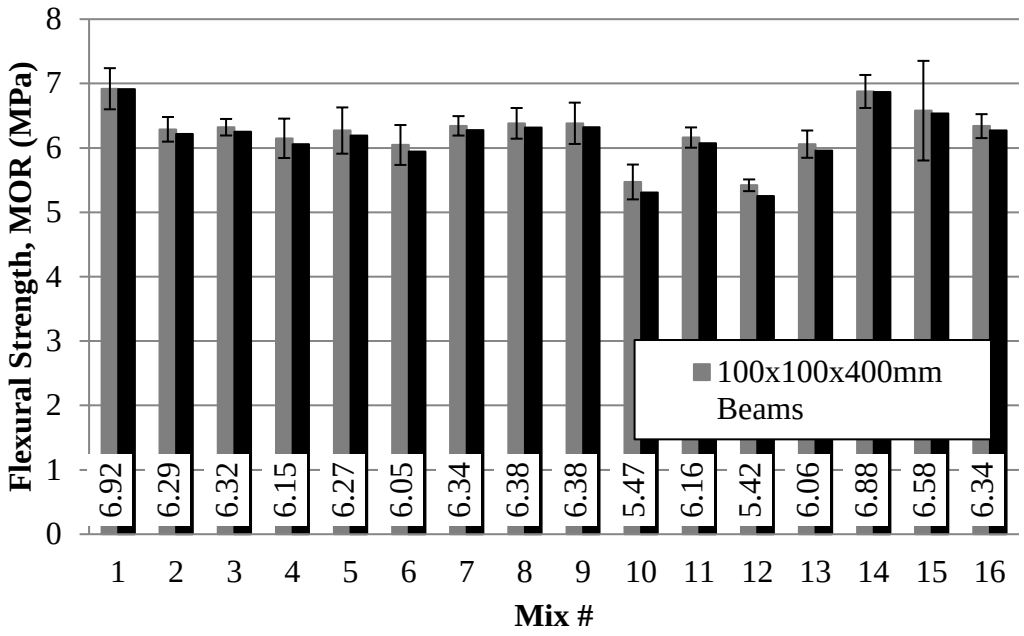

Figure 13. 28-Day RCC flexural strength for 100x100x400mm (4x4x16 in) specimens with error bars indicating +/- one standard deviation. MOR values of 150x150x525mm (6x6x21 in) beams were predicted from Tanesi et al. (2013); *(1 ksi = 6.89 MPa)*.

Table 8. Statistical Analysis of 28-Day Flexural Strength *(1 ksi = 6.89 MPa)*

Mix #	Flexural Strength, MOR (MPa)	Statistical Grouping		
1	6.92	A		
14	6.88	A		
15	6.58	A	B	
9	6.38	A	B	C
8	6.38	A	B	C
7	6.34	A	B	C
16	6.34	A	B	C
3	6.32	A	B	C
2	6.29	A	B	C
5	6.27	A	B	C
11	6.16	A	B	C
4	6.15	A	B	C
13	6.06	A	B	C
6	6.05	A	B	C
10	5.47		B	C
12	5.42			C

*Mixes that do not share the same statistical group(s) are statistically different.

2.4 FRACTURE PROPERTIES OF RCC MIXES

In addition to strength properties, fracture properties were also tested for the same set of RCC mixes. Fracture testing quantifies both the RCC material's resistance to crack initiation and crack propagation. It also defines fracture parameters, such as the critical stress intensity factor and critical crack tip opening displacement (Jenq and Shah, 1985) as well as total fracture energy (Hillerborg 1985). Fracture testing may be able to distinguish RCC mix designs better than typical strength testing and have been shown to be one of the most useful parameters for predicting the flexural capacity of concrete slabs (Ioannides et al. 2006; Gaedicke et al. 2012; Brand et al. 2014). The disk-shaped

compact tension (DCT) geometry shown in Figure 14 was chosen since RCC specimens for fracture testing can readily be fabricated from 150x300 mm (6x12 in) cylinders. While other specimen geometries (single-edge notched beam) have been used for RCC fracture testing (Ferrebee et al. 2014), there is not an ASTM standard for fabrication of these specimen geometries and therefore repeatability amongst operators and labs will be an issue. The testing and analysis procedure for the DCT geometry is detailed by Amirkhanian et al. (2015). The RCC fracture parameters are derived from the Jenq and Shah (1985) two-parameter fracture model (TPFM) and work of fracture method (Hillerborg 1985).

Li et al. (2002) tested uniaxial tensile fracture of RCC dam cores and found that fracture energy is proportional to compressive strength and maximum aggregate size with values ranging from 74-261 N/m (0.42-1.50 lb/in) depending on failure mode and specimen size/strength. Cui et al. (2014) performed wedge-split fracture tests on an RCC pavement mix to validate the double-k fracture model and found critical stress intensity factors in the range of 0.9 to 1.6 MPa-$m^{1/2}$ (0.82 to 1.46 ksi-$in^{1/2}$) depending on specimen size and notch-depth ratio. Zeng et al. (2011) performed fracture testing of an RCC dam mix and found higher compressive strengths led to increased brittleness (i.e., reduced fracture energy). However, no details were provided about specimen geometry or test procedure. The single-edge notched beam (SENB) geometry has also been used for testing of RCC pavement fracture properties (Albuquerque et al., 2011; Sachet et al., 2011; Ferrebee et al. 2014). Albuquerque et al. (2011) and Sachet et al. (2011) found values of K_{IC} ranging from 1.4 to 1.9 MPa-$m^{1/2}$ (1.27 to 1.73 ksi-$in^{1/2}$) and fracture energy values of approximately 490 N/m (2.8 lb/in). Ferrebee et al. (2014) found K_{IC} values ranging from 1.3 to 1.5 MPa-$m^{1/2}$ (1.18 to 1.37 ksi-$in^{1/2}$) and fracture energy values of 135 to 145 N/m (0.77 to 0.83 lb/in). Although the fracture properties of RCC mixtures have been previously tested, the characterization of RCC fracture properties over a wide range of mixture proportions, i.e., aggregate gradations, has not been reported in the literature.

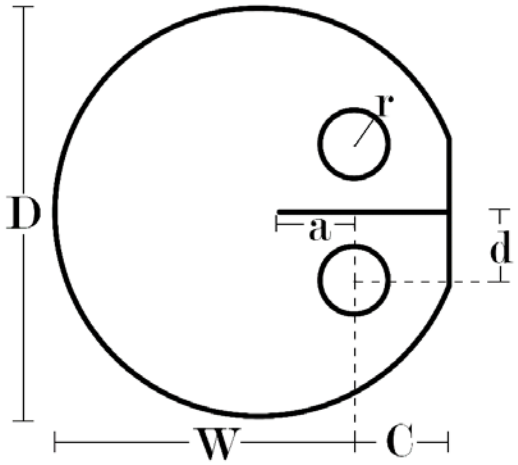

Figure 14. DCT geometry - D is 150 mm, W is 110 mm, C is 35 mm, d is 25 mm, a is 27.5 mm, and r is 12.5 mm (Amirkhanian et al. 2015); *(1 in = 25.4 mm)*.

The results of fracture testing at 28 days are shown in Table 9 along with fracture properties of conventional concrete pavement mixtures taken from the literature. A plot of load-crack mouth opening displacement (CMOD) curves from each RCC mix is shown in Figure 15. Plots of load-CMOD separated by gradation grouping (i.e. low fines, high fines, and 25.4 mm (1 in) NMAS) are shown in Figure 16. Observations from Figure 16 suggest there is not a significant difference in load-CMOD curves between the various mixes except in the peak load of some mixes. Fracture properties reported in Table 9 include: critical stress intensity factor (K_{IC}), elastic modulus (E), critical crack tip opening displacement ($CTOD_C$), initial fracture energy (G_f), and total fracture energy (G_F). Statistical analysis (Tukey test) was completed on K_{IC} (Table 10) and G_F (Table 11) for all RCC mixes.

While mix 1 produced a statistically greater flexural strength than mix 12, the opposite was true for critical stress intensity factor. In general, the high aggregate fines mixes (mixes 10-12), despite their lower mean strengths, yielded statistically similar or greater fracture properties relative to the low aggregate fines mixes (1-9 and 13-16). This behavior, mixes with lower strength properties yielding similar or greater fracture properties, has also been seen for recycled aggregates in RCC (LaHucik and Roesler, 2016). There was not a significant impact of the NMAS change (19 mm (3/4 in) to 25 mm (1 in) on fracture properties despite past concrete literature demonstrate higher fracture properties with large maximum size aggregate. Relative to conventional concrete pavement mixes, the 16 RCC mixes tested had similar or greater fracture properties. This confirms the findings of Ferrebee et al. (2014), which also showed that RCC produces similar or greater fracture properties with the SEN(B) specimen geometry than conventional paving concrete.

Figure 17 compares fracture properties (total fracture energy and critical stress intensity factor) to compressive strength for all 16 mixes. It can be seen that there is a positive relationship between compressive strength and total fracture energy while there is not a clear relationship between critical stress intensity factor and compressive strength. Zeng et al. (2011) found that increasing compressive strength resulted in increased brittleness (i.e. reduced total fracture energy). In this study, compressive strength varies with aggregate gradation only since the mixtures all have the same cement content whereas Zeng et al. (2011) produced different compressive strengths by changing cementitious content (i.e. changing the brittleness of the paste fraction). The data in Figure 17 suggests that there is more of an effect of aggregate gradation on total fracture energy than on critical stress intensity factor since increasing compressive strengths are solely a function of changing gradation.

Fracture properties have been shown to be a better predictor of the flexural capacity of concrete slabs than typical strength properties (Brand et al. 2014), especially when strength and fracture properties do not show the same trends. Therefore, it is expected that RCC constructed properly would produce similar or greater flexural slab capacities relative to conventional concrete pavements.

Table 9. 28-Day RCC Fracture Properties (COV, %) Compared with Conventional Paving Concrete (PCC) Fracture Properties *(1 MPa-m$^{1/2}$ = 0.910 ksi-in$^{1/2}$; 1 in = 25.4 mm; 1 GPa = 145 ksi; 1 lb/in = 175 N/m)*

Mix Group	Mix #	K_{IC} (MPa-m$^{1/2}$)	E	$CTOD_C$ (mm)	G_f (N/m)	G_F (N/m)
19 mm NMAS – Low Aggregate Fines	1	1.07 (6.6)	29.0 (7.2)	0.017 (29.3)	40.0 (18.1)	131.0 (9.7)
	2	1.45 (7.8)	34.0 (5.5)	0.018 (17.1)	62.5 (18.8)	179.2 (11.1)
	3	1.29 (4.1)	28.7 (4.4)	0.022 (9.5)	57.7 (4.6)	164.8 (11.7)
	4	1.12 (10.0)	30.8 (4.8)	0.016 (17.2)	40.8 (20.5)	171.8 (20.3)
	5	1.22 (10.9)	32.3 (3.9)	0.017 (24.8)	47.2 (21.6)	185.7 (14.4)
	6	1.23 (7.3)	28.7 (4.5)	0.020 (10.0)	52.8 (15.2)	148.9 (8.1)
	7	1.16 (7.9)	31.2 (3.0)	0.016 (21.5)	43.0 (16.8)	125.5 (12.0)
	8	1.31 (8.6)	29.5 (5.8)	0.022 (17.1)	58.9 (17.0)	168.3 (3.2)
	9	1.37 (5.9)	31.4 (4.1)	0.022 (14.4)	60.3 (13.8)	169.9 (6.0)
19 mm NMAS – High Aggregate Fines	10	1.23 (11.3)	32.6 (8.1)	0.020 (25.2)	47.0 (25.0)	147.9 (8.9)
	11	1.37 (11.7)	39.7 (6.3)	0.017 (25.1)	48.2 (25.7)	132.2 (16.0)
	12	1.54 (4.6)	39.4 (4.6)	0.018 (19.4)	60.3 (14.1)	145.6 (11.6)
25.4 mm NMAS – Low Aggregate Fines	13	1.41 (6.5)	39.5 (4.8)	0.018 (16.4)	50.7 (10.3)	157.4 (10.2)
	14	1.29 (13.8)	38.8 (10.2)	0.020 (24.7)	43.9 (29.7)	161.7 (12.3)
	15	1.06 (11.1)	33.3 (7.7)	0.017 (34.0)	34.3 (27.5)	140.9 (8.4)
	16	1.30 (8.9)	35.2 (9.1)	0.019 (25.9)	48.5 (16.2)	162.4 (6.4)
Roesler et al. (2007)[a]		1.01	-	0.016	38.3	120
Brand et al. (2014)[b]		1.15	-	0.019	44.3	73.8
Amirkhanian et al. (2015)[c,d]		1.33 (8.0)	-	0.017 (8.0)	49.1 (15.0)	120.3 (30.0)
		0.97 (4.0)	-	0.015 (6.0)	32.4 (12.0)	111.7 (14.0)

[a]Fracture properties of PCC were tested at an age of 7 days using SEN(B).

[b]Fracture properties of PCC were tested at an age of 39 days using SEN(B).

[c]Fracture properties of PCC were tested at an age of 142 days using DCT geometry.

[d]Fracture properties of PCC were tested at an age of 40 days using DCT geometry.

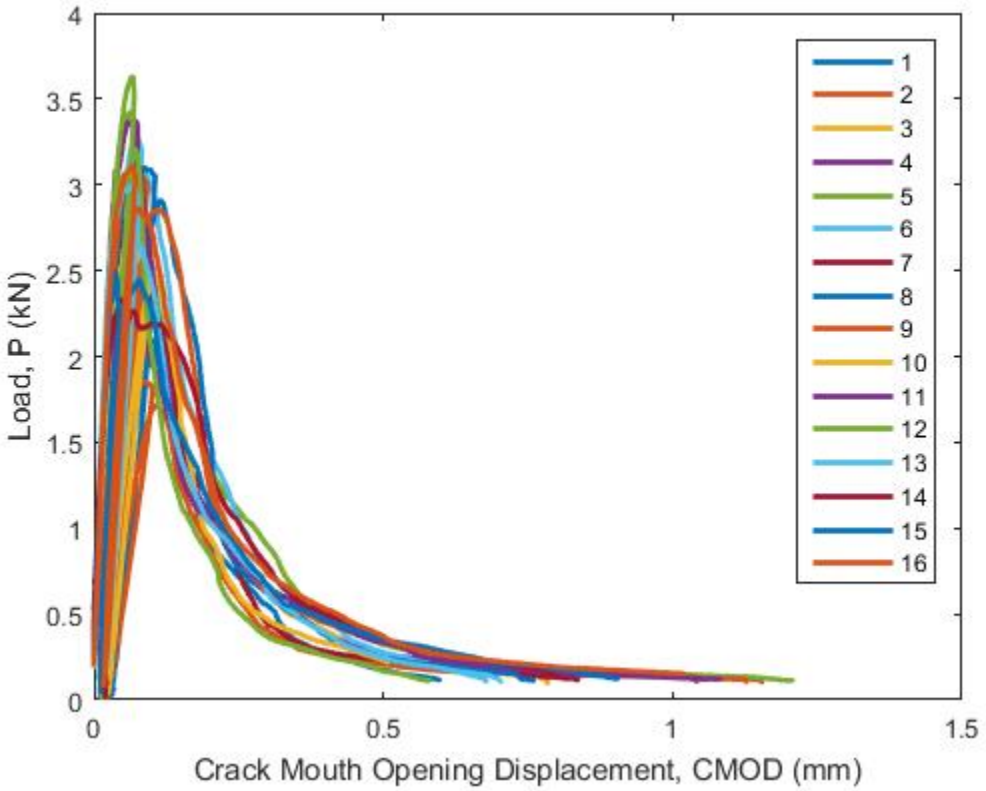

Figure 15. Example DCT load-CMOD plots for each RCC Mix *(1 kN = 224.8 lbf; 1 in = 25.4 mm)*.

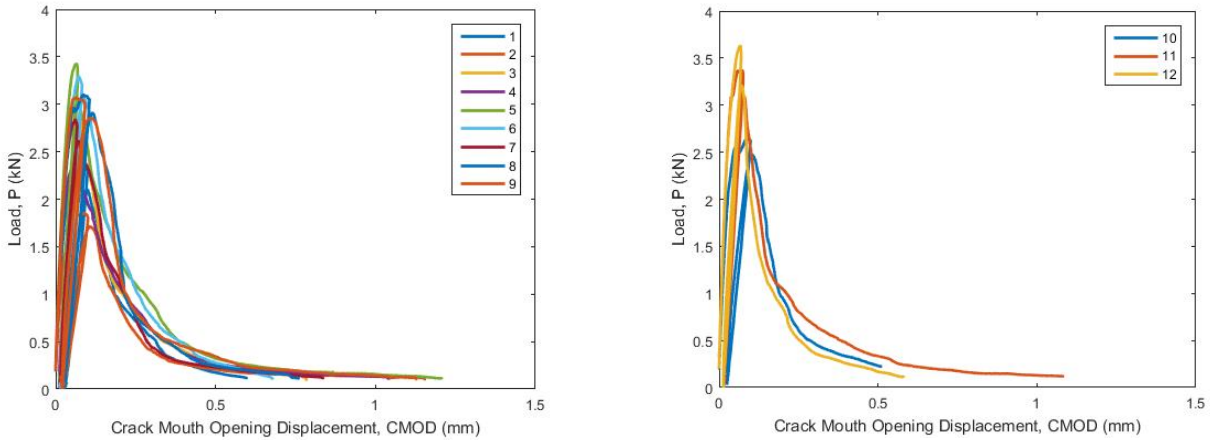

(a) **(b)**

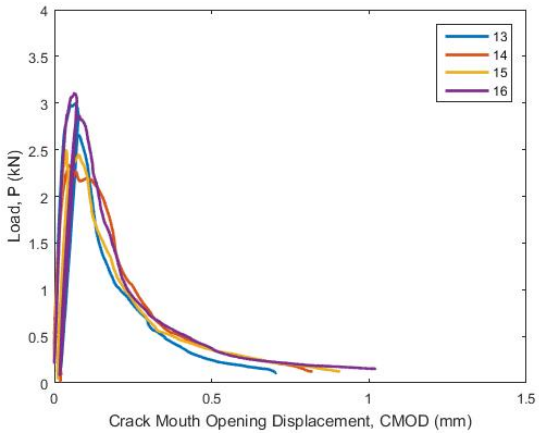

(c)

Figure 16. Example DCT fracture plots for each RCC mixture group. Mixes 1-9 (a), 10-12 (b), and 13-16 (c); *(1 kN = 224.8 lbf; 1 in = 25.4 mm)*.

Table 10. Statistical Analysis of 28-Day Critical Stress Intensity Factor *(1 MPa-$m^{1/2}$ = 0.910 ksi-$in^{1/2}$)*

Mix #	K_{IC} (MPa-$m^{1/2}$)	Statistical Grouping				
12	1.54	A				
2	1.45	A	B			
13	1.41	A	B			
9	1.37	A	B	C		
11	1.37	A	B	C	D	
8	1.31	A	B	C	D	E
16	1.30	A	B	C	D	E
14	1.29	A	B	C	D	E
3	1.29	A	B	C	D	E
6	1.23		B	C	D	E
10	1.23		B	C	D	E
5	1.22		B	C	D	E
7	1.16			C	D	E
4	1.12				D	E
1	1.07					E
15	1.06					E

*Mixes that do not share the same statistical group(s) are statistically different.

Table 11. Statistical Analysis of 28-Day Total Fracture Energy *(1 lb/in = 175.12 N/m)*

Mix #	G_F (N/m)	Statistical Grouping			
5	185.7	A			
2	179.2	A	B		
4	171.8	A	B	C	
9	169.9	A	B	C	
8	168.3	A	B	C	
3	164.9	A	B	C	D
16	162.5	A	B	C	D
14	161.7	A	B	C	D
13	157.4	A	B	C	D
6	148.9	A	B	C	D
10	147.9	A	B	C	D
12	145.6	A	B	C	D
15	140.9		B	C	D
11	132.3			C	D
1	131.0			C	D
7	125.5				D

*Mixes that do not share the same statistical group(s) are statistically different.

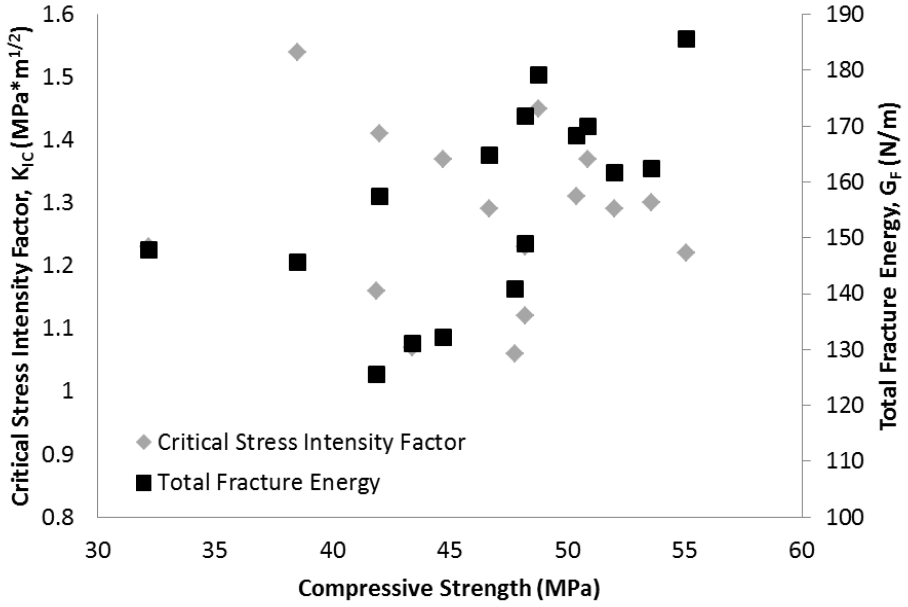

Figure 17. Relationship between fracture parameters and compressive strength for all RCC mixes; *(1 ksi = 6.89 MPa; 1 lb/in = 175.12 N/m; 1 MPa-m$^{1/2}$ = 0.910 ksi-in$^{1/2}$).*

2.5 DRYING SHRINKAGE

Previous research on drying shrinkage of RCC (Ghafoori and Cai, 1998; Pittman and Ragan, 1998; Jingfu et al. 2009; Damrongwiriyanupap et al. 2012; Khayat and Libre, 2014) has produced a relatively wide range of drying shrinkage strains with values ranging from 50 microstrain to 700 microstrain after 28 days of drying. However, the majority of researchers have shown 28-day RCC drying shrinkage strains to be approximately 250-300 microstrain (Ghafoori and Cai, 1998; Pittman and Ragan, 1998; Jingfu et al. 2009; Khayat and Libre, 2014) which is generally less than concrete pavement mixtures. As expected with RCC, increasing coarse aggregate content has shown to reduce drying shrinkage strains (Ghafoori and Cai, 1998; Pittman and Ragan, 1998).

Free drying shrinkage measurements were performed on the 16 RCC mixes in order to determine their volume change characteristics according to ASTM C157 (ASTM, 2008). Triplicate shrinkage prisms (100x100x281 mm (4x4x11 in) were fabricated for each mix. Since no standard procedure for fabricating and compacting RCC shrinkage prisms currently exists, a methodology similar to that proposed by Ferrebee et al. (2014) for fabrication of SEN(B) fracture specimens was used. A 90x260 mm (3.5x10.25 in) tamping plate (Figure 12) was used in conjunction with the vibratory hammer to compact the shrinkage prisms in two lifts with each lift being vibrated until a mortar ring formed around the tamping plate (typically 5-10 seconds). The shrinkage prisms were then cover-cured for 24 hours following which they were demolded and immediately placed in an environmentally-controlled chamber set to 50% relative humidity (RH) and 23°C (73.4°F). Length and mass measurements were taken at initiation of exposure to drying (i.e., 24 hours after casting) and 1, 3, 5, 7, 14, 28, 56, 90, and

180 days after exposure to drying. Variability in shrinkage measurements is expected because of the lower moisture content, higher surface irregularities, and 24-hour cover curing time.

Drying shrinkage strains were calculated using Equation 5 where shrinkage strain (ϵ_{sh}) is in units of microstrain, $L_{specimen}$ is in mm, $L_{reference\ bar}$ is in mm, and the gage length (GL) is equal to 254 mm (10 in). The plots of shrinkage strain versus time are shown in Figure 18. A hyperbolic model of the form shown in Equation 6 was used to fit the shrinkage strain data over time for each mix. Shrinkage strain (ϵ_{sh}) and ultimate shrinkage strain ($\epsilon_{ultimate}$) are in units of microstrain (με), t is time of drying in days, and α is a model coefficient (with units of days) that is approximately the time to 50% of ultimate shrinkage. Drying shrinkage strains after 7, 28, and 180 days of drying are shown in Figure 19 and the hyperbolic model fitting parameters of shrinkage strain are shown in Table 12.

$$\epsilon_{sh} = \frac{L_{specimen} - L_{reference\ bar}}{GL}(10^6) \quad \text{(Eq. 5)}$$

$$\epsilon_{sh} = \frac{\epsilon_{ultimate} \cdot t}{\alpha + t} \quad \text{(Eq. 6)}$$

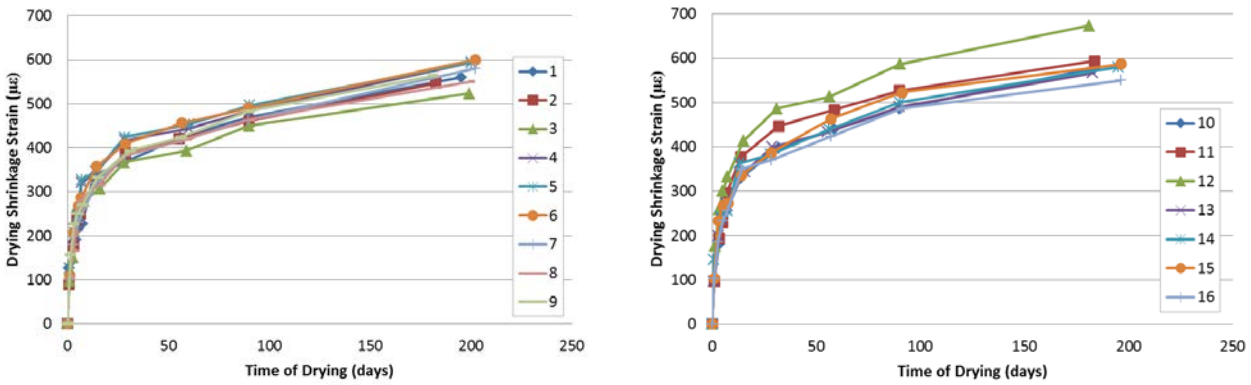

Figure 18. Drying shrinkage strains as a function of time for mixes 1-9 (left) and 10-16 (right).

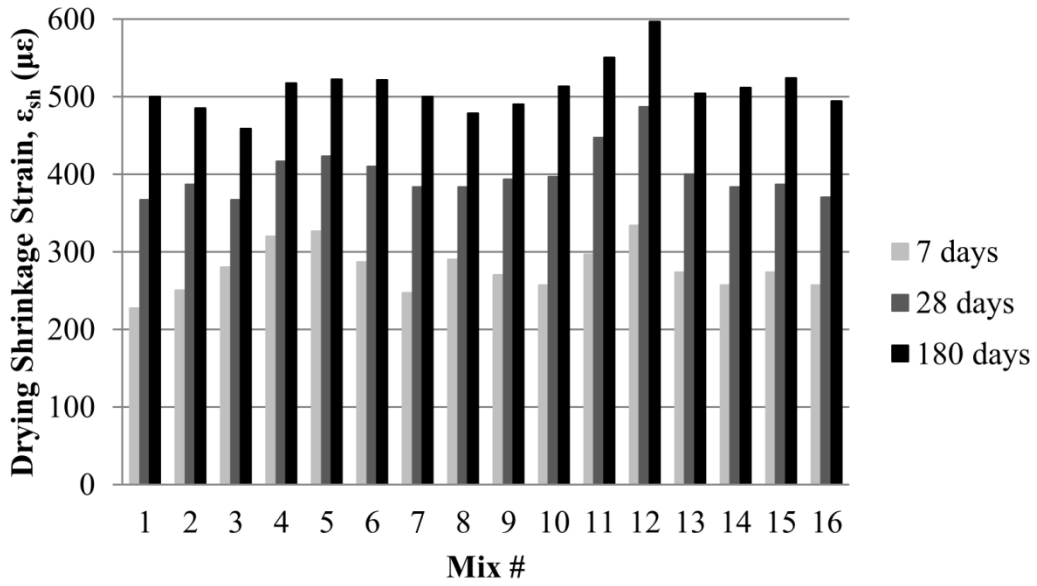

Figure 19. Drying shrinkage strains for RCC mixes.

From Figure 19, the 28-day shrinkage strains for most mixes were around 400 microstrain which is higher than most RCC shrinkage strains reported in the literature. The discrepancy between the shrinkage results presented here and those from the literature might be explained by the fact that the shrinkage results presented here are based on specimens that received no moist curing whereas all previous literature had some duration of moist curing (typically 28 days) before drying. In general, no effect of gradation on RCC shrinkage was seen with the exception that increasing aggregate fines content (mixes 10-12) appeared to result in increased shrinkage strains. The lack of any strong trends is not unexpected since all mixes were proportioned with the same cement content and relatively similar total water content. Compared to conventional concrete (PCC), shrinkage strains of these RCC mixes are lower because of the reduced paste content, i.e., water and cementitious materials.

Table 12. Hyperbolic Model Fit Parameters for Drying Shrinkage Strains

Mix #	R^2	$\epsilon_{ultimate}$ (microstrain)	α (days)
1	0.935	523.0	8.15
2	0.965	502.6	6.43
3	0.946	472.9	5.65
4	0.943	535.5	6.21
5	0.959	539.6	5.84
6	0.916	538.9	5.93
7	0.95	520.6	7.48
8	0.945	493.5	5.55
9	0.944	504.4	5.41
10	0.946	534.7	7.55
11	0.981	571.7	6.98
12	0.947	614.8	5.58
13	0.946	521.1	6.12
14	0.93	528.7	6.09
15	0.939	542.0	6.31
16	0.954	512.8	6.65

2.6 HARDENED VOID ANALYSIS

A procedure for determining hardened void content of concrete through a high-definition, flatbed scanner and use of image analysis (Song, 2014) was performed to determine approximate percentages of hardened voids in RCC. Four discs were cut from 100x200 mm (4x8 in) cylinders for mixes 1-5 to perform hardened void analysis. The cut section of each disc was then wet polished using successively finer grinding discs with the finest grinding disc being a #800 (25 µm) disc. The surface was then sprayed with phenolphthalein to provide good contrast. Once the phenolphthalein dried, an orange powder dye was applied to the surface and used to fill all the voids. The remaining

powder dye was then removed from the surface and the specimen was placed onto the flatbed scanner. The specimen was then scanned with a pixel resolution of approximately 5 µm (0.15 mil). The image analysis procedure is shown in Figure 20 below with the first step being obtaining the image. The following steps consist of distinguishing between aggregates and paste, overlaying the solid aggregates on top of the original image to remove the voids in the aggregates from the calculation, and thresholding the orange dye against the rest of the image to calculate the percent area of voids with respect to the area of the entire image. The void content of mixes 1 to 5 is: 2.40, 1.71, 2.35, 2.83, and 3.38% respectively. The average void content of these five RCC mixes is 2.53%, which is slightly higher than expected considering there is no air entrainment.

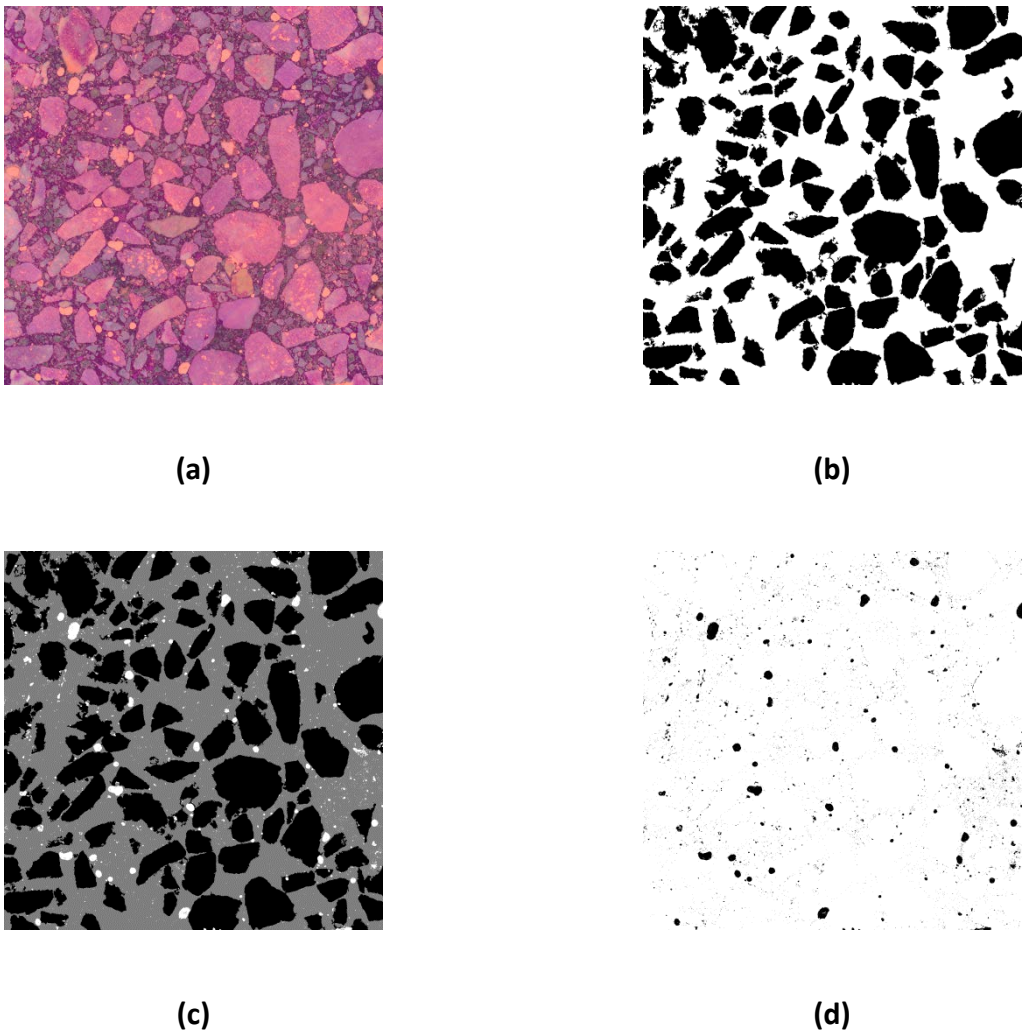

Figure 20. Image analysis of hardened concrete voids: scanned image (a), identifying aggregates and paste (b), overlaying aggregates onto original image (c), and final image of voids (d).

2.7 CONCLUSIONS

Sixteen RCC mixture designs were developed from the modified Proctor test that had a variety of gradations with the same aggregate sources. The gradations selected followed the maximum density line, were above or below it, and also included a significant amount of passing 75 micron (#200) sieve for several mixtures. The moisture-density relationship, workability, strength, fracture, and shrinkage properties were then quantified for these 16 RCC mixtures.

Modified Proctor compaction yielded a relatively narrow range of maximum dry densities (mostly between 2,330 and 2,400 kg/m^3 (145 and 150 lb/ft^3) and optimum moisture contents (mostly between 6.2 and 6.7%) for all gradations. However, wet density was shown to be a good indicator of moisture sensitivity. An RCC mix with a wet density vs. moisture content relationship that plateaus after the optimum moisture content has a lower sensitivity to moisture content fluctuations. The high aggregate fines content mixes produced Vebe times in the range recommended for RCC pavements (30 – 40 seconds) while all other gradations resulted in Vebe times less than 25 seconds. This suggests that it might be easier to achieve density for these higher fines mixes. However, construction issues such as roll down, edge slumping, or surface tearing might become an issue.

A methodology for fabricating 100x200 mm (4x8 in) cylinders was presented and validated with a side-by-side comparison of compressive strengths from 100x200 mm (4x8 in) and 150x300 mm (6x12 in) cylinders. A study on highly controlled aggregate gradation (sieved) versus blending aggregates (unsieved) in RCC mixes had a higher impact on compressive strength of 150x300 mm (6x12 in) cylinders than 100x200 mm (4x8 in) cylinders.

The aggregate gradations that followed the maximum density curve (0.45-power) did not yield the greatest modified Proctor densities or the greatest strength/fracture properties. The compressive strength—based on the laboratory compacted cylinders of all 16 mixes— typically satisfied specified strength values, e.g., 24 MPa (3.5 ksi) at 7 days and 31 MPa (4.5 ksi) at 28 days. In general, mixes with higher aggregate fines contents yielded lower strengths (compressive, split tensile, and flexural). However, this trend was not always statistically significant. The addition of aggregate fines effectively increased the powder content for RCC and potentially dispersed the coarse aggregates having some impact in reducing strength properties. Aggregate gradation had a larger impact on compressive strength of RCC than split tensile or flexural strength. Based on the strength properties, recommended gradation bands from the coarseness factor chart or Tarantula curve may not apply directly to RCC without further field investigation and adjustment.

Fracture properties of RCC were not significantly affected by aggregate fines content or small change in the nominal maximum aggregate size (NMAS). No significant effects of gradation were found on drying shrinkage strain because of the near constant paste content between mixes. Typical 28-day drying shrinkage strains of specimens with no moist curing prior to exposure to drying were around 400 microstrain. Drying shrinkage strains of RCC were found to be slightly less than those of conventional concrete; however, similar joint spacings to conventional concrete would be advisable to account for thermal and drying shrinkage contraction.

While it has been shown that strength properties from these 16 mixes were sufficient for current RCC specifications and fracture properties are similar or greater than those of PCC, this does not indicate that all of these gradations are optimal for field construction. Relatively low Vebe times of most gradations, along with those that exhibit moisture sensitivity, might suggest the potential for field constructability issues. Also, laboratory compaction methods are different from field compaction in terms of type of loading, breakdown, and compaction energy. Therefore, these results can only conclude that these RCC mixes with a variety of gradations have reasonable moisture-density relationships and sufficient mechanical properties to meet RCC specifications based on laboratory compacted specimens.

CHAPTER 3: MECHANICAL PROPERTIES OF ROLLER-COMPACTED CONCRETE PAVEMENTS FROM FIELD AND LABORATORY SAMPLES

This chapter presents a brief summary of RCC pavement construction specifications. Additionally, it compares the mechanical properties from laboratory compacted RCC and field cores using the same mix design and constituents. The mechanical properties investigated are densities, strength (compressive, split tensile, and flexural), fracture properties, and drying shrinkage. Modified Vebe time was also measured to determine the workability of the mixes.

3.1 REVIEW OF RCC PAVEMENT CONSTRUCTION SPECIFICATIONS

In order to compare lab and field data gathered in Illinois, a review of specifications relating to RCC pavement construction in the United States was conducted. The aim of this review was to determine typical RCC pavement construction methodologies, mix design parameters, and mechanical properties. Out of the 50 states, 15 states have a construction specification (supplemental specification or special provision) related to RCC. The Portland Cement Association (PCA) and American Concrete Pavement Association (ACPA) have published guide specifications relating to RCC (PCA, 2004; ACPA, 2014). The PCA's guide specification (PCA, 2004) has influenced many states' RCC specifications. The ACPA's guide specification (ACPA, 2014) was recently published at the time that many other states were publishing their RCC specifications. The following is a list of states that have published RCC specifications and their references:

- California (Caltrans, 2012)
- Georgia (GDOT, 2005)
- Illinois (IDOT, 2014)
- Indiana (Indiana LTAP Center, 2010)
- Kansas (City of Hutchinson, 2011)
- Kentucky (Kentucky Department of Highways, 2009)
- Minnesota (MnDOT, 2011)
- Missouri (Missouri Highways and Transportation Commission, 2013)
- North Carolina (NCDOT, 2014)
- Ohio (City of Columbus, 2010)
- Oklahoma (ODOT, 2000)

- South Carolina (SCDOT, 2001)
- Tennessee (TDOT, 2015)
- Texas (TxDOT, 2004)
- West Virginia (WVDOH, 2011)

3.1.1 Mixture Design

While most specifications have slightly different combined aggregate gradation requirements, none of them vary significantly from that recommended by the PCA (2004) guide specification. All specifications limit the nominal maximum aggregate size to 19.1 mm (3/4 in) with a minimum of 40% fine aggregate (when using the 4.75 mm (#4) sieve to differentiate between coarse and fine aggregate). The allowable percent passing the 0.074 mm (#200) sieve ranges between 0 and 12%.

Some specifications list minimum cement and/or cementitious contents as well as maximum supplementary cementitious material (SCM) replacement percentages (percent of cement content). Two states (Texas and Tennessee) require the cement content to be chosen by testing various cement contents and choosing the amount that achieves the specified compressive strength. As shown in Table 13, the minimum cement content ranges from 207.6 to 334.5 kg/m^3 (350 to 564 lb/yd^3), fly ash and ground granulated blast-furnace slag (GGBFS) maximum cement replacement percentages are no greater than 30%, and the maximum silica fume percentage is 10%. For two of the three specifications that have maximum limits on SCM's, the total SCM percentage is limited to 40%.

Table 13. Cementitious Material Requirements by State *(1 kg/m³ = 1.686 lb/yd³)*

State	Minimum Cement (kg/m^3)	Minimum Cementitious (kg/m^3)	Maximum Fly Ash (%)	Maximum Ground Granulated Slag (%)	Maximum Silica Fume (%)
California	-	252.0	-	-	-
Illinois	237.2	317.3	-	-	-
Kansas	237.2	-	-	-	-
Kentucky	-	-	20%* for class F, 30%* for class C	30%*	10%*
Minnesota	-	237.2	25%	30%	-
Missouri	-	237.2	25%*	30%*	8%*
Ohio	207.6	-	-	-	-
Oklahoma	334.5	-	-	-	-

*Maximum cement replacement with SCM's is 40%.

3.1.2 Strength Requirements

One of the main acceptance criteria for RCC pavements like conventional concrete pavements is compressive strength. Table 14 shows the compressive strength (and any other specified strength testing) requirements for each state, listed in order of increasing required compressive strength at 28 days. Compressive strength requirements (at 28 days) range from 20.7 to 34.5 MPa (3 to 5 ksi). Some states also specify compressive strength requirements at earlier ages (Illinois and South Carolina) while Ohio specifies split tensile and flexural strength requirements at 14 days age. For the majority of the states, 28-day compressive strength remains the only concrete strength-related acceptance criteria. According to the ACPA (2014) guide specification, minimum 28-day compressive strengths (based on cylinders cast according to ASTM C1435) of 27.6 and 31.0 MPa (4 and 4.5 ksi) are recommended for areas without freeze-thaw conditions and areas with freeze-thaw conditions, respectively.

The PCA (2004) guide specification, along with some of the state RCC specifications, recommends the fabrication of compressive strength cylinders using one of the following standards: ASTM D1557, ASTM C1435, or ASTM C1176. ASTM D1557 (i.e. modified Proctor compaction) yields a 150 mm (6 in) diameter specimen with a height of approximately 114 mm (4.5 in) whereas ASTM C1435 and C1176

requires 150 mm (6 in) diameter specimens with heights of 300 mm (12 in). Thus, it would be expected that the compressive strength results using specimens fabricated by different standards, would provide different results. Also, most state specifications require cores to validate strength requirements. The core strengths must meet the same strength requirements as companion cylinders.

Table 14. Strength Requirements. ***(1.0 ksi = 6.89 MPa)***

Compressive Strength at 28 days	Other Strength Requirement	States
20.7 MPa	n/a	Oklahoma
24.1 MPa	n/a	Kansas, Kentucky, Minnesota, Missouri
	2.76 MPa split tensile strength and 3.45 MPa flexural strength at 14 days	Ohio
27.6 MPa	n/a	Georgia, Tennessee, West Virginia
30.3 MPa	n/a	Texas
31.0 MPa	n/a	North Carolina
	24.1 MPa compressive strength at 7 days	Illinois
34.5 MPa	n/a	California and Indiana
	13.8 MPa compressive strength at 3 days	South Carolina

3.1.3 Opening to Traffic

The requirements for allowing traffic on newly-constructed RCC varied dramatically from specification-to-specification with one state allowing unrestricted traffic 12 hours after final compaction and other states not allowing any traffic until after 7 days. Most specifications that had provisions for when the pavement should be opened to traffic specified compressive strengths in the range of 13.8 to 20.7 MPa (2 to 3 ksi). Most of these specifications stipulated that in addition to the compressive strength requirements, the pavement should be at least 1 to 4 days old before opening.

3.1.4 Compaction Requirements

The acceptance criteria related to compaction is the wet density achieved in the field (expressed as a percentage of the laboratory maximum wet density), which is typically measured with a nuclear density gauge. Of the 15 states with RCC specifications, four (Oklahoma, Missouri, Minnesota, and California) did not specify a density requirement. The remaining states specified that field density must reach 98% of the laboratory maximum wet density (typically determined from ASTM D1557). Of the states that specified the 98% of laboratory maximum wet density, five stated that the density value should be an average of 5 separate readings with no single reading being below 95%. One state (Illinois) specified that the density value should be an average of 3 separate readings. In addition to measurement of wet density with the nuclear density gauge, moisture content is also typically measured to ensure that it complies with the project mix design.

There was more agreement on the issue of when final compaction should be complete. The compaction time is the time from when the RCC is mixed to the completion of final compaction. If the maximum compaction time is exceeded, the resulting joints are considered cold joints rather than fresh joints. Of the 12 states that specified a maximum compaction time: 10 specified 60 minutes, one specified 45 minutes, and one specified 90 minutes. Also, five states require a test strip prior to commencement of paving in order to verify that the contractor can achieve the specified density and strength(s). The minimum lift thickness was 100 mm (4 in), while the maximum lift thickness varied between 200 mm (8 in) and 254 mm (10 in), depending on whether the specification calls for a high density paver or not.

3.2 BACKGROUND

The recent resurgence of using RCC for pavements has been well documented (Piggott, 1987; Nanni and Johari, 1989; Nanni et al. 1996; Naik et al. 2001; Brotman et al. 2007; Kim, 2007; Plessis et al. 2012; Williams, 2014; Hossain and Ozyildirim, 2015; Wu and Mahdi, 2015) and is a result of its economics, equipment technology, early opening to traffic, structural capacity, and desire for more sustainable pavement choices. Although RCC pavement is becoming more of a recognized pavement option, the mix design process is different from conventional paving concrete and requires training on how to design and specify a quality RCC mix. Another challenge with RCC pavements is construction. Even though the construction process is similar to asphalt concrete, RCC is constructed in thicker lifts, to higher densities (i.e. 98% of modified Proctor maximum density), and must be compacted in a short time window that is controlled by the cement hydration reaction. All of these factors combined demand more training and knowledge by the engineers and contractors to achieve high quality and performing RCC pavement.

It is well known that RCC mechanical and durability properties are highly affected by density (Pittman, 1989; Shihata, 2000; Delatte and Storey, 2005; Harrington et al. 2010), which is the cause for construction specifications stating that RCC pavements must be compacted to at least 98% of the laboratory (i.e. modified Proctor) maximum density. Thus, if the RCC pavement does not achieve this density then mechanical properties of the in-situ pavement are not guaranteed to approach those of the laboratory specimens. The pavement design assumptions for elastic modulus, compressive strength, flexural strength, etc. will also be compromised. Researchers have shown that the density of

the RCC material decreases with depth (Nanni and Johari, 1989; Pittman, 1989; Nanni et al. 1996). Therefore, mechanical properties can be expected to vary as a function of depth due to varying compactive energy.

To address the issue of comparing field and laboratory properties of RCC pavements, a comparison study was undertaken. Four RCC pavement projects in Illinois were visited to view construction procedures and techniques, obtain cores, compact companion field specimens, and obtain raw materials (aggregate and cementitious materials) to replicate the mix design in the lab. The objective of this study was to determine a relationship between laboratory and field properties of RCC pavements.

3.3 SAMPLING AND TESTING PLAN

A total of four RCC pavement projects were visited in Illinois and are labeled sites A thru D (Table 15). Field cores (cylinders) were obtained following ASTM C42 (ASTM, 2013) to perform strength and fracture testing. The raw materials were obtained in order to replicate the mix design in the laboratory. Approximately 400 kg of each aggregate was retrieved along with approximately 200 kg of each cementitious material. Laboratory specimens were fabricated using the same mix designs as were used in the field.

Table 15. Description of Site Visits *(1 in =2.54 cm)*

Site Label	New Construction?	Thickness (cm)	Pavement Cores and Raw Materials Obtained?
Site A	Yes	17.8	Cores were tested by consultant of owner. No raw materials were obtained; companion cylinders cast
Site B	Yes	17.8	Yes
Site C	No. Pavement was 7 years old at time	12.7	Yes*
Site D	Yes	22.9	Yes

*Aggregate obtained from the same source as used during initial construction.

3.4 RCC MIX DESIGNS AND FRESH PROPERTIES

The mix designs (SSD aggregate weights) are shown in Table 16 along with maximum dry density (MDD), optimum moisture content (OMC) and modified Vebe time. The moisture-density properties (MDD and OMC) were obtained from the modified Proctor testing (ASTM 1557, 2012) and are the contractor's reported values. Of the four mix designs, two had binary cementitious blends (i.e. cement and fly ash) and one had a ternary blend of cement, fly ash, and slag. One mix design only contained straight cement. The optimum moisture contents varied between 5.8% and 6.5% while maximum dry densities varied from 2,317 to 2,355 kg/m^3 (145 to 147 lb/ft^3). The Vebe time is a measure of the workability/compactibility of an RCC mix. Modified Vebe times (ASTM 1170, 2008) ranged from 9.6 to 20.4 seconds which are similar Vebe times for most mix designs presented in this report (Chapters 2, 3, and 4 and Appendices F, J, and K) and below the time recommended by ACI (1995). The combined aggregate gradations, determined according to ASTM C136 (ASTM, 1996) are shown in Figure 21 and are quite similar among the four sites. All gradations have relatively low aggregate fines contents, i.e., less than 2.5% passing the 0.074 mm (#200) sieve. All four gradations are composed of three aggregates: coarse, intermediate, and fine. The three aggregates for site B are shown in Figure 22 and the aggregates for sites C and D, which used the same aggregates, are shown in Figure 23.

Table 16. Mix Designs (SSD) and Fresh Properties. ***(1 kg/m^3 = 1.686 lb/yd^3)***

Constituent (kg/m^3)	Site A	Site B	Site C	Site D
Coarse Aggregate	362.9	396.7	601.9	302.4
Intermediate Aggregate	808.9	591.2	667.1	817.2
Fine Aggregate	884.2	1091.7	839.1	902.5
Type I Cement	237.2	326.2	177.9	237.2
Fly Ash - Class C	74.1	-	59.3	100.8
Slag - Grade 100	-	-	59.3	-
Water	103.2	103.4	89.1	96.1
Maximum Dry Density (kg/m^3)	2318	2355	2355	2317
Optimum Moisture Content (%)	5.8	6.5	5.9	6.0
Modified Vebe Time (sec)	-	20.4	9.6	12.2

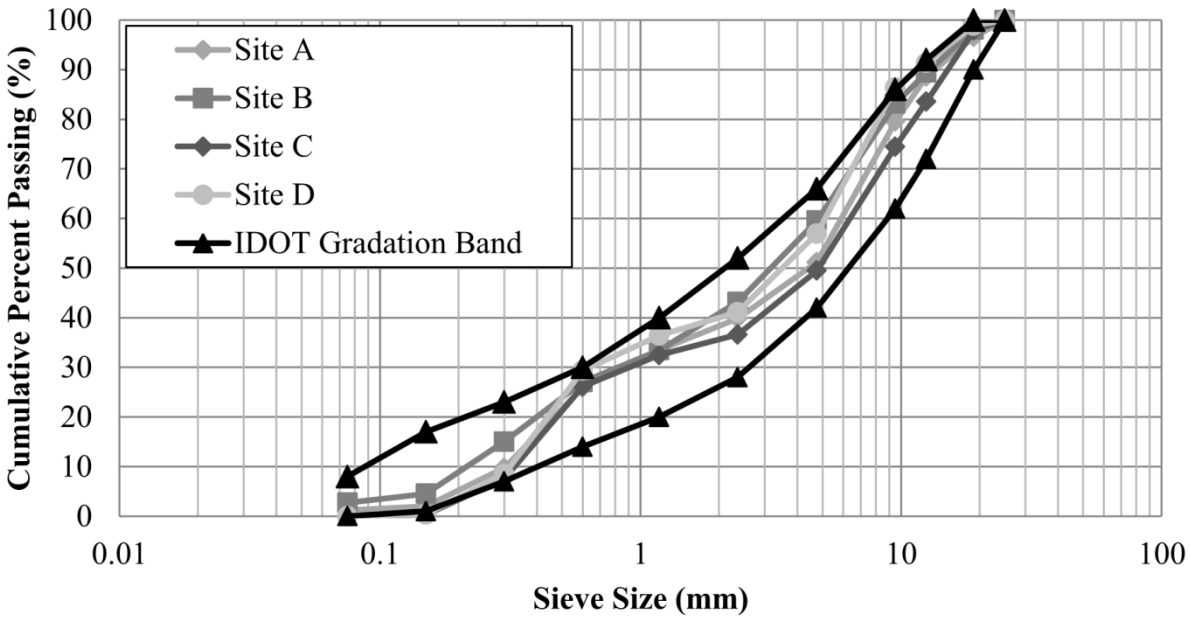

Figure 21. Combined aggregate gradations *(1 in = 25.4 mm)*.

Figure 22. Aggregate from site B - coarse (left), intermediate (center), and fine (right).

Figure 23. Aggregate from sites C and D - coarse (left), intermediate (center), and fine (right).

3.5 SPECIMEN PREPARATION AND DENSITIES

Laboratory specimens for sites B, C, and D were prepared by replicating the mix design in the lab. Laboratory specimens for site A were prepared on site and transported to the University of Illinois at Urbana-Champaign for testing. Laboratory specimens included cylinders (100x200 and 150x300 mm or 4x8 in and 6x12 in), flexural strength (MOR) beams (100x100x400 mm or 4x4x16 in), and shrinkage prisms (75x75x286 mm or 3x3x11.25 in). Compaction procedures for these specimen geometries can be found in Chapter 2. All RCC was mixed in accordance with ASTM C192 (ASTM, 2013). Cylindrical and flexural strength specimens were demolded after 24 hours and placed in a moist-curing room (23 degrees Celsius and 100% relative humidity) until the time of testing. Core specimens were also placed into the moist-curing room, after extraction from the pavement, until time of testing. The shrinkage prisms were introduced to the drying environment (23 degrees Celsius and 50% relative humidity) 24 hours after casting.

Density of the laboratory specimens was measured by weighing upon demolding and measuring specimen dimensions. Since the moisture content was known, the dry density (ρ_d) of each specimen was calculated according to Equation 7 where ρ_d is in units of kg/m^3, M is the mass of the specimen (kg), V is the volume of the specimen (m^3), and MC is the moisture content of the mix (decimal). The dry densities of the field cores were determined according to ASTM C642 (ASTM, 2013), and then the cores were tested for strength or fracture properties. The cores for fracture properties were cut into two or three discs (depending upon core length) corresponding to different depths of the RCC pavement. The densities for the laboratory specimens and field cores are shown in Table 17. It can be

seen that the laboratory specimens met the typical specification of 98% of modified Proctor density. With the exception of site C, which was only 12.7 cm (5 in) thick thereby making compaction easier, none of the field cores extracted met the specified 98% density. Two cores from sites B and D were taken directly over the center of a cold joint (Figure 24) and had resulting densities of 80.0% and 81.2% relative to their respective modified Proctor densities.

$$\rho_d = \frac{M}{V} \Big/ (1 + MC) \qquad \text{(Eq. 7)}$$

Since the fracture specimens (from field cores) were prepared in such a way that each one represented a different depth of the pavement, a relationship between density and depth was developed as shown in Figure 25 with each value being an average of two density measurements. From Figure 25, site C met the 98% density specification at both depths and is likely a result of the thinner RCC structure (12.7 cm or 5 in). While site D met the 98% density value near the surface, the bottom of the pavement showed a significantly lower density at 92.6% of the modified Proctor density. Site B did not meet the density specification at any depth. The decrease in density with depth has previously been shown for RCC pavements (Nanni and Johari, 1989; Pittman, 1989; Nanni et al. 1996). Nanni and Johari (1989) performed strength testing and elastic modulus testing on specimens from the top and bottom half of an RCC pavement and found approximately a 30% reduction in strength and 15% reduction in modulus from top to bottom. Figure 25 emphasizes the need for the use of the nuclear density gauge in direct transmission mode, where the density measurement is being taken at a particular depth—as opposed to backscatter mode, where the density measurement is more affected by the surface density and surface properties.

Table 17. Laboratory and Field Core Specimen Densities, kg/m^3 (Percent Compaction Relative to MDD, %) *(1 lb/ft^3 = 16.02 kg/m^3)*.

		Strength Testing Cylinders	Fracture Testing Cylinders	MOR Beams	Shrinkage Prisms
Site A	Lab	2329.6 (100.5)	2324.8 (100.3)	-	-
	Field	N/A			
Site B	Lab	2408.1 (102.2)	2387.2 (101.4)	2403.3 (102.0)	2371.2 (100.7)
	Field	2278.4 (96.7)	2243.1 (95.2)	-	-
Site C	Lab*	2350.0 (99.8)	2316.0 (98.3)	2305.8 (97.9)	2333.5 (99.1)
	Field	2363.0 (100.3)	2391.5 (101.5)	-	-
Site D	Lab	2340.7 (101.0)	2306.5 (99.6)	2337.6 (100.9)	2365.2 (102.1)
	Field	2250.3 (97.1)	2230.0 (96.2)	-	-

*Aggregate and cementitious materials were obtained from the original source however it was about 7 years after the pavement was constructed. It is likely that the aggregate has slightly different properties (i.e. gradation) from when the pavement was originally placed.

Figure 24. Core from cold joint.

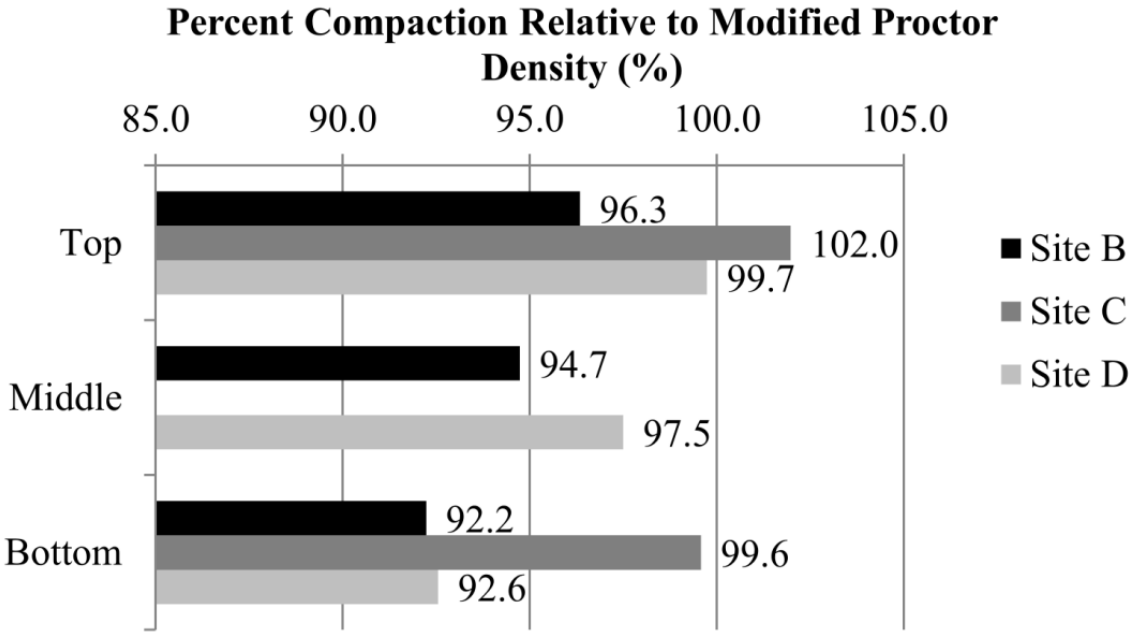

Figure 25. Core specimen density as a function of RCC pavement depth.

3.6 STRENGTH TESTING

Strength testing was performed on field cores as well as laboratory compacted specimens. Compressive and split tensile strength testing were performed on both sets of specimens while flexural strength was only determined from laboratory specimens because of difficulty in extracting sawed beams from a pavement. Compressive, split tensile, and flexural strength were determined according to ASTM C39 (ASTM, 2012), ASTM C496 (ASTM, 2011), and ASTM C78 (ASTM, 2010). Compressive and split tensile strength of laboratory specimens were measured at 1, 7, 28, and 90 days of moist-curing for sites B, C, and D. Site A had compressive strength tested at 7, 14, and 28 days while split tensile strength was only tested at 14 and 28 days. Flexural strength for sites B, C, and D was tested at 28 days. Elastic modulus of laboratory compacted 100x200 mm (4x8 in) cylinders was also tested at 28 days according to ASTM C469 (ASTM, 2010).

Figure 26 and Figure 27 show the laboratory strength gain curves for compressive and split tensile strength, respectively. As expected, the 1-day strengths of the mixes with supplementary cementitious materials (i.e. fly ash and slag) were lower than that of the straight-cement mix. Similar to results from Appendix J, the lowest 1-day compressive strength was 15.4 MPa (2.3 ksi) while the highest was 32.8 MPa (4.8 ksi). Despite this wide range of early-age strength, all four mixes had compressive strengths greater than 31 MPa (4.5 ksi) (the typically specified 28-day strength) at 7 days. Similar trends can be seen in the split tensile strengths, which had a range of 28-day strengths between 4.2 and 5.4 MPa (0.6 and 0.8 ksi). Flexural strengths at 28 days were 7.71, 6.38, and 6.70 MPa (1.12, 0.96 and 0.97 ksi) for sites B, C, and D, respectively. The relationship between split tensile strength and flexural strength (i.e., split tensile strength under predicted flexural strength for all three mixes) agrees with the literature on conventional concrete pavements (Brand et al. 2014). Elastic modulus testing at 28 days produced values of 40.5, 39.5, and 37.9 GPa (5875, 5730 and 5500 ksi) for sites B, C, and D, respectively.

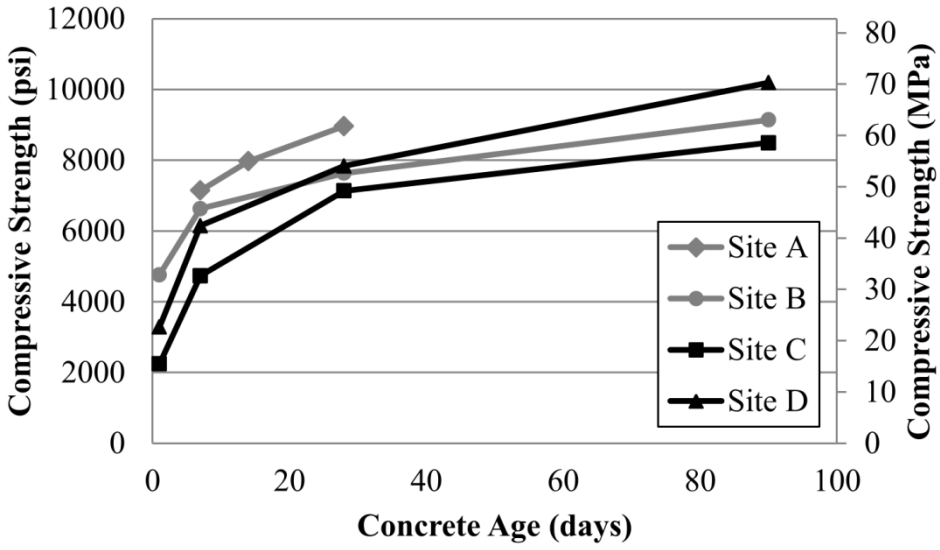

Figure 26. RCC compressive strength of laboratory compacted cylinders (100x200mm or 4x8 in).

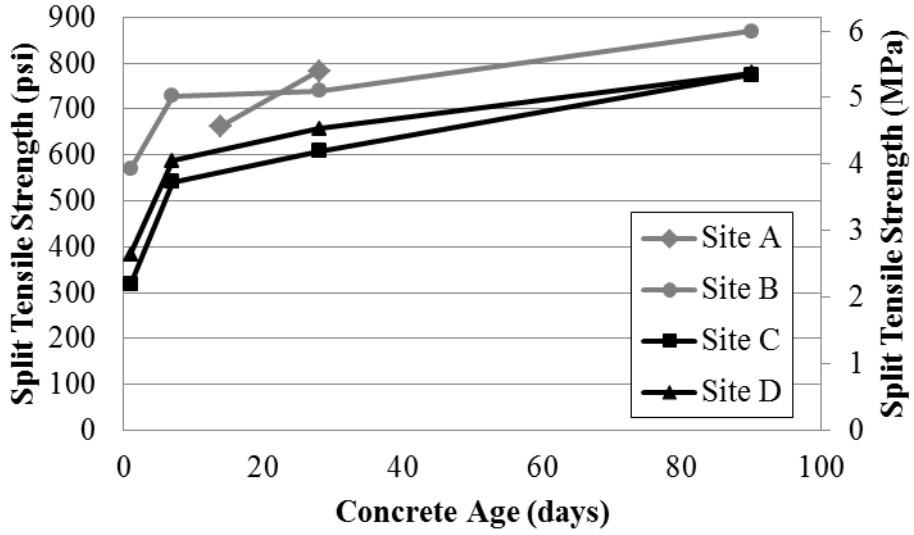

Figure 27. RCC split tensile strength of laboratory compacted cylinders (100x200mm or 4x8 in).

In addition to strength testing of laboratory specimens, the field cores were also tested for compressive and split tensile strength. In order to ensure compatibility, laboratory specimens were cored and/or cut to match the size of the field cores, i.e., 75x150 mm (3x6 in) cylinders were cored from 100x200 mm (4x8 in) laboratory cylinders in order to match 75x150 (3x6 in) mm field cores. Three different cylinder sizes were tested: 100x100 mm (4x4 in) (for site C which was only 12.7 cm (1/2 in) thick), 75x150 mm (3x6 in), and 100x200 mm (4x8 in). Table 18 and Table 19 compare

compressive and split tensile strengths, respectively, between lab and field core specimens from each site. The compressive strengths of lab and field core specimens are noticeably different. A t-test (95% confidence) was performed to determine if the compressive strengths are statistically different. All compressive strength pairs of lab and field core specimens (of the same size) were found to be statistically different. One reason for the statistical difference in compressive strength for site C is because of the large difference in age between lab and field core specimens. The main reasons for the statistical difference in compressive strength of the other field core and lab specimens is because of the lower density of the field cores and higher material variability, i.e., COV. Previous studies have shown that RCC strength properties are extremely sensitive, more so than conventional concrete, to density (Shihata, 2000).

When measured on 75x150 mm (3x6 in) cylinders, the field cores from sites B and D meet the specified 31 MPa (4.5 ksi) compressive strength at 28 days. However, the compressive strength from 75x150mm (3x6 in) RCC cylinders has been shown to be higher than the compressive strength determined from 100x200 mm (4x8 in) cylinders. This suggests that sites B and D might not have met the specified 31 MPa (4.5 ksi) 28-day compressive strength for freeze-thaw climates based on the standard cylinder size. Unlike compressive strength, there was no statistical difference in split tensile strength amongst the lab and field core specimens for sites B and D with site C being 7 years old.

Table 18. 28-Day Compressive Strength of Lab and Field Core RCC Mixes, MPa (COV, %); *(1 in = 25.4 mm; 1 ksi = 6.89 MPa)*

		Specimen Size		
Location		75x150 mm	100x100 mm	100x200 mm
Site A	Lab[a]			49.2 (3.5)
	Field Core[a]			39.3 (14.2)
Site B	Lab	57.0 (4.3)		52.6 (2.8)
	Field Core	32.2 (27.2)		
Site C	Lab		54.3 (4.0)	49.2 (3.6)
	Field Core[b]		75.0 (3.1)	
Site D	Lab	61.9 (4.0)		54.0 (5.2)
	Field Core	34.1 (8.4)		30.5 (12.4)

[a]Age at testing was 7 days.

[b]Age at testing was 2333 days.

Table 19. 28-Day Split Tensile Strength* of Lab and Field Core RCC Mixes, MPa (COV, %); *(1 in = 25.4 mm; 1 ksi = 6.89 MPa)*

		Specimen Size		
Location		75x150 mm	100x100 mm	100x200 mm
Site B	Lab	5.41 (4.7)		5.10 (2.6)
	Field Core	4.02 (18.6)		
Site C	Lab		3.92 (10.5)	4.20 (4.7)
	Field Core**		5.04 (7.43)	
Site D	Lab	4.70 (10.5)		4.53 (5.1)
	Field Core	4.02 (5.0)		

*Site A is not included since cores were not tested for split tensile strength.

**Age at testing was 2333 days.

3.7 FRACTURE TESTING

Fracture testing was performed using the disk-shaped compact tension (DCT) geometry and testing procedure (Amirkhanian et al. 2015). Fracture testing provides an indication of a material's resistance to cracking and has been positively linked to the structural capacity of concrete slabs (Ioannides et al. 2006; Gaedicke et al. 2012; Brand et al. 2014). One main advantage of using the DCT geometry is that it is easily fabricated from a 150 mm (6 in) diameter core or 150x300 mm (6x12 in) cylinder. Another advantage of this geometry is that fracture properties as a function of depth can be quantified given an extracted field core. The results of fracture testing from lab and field specimens are shown in Table 20 (along with RCC and PCC fracture properties from the literature) with each value indicating an average of at least 5 replicates. The fracture properties reported include critical stress intensity factor (K_{IC}), elastic modulus (E), critical crack tip opening displacement ($CTOD_C$), initial fracture energy (G_f), and total fracture energy (G_F).

Table 20 shows there is not a consistent relationship between lab and field core specimens with respect to fracture properties. For sites B and C, the critical stress intensity factor and initial fracture energy were both statistically different between the lab and field core specimens. Site C had field core samples that were 7 years old—so the observed trend of field core specimens having greater fracture properties than lab compacted specimens at 28-days—is not a fair conclusion. For the two sites (B and D) for which the lab and field fracture properties were tested at the same age (28-days), both mixes had at least one fracture property that was statistically different, i.e., field fracture properties were less than the lab. Relative to other RCC fracture properties from the literature (Ferrebee et al. 2014), the lab specimens in Table 20 had similar fracture properties except for elastic modulus and initial fracture energy. Relative to a conventional concrete pavement mix, all RCC

fracture properties shown in Table 20 are similar or greater. Since fracture properties are a good indicator of flexural slab capacity for conventional concrete pavements (Brand et al. 2014), statistically lower fracture properties from field cores (relative to laboratory compacted specimens) will likely result in lower flexural slab capacities in the field than expected. RCC thickness design is based currently on its lab flexural strength and laboratory RCC fatigue curve (Rodden, 2013) so the variation in lab to field fracture properties should not impact the current design methods. However, it is expected that this discrepancy will have an effect on predicted performance.

Table 20. 28-Day Fracture Properties of Field Cores and Lab Specimens* (COV, %); *(1 MPa-$m^{1/2}$ = 0.910 ksi-$in^{1/2}$; 1 in = 25.4 mm; 1 lb/in = 175 N/m)*

		K_{IC}, MPa-$m^{1/2}$	E, GPa	CTODc, mm	G_f, N/m	G_F, N/m
Site A	Lab	1.58 (6.1)	41.8 (8.1)	0.0204 (12.2)	60.2 (7.5)	144.2 (4.0)
	Field	n/a				
Site B	Lab	**1.60 (6.3)**	**45.6 (3.3)**	0.0172 (12.5)	**56.0 (10.5)**	165.5 (19.1)
	Field	**1.04 (29.4)**	**30.3 (23.7)**	0.0202 (22.0)	**35.7 (36.3)**	138.3 (10.5)
Site C	Lab	**1.32 (4.8)**	**41.5 (8.2)**	0.0183 (13.4)	**42.1 (12.1)**	161.8 (15.0)
	Field**	**1.64 (7.1)**	**46.3 (5.4)**	0.0192 (9.4)	**58.2 (9.3)**	216.0 (21.9)
Site D	Lab	1.20 (8.0)	42.0 (5.3)	0.0149 (15.5)	34.5 (18.7)	**178.4 (16.8)**
	Field	1.15 (22.6)	36.0 (19.0)	0.0168 (13.4)	37.0 (27.5)	**135.0 (21.8)**
RCC (Ferrebee et al. 2014)		1.50 (11.6)	32.7 (8.2)	0.017 (25.1)	68.4 (15.9)	144.5 (5.5)
PCC Paving Mix (Roesler et al. 2007)		1.01	N/A	0.016	38.3	120

*Values in bold indicate statistical difference between field and lab fracture parameter for given site.

**Age at testing was 2333 days.

3.8 SHRINKAGE

For the three sites for which raw materials were obtained, shrinkage prisms were cast in the lab. The shrinkage prisms (75x75x286 mm, 3x3x11.25 in) were demolded 24 hours after casting and immediately introduced to the drying environment (23°C (73.4°F) and 50% relative humidity). While this is different from the ASTM standard governing shrinkage (ASTM C157, 2008), which suggests

moist-curing for 28 days before exposing to drying environment, it is more representative of field curing for pavements. Drying shrinkage strains (Figure 28) were measured for a period of 90 days. As expected, the magnitude of drying shrinkage strain was dependent upon the cementitious content (i.e. higher cementitious content led to higher shrinkage strain). Shrinkage strains at 28 days ranged from approximately 270-380 microstrain (με) which is less than a conventional concrete pavement (Zhang et al. 2013).

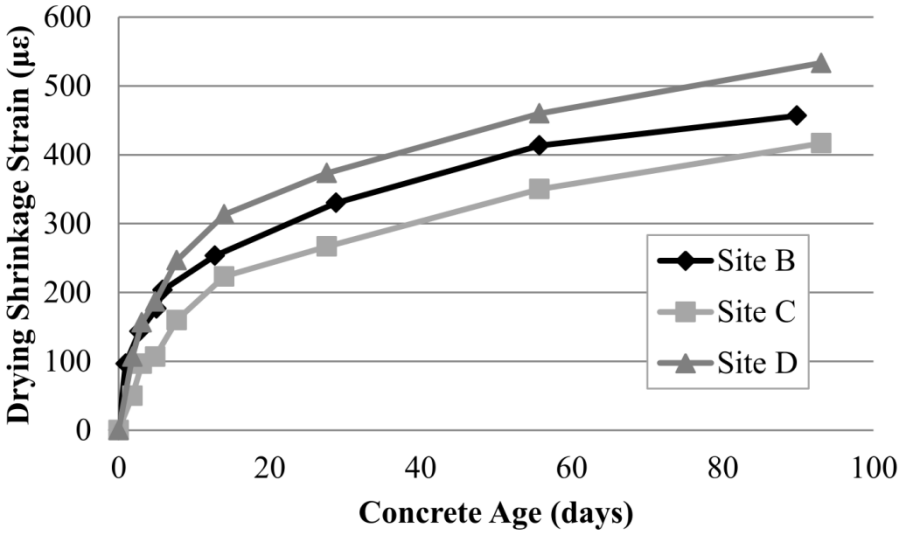

Figure 28. Free drying shrinkage strains for RCC mixes.

3.9 APPLICATION OF RESULTS TO RCC PAVEMENT CONSTRUCTION

While it is not typically specified that RCC pavements be constructed using high-density pavers or modified pavers with extra screeds or tamping bars, it is more difficult to attain proper density with depth using a conventional paver. If proper density is not achieved through the depth of the pavement, then lower quality material (i.e. lower density means weaker, less durable RCC) is left at the bottom of the structure where tensile stresses because of loading are usually the greatest (Huang, 2004). Likewise, lower RCC densities immediately behind the paver lead to more roll-down which increases surface roughness and can make it difficult to maintain grade, smoothness, and surface drainage profile.

It is common to specify nuclear density gauges to verify in-place density of RCC pavements. However, the exact method of operating the nuclear density gauge to check density is not always explicitly stated. The two main methods of operation (Figure 29) are backscatter (i.e., measuring density at the near surface) or direct transmission, which extends a nuclear source to a specific depth and then measures density between the pathway. In order to verify that proper density is being achieved throughout the RCC pavement thickness, it is recommended that the direct transmission mode be used with the probe being inserted, at a minimum, to the mid-depth of the RCC pavement. The direct transmission mode effectively measures the average density between the probe and the surface but

not beneath the probe. Researchers have demonstrated that the direct transmission mode yields higher precision than the backscatter mode (Davis et al. 1998). Therefore, in order to obtain an accurate density measurement for the full thickness of the pavement, the source probe should be hammered to the bottom of the RCC lift. The exposure time required to get an accurate density measurement will vary with the depth that the probe is hammered to, amongst other factors.

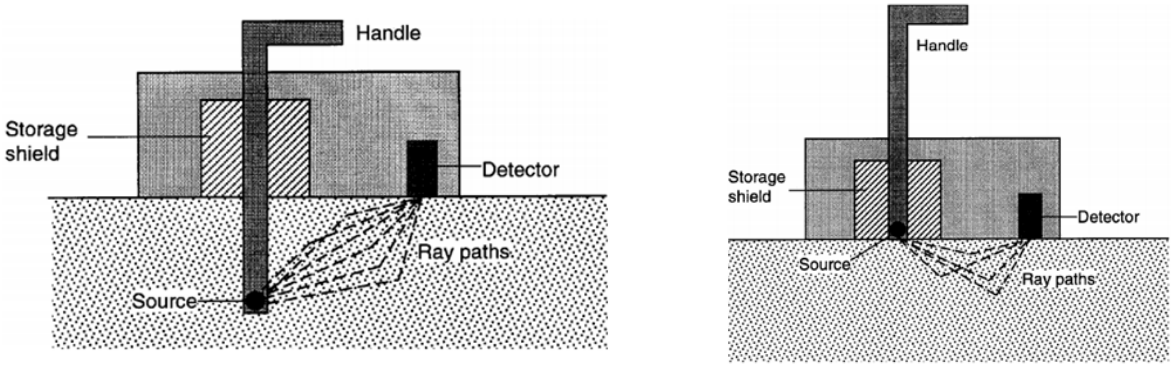

(a) **(b)**

Figure 29. Direct (a) and backscatter (b) transmission modes of nuclear density gauge (Davis et al. 1998).

Another means of improving density would be to tie the layer/ lift thicknesses to the stiffness of the base layer up to a maximum lift thickness. As shown by site C density measurements, the 98% density requirement was met at both the top and bottom of the 12.7 cm (5 in) thicknesses. Typical specifications limit lift thicknesses to 20 to 23 cm (8 to 9 in). However, RCC pavements in this thickness range (i.e. sites B and D) did not achieve proper density, especially at the bottom of the lift. Reducing the allowable lift thicknesses can introduce other problems such as difficulties associated with two-lift paving, reduced placement rates, and cold joints. The other means of making it easier to achieve proper density is ensuring a minimum base layer stiffness beneath the RCC to provide an adequate working platform to compact against. If the layer beneath the RCC pavement is not sufficiently stiff, it will be difficult to achieve the desired compaction throughout the depth of the RCC pavement.

3.10 CONCLUSIONS

Four RCC pavement sites in Illinois were visited with the objective of correlating lab and field properties. Field cores and lab/field fabricated specimens with the same mix proportions and constituents were tested in the lab. RCC pavement density taken from cores varied with depth with some sites significantly. Cores extracted from cold joints had significantly reduced densities (i.e. approximately 80% of modified Proctor density). None of the field cores, with the exception of site C, which was only 12.7 cm (5 in) thick, met the specified 98% of modified Proctor density. Nuclear density measurements of RCC pavements should be operated in the direct transmission mode rather than backscatter mode.

Lab compacted cylinders resulted in statistically different compressive strengths relative to field cores for the same sites. For all four project sites, lab cylinders far exceeded the 31 MPa (4.5 ksi) compressive strength specification at 28-days. However, field cores from one of the sites showed that the RCC pavement did not achieve the specified compressive strength. Split tensile strength did not show statistical differences between lab and field core specimens. Fracture testing was conducted using the disk-shaped compact tension geometry on field cores and lab specimens. Statistically lower fracture properties were observed for field cores relative to lab specimens—indicating that flexural slab capacities would be less under current lab compaction techniques—and could result in lower RCC pavement fatigue life than anticipated from the lab tested specimens. Drying shrinkage strains ranged from 270 to 380 microstrain with the magnitude of shrinkage strain being controlled by the total cementitious content of each mix.

Overall, lab and field mechanical properties of RCC did not always agree. The main factor contributing to the discrepancy between lab and field properties was linked to the field cores having inadequate densities. To improve compacted density of an RCC pavement in the field there are multiple strategies such as use of high-density pavers, stiffer foundation layer(s), reduced lift thicknesses, and improved RCC mix design to achieve density under lower compactive energy, e.g., less roller passes.

CHAPTER 4: INFLUENCE OF MIXTURE PROPORTIONS ON ROLLER COMPACTED CONCRETE PROPERTIES

An experimental design model was developed to characterize and predict the influence of aggregate gradation (percent sand content), cementitious materials content, and fly ash dosage on the fresh and hardened properties of RCC. Additionally, freeze-thaw testing was conducted on select mixtures to determine the effect of cementitious content on freeze-thaw resistance of RCC.

4.1 INTRODUCTION AND RCC EXPERIMENTAL DESIGN

As shown in previous chapters, it was shown that aggregate gradation, cementitious content, and fly ash dosage all affect RCC fresh and hardened properties. In order to predict the RCC properties magnitude and sensitivities to changes in these three independent variables, a statistically rigorous experimental design was developed to account for these. A circumscribed Box-Wilson model (Box and Wilson, 1951) was chosen as the appropriate model because of its ability to handle cross-interactions of three independent variables. The model contains 1 central point, 8 corner points (radially 1 factor away from central point), and 6 circular points (radially 1.682 factors away from central point) for a total of 15 different mixture designs. In order to assess the variability of the model, the central point had 6 replicates, for a total of 20 experimental design points. The model assumes variation at any point equidistant from the central point is equivalent (Box and Wilson, 1951).

A visual representation of the experimental design space can be found in Figure 30. The model was developed such that the range of each independent variable (Table 21) was reasonable, practical, and applicable to RCC pavement mix design. The 20 experimental design points and the values of the three independent variables for each design point are shown in Table 22 along with their factors (i.e. distance from central point). The objective of developing this model and the corresponding response-surfaces is to provide practicing engineers, researchers, and those responsible for RCC mixture design with a starting point for choosing mixture proportions (aggregate gradation in terms of % sand, cementitious content, and fly ash dosage). The measured responses include fresh properties (maximum dry density and optimum moisture content from modified Proctor testing, Vebe time and density), strength properties (compressive, split tensile, and flexural) at various ages, 28-day elastic modulus, and drying shrinkage. The subsequent contour plots that are developed from the experimentally-calibrated model are a comparison of the effect of two independent variables on the chosen response, i.e., RCC fresh or hardened properties. Therefore, three contour plots are made for each response in order to capture the three pairs of independent variables. Since each contour plot only involves two of the three independent variables, the effect of the third variable is fixed at the central point. For example, a contour plot comparing the effect of fly ash dosage and sand percentage would be valid for the central value of cementitious content (281.7 kg/m^3 or 475 lb/yd^3). All raw data used to generate the response equations and contour plots is shown in Appendix D.

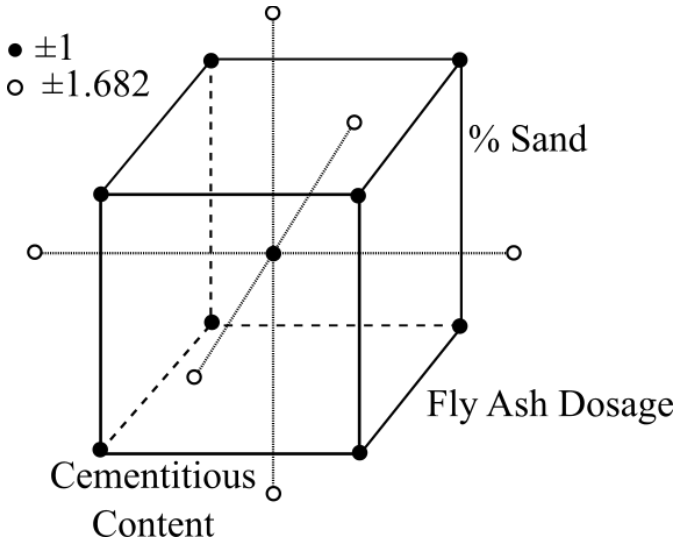

Figure 30. Schematic of box-wilson experimental design space.

Table 21. Independent Variables and Range for RCC Response Surface *(1 kg/m^3 = 1.686 lb/yd^3)*

Independent Variable	Range Tested	Points Tested
Percent Sand (%)	40 - 60	40.00, 44.05, 50.00, 55.95, 60.00
Cementitious Content (kg/m^3)	237.2 - 326.2	237.2, 255.2, 281.7, 308.1, 326.2
Fly Ash Dosage (weight % of cementitious materials)	0 - 25	0.00, 5.07, 12.50, 19.93, 25.00

Table 22. Experimental Design Points (non-dimensional distance from central point); *(1 kg/m³ = 1.686 lb/yd³)*

Design Point Label	Percent Sand, %	Total Cementitious Content, kg/m³	Fly Ash Dosage, weight % of cementitious materials
A	50.00 (0)	281.7 (0)	12.50 (0)
B	50.00 (0)	326.2 (+1.682)	12.50 (0)
C	44.05 (-1)	255.2 (-1)	19.93 (+1)
D	50.00 (0)	281.7 (0)	0.00 (-1.682)
E	50.00 (0)	281.7 (0)	12.50 (0)
F	60.00 (+1.682)	281.7 (0)	12.50 (0)
G	55.95 (+1)	255.2 (-1)	5.07 (-1)
H	44.05 (-1)	308.1 (+1)	5.07 (-1)
I	55.95 (+1)	308.1 (+1)	5.07 (-1)
K	55.95 (+1)	255.2 (-1)	19.93 (+1)
L	55.95 (+1)	308.1 (+1)	19.93 (+1)
M	50.00 (0)	281.7 (0)	12.50 (0)
N	50.00 (0)	281.7 (0)	12.50 (0)
O	50.00 (0)	237.2 (-1.682)	12.50 (0)
P	40.00 (-1.682)	281.7 (0)	12.50 (0)
Q	44.05 (-1)	308.1 (+1)	19.93 (+1)
R	50.00 (0)	281.7 (0)	25.00 (+1.682)
S	50.00 (0)	281.7 (0)	12.50 (0)
T	44.05 (-1)	255.2 (-1)	5.07 (-1)
U	50.00 (0)	281.7 (0)	12.50 (0)

For each response (e.g., 1-day compressive strength, Vebe time, etc.), a response surface model was produced that accounts for all three independent variables and their interactions. The general form of the response model is shown in Equation 8 where α is a constant, α_C (Equation 9) is the coded coefficient for cementitious content, α_F (Equation 10) is the coded coefficient for fly ash dosage, and α_S (Equation 11) is the coded coefficient for sand percentage. All coded coefficients (Equations 9, 10, and 11) are valid in the range of -1.68 to 1.68. Outside of this range, the experimental design model is not valid. All response equations do not include every term shown in Equation 8. Only those terms shown to be statistically significant at a 95% confidence level (p-value less than 0.05) were included in the response equation.

$$Response = \alpha + \alpha_C + \alpha_F + \alpha_S + \alpha_C^2 + \alpha_F^2 + \alpha_S^2 + \alpha_C \cdot \alpha_S + \alpha_C \cdot \alpha_F + \alpha_S \cdot \alpha_F \quad \text{(Eq. 8)}$$

$$\alpha_C = \frac{Cementitious\ Content\ (kg/m^3) - 281.7}{26.5} \quad \text{(Eq. 9)}$$

$$\alpha_F = \frac{Fly\ Ash\ Dosage\ (\%) - 12.5}{7.43} \quad \text{(Eq. 10)}$$

$$\alpha_S = \frac{Sand\ Percentage\ (\%) - 50}{5.95} \quad \text{(Eq. 11)}$$

4.2 RCC MIXTURE DESIGNS AND FRESH PROPERTIES

The aggregate gradations for each experimental design point are shown in Figure 31 and Table 23. In general, the aggregate gradations agree with the recommendations from ACPA (2014) with the exception of the low-fines content. Modified Proctor testing (ASTM D1557, 2012) was conducted to evaluate the moisture-density relationship of each design point. Based on the maximum dry density (MDD) and optimum moisture content (OMC) from the modified Proctor testing, the final mixture proportions for each experimental design point were developed (Table 24). Since the central experimental design point has a total of 6 replicates, variability of modified Proctor testing was assessed. The coefficient of variation for MDD was only 0.2% and OMC was 2.8%. This suggests that single-operator variability for modified Proctor-based mixture design can be quite low.

Table 23. Combined Aggregate Gradations (Cumulative % Passing) for Each Sand Percentage. ***(1 in = 25.4 mm)***

Sieve Size (mm)	40% Sand	44.05% Sand	50% Sand	55.95% Sand	60% Sand
19	100.0	100.0	100.0	100.0	100.0
12.7	72.9	74.7	77.4	80.1	81.9
9.5	67.7	69.9	73.1	76.3	78.5
4.76	40.0	44.1	50.0	55.9	60.0
2.38	28.0	32.1	38.2	44.3	48.5
1.19	26.1	30.0	35.8	41.5	45.4
0.595	17.9	20.6	24.5	28.5	31.1
0.3	2.1	2.4	2.9	3.3	3.6
0.15	0.1	0.1	0.2	0.2	0.2
0.075	0.0	0.0	0.0	0.0	0.0

Table 24. Mixture Proportions *(1 kg/m³ = 1.686 lb/yd³ or 0.062 lb/ft³)*

Design Point	OMC (%)	MDD (kg/m³)	Class C Fly Ash (kg/m³)	Type I/II Cement (kg/m³)	Oven-Dry Aggregate (kg/m³)	Water (kg/m³)
A	6.59	2391.6	35.2	246.5	2110.0	157.5
B	6.26	2364.1	40.8	285.4	2037.9	147.9
C	5.95	2394.2	50.9	204.4	2139.0	142.4
D	6.44	2382.7	0.0	281.7	2101.0	153.5
E	6.23	2387.2	35.2	246.5	2105.5	148.8
F	6.64	2324.4	35.2	246.5	2042.7	154.3
G	6.84	2301.5	12.9	242.3	2046.2	157.3
H	6.31	2411.5	15.6	292.5	2103.4	152.0
I	6.52	2319.9	15.6	292.5	2011.8	151.2
K	6.57	2358.7	50.9	204.4	2103.4	154.9
L	6.24	2358.8	61.4	246.7	2050.7	147.2
M	6.45	2387.3	35.2	246.5	2105.6	154.0
N	6.45	2387.3	35.2	246.5	2105.6	154.0
O	6.39	2390.5	29.7	207.6	2153.3	152.8
P	6.00	2407.0	35.2	246.5	2125.4	144.4
Q	6.05	2411.3	61.4	246.7	2103.2	145.9
R	6.11	2371.9	70.4	211.3	2090.3	144.9
S	6.45	2387.3	35.2	246.5	2105.6	154.0
T	6.16	2414.2	12.9	242.3	2159.0	148.6
U	6.45	2387.3	35.2	246.5	2105.6	154.0

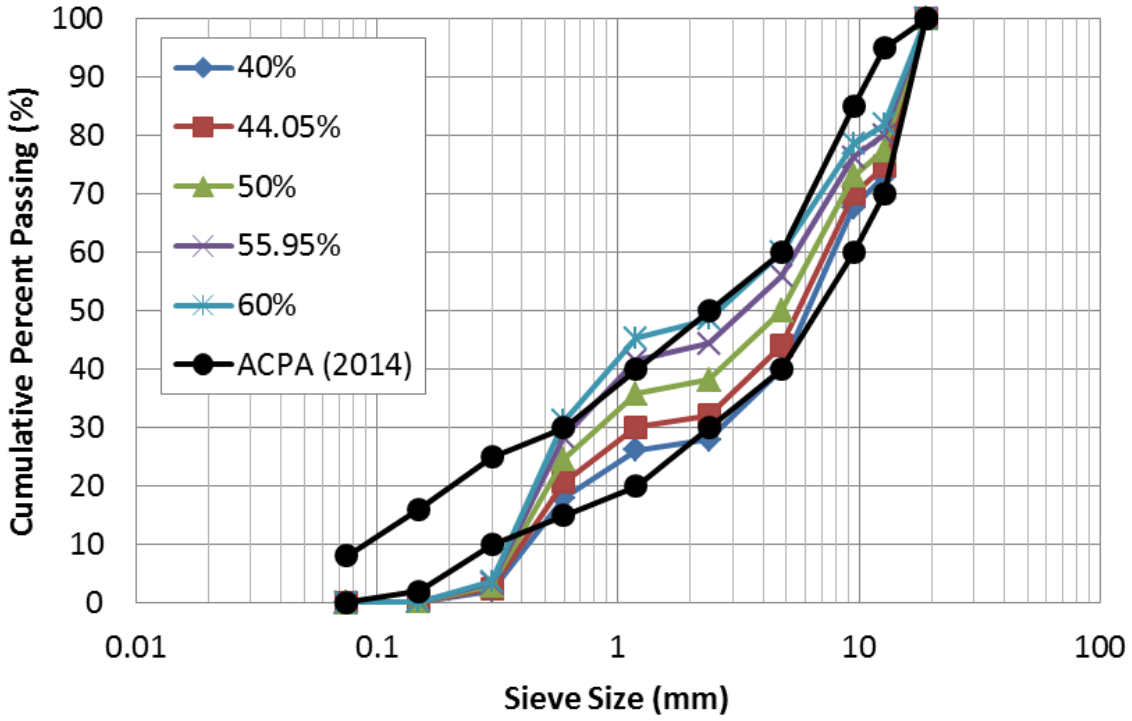

Figure 31. Combined aggregate gradations for RCC mixes (indicates % sand values); *(1 in = 25.4 mm)*.

Based on the MDD and OMC values from each design point, contour plots were generated to determine the effect of the three independent variables on the MDD and OMC for each RCC mixture as shown in Figure 32. The response equation for MDD has a standard error of 12.2 kg/m^3 (0.75 lb/ft^3) shown in Equation 12 and the response equation for OMC has a standard error of 0.1%, which is shown in Equation 13. The sand percentage has an inverse relation with the MDD, i.e., decreasing sand percentage increased the MDD of the RCC mix. Based on contour plots of OMC (Figure 33), increasing sand percentage also increases the OMC. The impact of cementitious content and fly ash dosage changes on MDD and OMC were much less significant relative to the effect of sand percentage.

$$MDD\ (kg/m^3) = 2382 - 31.6\alpha_S - 7.43\alpha_S^2 + 14.54\alpha_S\alpha_F \quad \text{(Eq. 12)}$$

$$OMC\ (\%) = 6.35 + 0.204\alpha_S - 0.115\alpha_F - 0.112\alpha_C\alpha_S \quad \text{(Eq. 13)}$$

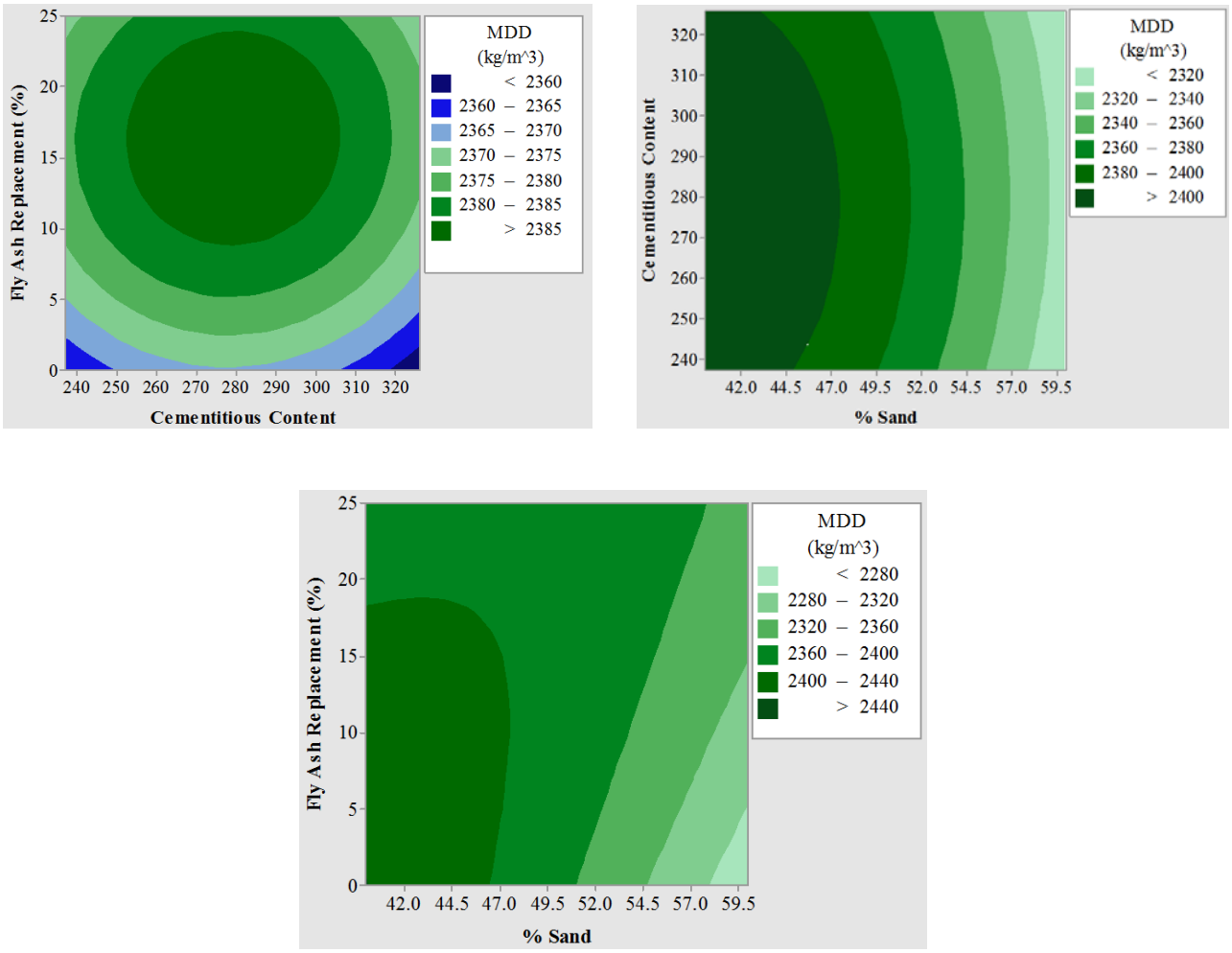

Figure 32. Contour plots for maximum dry density (MDD); *(1 kg/m³ = 0.062 lb/ft³)*.

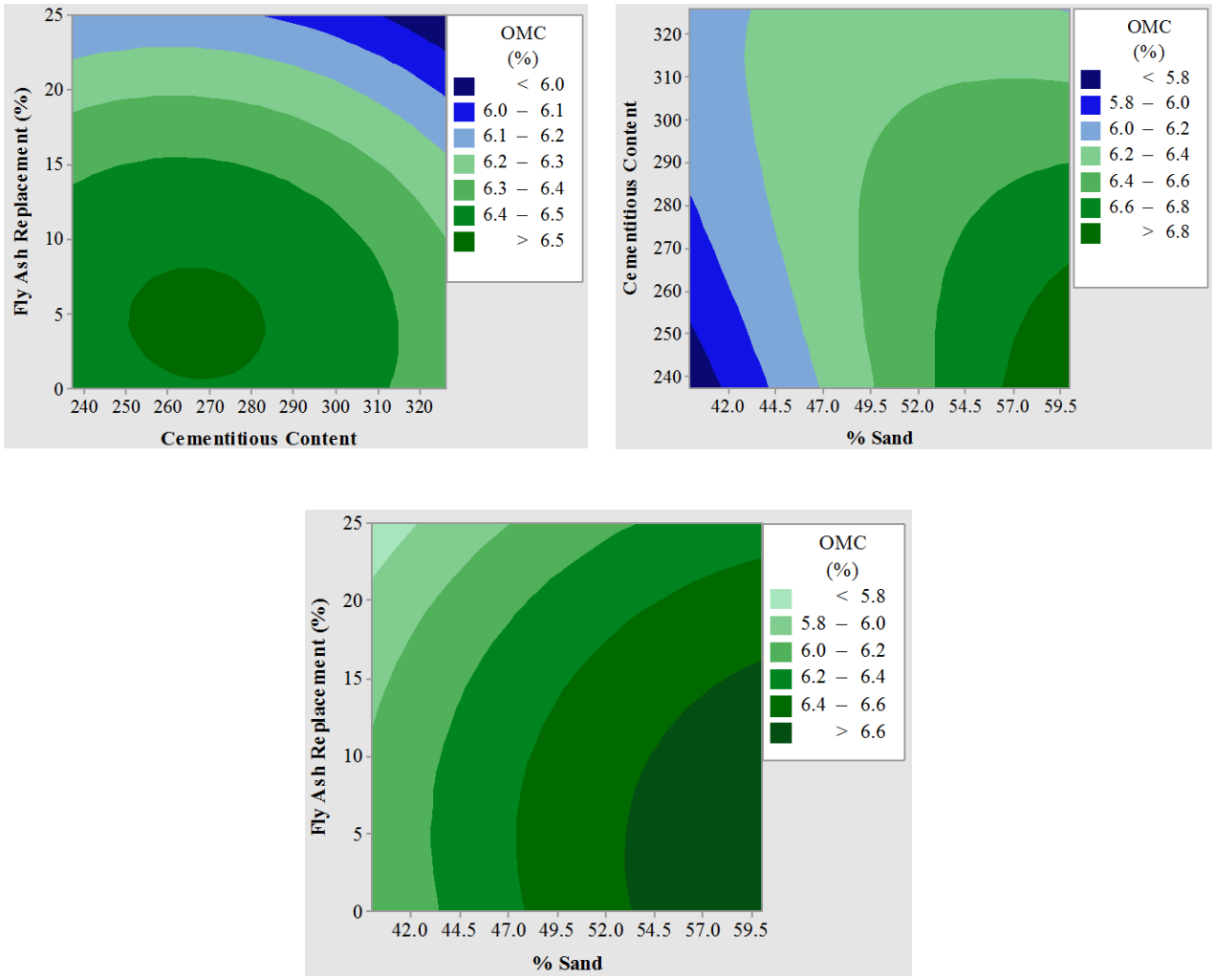

Figure 33. Contour plots for optimum moisture content (OMC); *(1 kg/m³ = 0.062 lb/ft³)*.

The modified Vebe time (ASTM C1170, 2008) was measured to quantify the compactability of each RCC mixture in the experimental design. Figure 34 shows there is not a consistent relationship between any of the independent variables and Vebe time. This is likely a result of both the user subjectivity of the modified Vebe test and the narrow range of measured Vebe times (approximately 10 to 22 seconds). The response equation for Vebe time had a standard error of 2.7 seconds but is not presented because there are no statistically significant parameters. Density measurements were also performed on cores from the Vebe specimens according to ASTM C542 (2013). Contour plots of density from the Vebe specimens are shown in Figure 35. Similar trends to modified Proctor MDD (Figure 32) can be seen, i.e., reducing the percentage of sand results in an increase in density while cementitious content and fly ash dosage have relatively insignificant effects on Vebe density. The response Equation 14 for Vebe density has a standard error of 28.9 kg/m^3 (1.8 lb/ft^3) and is shown next.

$$Vebe\ Density\ (kg/m^3) = 2268.8 - 24.31\alpha_s \qquad \text{(Eq. 14)}$$

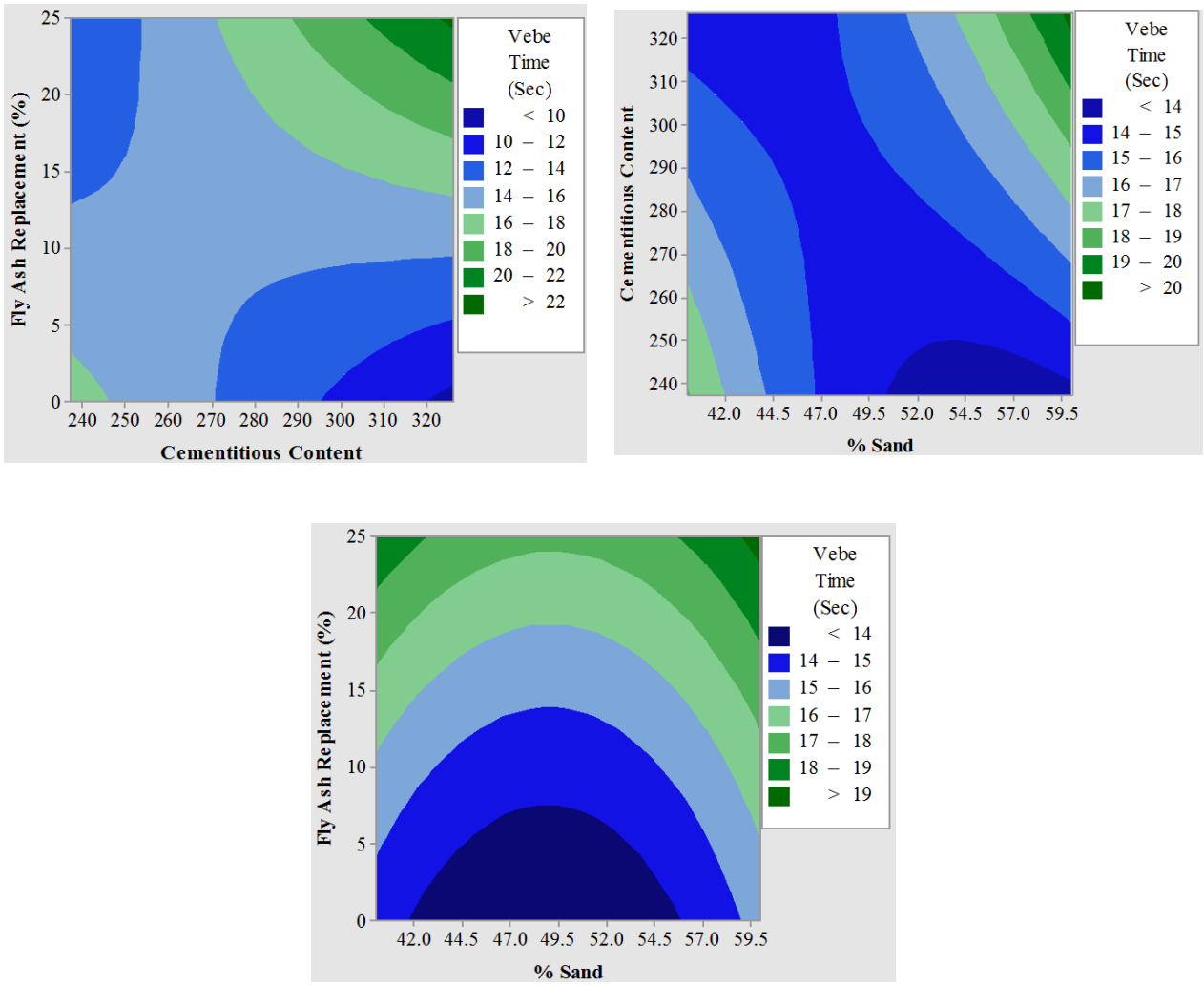

Figure 34. Contour plots for vebe time *(1 kg/m³ = 0.062 lb/ft³)*.

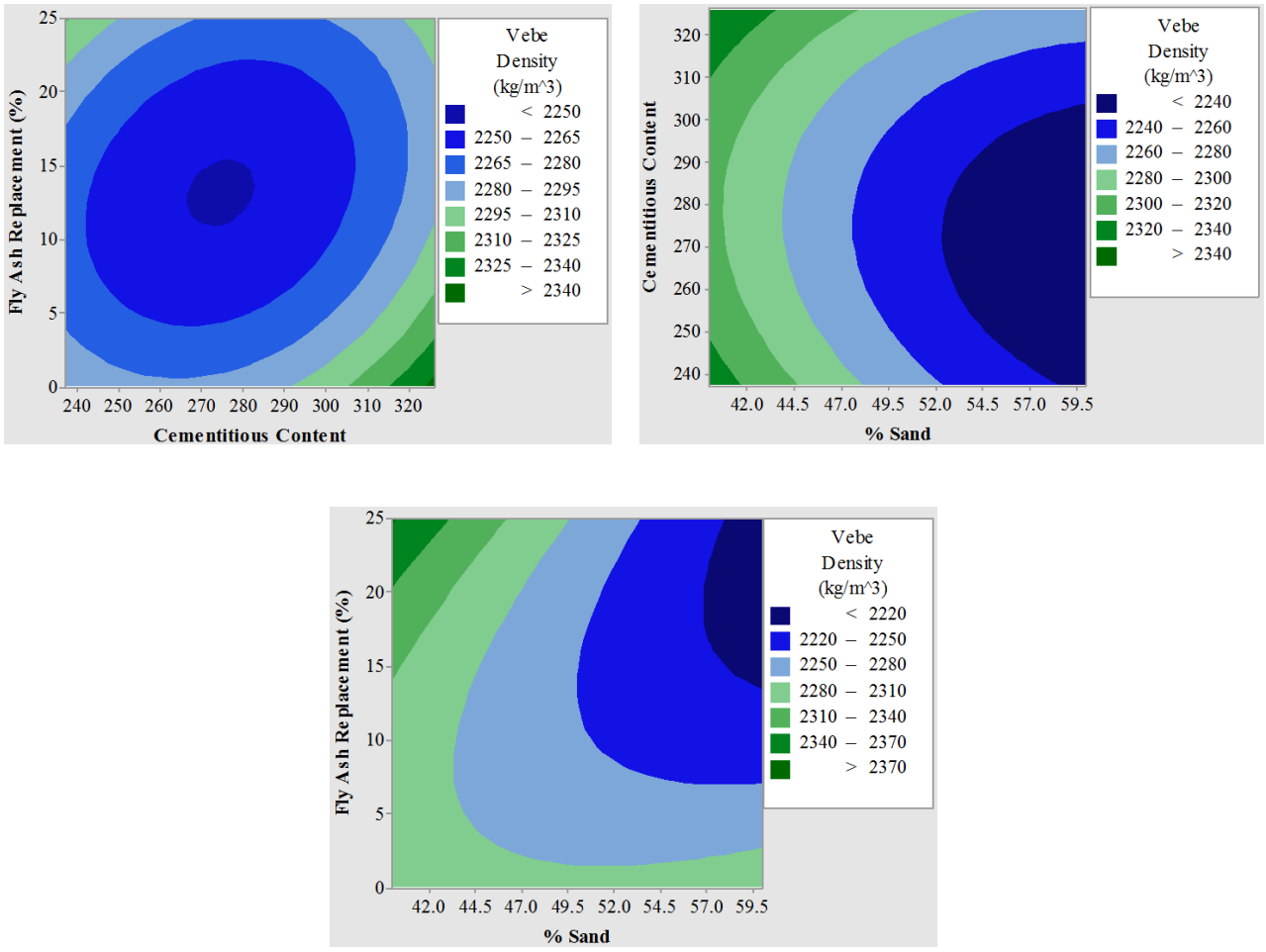

Figure 35. Contour plots for vebe density *(1 kg/m³ = 0.062 lb/ft³)*.

4.3 STRENGTH PROPERTIES

4.3.1 Compressive Strength

Compressive strength testing was carried out at a minimum of 3 different ages. The 3 ages that had compressive strength testing for all experimental design points were 1, 7, and 28 days. Compressive strength was tested according to ASTM C39 (2012) on triplicate 100x200 mm (4x8 in) cylinders for each testing age and experimental design point. Specimens were stored in a fog curing room at 100% relative humidity (RH) and 23°C (73.4°F) until the time of testing. Contour plots based on 1-day, 7-day, and 28-day compressive strengths are shown in Figure 36, Figure 37, and Figure 38 respectively. As expected, increasing cementitious content resulted in increased compressive strength for all testing ages. The influence of fly ash on compressive strength was more prominent at early ages (1-day) than later ages (7 and 28 days). Increasing fly ash dosages led to reductions in 1-day compressive

strength, as expected. The sand percentage had a significant effect on compressive strength at testing ages of 7 and 28 days with increasing sand percentage leading to reductions in compressive strength for all testing ages. This supports previous research that has shown strength of RCC to be positively correlated to coarse-to-fine aggregate ratio (Qasrawi et al. 2005; LaHucik and Roesler, 2015). At a testing age of 1 day, the cement content and fly ash content significantly impact compressive strength more than sand percentage. The response Equations 15, 16, and 17 for 1-, 7-, and 28-day are respectively shown for compressive strength. The standard errors for 1-, 7-, and 28-day compressive strength are 3.1 MPa (0.44 ksi), 5.4 MPa (0.78 ksi), and 3.3 MPa (0.48 ksi), respectively.

$$1 - Day\ Compressive\ Strength\ (MPa) = 22.9 + 4.03\alpha_C - 2.63\alpha_F \quad \text{(Eq. 15)}$$

$$7 - Day\ Compressive\ Strength\ (MPa) = 45.3 - 4.84\alpha_S + 5.76\alpha_C \quad \text{(Eq. 16)}$$

$$28 - Day\ Compressive\ Strength\ (MPa) = 57.9 - 3.21\alpha_S + 4.93\alpha_C \quad \text{(Eq. 17)}$$

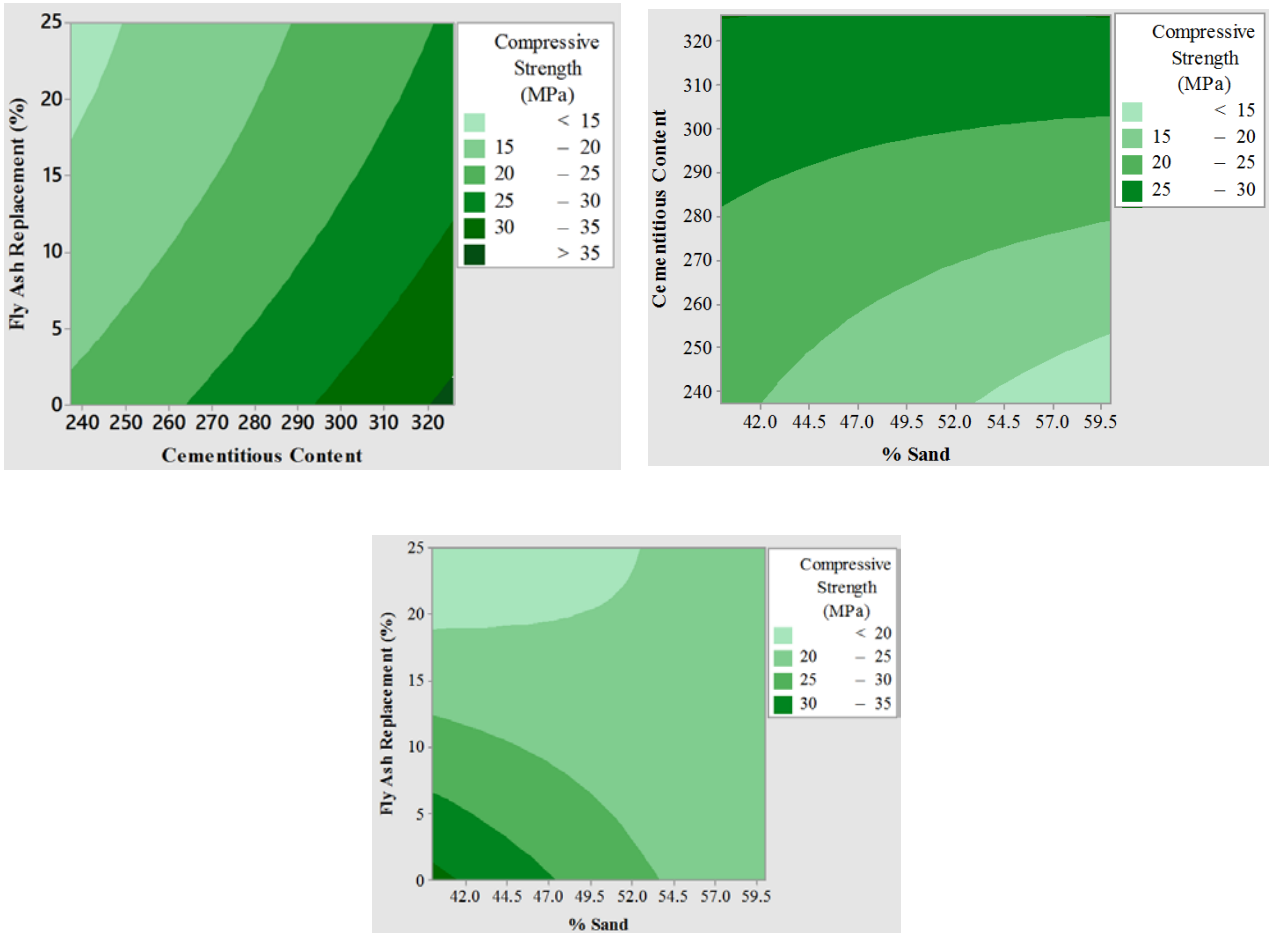

Figure 36. Contour plots for 1-day compressive strength *(1 ksi = 6.89 MPa; 1 kg/m³ = 1.686 lb/yd³)*.

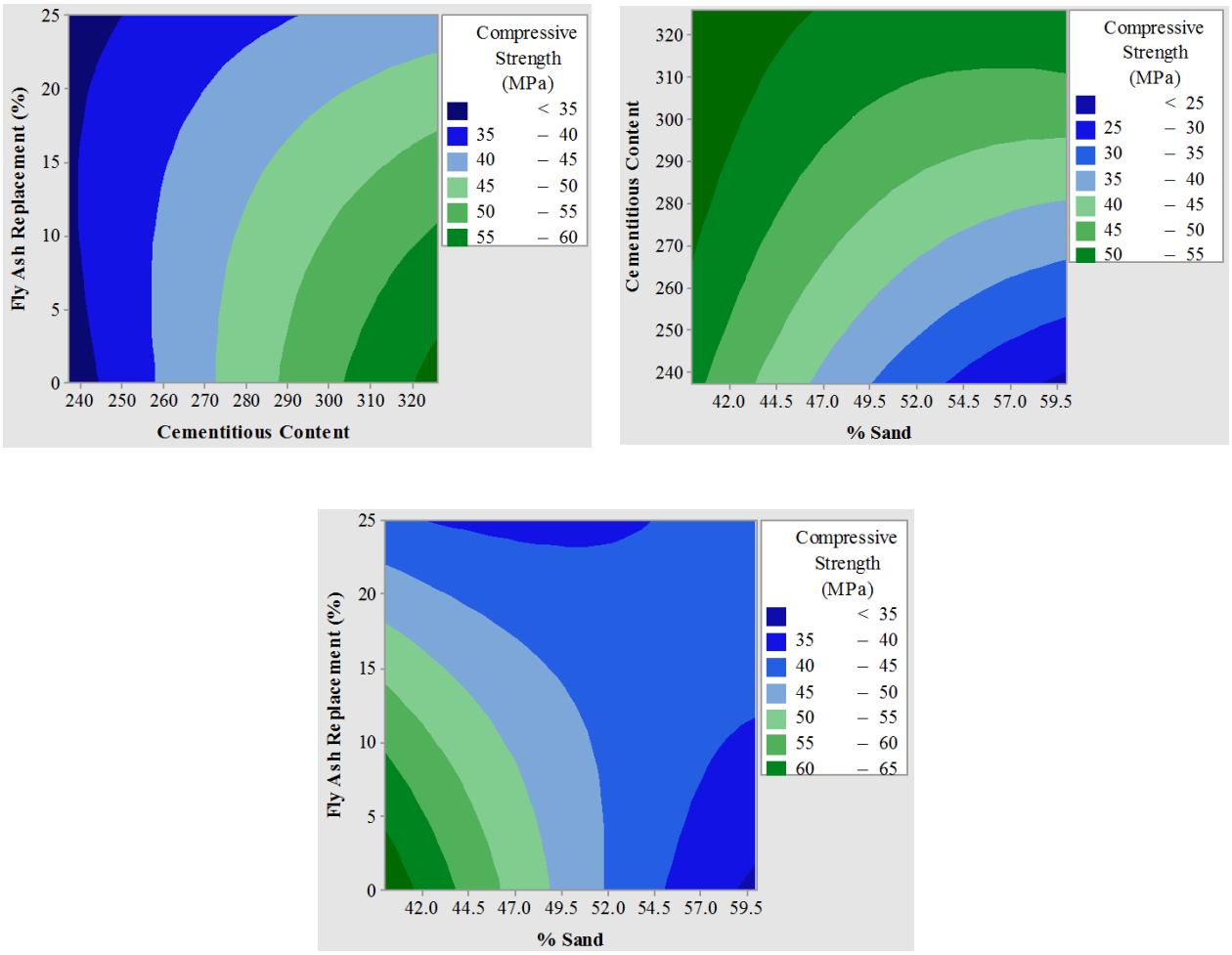

Figure 37. Contour plots for 7-day compressive strength *(1 ksi = 6.89 MPa; 1 kg/m^3 = 1.686 lb/yd^3)*.

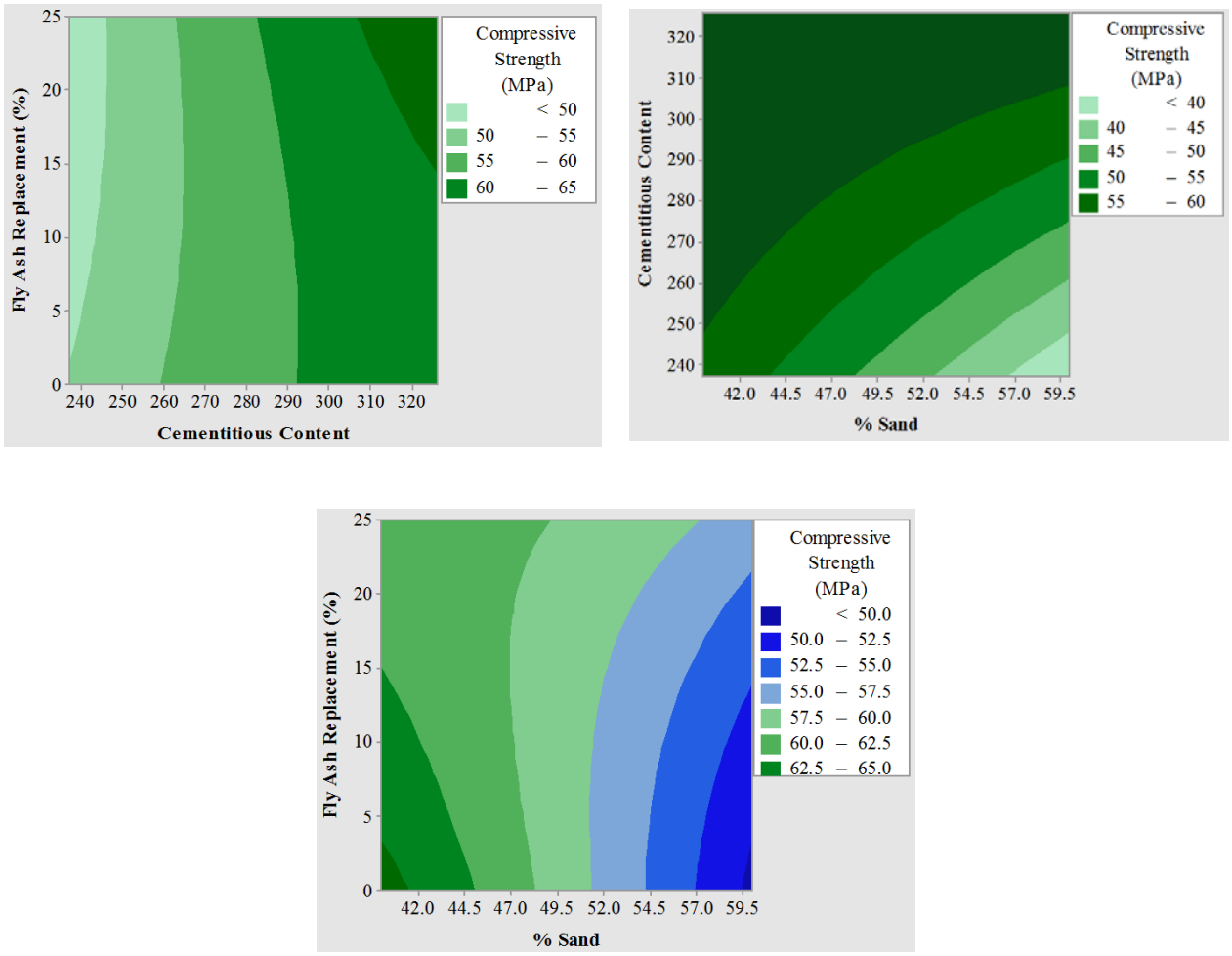

Figure 38. Contour plots for 28-day compressive strength *(1 ksi = 6.89 MPa; 1 kg/m^3 = 1.686 lb/yd^3)*.

4.3.2 Split Tensile Strength

Split tensile strength testing was carried out at a minimum of 3 different ages. The 3 ages that had split tensile strength testing for all experimental design points were 1, 7, and 28 days. Split tensile strength was tested according to ASTM C496 (2011) on triplicate 100x200 mm (4x8 in) cylinders for each testing age and design point. Specimens were stored in a fog curing room at 100% relative humidity (RH) and 23°C (73.4°F) until the time of testing. Contour plots of 1-day, 7-day, and 28-day split tensile strength are shown in Figure 39, Figure 40, and Figure 41 respectively. Trends in split tensile strength for 1 and 7-day strengths mirror those found for compressive strength. At early ages (i.e. 1-day) split tensile strength was largely dominated by cementitious content whereas sand percentage becomes a controlling factor at 7 days. Also, similar to trends in compressive strength, sand percentage and cementitious content both had a greater effect on split tensile strength than fly ash dosage. The response equations for 1 and 7-day split tensile strength are shown in Equations 18

and 19 respectively. There were no statistically significant parameters for 28-day split tensile strength and therefore no equation is shown. Standard errors for 1-, 7-, and 28-day split tensile strength are 0.49 MPa, 0.38 MPa and 0.65 MPa (71, 55 and 94 lb/in^2), respectively.

$$1 - Day\ Split\ Tensile\ Strength\ (MPa) = 2.82 + 0.37\alpha_C \quad \text{(Eq. 18)}$$

$$7 - Day\ Split\ Tensile\ Strength\ (MPa) = 3.78 - 0.26\alpha_S \quad \text{(Eq. 19)}$$

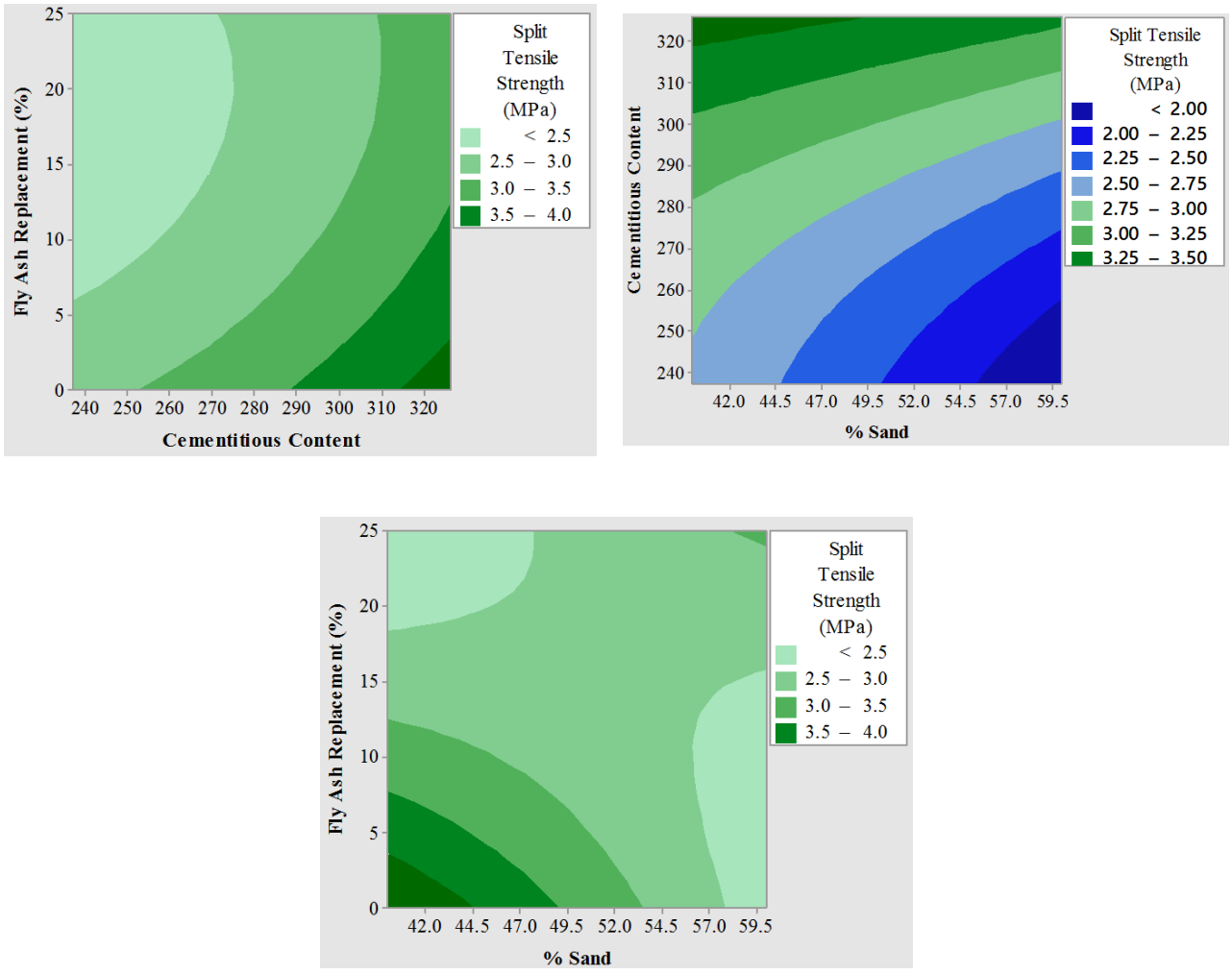

Figure 39. Contour plots for 1-day split tensile strength *(1 ksi = 6.89 MPa; 1 kg/m^3 = 1.686 lb/yd^3)*.

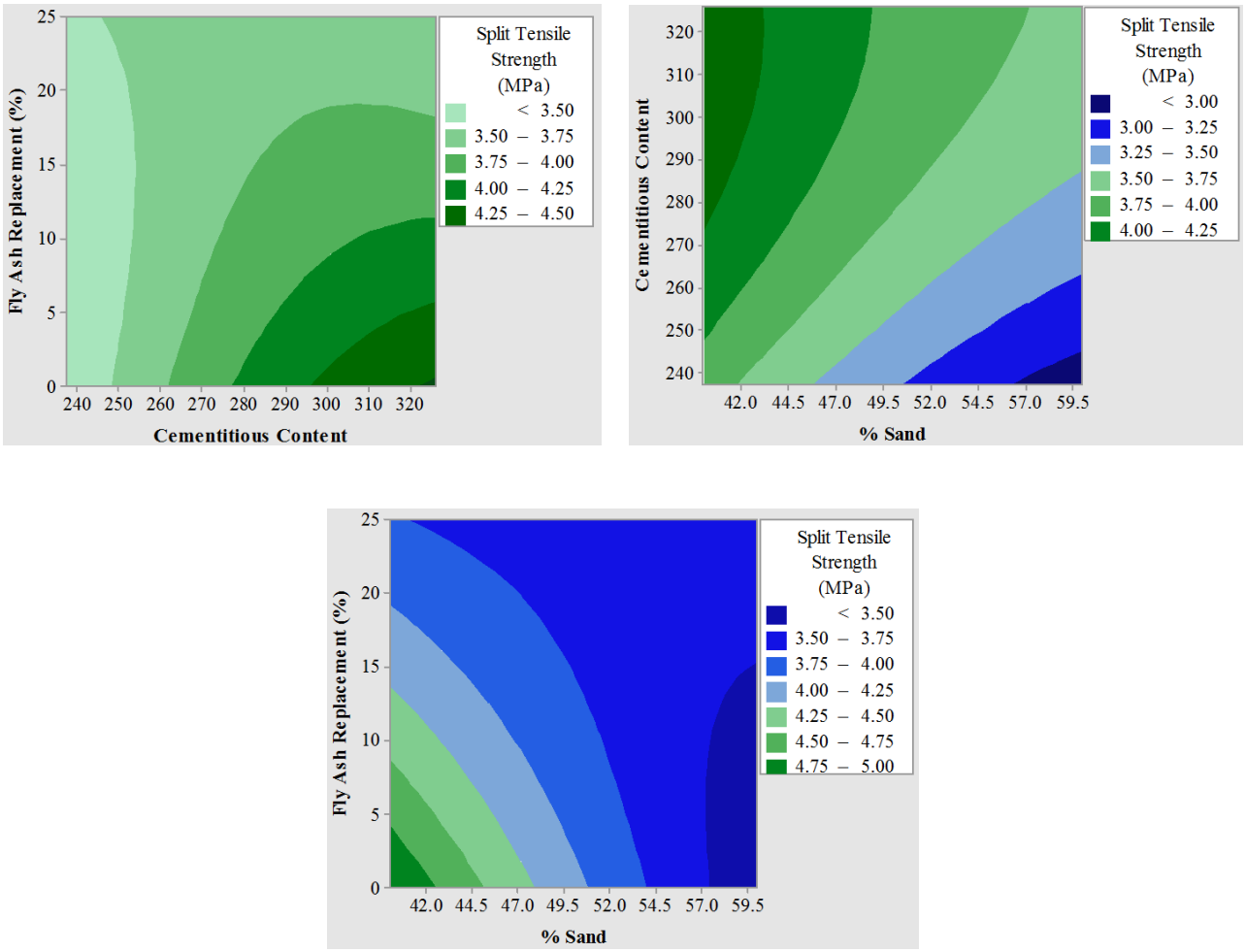

Figure 40. Contour plots for 7-day split tensile strength *(1 ksi = 6.89 MPa; 1 kg/m³ = 1.686 lb/yd³)*.

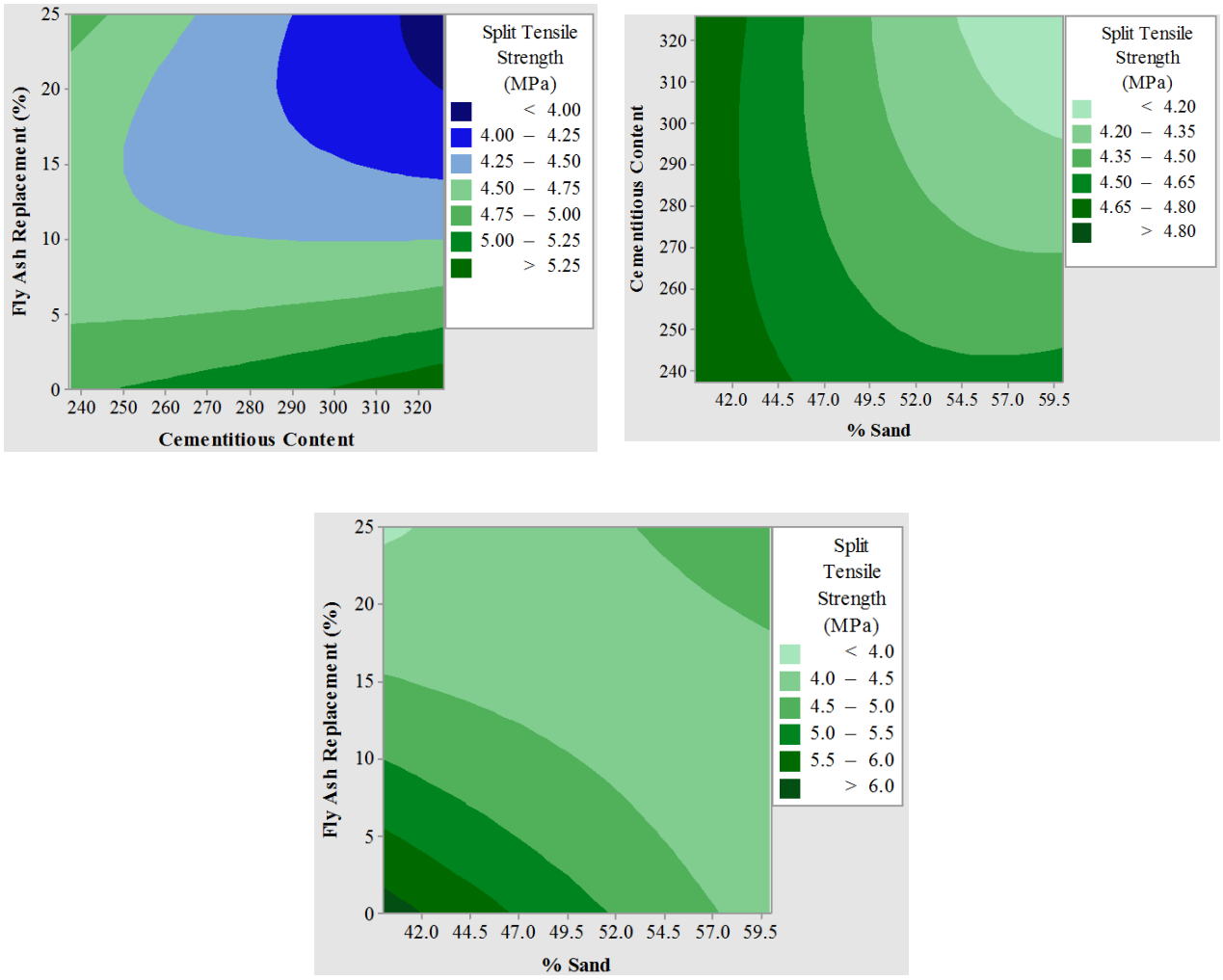

Figure 41. Contour plots for 28-day split tensile strength *(1 ksi = 6.89 MPa; 1 kg/m³ = 1.686 lb/yd³)*.

4.3.3 Flexural Strength

Flexural strength testing was performed at an age of 28-days on 100x100x400 mm (4x4x16 in) beam specimens according to ASTM C78 (2010). Triplicate specimens were tested per experimental design point. Specimens were stored in a fog curing room at 100% relative humidity (RH) and 23°C (73.4°F) until the time of testing. Contour plots for 28-day flexural strength (MOR) are shown in Figure 42. The primary variable increasing flexural strength was decreasing sand percentages. The response equation for 28 day MOR has a standard error of 0.43 MPa (62 psi) and is shown in Equation 20.

$$28 - Day\ MOR\ (MPa) = 6.61 - 0.43\alpha_S - 0.28\alpha_C^2 \qquad \text{(Eq. 20)}$$

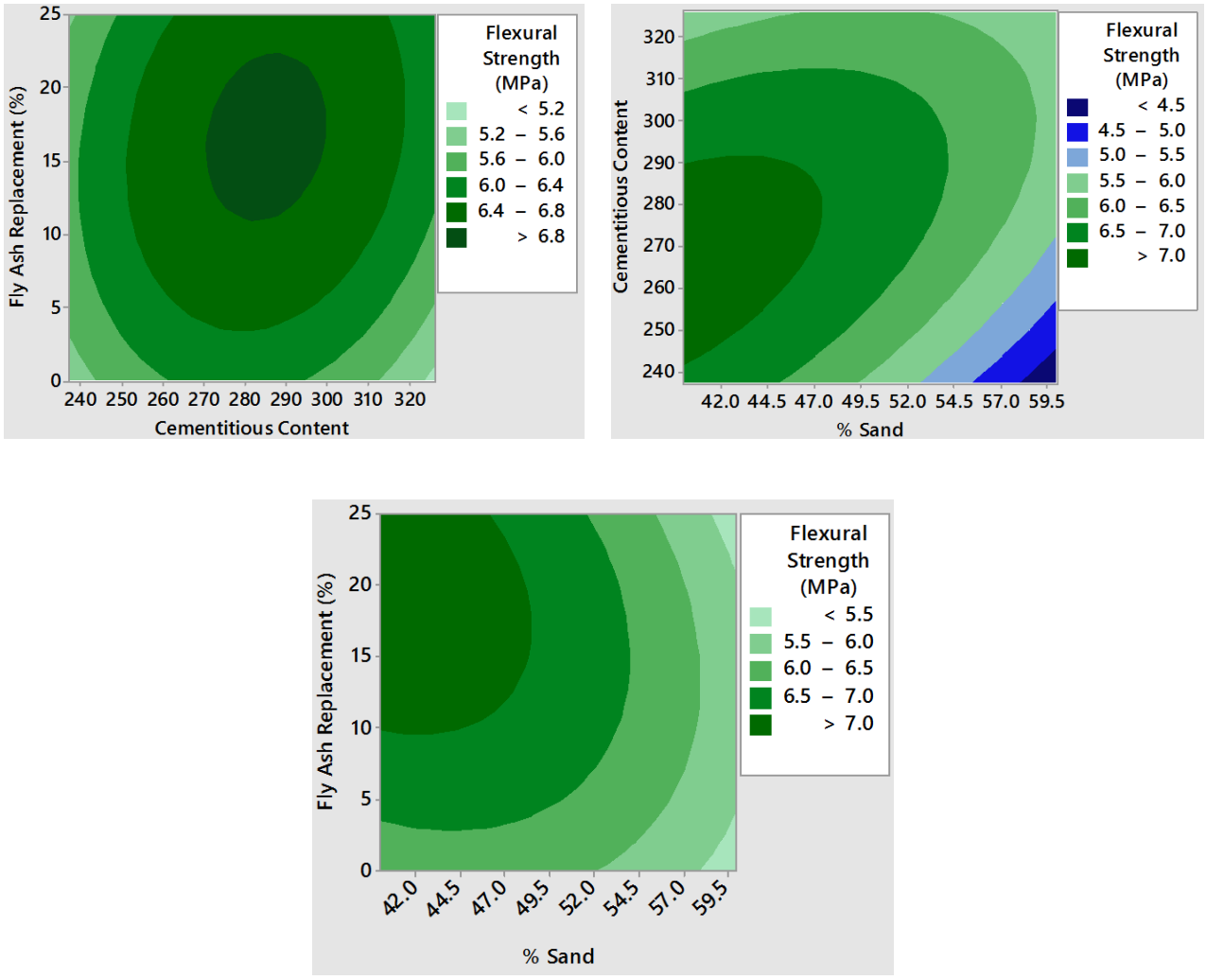

Figure 42. Contour plots for 28-day flexural strength *(1 ksi = 6.89 MPa; 1 kg/m³ = 1.686 lb/yd³)*.

4.4 ELASTIC MODULUS PROPERTIES

Elastic modulus testing was performed on 100x200 mm cylinders at an age of 28 days according to ASTM C469 (2010). Triplicate specimens were tested for each design point. Specimens were stored in a fog curing room at 100% relative humidity (RH) and 23°C (73.4°F) until the time of testing. Contour plots for elastic modulus testing are shown in Figure 43. Response Equation 21 for 28-day elastic modulus has a standard error of 1.30 GPa (189 ksi). Similar to strength properties, an increase in sand percentage correlates to a decrease in elastic modulus. However, increasing cementitious content also led to an increase in elastic modulus. Figure 44 shows elastic modulus (average of 3 cylinders) plotted against compressive strength (average of 3 cylinders) measured on the same specimens as elastic modulus testing. Figure 44 shows data from Chapters 3 and 4 and Appendix J along with the

relationship between elastic modulus and compressive strength (Equation 22) proposed by the American Concrete Institute (ACI, 2008). Equation 22 gives 28-day elastic modulus (*E*) in units of GPa with 28-day compressive strength (σ_c) in units of MPa. For the majority of the data points in Figure 44, the relationship between elastic modulus and compressive strength proposed by ACI (2008) over predicts the measured elastic modulus.

$$28 - Day\ Elastic\ Modulus\ (GPa) = 32.27 - 0.86\alpha_S + 0.97\alpha_C^2 - 1.07\alpha_C\alpha_F \qquad \text{(Eq. 21)}$$

$$E = 4.73\sqrt{\sigma_c} \qquad \text{(Eq. 22)}$$

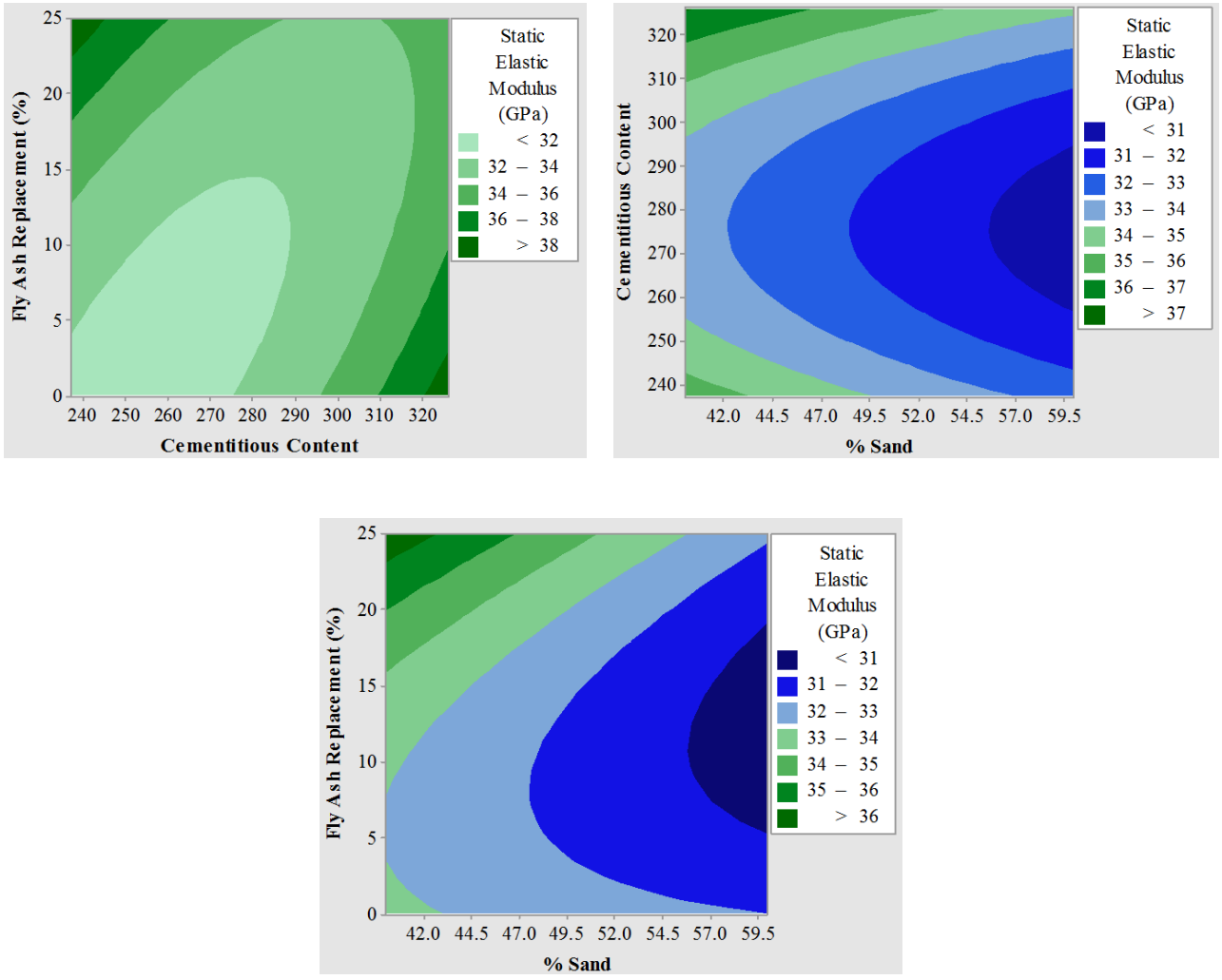

Figure 43. Contour plots of 28-day elastic modulus *(1 ksi = 6.89 MPa; 1 kg/m³ = 1.686 lb/yd³)*.

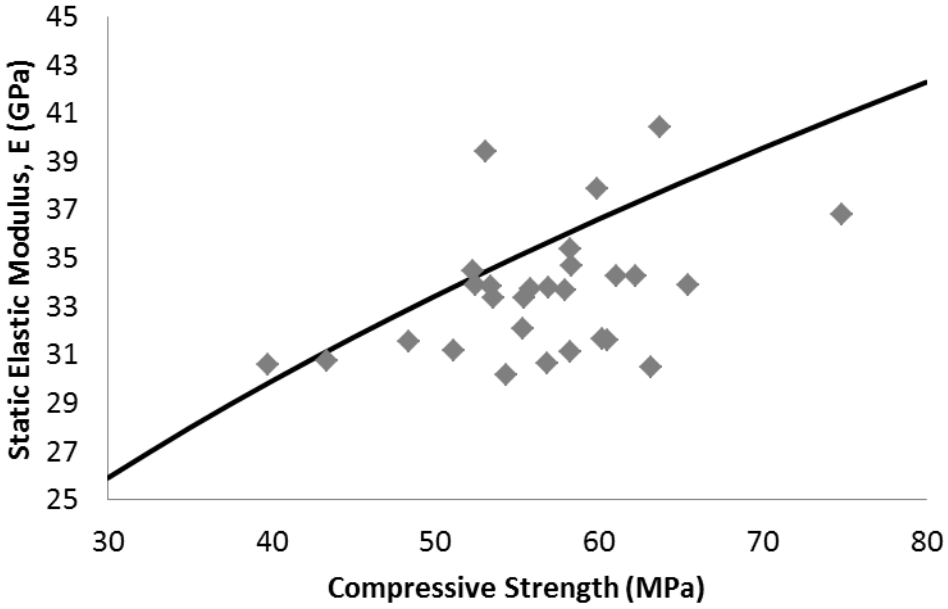

Figure 44. Relationship between elastic modulus and compressive strength. Black line indicates ACI-318 (2008) equation *(1 GPa = 145 ksi)*.

4.5 DRYING SHRINKAGE

Drying shrinkage measurements were conducted according to ASTM C157 (2008) for each of the experimental design points. Triplicate 75x75x281 mm (3x3x11 in) beams were cast per design point and were cover-cured for 24 hours after casting before being introduced to a drying environment (50% relative humidity and 23°C (73.4°F)). Length change was measured for at least 28 days after exposure to the drying environment. Contour plots of the drying shrinkage strains (microstrain) after 7 and 28 days of drying are shown in Figure 45 and Figure 46, respectively. Response Equations 23 and 24 for 7 and 28 day drying shrinkage (microstrain, με), respectively have standard errors of 31.0 με and 47.7 με, respectively. The most apparent trend in the drying shrinkage results is that reducing cementitious content tends to reduce drying shrinkage strains which was also found in Chapter 3. Unlike all other properties (density, optimum moisture, strength, and modulus), there does not appear to be a significant and consistent effect of sand percentage on drying shrinkage measurements at 7 or 28 days. The drying shrinkage values in Figure 45 and Figure 46 tend to agree with other drying shrinkage tests on RCC in this report as well as in the RCC literature (Ghafoori and Cai, 1998; Pittman and Ragan, 1998; Jingfu et al. 2009; Damrongwiriyanupap et al. 2012; Khayat and Libre, 2014).

$$7 - Day\ Drying\ Shrinkage\ Strain\ (\mu\epsilon) = 214.3 - 17.5\alpha_S^2 - 25.0\alpha_C\alpha_F \qquad \text{(Eq. 23)}$$

$$28 - Day\ Drying\ Shrinkage\ Strain\ (\mu\epsilon) = 312.3 - 39.2\alpha_C\alpha_F \qquad \text{(Eq. 24)}$$

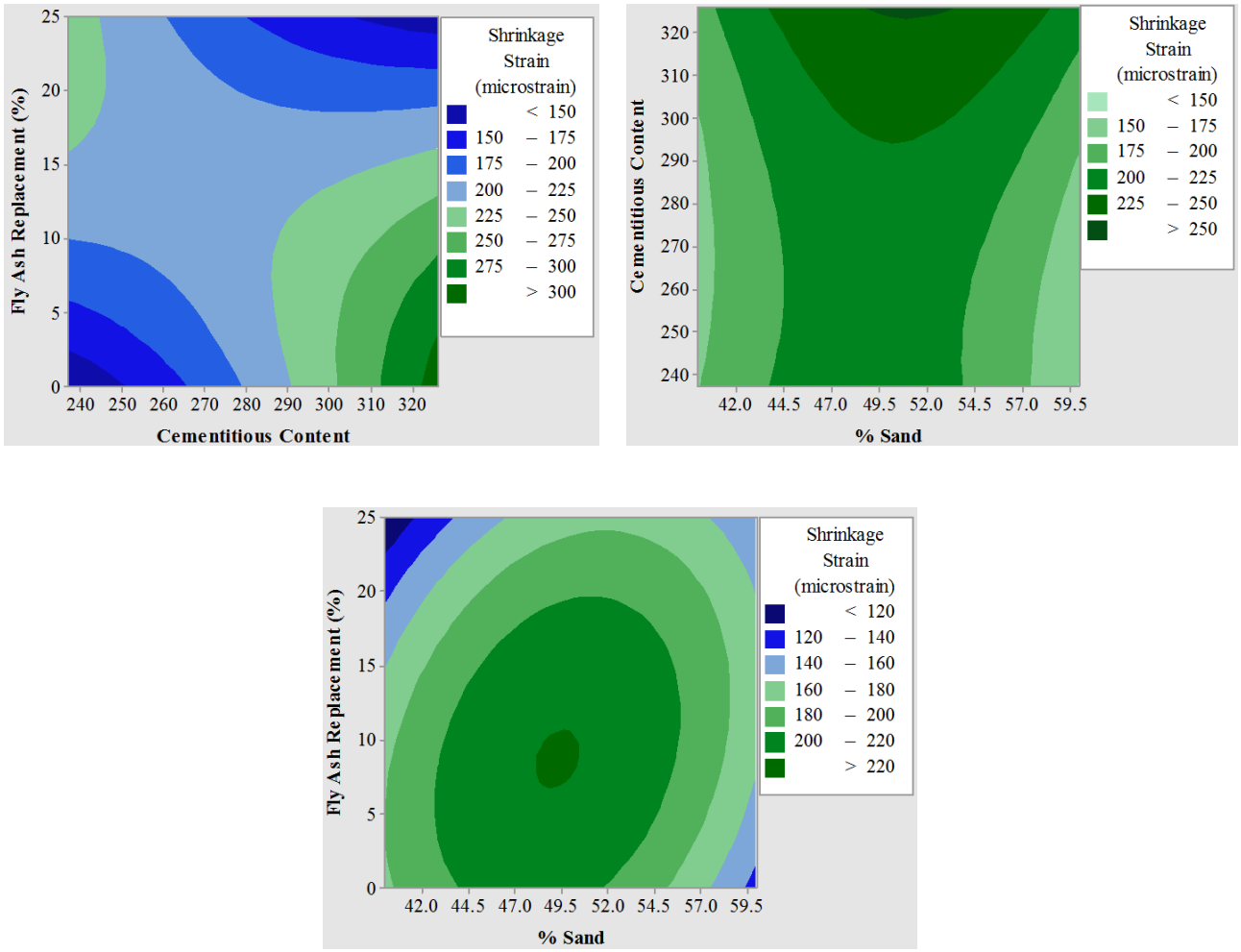

Figure 45. Contour plots of 7-day drying shrinkage strains *(1 ksi = 6.89 MPa; 1 kg/m³ = 1.686 lb/yd³)*.

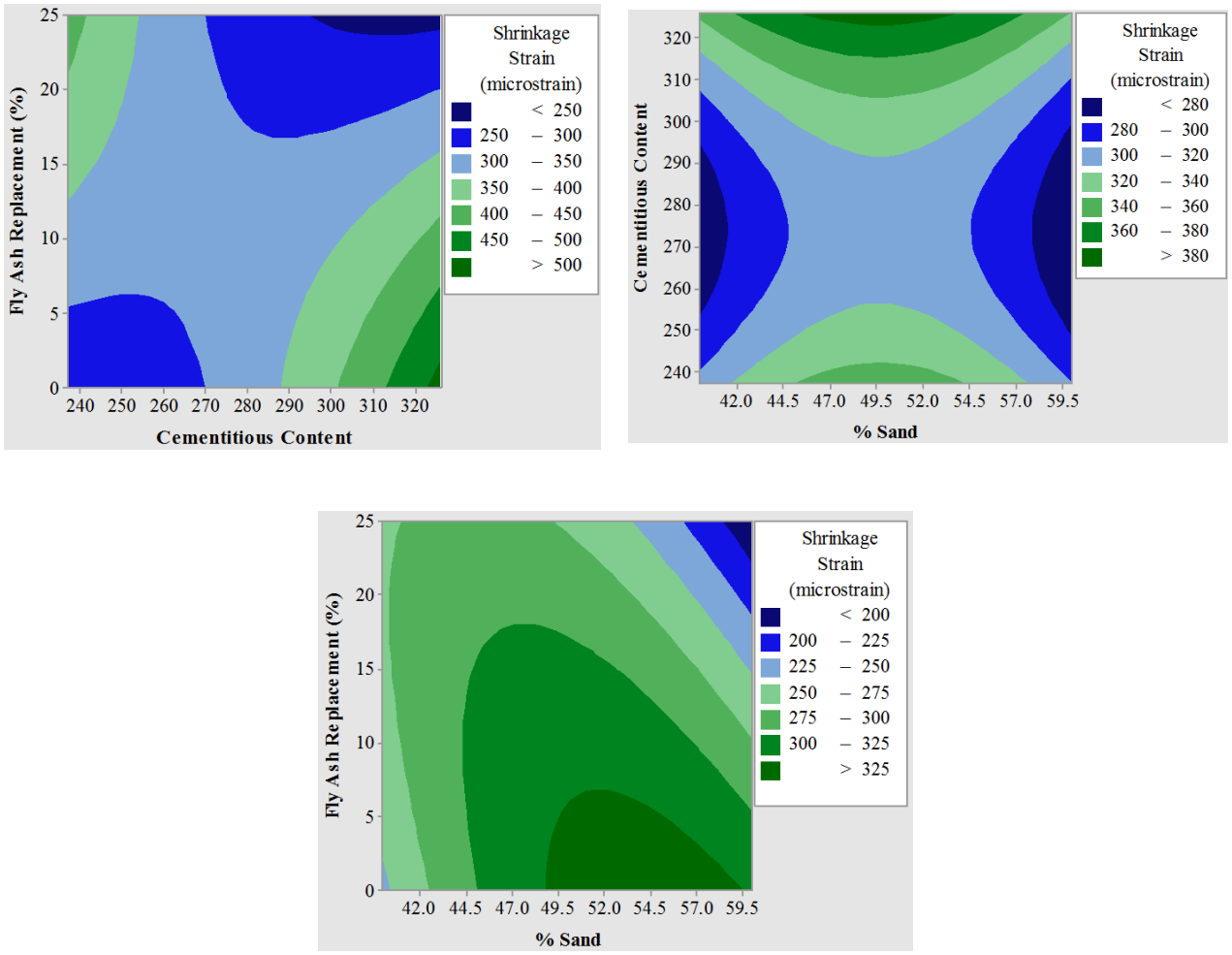

Figure 46. Contour plots of 28-day drying shrinkage strains *(1 ksi = 6.89 MPa; 1 kg/m³ = 1.686 lb/yd³)*.

4.6 FREEZE-THAW RESISTANCE

Previous research on freeze-thaw resistance of RCC has conflicting findings as summarized in Table 25. Ghafoori and Cai (1998) as well as Vahedifard et al. (2010) showed that RCC could achieve a relative dynamic modulus of 80% or greater at 300 cycles for non-air entrained RCC with cementitious contents as low as 216 kg/m^3 (365 lb/yd^3). However, Delatte and Storey (2005) found significantly higher mass loss than all other RCC studies even with cement contents of 326 kg/m^3 (550 lb/yd^3), while Mardani et al. (2013) and Hazaree et al. (2011) found relative dynamic moduli at 300 cycles less than 80% even for cement contents as high as 450 kg/m^3 (760 lb/yd^3). Hazaree et al. (2011) showed that it was possible to include air-entraining agent in RCC effectively and this change resulted in significantly improved freeze-thaw resistance. It is clear that RCC made with different aggregate sources and gradations, different compaction methods, and different cementitious materials will

yield significantly different resistance to freeze-thaw even for a constant cementitious content. Ragan (1986) cut specimens from in service RCC pavements and tested them for freeze-thaw resistance in the laboratory with results showing generally good freeze-thaw performance of RCC field specimens, especially those with relatively small spacing factors. Anecdotal evidence of RCC having good freeze-thaw performance in the field can be found in the literature (Piggott, 1987).

A review of the theory and underlying principles of freeze-thaw resistance and damage mechanisms for concrete materials can be useful for predicting potential RCC mechanisms. Freeze-thaw damage can be seen in the cement paste and/or the aggregates. Assuming that the aggregates used are freeze-thaw resistant, the main concern is then freeze-thaw damage in the cement paste. The overarching cause for freeze-thaw damage in cementitious materials is the dilation of the specimens which induces micro-cracking. The dilation is caused by three main phenomena: hydraulic, osmotic, and vapor pressures (Mindess et al. 2003). These three forms of pressure are caused by different physio-chemical methods, but they all have the same effect of inducing micro-cracking in the surrounding paste. As the material is cycled through freezing and thawing conditions repeatedly, the micro-cracking progresses outward into the bulk of the material and reduces its integrity. The material properties that control freeze-thaw resistance of cementitious materials are its permeability, degree of paste saturation, amount of freezable water, and average maximum distance from any point in the paste to a free surface where ice can form safely (Mindess et al. 2003). Due to the dense nature of RCC and low water contents relative to conventional concrete, it is expected to have lower permeability and less available water to saturate the paste as well as less freezable water. Based on material properties of RCC, it is expected to have similar or better freeze-thaw resistance relative to conventional (non-air entrained) concrete.

A small study was undertaken to evaluate the freeze-thaw resistance of RCC mixes that contain Dolomite (coarse and intermediate) and natural sand, 12.5% fly ash (by weight of total cementitious materials), and were compacted with a vibratory hammer. The three mix designs that were tested for resistance to freeze-thaw were the two extreme values of cementitious content (experimental design points B and O) as well as the central experimental design point (A). The corresponding total cementitious contents were 237.2 (400) (mix O), 281.7 (475) (mix A), and 326.2 (550) kg/m^3 (lb/yd^3) (mix B). Duplicate 75x75x281 mm (3x3x11 in) prisms were cast per mix according to the procedure for compacting shrinkage prisms (Chapter 2). These prisms were then tested for freeze-thaw resistance according to ASTM C666 Procedure B (2008) for a total of 322 cycles. Unfortunately, dynamic modulus measurements versus cycles were not obtained during testing so only measurements prior to commencing testing and measurements after completion of testing were collected. A duplicate set of prisms were also tested according to ASTM C666 Procedure A (2008) for a total of 12 total cylinders tested

Table 25. Summary of RCC Freeze-Thaw Resistance Literature *(1 in = 25.4 mm; 1 kg/m³ = 1.686 lb/yd³)*

Researcher(s)	Cementitious Content	Mass Loss at 300 Cycles	Relative Dynamic Modulus at 300 Cycles
Ghafoori and Cai (1998)	216, 288, 360 kg/m^3	< 2%	90, 94, 97%
Mardani et al. (2013)	250 kg/m^3	< 2%	< 70%
Hazaree et al. (2011)	100 – 250 kg/m^3	n/a	< 60%
	300 – 450 kg/m^3	n/a	60 – 80%
	350 – 450 kg/m^3 with air entraining agent	n/a	90%
Vahedifard et al. (2010)	288 and 360 kg/m^3	< 1.5%	80%
Delatte and Storey (2005)*	261 – 326 kg/m^3	> 7%	n/a

*Specimens were compacted using gyratory compactor with a resultant length of 160 mm instead of the standard 281 mm.

Dynamic modulus values were obtained from transverse resonance frequency testing according to ASTM C215 (2002). Triplicate resonance frequency measurements were carried out on each prism for a total of 6 resonance frequency measurements per set of prisms. The MATLAB code used to calculate transverse resonance frequency from testing according to ASTM C215 (2002) is shown in Appendix B. Typical frequency-domain signals from each set of prisms after completion of freeze-thaw testing are shown in Figure 47 as a function of cementitious content. The initial and final dynamic moduli (averages of 6 replicates) for each set of prisms are shown in Table 26 along with relative dynamic modulus after 322 cycles. For procedure B, the lowest cementitious content (237.2 kg/m^3 or 400 lb/yd^3) produced a relative dynamic modulus of 83.7% while the other two cementitious contents produced relative dynamic moduli greater than 100%. The same trend was observed for procedure A. However, all cementitious contents had relative dynamic modulus less than 100% after 300 cycles. Relative dynamic modulus was inversely proportional to w/cm ratio, as expected based on Mindess et al. (2003). These results would suggest that these three mixtures are potentially suitable for freeze-thaw climates. Figure 48 shows the RCC specimens prior to freeze-thaw testing and after completion of testing. It can be seen that there is not any significant damage to the specimens after 322 cycles of freezing and thawing.

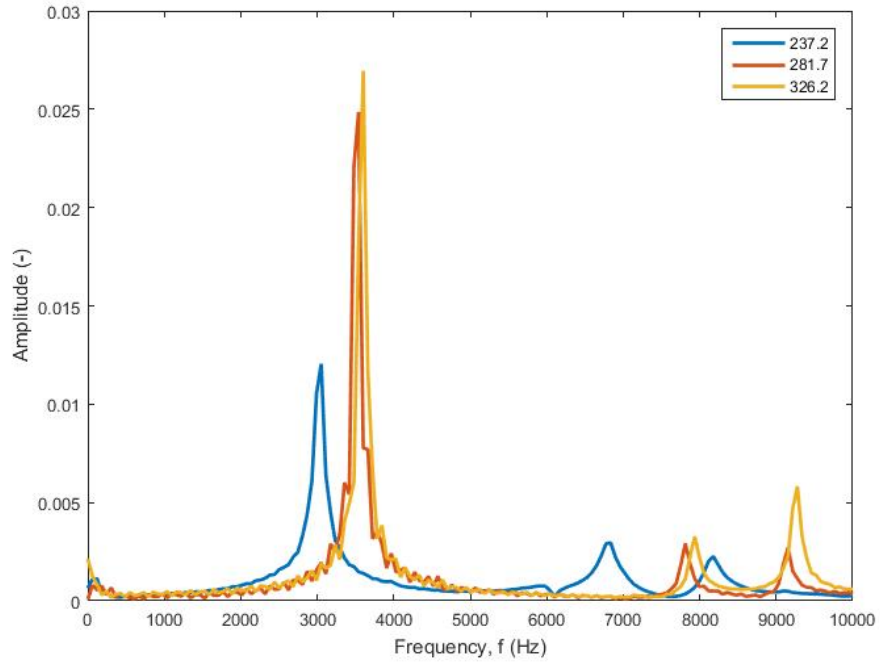

Figure 47. Frequency-domain response of freeze-thaw specimens after completion of testing (values represent cementitious content in kg/m^3); *(1 kg/m^3 = 1.686 lb/yd^3)*.

Table 26. Freeze-Thaw Testing Results *(1 GPa = 145.03 ksi; 1 kg/m^3 = 1.686 lb/yd^3)*

Mix ID	Cementitious Content (kg/m^3)	W/CM	Procedure A – Relative Dynamic Modulus after 300 Cycles (%)	Procedure B - Initial Dynamic Modulus (GPa)	Procedure B - Dynamic Modulus after 322 Cycles (GPa)	Procedure B - Relative Dynamic Modulus after 322 Cycles (%)
O	237.2	0.49	83.0	41.91	35.08	83.7
A	281.7	0.43	84.0	45.17	46.84	103.7
B	326.2	0.35	92.5	46.72	50.66	108.4

(a)

(b)

Figure 48. RCC freeze-thaw specimens prior to testing (a) and after completion of testing (b). Mix O (RCC1/2), Mix A (RCC3/4), and Mix B (RCC5/6).

4.7 CONCLUSIONS

An experimental design was developed to quantify the combined effects of sand percentage, cementitious content, and fly ash dosage on the fresh and hardened properties of RCC. A total of 20 mix designs were created to populate the experimental design space. Sand percentage has a relatively significant effect on most fresh and hardened properties of RCC. Increasing sand percentage resulted in decreased Proctor densities, strength properties (compressive, split tensile, and flexural), and elastic modulus—while increasing sand percentage led to increased optimum moisture contents. The effect of sand percentage on RCC properties agrees with the limited RCC literature that has investigated sand percentage (similar parameter to coarse-to-fine aggregate ratio). As expected, increasing cementitious content led to increases in strength and modulus properties. The interaction between cementitious content and fly ash dosage appeared to be the controlling factor with regards to drying shrinkage.

A study on RCC freeze-thaw durability was conducted to assess the physical resistance of three RCC mixes utilized in this experimental design, knowing that the literature has conflicting results for RCC. The three mix designs represented the extreme points of cementitious content and the central point: 237.2, 281.7, and 326.2 kg/m^3 (400, 475 and 550 lb/yd^3) while fixing the fly ash content (12.5%) and

sand percentage (50%). All three mixes maintained relative dynamic moduli of at least 80% through 322 freeze-thaw cycles according to Procedure B of ASTM C666. The two higher cementitious content mixes produced relative dynamic moduli values greater than 100%. These preliminary results, along with visible inspection of the tested specimens, would suggest that these RCC mixes might perform well in a freeze-thaw climate.

CHAPTER 5: CONCLUSIONS AND FUTURE WORK

5.1 CONCLUSIONS

A research program was initiated to characterize the main parameters that affect RCC mix design for pavements as well as the relationship between field and laboratory RCC properties. The effect of aggregates on RCC mix design and mechanical properties was investigated in terms of combined aggregate gradation, aggregate packing efficiency, and aggregate sources (recycled, dolomite, trap rock, gravel, sand, etc.). The impact of various cementitious materials (cement, fly ash, silica fume, and ground-granulated blast furnace slag) and content on RCC mix design and properties was also part of the experimental factorial in the laboratory. Discrete macro-fibers were introduced to a subset of RCC and lightly cement-treated bases to determine the change in strength, flexural toughness, and fracture properties. Several existing RCC compaction methods (modified Proctor, vibrating table with surcharge weight, and vibrating hammer) were evaluated with respect to the gyratory compactor to better define laboratory mixture procedures that produce the observed field properties under modern construction equipment. In total, 74 RCC mixes were tested for moisture-density, Vebe time, strength, durability, shrinkage, creep, and fracture properties. Throughout the range of material constituents and proportions tested, almost all RCC mixes met typical hardened property specifications.

The aggregate gradation had the most significant effect on RCC properties with the largest change occurring in 28-day compressive strength ranging from 32.2 MPa to 55.1 MPa (4.75 to 8 ksi) for the same cement content. Variations in the aggregate gradation had much less effect on RCC split tensile and flexural strengths as well as fracture and shrinkage properties. Application of the modified Proctor testing to a wide range of aggregate gradations produced no significant difference in the maximum dry density and optimum moisture content (OMC) for a given aggregate source. However, the modified Proctor did demonstrate that certain aggregate gradations produced densities more sensitive to changes in moisture contents once above the OMC. A design of experiment response model validated that the percent sand (or coarse-fine aggregate ratio) in RCC was one of the most important mixture parameters, with increasing sand percentage leading to reductions in strength, density, and elastic modulus. An aggregate packing model developed for RCC aggregates reinforced that low packing efficiency leads to lower RCC compressive strengths.

The effect of cementitious content and supplementary cementitious materials (SCMs) was also characterized for RCC mixtures. A lightly cement-treated base course (2 to 4%) incorporating recycled/marginal aggregates was tested with the mechanical and toughness properties being highly dependent on cement contents. Several RCC mixes containing SCMs, class C fly ash, ground granulated blast furnace slag, and silica fume, were tested near their maximum dosage levels—and did not detrimentally effect RCC mechanical properties—with the exception of reduced 1-day strengths for the fly ash and slag mixtures. RCC pavements incorporating higher SCM dosages may require slightly longer curing times before opening to traffic. Cementitious content (in the range of 237.2 to 326.2 kg/m^3 (400 to 550 lb/yd^3) had a significant effect on RCC strength properties. Drying shrinkage of RCC was less than conventional concrete (PCC). In general, compressive creep of RCC was similar or lower than PCC whereas tensile creep was similar or greater relative to PCC. Freeze-

thaw durability testing of RCC with cement contents of 237.2, 281.7, and 326.2 kg/m^3 (400, 475 and 550 lb/yd^3) passed the minimum durability factor of 80% after 322 freeze-thaw cycles, i.e., 83.7, 103.7, and 108.4% respectively.

Current RCC pavement mix design uses the modified Proctor test procedure. Based on past experience, the modified Proctor compaction method has produced RCC mix designs with acceptable MDD and OMC required for field compaction. However, it was shown in this research to be relatively insensitive to changes in gradation and cementitious content with regards to density as well as overestimate field density, strength, and fracture properties. Like the modified Proctor test, the modified Vebe test is also relatively insensitive to key mixture parameters such as aggregate gradation/type and cementitious content. Thus, the gyratory compactor was investigated as an alternative for the RCC mix design process, indicator of workability/compactibility, and for fabricating specimens for hardened properties. A total of 17 mix designs with various cementitious contents and aggregate gradations were compared between these compaction methods. The gyratory compactor was found to be better suited for determining combinations of aggregate gradations and cementitious contents that will have a greater likelihood of achieving density and sufficient mechanical properties in the field.

5.2 FUTURE RCC RESEARCH WORK

One of the main objectives of this report was to investigate the effects of mixture parameters and compaction methods on laboratory properties of RCC. In order to validate the effectiveness of the gyratory compactor for RCC mix design and for matching lab and in-situ properties, further lab work that shadows field projects is recommended. One of the remaining questions with regards to use of the gyratory compactor is the optimal set of compaction parameters that provides the best relationship between properties (density and mechanical properties) from laboratory and field specimens. Field projects where the gyratory compactor is used to compact specimens (with a suite of compaction parameters) and then comparing the resulting specimen densities and mechanical properties with those from field cores would help validate a final mix design procedure using the gyratory compactor in lieu of the modified Proctor. Additionally, sawed beams should be extracted from the field project pavements in order to determine correlations between compressive and/or split tensile strength from the gyratory compactor and flexural strength.

Another area of future work that could prove useful for RCC pavement design would be flexural slab capacity testing (monotonic tests or accelerated pavement testing) of RCC incorporating virgin and/or recycled aggregates. Durability testing, such as freeze-thaw resistance, would also be of interest to determine whether or not these recycled aggregates have negative effects on durability of RCC pavements.

Full-scale test batching and placing of fiber-reinforced RCC in the field is also an area that needs to be investigated since it has been shown to be promising in the laboratory. Ideally, an accelerated pavement testing plan could be developed to validate RCC slab capacity, crack control, and performance of RCC joint load transfer with fibers. This testing plan would allow for determination of the thicknesses of fiber-reinforced and non-reinforced RCC pavement that produce equivalent structural capacities.

REFERENCES

AASHTO T 318-02, "Standard Method Of Test For Water Content Of Freshly Mixed Concrete Using Microwave Oven Drying," In 2011.

Achilleos, C., Hadjimitsis, D., Neocleous, K., Pilakoutas, K., Neophytou, P. O., & Kallis, S. (2011). Proportioning of steel fibre reinforced concrete mixes for pavement construction and their impact on environment and cost.*Sustainability*, *3*(7), 965-983.

ACI 325.10R-95, "State-Of-The-Art Report On Roller Compacted Concrete Pavements," *State-Of-The-Art Report On Roller-Compacted Concrete Pavements, ACI,* 1995.

ACI Committee, American Concrete Institute, & International Organization for Standardization. (2008). Building code requirements for structural concrete (ACI 318-08) and commentary. American Concrete Institute.

Aïssoun, B. M., Hwang, S. D., & Khayat, K. H. (2016). Influence of aggregate characteristics on workability of superworkable concrete. *Materials and Structures*, *49*(1-2), 597-609.

Akkaya, Y., Ouyang, C., & Shah, S. P. (2007). Effect of supplementary cementitious materials on shrinkage and crack development in concrete.*Cement and Concrete Composites*, *29*(2), 117-123.

Albuquerque, M., Balbo, J., Sansone, E., Pinto, P. (2011). "Fracture Characterization of Roller Compacted Concrete Mixtures with Blast Furnace Slag and Industrial Sand." *International Journal of Pavement Research and Technology*, 4 (4), 244-251.

Altoubat, S., J. Roesler, D. Lange, and K.A. Rieder. (2008). "Simplified method for concrete pavement design with discrete structural fibers." *Construction and Building Materials 22*, Elsevier Ltd.: 384-393.

Amer, N., Delatte, N., & Storey, C. (2003). Using gyratory compaction to investigate density and mechanical properties of roller-compacted concrete.*Transportation Research Record: Journal of the Transportation Research Board*, (1834), 77-84.

Amer, N., Storey, C., & Delatte, N. (2004). Roller-compacted concrete mix design procedure with gyratory compactor. *Transportation Research Record: Journal of the Transportation Research Board*, (1893), 46-52.

American Concrete Institute (ACI). (1995). ACI 325.10R-95 State-of-the-art report on roller-compacted concrete pavements. ACI, Farmington Hills, Michigan.

American Concrete Pavement Association (ACPA). (2014). ACPA guide specification: roller-compacted concrete pavements as exposed wearing surface. ACPA, Rosemont, Illinois.

Amirkhanian, A.N. (2012). "Properties of Functionally-Graded Concrete Slabs." MS thesis. University of Illinois at Urbana-Champaign.

Amirkhanian, A.N. (2016). "Effects of fine lightweight aggregates on curling and moisture gradient development in drying concrete materials." Ph.D. Dissertation, University of Illinois at Urbana-Champaign.

Amirkhanian, A., Spring, D., Roesler, J., Paulino, G. (2015). "Forward and Inverse Analysis of Concrete

Fracture Using the Disk-Shaped Compact Tension Test." *Journal of Testing and Evaluation*.

Angelakopoulos, H., Papastergiou, P., Pilakoutas, K. (2015). "Fibrous Roller-Compacted Concrete with Recycled Materials – Feasibility Study." *Magazine of Concrete Research*, 67 (15), 801-811.

Arman, A. Louisiana. Dept. Of Highways. And Louisiana State University (Baton Rouge,La.).Division Of Engineering Research., "Counteraction Of Detrimental Effects Of Delayed Compaction." 1972.

Ashtiani, R. S., Little, D. N. (2007). Acceptability criteria for high fines content aggregate pavement layers. *Rep. No. ICAR/401131, International Center for Aggregates Research (ICAR), Texas Transportation Institute, Austin, TX*, 1-100.

ASTM C29. (1997). Standard test method for bulk density ("unit weight") and voids in aggregate. ASTM International: West Conshohocken, 4 p.

ASTM C39. (2012). Standard test method for compressive strength of cylindrical concrete specimens. ASTM International: West Conshohocken, 7 p.

ASTM C42. (2013). Standard test method for obtaining and testing drilled cores and sawed beams of concrete. ASTM International, West Conshohocken, 7 p.

ASTM C78. (2010). Standard test method for flexural strength of concrete (using simple beam with third-point loading). ASTM International, West Conshohocken, 4 p.

ASTM C136. (1996). Standard test method for sieve analysis of fine and coarse aggregates. ASTM International: West Conshohocken, 5 p.

ASTM C127-15, "Standard Test Method For Specific Gravity And Absorption of Coarse Aggregate," In 2015.

ASTM C128-15. Standard Test Method For Relative Density (Specific Gravity) And Absorption of Fine Aggregate. 2015.

ASTM C157. (2008). Standard test method for length change of hardened hydraulic-cement mortar and concrete. ASTM International: West Conshohocken, 7 p.

ASTM C192. (2013). Standard practice for making and curing concrete test specimens in the laboratory. ASTM International: West Conshohocken, 8 p.

ASTM C215. (2002). Standard test method for fundamental transverse, longitudinal, and torsional resonant frequencies of concrete specimens. ASTM International: West Conshohocken, 7 p.

ASTM C469. (2010). Standard test method for static modulus of elasticity and Poisson's ratio of concrete in compression. ASTM International: West Conshohocken, 5 p.

ASTM C496. (2011). Standard test method for splitting tensile strength of cylindrical concrete specimens. ASTM International: West Conshohocken, 5 p.

ASTM C512. (2015). Standard test method for creep of concrete in compression. ASTM International: West Conshohocken, 5 p.

ASTM C542. (2013). Standard test method for density, absorption, and voids in hardened concrete. ASTM International: West Conshohocken, 3 p.

ASTM C666. (2008). Standard test method for resistance of concrete to rapid freezing and thawing. ASTM International: West Conshohocken, 6 p.

ASTM C1170. (2008). Standard test method for determining consistency and density of roller-compacted concrete using a vibrating table. ASTM International: West Conshohocken, 5 p.

ASTM C1176. (2013). Standard practice for making roller-compacted concrete in cylinder molds using a vibrating table. ASTM International: West Conshohocken, 5 p.

ASTM C1435. (2008). Standard practice for molding roller-compacted concrete in cylinder molds using a vibrating hammer. ASTM International: West Conshohocken, 5 p.

ASTM C1609. (2010). Standard test method for flexural performance of fiber-reinforced concrete (using beam with third-point loading). ASTM International: West Conshohocken, 9 p.

ASTM D1557. (2012). Standard test methods for laboratory compaction characteristics of soil using modified effort. ASTM International: West Conshohocken, 14 p.

Atiş, C. D. (2005). Strength properties of high-volume fly ash roller compacted and workable concrete, and influence of curing condition. *Cement and Concrete Research*, *35*(6), 1112-1121.

Atrushi, D. S. (2003). Tensile and compressive creep of early age Concrete. Ph.D. Thesis. The Norwegian University of Science and Technology. 314 p.

Banthia, N. and S. Islam. (2013). "Loading Rate Concerns in ASTM C1609." *Journal of Testing and Evaluation 41(6), ASTM.* West Conshohocken, PA: 1-5.

Bernard, E. (2014). Influence of friction in supporting rollers on the apparent flexural performance of third-point loaded fiber-reinforced concrete beams. *Advances in Civil Engineering Materials*, 3.

Bilodeau, K., Sauzéat, C., Benedetto, H.D., Olard, F., Bonneau, D. (2011). "Laboratory and In Situ Investigations of Steel Fiber Reinforced Compacted Concrete Containing Reclaimed Asphalt Pavement." Presented at the Transportation Research Board 90th Annual Meeting, Washington, D.C.

Bilodeau, K., Sauzéat, C., Benedetto, H.D., Olard, F. (2012). "Roller Compacted Concrete for Road Base Layer with RAP and Steel Fibers: Viscous Properties and Description of Experimental Sites." In *10th International Conference on Concrete Pavements*, Québec City, Canada, 435-448.

Bissonnette, B., & Pigeon, M. (1995). Tensile creep at early ages of ordinary, silica fume and fiber reinforced concretes. *Cement and Concrete Research*, *25*(5), 1075-1085.

Bordelon, A., Cervantes, V., & Roesler, J. R. (2009). Fracture properties of concrete containing recycled concrete aggregates. *Magazine of Concrete Research*, *61*(9), 665-670.

Bordelon, A. and J. Roesler. (2009). "Fiber-Reinforced Concrete Pavement Design and Material Requirements." *8th International Conference on the Bearing Capacity of Roads, Railways, and Airfield*

Bordelon, A., & Roesler, J. (2011). Design with fiber reinforcement for thin concrete overlays bonded to asphalt. *Journal of Transportation Engineering*,*138*(4), 430-435.

Box, G. and K.B. Wilson. On the experimental attainment of optimum conditions. Journal of the

Royal Statistical Society. Series B (Methodological), 13(1):145, 1951.

Brand, A.S. and J.R. Roesler. (2014). “Concrete with Steel Furnace Slag Fractionated Reclaimed Asphalt Pavement.” *Report No. ICT-14-015*, Illinois Center for Transportation, Illinois State Toll Highway Authority, National Slag Association, Urbana, IL.

Brand, A.S. and J.R. Roesler. (2015a). “Steel Furnace Slag Aggregate Expansion and Hardened Concrete Properties.” *Cement and Concrete Composites,* 60, 1-9.

Brand, A.S. and J.R. Roesler. (2015b). “Expansive and Concrete Properties of SFS-FRAP Aggregates.” *Journal of Materials in Civil Engineering*, in preprint.

Brand, A.S. and J.R. Roesler. (2015c). “Ternary Concrete with Fractionated Reclaimed Asphalt Pavement.” *ACI Materials Journal*, 112 (1), 155-163.

Brand, A., Amirkhanian, A., & Roesler, J. (2014). Flexural capacity of full-depth and two-lift concrete slabs with recycled aggregates. *Transportation Research Record: Journal of the Transportation Research Board*, (2456), 64-72.

Brand, A.S., Roesler, J.R., Salas, A. (2015). “Initial Moisture and Mixing Effects on Higher Quality Recycled Coarse Aggregate Concrete.” *Construction and Building Materials*, 79, 83-89.

Brooks, J. J., & Johari, M. M. (2001). Effect of metakaolin on creep and shrinkage of concrete. *Cement and Concrete Composites*, *23*(6), 495-502.

Brooks, J. J., & Neville, A. M. (1977). A comparison of creep, elasticity and strength of concrete in tension and in compression. *Magazine of Concrete research*, *29*(100), 131-141.

Brooks, R.M., F. Udoeyo And K. V. Takkalapelli, "Compaction Delay Characteristics Of Clay With Cement Kiln Dust," *Proceedings Of The Institution Of Civil Engineers-Geotechnical Engineering,* Vol. 162, Pp. 283-286, 2009.

Brotman, I., Crist, M., & Gaul, J. (2007). Roller Compacted Concrete Pavement: Properties, Design, and Construction. In *Soil and Material Inputs for Mechanistic-Empirical Pavement Design* (pp. 1-10). ASCE.

Buratti, N., Mazzotti, C., & Savoia, M. (2011). Post-cracking behaviour of steel and macro-synthetic fibre-reinforced concretes. *Construction and Building Materials*, *25*(5), 2713-2722.

Caltrans. Special Provisions for Construction on State Highway in Los Angeles County, State of California Department of Transportation, 2012.

Cao, C., Sun, W., & Qin, H. (2000). The analysis on strength and fly ash effect of roller-compacted concrete with high volume fly ash. *Cement and concrete research*, *30*(1), 71-75.

Cervantes, V. and J. Roesler. (2009). “Performance of Concrete Pavements with Optimized Slab Geometry.” *Illinois Center for Transportation Research Report.* ICT-09-053.

Cha, Y.H., K.S. Kim, and D.J. Kim. (1998). “Evaluation of the Fracture Toughness and Strength of Fiber Reinforced Brittle Matrix Composites.” *KSME International Journal, 12-3:* 370-379.

Chi, M., & Huang, R. (2014). Effect of circulating fluidized bed combustion ash on the properties of roller compacted concrete. *Cement and Concrete Composites*, *45*, 148-156.

Chupanit, P. and Roesler, J.R. (2005), "Improvement of Concrete Cracking Resistance and Joint Load Transfer through Coarse Aggregate Selection," *Transportation Research Record 1913, Journal of Transportation Research Board*, National Research Council, Washington, D.C, pp. 3-10.

City of Columbus. Supplemental Specification 1523 Roller Compacted Concrete Pavements (RCC), Columbus, Ohio, 2010.

City of Hutchinson. Specifications and Contract Documents for City of Hutchinson NEGVI Trail Project (Phase III), City of Hutchinson, Kansas, 2011.

Cook, D., Ghaeezadeh, A., Ley, T., & Russell, B. (2013). Investigation of optimized graded concrete for Oklahoma–Phase I. *Report-FHWA-OK-13-12*.

Courard, L., Michel, F., Delhez, P. (2010). "Use of Concrete Road Recycled Aggregates for Roller Compacted Concrete." *Construction and Building Materials*, 24 (3), 390-395.

Cui, X., Zhang, J., Gao, Z., Wang, Z., & Sui, W. (2014, June). Effects of specimen size and crack depth ratio on double-K fracture model parameters of roller compacted concrete. In *Recent Developments in Evaluation of Pavements and Paving Materials* (pp. 98-105). ASCE.

D'Ambrosia, M. (2011). Early age creep and shrinkage of emerging concrete materials. Ph.D. Thesis. University of Illinois at Urbana-Champaign. 212 p.

Damrongwiriyanupap, N., Liang, Y. C., & Xi, Y. (2012). *Application of Roller Compacted Concrete in Colorado's Roadways* (No. CDOT-2012-11).

Dasmeh, A., A. Fakher, M. Shekarchi And M. Gharavy, "The Influence Of Compaction Time On The Mechanical Properties Of RCC," *Int J Hydropower Dams,* Vol. 7, Pp. 60-63, 2000.

Davis, A. G., Ansari, F., Gaynor, R. D., Lozen, K. M., Rowe, T. J., Caratin, H., ... & Hertlein, B. H. (1998). Nondestructive test methods for evaluation of concrete in structures. *American Concrete Institute, ACI*, *228*.

De Larrard, F., & Sedran, T. (2002). Mixture-proportioning of high-performance concrete. *Cement and concrete research*, *32*(11), 1699-1704.

Debieb, F., Courard, L., Kenai, S., Degeimbre, R. (2009). "Roller Compacted Concrete with Contaminated Recycled Aggregates." *Construction and Building Materials*, 23 (11), 3382-3387.

Delagrave, A., Marchand, J., Pigeon, M., & Boisvert, J. (1997). Deicer salt scaling resistance of roller-compacted concrete pavements. *ACI Materials Journal*, *94*, 164-169.

Delatte, N., & Storey, C. (2005). Effects of density and mixture proportions on freeze-thaw durability of roller-compacted concrete pavement. *Transportation Research Record: Journal of the Transportation Research Board*, (1914), 45-52.

Delgadillo, R., & Bahia, H. U. (2008). Effects of temperature and pressure on hot mixed asphalt compaction: field and laboratory study. *Journal of materials in civil engineering*, *20*(6), 440-448.

Federal Highway Administration (FHWA). (2010). Superpave Gyratory Compactors. FHWA, Washington, D.C.

Ferrebee, E., Brand, A., Kachwalla, A., Roesler, J., Gancarz, D., & Pforr, J. (2014). Fracture properties of

roller-compacted concrete with virgin and recycled aggregates. *Transportation Research Record: Journal of the Transportation Research Board*, (2441), 128-134.

Gaedicke, C., Roesler, J., Evangelista, F. (2012). "Three-Dimensional Cohesive Crack Model Prediction of the Flexural Capacity of Concrete Slabs on Soil. *Engineering Fracture Mechanics*, 94, 1-12.

Gao, P. W., Wu, S. X., Lin, P. H., Wu, Z. R., & Tang, M. S. (2006). The characteristics of air void and frost resistance of RCC with fly ash and expansive agent. *Construction and Building Materials*, *20*(8), 586-590.

Gardiner, M. and Komas, T.. (2013). "NCHRP Synthesis 435: Recycled Materials and Byproducts in Highway Applications – Summary Report." Transportation Research Board, Washington, D.C.

Garg, N., and M. Thompson. (1996) "Lincoln Avenue Reclaimed Asphalt Pavement Base Project." *Transportation Research Record: Journal of the Transportation Research Board*, *No 1547*, Transportation Research Board of the National Academies, Washington, D.C.: 89-95.

GDOT. Section 442 - Roller Compacted Concrete Pavement, Georgia Department of Transportation, 2005.

Ghafoori, N., & Cai, Y. (1998). Laboratory-Made RCC containing Dry Bottom Ash: Part I—Mechanical Properties. *Materials Journal*, *95*(2), 121-130.

Ghafoori, N., & Cai, Y. (1998). Laboratory-made roller compacted concretes containing dry bottom ash: Part ii—long-term durability. *Materials Journal*,*95* (3), 244-251.

Gharavi, M. "Optimization Of Compacting Time With The Effects Of Different Pozzolans (Type And Dosage) On The Mechanical Properties Of RCC," In *Fourth International Symposium On Roller Compacted Concrete (RCC) Dams, Madrid, Spain,* 2003.

Gopalaratnam, V. S., Shah, S. P., Batson, G., Criswell, M., Ramakishnan, V., & Wecharatana, M. (1991). Fracture toughness of fiber reinforced concrete. *Materials Journal*, *88*(4), 339-353.

Graeff, A. G., Pilakoutas, K., Neocleous, K., & Peres, M. V. N. (2012). Fatigue resistance and cracking mechanism of concrete pavements reinforced with recycled steel fibres recovered from post-consumer tyres.*Engineering Structures*, *45*, 385-395.

Greene, J., A. Nazef, and B. Choubane. (2011). "Thirty-Year Performance Evaluation of Two-Layer Concrete Pavement System." *Transportation Research Record: Journal of the Transportation Research Board No. 2226*, Transportation Research Board of the National Academies, Washington D.C.: 21-29.

Grilli, A., M. Bocci, and A.M. Tarantino. (2013). "Experimental Investigation on Fiber-Reinforced Cement-Treated Materials Using Reclaimed Asphalt." *Construction and Building Materials 38*: 491-496.

Guinea, G. V., El-Sayed, K., Rocco, C. G., Elices, M., & Planas, J. (2002). The effect of the bond between the matrix and the aggregates on the cracking mechanism and fracture parameters of concrete. *Cement and concrete research*, *32*(12), 1961-1970.

Guthrie, W., J. Michener, B. Wilson and D. Eggett, "Effects of Environmental Factors On Construction Of Soil-Cement Pavement Layers," *Transportation Research Record: Journal Of The Transportation*

Research Board, Pp. 71-79, 2009.

Halsted, G.E. "Roller-Compacted Concrete Pavements For Highways And Streets," In *2009 Annual Conference Of The Transportation Association Of Canada,* Vancouver, British Columbia, 2009.

Halsted, G. E., Luhr, D. R., & Adaska, W. S. (2006). *Guide to Cement-Treated Base (CTB)*.

Haque, M. and Ward, M. (1986). "Marginal Materials in Roller Compacted Concrete for Pavement Construction." *Journal of the American Concrete Institute*, 83 (4), 674-679.

Harrington, D., Abdo, F., Adaska, W., Hazaree, C. V., Ceylan, H., & Bektas, F. (2010). Guide for roller-compacted concrete pavements.

Harris, B., J. Varlow, and C. Ellis. (1972). "The Fracture Behavior of Fiber Reinforced Concrete." *Cement and Concrete Research, Vol. 2*, Pergamon Press: 447-461.

Hazaree, C., Ceylan, H., & Wang, K. (2011). Influences of mixture composition on properties and freeze–thaw resistance of RCC. *Construction and Building Materials*, *25*(1), 313-319.

Hazaree, C. V. (2010). Workability and strength attributes of RCC: Effects of different chemical admixtures and resulting paste.*Graduate Theses and Dissertations.* Paper 11250. http://lib.dr.iastate.edu/etd/11250

Hesami, S., Modarres, A., Soltaninejad, M., & Madani, H. (2016). Mechanical properties of roller compacted concrete pavement containing coal waste and limestone powder as partial replacements of cement.*Construction and Building Materials*, *111*, 625-636.

Hillerborg, A. (1985). "The Theoretical Basis of a Method to Determine the Fracture Energy G_F of Concrete." *Materials and Structures,* 18 (4), 291-296.

Hoppe, E. J., Lane, D. S., Fitch, G. M., & Shetty, S. (2015). *Feasibility of Reclaimed Asphalt Pavement (RAP) Use as Road Base and Subbase Material* (No. VCTIR 15-R6).

Hossain, M. S., & Ozyildirim, H. C. (2015, June). Roller Compacted Concrete Pavement in Virginia. In *Airfield and Highway Pavements 2015*.

Hou, X., P. Zhang, and M. Zhang. (2011). "Study on Fracture Toughness of Cement Treated Aggegate." *Advanced Materials Research, Vol. 280*. Trans Tech Publications, Switzerland: 76-79.

Huang, Y. (2004). "Pavement Analysis and Design." *Pearson Prentice Hall, 2nd ed.*, Upper Saddle River, NJ.

Huber, G. A., Harrigan, E. T., Cominsky, R. J., Hughes, C. S., Von Quintus, H., & Moulthrop, J. S. (1994). *Superior performing asphalt pavements (Superpave): The product of the SHRP asphalt research program* (No. SHRP-A-410). Strategic Highway Research Program, National Research Council.

IDOT. Circular Letter 2014-07: Roller Compacted Concrete Experimental Feature. Illinois Department of Transportation, Springfield, Illinois, 2014.

Indiana LTAP Center. The Indiana Local Technical Assistance Program Roller Compacted Concrete Pavement Manual for Local Government Agencies, TR-2-2010, Purdue University School of Civil Engineering, Nov. 2010.

Ioannides, A.M., Peng, J., Swindler, J.R. (2006). “ABAQUS Model for PCC Slab Cracking.” *International Journal of Pavement Engineering*, 7 (4), 311-321.

Jafarifar, N., Pilakoutas, K., & Bennett, T. (2015). The effect of shrinkage cracks on the load bearing capacity of steel-fibre-reinforced roller-compacted-concrete pavements. *Materials and Structures*, 1-19.

Jenq, Y. and Shah, S.P. (1985). “Two Parameter Fracture Model for Concrete.” *ASCE Journal of Engineering Mechanics*, 111 (10), 1227-1241.

Jingfu, K., Chuncui, H., & Zhenli, Z. (2009). Strength and shrinkage behaviors of roller-compacted concrete with rubber additives. *Materials and structures*, *42*(8), 1117-1124.

Johnston, C. and R. Zemp. (1991). “Flexural Fatigue Performance of Steel Fiber Reinforced Concrete-Influence of Fiber Content, Aspect Ratio, and Type.” *ACI Materials Journal, Vol. 88, Title No. 88-M44.* American Concrete Institute: 374-383.

Johnston, C. D., & Skarendahl, Å. (1992). Comparative flexural performance evaluation of steel fibre-reinforced concretes acoording to ASTM C1018 shows importance of fibre parameters. *Materials and Structures*, *25*(4), 191-200.

Käppi, A., & Nordenswan, E. (2007). Workability of no-slump concrete.*Concrete international*, *29*(03), 37-41.

Kar, A., Ray, I., Unnikrishnan, A., & Davalos, J. F. (2013). Composite modeling to predict shrinkage of concretes containing supplementary cementitious materials from paste volumes. *Construction and Building Materials*, *43*, 139-155.

Karimpour, A. (2010). Effect of time span between mixing and compacting on roller compacted concrete (RCC) containing ground granulated blast furnace slag (GGBFS). *Construction and Building Materials*, *24*(11), 2079-2083.

Kentucky Department of Highways. Bid Packet for Irvine-Winchester Road (KY 89), Kentucky Department of Highways, 2009.

Khayat, K. H., & Libre, P. N. A. (2014). *Roller Compacted Concrete: Field Evaluation and Mixture Optimization* (No. NUTC R363).

Kim, Y. (2007). Roller-compacted concrete shoulder construction on interstate highway in Georgia. *Transportation Research Record: Journal of the Transportation Research Board*, (2040), 71-79.

Kogan, E. A. (1991). Creep of roller-compacted concrete. *Hydrotechnical Construction*, *25*(3), 147-152.

Kokubun, S., & Kagaya, M. (2001). A study on properties of steel fibre reinforced roller compacted concrete for pavements. In *Akita University, Proceedings of the Fourth International Conference on Materials Enginering Resources,* (Vol. 1, pp. 65-70).

LaHucik, J. (2016) "Improving Material Constituents and Proportion Selection for Roller-Compacted Concrete Mix Design and Mechanical Properties." MS thesis. University of Illinois at Urbana-Champaign.

LaHucik, J., & Roesler, J. (2015). Low fines content roller-compacted concrete. In *International Airfield*

and Highway Pavements Conference, ASCE, Miami, Florida, 441-452.

LaHucik, J., & Roesler, J. (2016). Recycled aggregates in roller-compacted concrete. In *11th International Conference on Concrete Pavements*, San Antonio, Texas. Accepted for publication.

Lamond, J.F. and J. H. Pielert, "Significance Of Tests And Properties Of Concrete And Concrete-Making Materials," In Anonymous ASTM International, 2006, Pp. 595-604.

Lange, D., & Shin, H. C. (2001). Early age stresses and debonding in bonded concrete overlays. *Transportation Research Record: Journal of the Transportation Research Board*, (1778), 174-181.

Lecomte, A. (2006). The measurement of real and virtual packing density of soft grains. *Materials and structures*, *39*(1), 63-80.

Lee, C. J., Lange, D. A., & Liu, Y. S. (2011). Prediction of moisture curling of concrete slab. *Materials and structures*, *44*(4), 787-803.

Ley, T. and D. Cook. (2014). Aggregate gradations for concrete pavement mixtures. Federal Highway Administration.

Li, Q., Zhang, F., Zhang, W., & Yang, L. (2002). Fracture and tension properties of roller compacted concrete cores in uniaxial tension. *Journal of materials in civil engineering*, *14*(5), 366-373.

Lindquist, W., Darwin, D., Browning, J., McLeod, H. A., Yuan, J., & Reynolds, D. (2015). Implementation of concrete aggregate optimization.*Construction and Building Materials*, *74*, 49-56.

Loukili, A., Khelidj, A., & Richard, P. (1999). Hydration kinetics, change of relative humidity, and autogenous shrinkage of ultra-high-strength concrete.*Cement and Concrete Research*, *29*(4), 577-584.

Luhr, D.R. "Design and Construction Of Roller-Compacted Concrete Pavements For Container Terminals," In *Port Development In The Changing World. Ports 2004,* 2004.

Madhkhan, M., Azizkhani, R., & Harchegani, M. T. (2012). Effects of pozzolans together with steel and polypropylene fibers on mechanical properties of RCC pavements. *Construction and Building Materials*, *26*(1), 102-112.

Mardani-Aghabaglou, A., Andiç-Çakir, Ö., & Ramyar, K. (2013). Freeze–thaw resistance and transport properties of high-volume fly ash roller compacted concrete designed by maximum density method. *Cement and Concrete Composites*, *37*, 259-266.

Mardani-Aghabaglou, A., & Ramyar, K. (2013). Mechanical properties of high-volume fly ash roller compacted concrete designed by maximum density method. *Construction and Building Materials*, *38*, 356-364.

Mason, R.L., Gunst R.F., Hess, J.L. (2003). *Statistical Design and Analysis of Experiments*. Hoboken: John Wiley & Sons.

Matsumoto, T. and V. Li. (1999). “Fatigue Life Analysis of Fiber Reinforced Concrete with a Fracture Mechanics Based Model.” *Cement & Concrete Composites 21*. Elsevier: 249-261.

Millard, S. G., & Johnson, R. P. (1984). Shear transfer across cracks in reinforced concrete due to aggregate interlock and to dowel action. *Magazine of concrete research*, *36*(126), 9-21.

Mindess, S., Young, J. F., & Darwin, D. (2003). *Concrete*.

Missouri Highways and Transportation Commission. General Provisions and Supplemental Specifications to 2011 Missouri Standard Specifications for Highway Construction, Missouri Highways and Transportation Commission, Jefferson City, Missouri, 2013.

MnDOT. Specification for Roller Compacted Concrete (RCC), Minnesota Department of Transportation, 2011.

Modarres, A. and Hosseini, Z. (2014). "Mechanical Properties of Roller Compacted Concrete Containing Rice Husk Ash with Original and Recycled Asphalt Pavement Material." *Materials and Design*, 64, 227-236.

Mohammadinia, A., Arulrajah, A., Sanjayan, J., Disfani, M. M., Bo, M. W., & Darmawan, S. (2015). Geotechnical Properties of Lightly Stabilized Recycled Demolition Materials in Base/Sub-Base Applications. In *IFCEE 2015* (pp. 2767-2776). ASCE.

Montgomery, D.G. and Wang, G. (1992). "Instant-Chilled Steel Slag Aggregate in Concrete – Fracture Related Properties." *Cement and Concrete Research*, 22, 755-760.

Muscalu, M., Radu, A., Budescu, M., Taranu, N., Florescu, E. (2013). "Use of Recycled Materials in the Construction of Roller Compacted Concrete (RCC) Pavements." *Advanced Materials Research*, 649, 262-265.

Mushota, C., M. Mwale, G. Mutembo, M. Muya, and L. Walubita. (2014). "Reflective Cracking on Cement Treated Base (CTB) Pavements in Zambia: An Analytical Study." *Application of Nanotechnology in Pavements, Geological Disasters, and Foundation Settlement Control Technology.* ASCE: 62-69.

Mwumvaneza, V., W. Hou, H. Ozer, E. Tutumluer, I. Al-Qadi, and S. Beshears. (2015). "Characterization and Stabilization of Quarry Byproducts for Sustainable Pavement Applications." *Transportation Research Board 94th Annual Meeting 15-4464*, Transportation Research Board, Washington, D.C.: 17.

Naik, T. R., Chun, Y. M., Kraus, R. N., Singh, S. S., Pennock, L. L. C., & Ramme, B. W. (2001). Strength and durability of roller-compacted HVFA concrete pavements. *Practice Periodical on Structural Design and Construction*, *6*(4), 154-165.

Nanni, A. (1988). "Limestone Crusher-run and Tailings in Compaction Concrete for Pavement Applications." *ACI Materials Journal*, 85 (3), 158-163.

Nanni, A., & Johari, A. (1989). RCC pavement reinforced with steel fibers.*Concrete International*, *11*(3), 64-69.

Nanni, A., Ludwig, D. A., & Shoenberger, J. E. (1996). Physico-Mechanical Properties and Load Transfer Efficiency of RCC Pavement. *ACI Materials Journal*, *93*, 356-361.

NCDOT. Final Request for Proposals on I-85 Design-Build Project, North Carolina Department of Transportation, Raleigh, North Carolina, 2014.

Neocleous, K., Angelakopoulos, H., Pilakoutas, K., & Guadagnini, M. (2011). Fibre-reinforced roller-compacted concrete transport pavements.*Proceedings of the ICE-Transport*, *164*(TR2), 97-109.

Nguyen, M, Jones, D, Harvey, J. (2012). "Accelerated Pavement Testing Experiment of a Pavement Made of Fiber-Reinforced Roller-Compacted Concrete. In *Advances in Pavement Design Through Full-scale Accelerated Pavement Testing*. Hoboken: CRC Press. 299-311.

Nili, M., & Zaheri, M. (2011). Deicer salt-scaling resistance of non-air-entrained roller-compacted concrete pavements. *Construction and Building Materials*, *25*(4), 1671-1676.

ODOT. Special Provisions for Roller Compacted Concrete Pavement, Oklahoma Department of Transportation, 2000.

Olubanwo, A. O., & Karadelis, J. N. (2015). Applied mixture optimization techniques for paste design of bonded roller-compacted fibre reinforced polymer modified concrete (BRCFRPMC) overlays. *Materials and Structures*,*48* (7), 2023-2042.

Østergaard, L., Lange, D. A., Altoubat, S. A., & Stang, H. (2001). Tensile basic creep of early-age concrete under constant load. *Cement and concrete research*, *31*(12), 1895-1899.

Pavan, S., & Rao, S. K. (2014). Effect of Fly Ash on Strength Characteristics of Roller Compacted Concrete Pavement. *IOSR Journal of Mechanical and Civil Engineering (IOSR-JMCE)*, *11*(6), 04-08.

PCA. Guide Specification for Construction of Roller-Compacted Concrete Pavements, IS009, Portland Cement Association, Skokie, IL, 2004.

Peng, G. F., Niu, X. J., & Long, Q. Q. (2015). Experimental Study of Strengthening and Toughening for Recycled Steel Fiber Reinforced Ultra-High Performance Concrete. In *Key Engineering Materials* (Vol. 629, pp. 104-111). Trans Tech Publications.

Piggott, R. W. (1987). Ten Years of Heavy-Duty Pavement in Western Canada. *Concrete International*, *9*(2), 49-54.

Pittman, D. W. (1989). *The Effects of the Construction Process on Selected Fresh and Hardened Properties of Roller-Compacted Concrete (RCC) Pavements* (No. WES/MP/GL-89-22). ARMY ENGINEER WATERWAYS EXPERIMENT STATION VICKSBURG MS GEOTECHNICAL LAB.

Pittman, D. W., & Ragan, S. A. (1998). Drying shrinkage of roller-compacted concrete for pavement applications. *Materials Journal*, *95*(1), 19-26.

Plessis, L., Louw, S. J. H., Rugodho, G., & Musundi, S. (2012). Provisional results from accelerated pavement testing of roller-compacted concrete in South Africa. *Advances in Pavement Design through Full-scale Accelerated Pavement Testing*, 313.

Popovics, J., J. Roesler, C. Peterson, A. Salas, S. Ham, "High Plastic Concrete Temperature Specifications For Paving Mixtures," Tech. Rep. FHWA-ICT-11-087, August. 2011.

Prusinski, J. (2016). Evolution of RCC Construction in Texas. Presented at *Spring 2016 American Concrete Institute Convention,* Milwaukee, Wisconsin.

Puppala, A.J., S. Saride, S.K. Sirigiripet, and R. Williammee. (2008). "Evaluation of Cemented Quarry Fines as a Pavement Base Material." *ASCE Geotechnical Special Publication 177, Geo-Congress*, New Orleans, Louisiana: 312-319.

Puppala, Anand J., S. Saride, and R. Williammee. (2012). “Sustainable Reuse of Limestone Quarry Fines and RAP in Pavement Base/Subbase Layers.” *Journal of Materials in Civil Engineering 24(4),* ASCE 2012: 418-29.

Qasrawi, H. Y., Asi, I. M., & Wahhab, H. A. (2005). Proportioning rccp mixes under hot weather conditions for a specified tensile strength. *Cement and Concrete Research*, *35*(2).

Ragan, S.A. (1986). Evaluation of the frost resistance of roller-compacted concrete pavements. Miscellaneous Paper SL-86-16, U.S. Army Corps of Engineers, Washington, D.C., USA.

Ranaivomanana, N., Multon, S., & Turatsinze, A. (2013). Tensile, compressive and flexural basic creep of concrete at different stress levels. *Cement and Concrete Research*, *52*, 1-10.

Rao, S. K., Sravana, P., & Rao, T. C. (2016). Experimental studies in ultrasonic pulse velocity of roller compacted concrete containing GGBS and M-sand. *ARPN Journal of Engineering and Applied Sciences*, *11*(3).

Rezende, L., L. Silveira, W. Araújo, and M. Luz. (2014). “Reuse of Fine Quarry Wastes in Pavement: Case Study in Brazil.” *Journal of Materials in Civil Engineering*, 26(8). ASCE 2014: Case Study.

Richardson, D. N. (2005). Aggregate gradation optimization: literature search.

Rodden, R. (2013). RCC fatigue model development by the American Concrete Pavement Association (ACPA) – interim report. *American Concrete Pavement Association (ACPA)*.

Roesler, J, D. Lange, S. Altoubat, K. Rieder, and G. Ulreich. (2004). “Fracture of Plain and Fiber-Reinforced Concrete Slabs under Monotonic Loading.” *Journal of Materials in Civil Engineering, Sept/Oct*. ASCE: 452-460.

Roesler, J., G. Paulino, C. Gaedicke, A. Bordelon, and K. Park. (2007). “Fracture Behavior of Functionally Graded Concrete Materials for Rigid Pavements.” *Transportation Research Record: Journal of the Transportation Research Board No. 2037*, Transportation Research Board of the National Academies, Washington D.C.: 40-49.

Roesler, J., V. Cervantes, and A. Amirkhanian. (2012). “Accelerated Performance Testing of Concrete Pavement with Short Slabs.” *International Journal of Pavement Engineering, 13:6,* 494-507.

Rossi, P., Tailhan, J. L., Le Maou, F., Gaillet, L., & Martin, E. (2012). Basic creep behavior of concretes investigation of the physical mechanisms by using acoustic emission. *Cement and Concrete Research*, *42*(1), 61-73.

Rupnow, T., Schaefer, V., & White, D. (2010). Investigation of the Use of Limestone Screenings in Roadway Construction. *Transportation Research Record: Journal of the Transportation Research Board*, (2167), 53-60.

Sachet, T., Albuquerque, M.C.F., Balbo, J.T., Sansone, C.E. (2011). “Investigation of Resistance and Fracture Parameters for Compacted Concrete with Incorporation of Reclaimed Asphalt Pavement.” *International Journal of Pavements*, 10, 83-93.

Sachet, T., Balbo, J.T., Bonsembiante, F.T. (2013). “Rendering the Loss of Strength in Dry Concretes with Addition of Milled Asphalt Through Microscopic Analysis.” *IBRACON Structures and Materials Journal*, 6, 933-943.

Sagoe-Crentsil, K. K., Brown, T., & Taylor, A. H. (2001). Performance of concrete made with commercially produced coarse recycled concrete aggregate. *Cement and concrete research*, *31*(5), 707-712.

Şahin, Y., & Köksal, F. (2011). The influences of matrix and steel fibre tensile strengths on the fracture energy of high-strength concrete.*Construction and Building Materials*, *25*(4), 1801-1806.

SCDOT. Proposal for Construction on Road S-2304 (Powell Pond Rd.), South Carolina Department of Transportation, Columbia, South Carolina, 2001.

Schroeder, R.L. (1994). The use of recycled materials in highway construction. *Public Roads*, 57(2).

Senol, A., T.B. Edil And M.S.B. Shafique, "Laboratory Evaluation Of Stabilization Of Soft Subgrades By Class C Fly Ash," In *15th Southeast Asian Geotechnical Society Conference,* Bangkok, Thailand, 2004.

Shihata, S. A. (2000). Strength and Density of Laboratory-Prepared RCC Specimens: Effect of Compaction Procedure. *Cement, Concrete and Aggregates*, *22*(1), 1-9.

Shilstone, J. S. (1990). Concrete mixture optimization. *Concrete International*, *12*(6), 33-39.

Sobhan, K and Mashnad, M. (2001). "Roller-Compacted Fiber Concrete Pavement Foundation with Recycled Aggregate and Waste Plastics." *Transportation Research Record*, 1775, 53-63.

Sobhan, K. and Mashnad, M. (2002). "Fatigue Damage in Roller-Compacted Pavement Foundation with Recycled Aggregate and Waste Plastic Strips." *Transportation Research Record*, 1798, 8-16.

Sobhan, K. and R. Krizek. (1999). "Fatigue Behavior of Fiber-Reinforced Recycled Aggregate Base Course." *Journal of Materials in Civil Engineering, May, 11:2.* ASCE: 124-130.

Song, Y. (2014). Analysis of air-void system in hardened concrete from a three-dimensional perspective. University of Illinois at Urbana-Champaign Master's Thesis.

Soroushian, P., Obaseki, K., & Choi, K. B. (1988). Analysis of aggregate interlock behaviour at cracks in reinforced concrete. *Magazine of Concrete Research*, *40*(142), 43-49.

Syed, I., & Scullion, T. (2001). Performance evaluation of recycled and stabilized bases in Texas. *Transportation Research Record: Journal of the Transportation Research Board*, (1757), 14-21.

Symons, I.F. (1970). The effect of size and shape of specimen upon the unconfined compressive strength of cement-stabilized materials. *Magazine of Concrete Research,* 22(70), 45-50.

Taha, R., A. Al-Harthy, K. Al-Shamsi, and M. Al-Zubeidi. (2002). "Cement Stabilization of Reclaimed Asphalt Pavement Aggregate for Road Bases and Subbases." *Journal of Materials in Civil Engineering 14(3)*, ASCE 2002: 239-245.

Tanesi, J., Ardani, A., & Leavitt, J. (2013). Reducing the Specimen Size of the AASHTO T 97 Concrete Flexural Strength Test for Safety and Ease of Handling. *Transportation Research Record: Journal of the Transportation Research Board*, (2342), 99-105.

Tangtermsirikul, S., Kaewkhluab, T., & Jitvutikrai, P. (2004). A compressive strength model for roller-compacted concrete with fly ash. *Magazine of Concrete Research*, *56*(1), 35-44.

Tayabji, S. and Okamoto, P. (1987). Engineering properties of roller-compacted concrete. *Transportation Research Record*, 1136, 33-45.

Taylor, P. (2015). Blended aggregates for concrete mixture optimization – best practices for jointed concrete pavements. Federal Highway Administration: FHWA-HIF-15-019.

TDOT. Special Provision Regarding Roller Compacted Concrete Pavement, Tennessee Department of Transportation, 2015.

Topçu, İ.B. and V. B. Elgün, "Influence Of Concrete Properties On Bleeding And Evaporation," *Cem. Concr. Res.,* Vol. 34, Pp. 275-281, 2004.

Tutumluer, E. (2013). Practices for unbound aggregate pavement layers: a synthesis of highway practice. *National Cooperative Highway Research Program (NCHRP), NCHRP Synthesis*, *445*.

TxDOT. Special Specification 3258 Roller Compacted Concrete, Texas Department of Transportation, 2004.

Vahedifard, F., Nili, M., & Meehan, C. L. (2010). Assessing the effects of supplementary cementitious materials on the performance of low-cement roller compacted concrete pavement. *Construction and Building Materials*,*24*(12), 2528-2535.

Van Dam, T., Taylor, P., Fick, G., Gress, D., VanGeem, M., Lorenz, E. (2011). "Sustainable Concrete Pavements: A Manual of Practice." National Concrete Pavement Technology Center, Ames, Iowa.

Vandenbossche, J. M., Dufalla, N., & Li, Z. (2016). Bonded concrete overlay of asphalt mechanical-empirical design procedure. *International Journal of Pavement Engineering*, 1-12.

Villena, J, Trichês, G, Prudêncio, L. (2011). "Replacing the Aggregate by Rice Husk Ash in Roller Compacted Concrete for Composite Pavements." *ASCE Geotechnical Special Publication No. 212*, 19-27.

Williams, S. (2013). Comparison of the Superpave Gyratory and Proctor Compaction Methods for the Design of Roller-Compacted Concrete Pavements. *Transportation Research Record: Journal of the Transportation Research Board*, (2342), 106-112.

Williams, S. (2014). Construction of Roller-Compacted Concrete Pavement in the Fayetteville Shale Play Area, Arkansas. *Transportation Research Record: Journal of the Transportation Research Board*, (2408), 47-54.

Wu, Z., & Mahdi, M. (2015). Roller Compacted Concrete over Soil Cement under Accelerated Loading. In *Airfield and Highway Pavements 2015*(pp. 418-428).

WVDOH. Supplemental Specifications to Accompany the 2010 Edition of the Standard Specifications Roads and Bridges, West Virginia Division of Highways, 2011.

Xie, J. B., He, T. C., Fan, J., & Ai, Y. P. (2011). Study on the Properties of Roller Compacted Concrete in the Dam of Jinghong Hydropower Station. *Applied Mechanics and Materials*, *90*, 2541.

Yandong, J., Zhou, Z. W., Qu, Y. D., & Tian, A. S. (2011). Experimental Research on the Fracture Properties of Roller Compacted Steel Fiber Recycled Concrete. In *Advanced Materials Research* (Vol. 299, pp. 135-138).

Yazici, S., Mardani-Aghabaglou, A., Tuyan, M., & Ute, A. A. (2015). Mechanical properties and impact resistance of roller-compacted concrete containing polypropylene fibre. *Magazine of Concrete Research*, *67*(16), 867-875.

Yeon, J. H., Choi, S., Ha, S., & Won, M. C. (2012). Effects of creep and built-in curling on stress development of Portland cement concrete pavement under environmental loadings. *Journal of Transportation Engineering*, *139*(2), 147-155.

Yerramala, A., & Babu, K. G. (2011). Transport properties of high volume fly ash roller compacted concrete. *Cement and Concrete Composites*, *33*(10), 1057-1062.

Zeng, L., Wu, D., Zhang, Y. (2011). Research on crack resistance of roller compacted concrete (RCC). *Advanced Materials Research, 168,* 1900-1903.

Zhang, J., Hou, D., & Gao, Y. (2013). Calculation of shrinkage stress in early-age concrete pavements. I: Calculation of shrinkage strain. *Journal of Transportation Engineering*, *139*(10), 961-970.

APPENDIX A: AGGREGATE PACKING TEST DATA

This appendix contains raw data from aggregate packing tests in Appendix F that was used to calibrate the aggregate packing model.

A.1 COARSE DOLOMITE

Table A1. Data from Vibrating Table Compaction of Coarse Dolomite (1 in = 25.4 mm)

Test #	Broken Particles (%)	Experimental Packing Density	Volume Fraction of Aggregate Sieve Size (mm)						
			19	12.7	9.5	4.75	2.38	1.19	Pass 1.19
1	5.977	0.531	0.940	0.057	0.001	0.000	0.000	0.000	0.002
2	6.768	0.538	0.932	0.062	0.001	0.001	0.001	0.001	0.002
3	6.207	0.543	0.938	0.060	0.001	0.000	0.000	0.000	0.001
4	4.914	0.546	0.013	0.938	0.040	0.000	0.000	0.000	0.009
5	2.760	0.552	0.033	0.939	0.025	0.001	0.000	0.000	0.002
6	2.269	0.538	0.015	0.963	0.020	0.001	0.000	0.000	0.001
7	1.897	0.547	0.000	0.022	0.959	0.018	0.000	0.000	0.001
8	2.583	0.535	0.000	0.023	0.952	0.025	0.000	0.000	0.001
9	2.503	0.545	0.000	0.017	0.957	0.023	0.000	0.000	0.001
10	1.945	0.560	0.000	0.000	0.013	0.968	0.016	0.001	0.002
11	1.701	0.566	0.000	0.000	0.015	0.968	0.016	0.000	0.001
12	1.432	0.551	0.000	0.000	0.029	0.957	0.010	0.002	0.001
13	1.429	0.571	0.000	0.000	0.000	0.011	0.974	0.014	0.001
14	2.003	0.573	0.000	0.000	0.000	0.008	0.972	0.018	0.002
15	1.541	0.568	0.000	0.000	0.000	0.008	0.976	0.014	0.001
16	1.078	0.564	0.000	0.000	0.000	0.001	0.047	0.941	0.011
17	1.099	0.571	0.000	0.000	0.000	0.000	0.028	0.961	0.011
18	0.904	0.571	0.000	0.000	0.000	0.000	0.044	0.947	0.009

Table A2. Data from Modified Proctor Compaction of Coarse Dolomite (1 in = 25.4 mm)

Test #	Broken Particles (%)	Experimental Packing Density	Volume Fraction of Aggregate Sieve Size (mm)						
			19	12.7	9.5	4.75	2.38	1.19	Pass 1.19
1	45.405	0.728	0.546	0.227	0.045	0.071	0.042	0.024	0.044
2	39.038	0.705	0.610	0.187	0.041	0.065	0.038	0.021	0.039
3	34.595	0.709	0.654	0.173	0.034	0.053	0.030	0.017	0.038
4	42.126	0.711	0.000	0.579	0.160	0.117	0.054	0.033	0.057
5	36.193	0.698	0.000	0.638	0.139	0.098	0.047	0.025	0.054
6	39.450	0.681	0.000	0.606	0.147	0.107	0.052	0.030	0.059
7	50.723	0.717	0.000	0.000	0.493	0.315	0.079	0.044	0.070
8	53.345	0.727	0.000	0.000	0.467	0.337	0.081	0.045	0.071
9	51.130	0.705	0.000	0.000	0.489	0.340	0.069	0.038	0.064
10	31.667	0.699	0.000	0.000	0.000	0.683	0.166	0.057	0.094
11	32.290	0.697	0.000	0.000	0.000	0.677	0.182	0.057	0.084
12	31.506	0.661	0.000	0.000	0.000	0.685	0.178	0.051	0.086
13	26.654	0.689	0.000	0.000	0.000	0.000	0.733	0.147	0.120
14	29.142	0.694	0.000	0.000	0.000	0.000	0.709	0.156	0.136
15	25.724	0.675	0.000	0.000	0.000	0.000	0.743	0.128	0.129
16	22.832	0.681	0.000	0.000	0.000	0.000	0.000	0.772	0.228
17	25.923	0.699	0.000	0.000	0.000	0.000	0.000	0.741	0.259
18	24.949	0.686	0.000	0.000	0.000	0.000	0.000	0.751	0.249

Table A3. Data from Gyratory Compaction of Coarse Dolomite (1 in = 25.4 mm)

Test #	Broken Particles (%)	Experimental Packing Density	Volume Fraction of Aggregate Sieve Size (mm)						
			19	12.7	9.5	4.75	2.38	1.19	Pass 1.19
1	36.459	0.642	0.635	0.228	0.029	0.045	0.024	0.014	0.025
2	39.440	0.644	0.606	0.244	0.032	0.048	0.027	0.016	0.027
3	29.872	0.615	0.701	0.185	0.034	0.036	0.019	0.009	0.016
4	32.040	0.648	0.000	0.680	0.156	0.080	0.036	0.018	0.030
5	30.169	0.653	0.038	0.661	0.134	0.076	0.032	0.024	0.035
6	26.800	0.664	0.054	0.678	0.111	0.076	0.031	0.020	0.031
7	27.286	0.677	0.000	0.413	0.314	0.155	0.049	0.027	0.042
8	28.667	0.652	0.000	0.273	0.440	0.179	0.047	0.027	0.033
9	33.031	0.643	0.000	0.086	0.584	0.220	0.050	0.026	0.034
10	24.710	0.677	0.000	0.000	0.008	0.745	0.144	0.046	0.057
11	25.838	0.649	0.000	0.000	0.006	0.736	0.162	0.049	0.047
12	25.227	0.634	0.000	0.000	0.006	0.742	0.169	0.043	0.040
13	13.512	0.620	0.000	0.000	0.000	0.008	0.857	0.089	0.046
14	12.908	0.616	0.000	0.000	0.000	0.009	0.861	0.083	0.046
15	14.624	0.621	0.000	0.000	0.000	0.008	0.845	0.097	0.049
16	11.479	0.613	0.000	0.000	0.000	0.000	0.003	0.882	0.115
17	10.722	0.617	0.000	0.000	0.000	0.000	0.005	0.888	0.107
18	10.422	0.618	0.000	0.000	0.000	0.000	0.005	0.891	0.104

Table A4. Data for Gyratory Compaction Evolution of Coarse Dolomite. (1 in = 25.4 mm & 1 kg = 2.2 lbs)

Test #	Weight (kg)	Height of Aggregate Sample (mm) as a Function of Number of Gyrations											
		1	5	10	20	30	40	50	60	70	80	90	100
1	3.907	157.4	151.6	147.7	141.9	138.1	135.4	133	130.7	128.8	127.4	126	125
2	3.620	150.5	145.2	140.7	134.6	130	126.9	124.3	122.1	120.4	118.6	116.9	115.4
3	3.922	158.7	154.6	151.2	146.3	142.7	140.3	138.6	136.9	135.1	133.6	132.2	130.9
4	3.711	151.6	145.6	141.5	135.8	132.1	129.1	126.3	123.6	121.7	120.1	118.8	117.6
5	3.799	153.6	147.3	143.3	138	134	130.4	127.8	125.7	124	121.9	120.6	119.4
6	3.707	145.6	141	137.1	131.3	127.1	124.2	121.8	120.2	118.8	117.1	115.9	114.7
7	3.463	139.7	134.6	130.1	123.7	118.5	115.1	112.6	110.2	108.6	107.5	105.9	105
8	3.817	157.3	149.5	145	139.7	135.6	132.2	129	126.8	124.5	123	121.4	120.2
9	3.781	152.2	146.6	143.2	137.9	134.2	131.1	128.7	126.8	125.1	123.5	122.1	120.8
10	3.545	139.8	134.8	130.9	124.9	120.8	117.5	115	113.1	111.4	110.1	108.9	107.5
11	4.188	165	158.7	154.7	150.1	146.4	145.4	141	138.9	137.1	135.5	133.9	132.5
12	4.191	169.5	161.4	156.9	152	148.3	145.3	143	141.1	139.3	138	136.8	135.7
13	4.228	163.6	158.2	155.1	151.7	149.2	146.9	145.3	143.9	142.6	141.7	140.8	140.1
14	4.315	170.1	163.3	159.9	156.1	153.5	151.1	149.4	148.1	146.7	145.7	144.9	143.9
15	4.209	163.8	158.3	155.2	151.6	148.7	146.6	144.7	143.4	142.1	141.1	140	139.2
16	4.149	164.5	158	154.7	150.9	147.8	145.8	144	142.8	141.5	140.6	139.6	139
17	4.224	163	158.1	155.2	151.4	148.9	146.9	145.5	144	142.9	142.1	141.2	140.6
18	4.289	167	160.7	157.6	153.8	151.1	149.2	147.5	146.1	145.2	144.1	143.5	142.6

A.2 COARSE TRAP ROCK

Table A5. Data from Vibrating Table Compaction of Coarse Trap Rock* (1 in = 25.4 mm)

Test #	Broken Particles (%)	Experimental Packing Density	Volume Fraction of Aggregate Sieve Size (mm)			
			12.7	9.5	4.75	Pass 4.75
1	26.544	0.482	0.961	0.037	0.001	0.000
2	26.517	0.479	0.975	0.024	0.001	0.000
3	23.712	0.478	0.966	0.032	0.001	0.001
4	42.968	0.483	0.056	0.900	0.044	0.000
5	10.991	0.476	0.000	0.104	0.891	0.005
6	10.643	0.489	0.007	0.129	0.857	0.007
7	11.941	0.476	0.001	0.122	0.869	0.008
8	5.605	0.478	0.541	0.456	0.003	0.000
9	4.446	0.480	0.511	0.483	0.005	0.000
10	4.989	0.481	0.510	0.481	0.008	0.001
11	5.778	0.486	0.040	0.594	0.365	0.001
12	6.128	0.490	0.042	0.574	0.382	0.001
13	6.260	0.490	0.045	0.526	0.427	0.002
14	4.806	0.504	0.483	0.103	0.412	0.003
15	8.326	0.493	0.514	0.106	0.378	0.002
16	7.676	0.508	0.529	0.086	0.383	0.003
17	7.351	0.498	0.348	0.368	0.282	0.002
18	7.712	0.490	0.358	0.363	0.277	0.001
19	8.469	0.496	0.367	0.357	0.275	0.001
20	7.413	0.491	0.500	0.295	0.203	0.001
21	6.626	0.499	0.489	0.279	0.231	0.001
22	5.379	0.496	0.469	0.305	0.226	0.001
23	4.577	0.494	0.272	0.284	0.443	0.002
24	4.722	0.496	0.278	0.320	0.400	0.002

*Bold values indicate blended gradations (i.e. not mono-sized particles)

Table A6. Data from Modified Proctor Compaction of Coarse Trap Rock* (1 in = 25.4 mm)

Test #	Broken Particles (%)	Experimental Packing Density	Volume Fraction of Aggregate Sieve Size (mm)			
			12.7	9.5	4.75	Pass 4.75
1	32.493	0.627	0.675	0.171	0.075	0.079
2	32.768	0.582	0.672	0.195	0.068	0.065
3	29.589	0.583	0.704	0.161	0.067	0.067
4	31.085	0.567	0.000	0.689	0.222	0.089
5	27.897	0.569	0.006	0.715	0.200	0.079
6	25.923	0.564	0.009	0.732	0.183	0.076
7	14.647	0.539	0.000	0.000	0.854	0.146
8	14.507	0.553	0.000	0.000	0.855	0.145
9	13.866	0.547	0.000	0.000	0.861	0.139
10	3.413	0.560	0.448	0.341	0.178	0.034
11	8.305	0.585	0.377	0.342	0.198	0.083
12	8.009	0.567	0.350	0.337	0.233	0.080
13	10.528	0.584	0.008	0.275	0.612	0.105
14	13.400	0.550	0.011	0.310	0.544	0.134
15	8.353	0.553	0.004	0.353	0.559	0.084
16	7.123	0.596	0.325	0.033	0.570	0.071
17	7.641	0.583	0.282	0.042	0.600	0.076
18	8.201	0.558	0.269	0.051	0.598	0.082
19	8.005	0.567	0.185	0.275	0.459	0.080
20	7.412	0.614	0.203	0.257	0.465	0.074
21	7.174	0.601	0.239	0.291	0.398	0.072
22	6.860	0.609	0.296	0.292	0.344	0.069
23	6.325	0.602	0.348	0.270	0.318	0.063
24	2.936	0.604	0.370	0.300	0.300	0.029
25	2.887	0.598	0.182	0.257	0.532	0.029
26	4.246	0.592	0.193	0.259	0.505	0.042
27	5.667	0.599	0.135	0.261	0.547	0.057

*Bold values indicate blended gradations (i.e. not mono-sized particles)

Table A7. Data from Gyratory Compaction of Coarse Trap Rock* (1 in = 25.4 mm)

Test #	Broken Particles (%)	Experimental Packing Density	Volume Fraction of Aggregate Sieve Size (mm)			
			12.7	9.5	4.75	Pass 4.75
1	26.544	0.563	0.735	0.171	0.046	0.048
2	26.517	0.571	0.735	0.159	0.054	0.052
3	23.712	0.567	0.763	0.113	0.064	0.061
4	42.968	0.563	0.011	0.559	0.357	0.073
5	44.834	0.561	0.010	0.542	0.368	0.080
6	40.235	0.576	0.007	0.590	0.320	0.082
7	10.991	0.563	0.000	0.010	0.880	0.110
8	10.643	0.562	0.000	0.016	0.878	0.106
9	11.941	0.560	0.000	0.012	0.869	0.119
10	5.605	0.570	0.393	0.432	0.119	0.056
11	4.446	0.570	0.430	0.436	0.090	0.044
12	4.989	0.570	0.411	0.432	0.107	0.050
13	5.778	0.565	0.006	0.394	0.542	0.058
14	6.128	0.562	0.001	0.366	0.572	0.061
15	6.260	0.562	0.000	0.374	0.564	0.063
16	4.806	0.594	0.268	0.261	0.423	0.048
17	8.326	0.583	0.417	0.068	0.432	0.083
18	7.676	0.579	0.418	0.076	0.430	0.077
19	7.351	0.570	0.279	0.289	0.358	0.074
20	7.712	0.571	0.211	0.315	0.397	0.077
21	8.469	0.575	0.279	0.283	0.353	0.085
22	7.413	0.581	0.406	0.271	0.249	0.074
23	6.626	0.576	0.453	0.260	0.221	0.066
24	5.379	0.571	0.487	0.247	0.212	0.054
25	4.577	0.566	0.247	0.274	0.433	0.046
26	4.722	0.564	0.267	0.239	0.446	0.047

*Bold values indicate blended gradations (i.e. not mono-sized particles)

Table A8. Data for Gyratory Compaction Evolution of Coarse Trap Rock (1 kg = 2.2 lbs)

Test #	Weight (kg)	Height of Aggregate Sample (mm) as a Function of Number of Gyrations											
		1	5	10	20	30	40	50	60	70	80	90	100
1	4.707	190.9	184.1	179.1	173.9	170.9	168.3	166.6	165	163.8	162.8	161.4	160.4
2	4.721	191.7	184.2	179.4	173.9	169.9	167.1	165.2	163.3	161.9	160.7	159.6	158.5
3	4.666	192.6	185.7	179.8	173.8	170.1	167.6	165.3	163.5	161.7	160.2	158.9	157.9
4	4.596	191.9	182.8	177.2	171	167.6	164.9	163.1	161.3	159.9	158.5	157.4	156.4
5	4.535	190	183.4	177.8	171.4	167.1	163.9	161.8	159.9	158.4	157.1	156.1	154.9
6	3.550	144.5	138	134.1	129.6	126.7	124.7	123.3	122.3	121.2	120.2	119.1	118.1
7	4.548	184.5	178.2	173.5	168.3	165	162.9	160.8	159.3	158.2	156.9	156	155
8	4.390	182	174.3	169.2	163.5	160	157.4	155.7	154	152.8	151.5	150.6	149.8
9	4.515	186.9	180.5	175.4	169.6	166	163.1	161.3	159.4	157.8	156.7	155.4	154.5
10	4.839	193	186.6	182	177	173.6	171	169.3	167.6	166.5	165.1	164.1	162.9
11	4.831	188.1	182.6	178.9	174.4	171.7	169.3	167.8	166.3	165.3	164.1	163.2	162.4
12	4.950	192.2	186.8	183.1	178.8	176	174.3	172.6	171	169.8	168.6	167.6	166.5
13	4.734	186	179.8	176.2	172.3	169.6	167.5	165.8	164.8	163.5	162.5	161.5	160.7
14	4.841	191.3	185.7	181.7	177.3	174.4	172.3	170.6	169.2	167.8	166.7	165.7	165.1
15	4.916	195.1	188.4	184.6	180.1	177.3	175.2	173.5	172	170.7	169.6	168.6	167.6
16	5.130	197.1	190.4	185.4	179.5	176.1	173.7	171.8	169.9	168.5	167.4	166.3	165.5
17	4.870	191.7	186.8	182.8	176	171.8	168.9	166.5	164.9	163.4	162	161.1	160.1
18	5.120	198.8	193.3	188.8	183.1	179.9	177.5	175.8	174.2	172.7	171.5	170.5	169.5
19	4.989	197.8	192.8	188.4	182.5	178.9	176.3	174.3	172.6	171	169.8	168.7	167.8
20	4.967	199.7	192.8	187.6	181.5	178	175.6	173.6	171.9	170.4	169.1	167.8	166.8
21	4.764	190.6	185.7	180.8	174.4	170.8	168	166	164.2	162.6	161.2	160	158.8
22	4.745	189.4	182.7	177.7	171.8	168	165.2	163.3	161.7	160.2	158.8	157.7	156.6
23	4.888	194.5	189.2	184.4	178.4	174.9	172	169.8	168	166.3	164.8	163.6	162.7
24	4.908	193.2	187.3	183	177.9	174.7	172.5	170.6	169	167.7	166.7	165.6	164.8
25	5.168	197.8	193.9	190.6	186.2	183.4	181.4	179.9	178.4	177.5	176.6	175.6	175
26	5.048	197.2	192.6	188.3	183.1	180.1	178	176.4	175.2	174.2	173.3	172.3	171.6

*Bold values indicate blended gradations (i.e. not mono-sized particles)

A.3 INTERMEDIATE DOLOMITE

Table A9. Data from Vibrating Table Compaction of Intermediate Dolomite (1 in = 25.4 mm)

Test #	Broken Particles (%)	Experimental Packing Density	Volume Fraction of Aggregate Sieve Size (mm)			
			9.5	4.75	2.36	Pass 2.36
1	4.426	0.558	0.956	0.044	0.000	0.000
2	4.728	0.554	0.953	0.046	0.000	0.002
3	4.088	0.549	0.959	0.041	0.000	0.000
4	1.689	0.543	0.000	0.983	0.017	0.000
5	2.682	0.524	0.000	0.973	0.027	0.000
6	4.143	0.554	0.000	0.959	0.033	0.009
7	1.622	0.559	0.000	0.000	0.984	0.016
8	1.433	0.554	0.000	0.000	0.986	0.014
9	1.007	0.565	0.000	0.000	0.990	0.010

Table A10. Data from Modified Proctor Compaction of Intermediate Dolomite* (1 in = 25.4 mm)

Test #	Broken Particles (%)	Experimental Packing Density	Volume Fraction of Aggregate Sieve Size (mm)			
			9.5	4.75	2.36	Pass 2.36
1	36.609	0.686	0.634	0.260	0.045	0.061
2	44.759	0.705	0.552	0.304	0.061	0.083
3	33.371	0.675	0.666	0.249	0.038	0.047
4	30.827	0.684	0.000	0.692	0.158	0.151
5	29.622	0.683	0.000	0.704	0.156	0.140
6	33.503	0.703	0.000	0.665	0.181	0.154
7	23.213	0.672	0.000	0.000	0.768	0.232
8	24.480	0.696	0.000	0.000	0.755	0.245
9	27.731	0.716	0.000	0.000	0.723	0.277

Table A11. Data from Gyratory Compaction of Intermediate Dolomite* (1 in = 25.4 mm)

Test #	Broken Particles (%)	Experimental Packing Density	Volume Fraction of Aggregate Sieve Size (mm)			
			9.5	4.75	2.36	Pass 2.36
1	37.025	0.611	0.630	0.272	0.049	0.049
2	38.450	0.621	0.615	0.283	0.049	0.052
3	39.709	0.622	0.603	0.297	0.050	0.050
4	24.038	0.620	0.000	0.760	0.162	0.078
5	20.756	0.601	0.000	0.792	0.144	0.064
6	23.402	0.627	0.000	0.766	0.158	0.076
7	15.841	0.621	0.000	0.000	0.842	0.158
8	18.062	0.638	0.000	0.000	0.819	0.181
9	13.655	0.609	0.000	0.000	0.863	0.137

Table A12. Data for Gyratory Compaction Evolution of Intermediate Dolomite (1 in = 25.4 mm; 1 kg = 2.2 lbs)

Test #	Weight (kg)	Height of Aggregate Sample (mm) as a Function of Number of Gyrations											
		1	5	10	20	30	40	50	60	70	80	90	100
1	4.446	179.8	173.7	169.9	165.5	161.8	159.4	157.2	155.7	153.8	152.6	151.0	150.0
2	4.404	179.4	171.0	166.9	161.9	158.2	156.0	153.8	151.7	150.4	148.7	147.7	146.3
3	4.484	176.2	170.5	166.9	162.6	159.6	157.3	155.3	153.5	152.1	150.9	149.8	148.6
4	4.529	179.9	173.6	169.4	164.6	161.4	159.1	157.2	155.7	154.5	153.2	151.4	150.5
5	4.702	189.7	181.9	178.3	174.3	171.9	169.8	168.0	166.4	164.8	163.6	162.5	161.2
6	4.148	170.3	162.2	158.0	152.8	149.1	146.1	144.0	142.1	140.6	139.0	137.8	136.5
7	4.536	181.7	173.4	169.2	164.1	161.0	158.8	157.1	155.5	154.1	152.9	151.7	150.7
8	4.091	163.8	156.9	152.5	146.8	143.4	140.8	138.8	137.1	135.9	134.3	133.2	132.2
9	4.858	191.7	184.6	180.1	175.2	172.5	170.6	169.0	167.7	166.7	165.8	165.0	164.4

A.4 INTERMEDIATE RIVER GRAVEL

Table A13. Data from Vibrating Table Compaction of Intermediate River Gravel (1 in = 25.4 mm)

Test #	Broken Particles (%)	Experimental Packing Density	Volume Fraction of Aggregate Sieve Size (mm)				
			9.5	4.75	2.38	1.19	Pass 1.19
1	8.508	0.631	0.915	0.085	0.000	0.000	0.000
2	8.766	0.642	0.912	0.087	0.000	0.000	0.000
3	2.336	0.635	0.977	0.017	0.000	0.002	0.005
4	3.013	0.641	0.000	0.970	0.030	0.000	0.000
5	0.523	0.635	0.000	0.995	0.005	0.000	0.000
6	1.126	0.634	0.000	0.989	0.010	0.000	0.000
7	0.229	0.625	0.000	0.053	0.945	0.002	0.000
8	0.405	0.637	0.000	0.080	0.916	0.004	0.000
9	0.419	0.631	0.000	0.068	0.928	0.004	0.000
10	0.721	0.619	0.000	0.000	0.087	0.906	0.007
11	0.965	0.621	0.000	0.000	0.067	0.923	0.010
12	1.372	0.628	0.000	0.000	0.000	0.986	0.014
13	2.490	0.709	0.062	0.264	0.293	0.356	0.025
14	2.259	0.711	0.038	0.242	0.344	0.353	0.023
15	1.594	0.698	0.023	0.302	0.343	0.315	0.016

Table A14. Data from Modified Proctor Compaction of Intermediate River Gravel (1 in = 25.4 mm)

Test #	Broken Particles (%)	Experimental Packing Density	Volume Fraction of Aggregate Sieve Size (mm)				
			9.5	4.75	2.38	1.19	Pass 1.19
1	14.354	0.721	0.856	0.083	0.023	0.013	0.024
2	15.868	0.679	0.841	0.107	0.017	0.012	0.023
3	18.297	0.739	0.817	0.115	0.024	0.015	0.029
4	17.400	0.761	0.000	0.826	0.091	0.032	0.051
5	17.774	0.748	0.000	0.822	0.093	0.032	0.053
6	16.265	0.739	0.000	0.837	0.088	0.026	0.049
7	14.832	0.720	0.000	0.000	0.852	0.062	0.086
8	16.406	0.751	0.000	0.000	0.836	0.071	0.093
9	15.641	0.710	0.000	0.000	0.844	0.063	0.094
10	13.242	0.720	0.000	0.000	0.000	0.868	0.132
11	13.259	0.715	0.000	0.000	0.000	0.867	0.133
12	14.169	0.702	0.000	0.000	0.000	0.858	0.142
13	10.060	0.776	0.000	0.242	0.324	0.334	0.101
14	8.698	0.778	0.000	0.248	0.335	0.330	0.087
15	9.419	0.793	0.000	0.244	0.307	0.355	0.094

Table A15. Data from Gyratory Compaction of Intermediate River Gravel (1 in = 25.4 mm)

Test #	Broken Particles (%)	Experimental Packing Density	Volume Fraction of Aggregate Sieve Size (mm)				
			9.5	4.75	2.38	1.19	Pass 1.19
1	18.287	0.671	0.817	0.124	0.026	0.011	0.022
2	15.961	0.661	0.840	0.116	0.015	0.006	0.022
3	16.235	0.656	0.838	0.119	0.016	0.007	0.021
4	14.329	0.686	0.023	0.834	0.084	0.023	0.036
5	14.375	0.689	0.014	0.842	0.084	0.023	0.036
6	14.379	0.690	0.013	0.843	0.084	0.023	0.036
7	6.342	0.632	0.001	0.014	0.922	0.034	0.030
8	8.576	0.683	0.000	0.015	0.899	0.045	0.041
9	8.339	0.662	0.001	0.012	0.904	0.045	0.039
10	8.403	0.649	0.000	0.001	0.005	0.910	0.084
11	8.233	0.670	0.000	0.000	0.000	0.918	0.082
12	8.332	0.668	0.000	0.000	0.000	0.917	0.083
13	5.223	0.717	0.000	0.290	0.312	0.345	0.052
14	4.362	0.716	0.000	0.332	0.322	0.303	0.044
15	4.811	0.715	0.000	0.352	0.348	0.252	0.048

Table A16. Data for Gyratory Compaction Evolution of Intermediate River Gravel (1 in = 25.4 mm; 1 kg = 2.2 lbs)

Test #	Weight (kg)	Height of Aggregate Sample (mm) as a Function of Number of Gyrations											
		1	5	10	20	30	40	50	60	70	80	90	100
1	5.050	183.3	179.8	177.3	173.7	171.1	169.2	167.7	166.4	165.6	164.6	163.7	163.1
2	4.985	183.8	180.6	178.3	175.0	172.5	170.4	168.8	167.3	166.0	165.0	164.1	163.5
3	5.053	188.8	184.8	182.7	179.0	176.1	174.2	172.4	170.9	169.6	168.6	167.7	167.0
4	5.296	192.6	188.3	185.3	180.8	177.5	175.1	173.4	171.8	170.6	169.5	168.4	167.4
5	5.175	188.8	183.7	180.4	176.0	173.0	170.3	168.5	167.0	165.8	164.7	163.8	162.9
6	5.254	189.7	185.1	181.8	177.5	174.6	172.0	170.6	169.2	168.0	166.9	166.0	165.2
7	4.835	188.0	183.3	180.2	176.0	173.5	171.7	170.2	169.0	168.0	167.2	166.9	166.0
8	5.377	190.3	186.4	183.4	180.3	178.1	176.5	175.2	174.0	173.0	172.1	171.3	170.6
9	5.306	193.4	188.6	185.4	181.8	179.8	178.5	177.0	176.4	175.6	174.9	174.3	173.7
10	5.155	188.0	184.4	182.0	179.6	177.9	176.6	175.7	174.9	174.1	173.4	172.8	172.3
11	4.664	171.3	168.0	165.2	161.5	159.1	157.3	155.9	154.4	153.4	152.5	151.8	151.0
12	4.750	173.7	170.8	168.1	164.5	162.1	160.2	158.8	157.6	156.6	155.7	155.0	154.3
13	5.294	179.3	175.7	173.1	169.6	167.4	165.5	164.3	163.3	162.2	161.5	160.8	160.0
14	5.299	178.1	175.0	173.0	169.9	167.4	165.8	164.6	163.5	162.5	161.9	161.0	160.4
15	4.856	166.6	165.3	160.9	157.4	155.1	153.3	152.1	150.9	149.9	149.0	148.0	147.3

A.5 NATURAL SAND

Table A17. Data from Vibrating Table Compaction of Natural Sand (1 in = 25.4 mm)

Test #	Broken Particles (%)	Experimental Packing Density	Volume Fraction of Aggregate Sieve Size (mm)						
			4.75	2.38	1.19	0.595	0.30	0.149	0.075
1	2.354	0.575	0.976	0.020	0.003	0.000	0.000	0.000	0.001
2	3.742	0.571	0.963	0.037	0.000	0.000	0.000	0.000	0.000
3	1.996	0.565	0.980	0.018	0.002	0.000	0.000	0.000	0.000
4	1.705	0.548	0.000	0.983	0.015	0.000	0.000	0.000	0.001
5	1.332	0.540	0.000	0.987	0.007	0.001	0.001	0.001	0.003
6	1.486	0.558	0.000	0.985	0.015	0.000	0.000	0.000	0.000
7	1.371	0.558	0.000	0.000	0.986	0.013	0.000	0.000	0.001
8	1.242	0.561	0.000	0.000	0.988	0.012	0.000	0.000	0.000
9	0.563	0.557	0.000	0.000	0.994	0.006	0.000	0.000	0.000
10	8.906	0.582	0.000	0.000	0.000	0.911	0.070	0.019	0.000
11	4.330	0.576	0.000	0.000	0.000	0.957	0.037	0.007	0.000
12	3.556	0.564	0.000	0.000	0.000	0.964	0.033	0.002	0.000
13	4.396	0.594	0.000	0.000	0.000	0.000	0.956	0.044	0.000
14	5.566	0.592	0.000	0.000	0.000	0.000	0.944	0.056	0.000
15	3.280	0.592	0.000	0.000	0.000	0.000	0.967	0.033	0.000
16	0.393	0.572	0.000	0.000	0.000	0.000	0.000	0.996	0.004
17	0.439	0.582	0.000	0.000	0.000	0.000	0.000	0.996	0.004
18	0.120	0.578	0.000	0.000	0.000	0.000	0.000	0.999	0.001

Table A18. Data from Modified Proctor Compaction of Natural Sand (1 in = 25.4 mm)

Test #	Broken Particles (%)	Experimental Packing Density	Volume Fraction of Aggregate Sieve Size (mm)						
			4.75	2.38	1.19	0.595	0.30	0.149	0.075
1	19.334	0.626	0.807	0.090	0.040	0.021	0.011	0.020	0.012
2	21.511	0.630	0.785	0.104	0.045	0.024	0.012	0.019	0.012
3	24.227	0.622	0.758	0.116	0.043	0.028	0.015	0.010	0.031
4	23.380	0.624	0.000	0.766	0.100	0.050	0.027	0.016	0.041
5	26.418	0.635	0.000	0.736	0.115	0.055	0.029	0.018	0.047
6	24.481	0.617	0.000	0.755	0.109	0.048	0.026	0.016	0.045
7	23.394	0.624	0.000	0.000	0.766	0.087	0.036	0.026	0.084
8	20.528	0.610	0.000	0.000	0.795	0.081	0.034	0.028	0.063
9	20.603	0.582	0.000	0.000	0.794	0.087	0.035	0.022	0.062
10	30.616	0.600	0.000	0.000	0.000	0.694	0.227	0.043	0.036
11	26.841	0.600	0.000	0.000	0.000	0.732	0.194	0.037	0.037
12	20.072	0.593	0.000	0.000	0.000	0.799	0.134	0.024	0.043
13	11.747	0.606	0.000	0.000	0.000	0.000	0.883	0.100	0.018
14	10.928	0.602	0.000	0.000	0.000	0.000	0.891	0.093	0.016
15	9.776	0.599	0.000	0.000	0.000	0.000	0.902	0.083	0.014
16	1.251	0.600	0.000	0.000	0.000	0.000	0.000	0.987	0.013
17	1.653	0.599	0.000	0.000	0.000	0.000	0.000	0.983	0.017
18	1.003	0.599	0.000	0.000	0.000	0.000	0.000	0.990	0.010

Table A19. Data from Gyratory Compaction of Natural Sand (1 in = 25.4 mm)

Test #	Broken Particles (%)	Experimental Packing Density	Volume Fraction of Aggregate Sieve Size (mm)						
			4.75	2.38	1.19	0.595	0.30	0.149	0.075
1	19.477	0.632	0.805	0.120	0.032	0.014	0.007	0.005	0.017
2	22.066	0.652	0.779	0.125	0.039	0.018	0.009	0.007	0.023
3	21.590	0.640	0.784	0.123	0.039	0.018	0.009	0.006	0.021
4	19.392	0.615	0.000	0.806	0.113	0.033	0.014	0.009	0.025
5	18.918	0.629	0.000	0.811	0.110	0.032	0.014	0.008	0.025
6	17.788	0.634	0.000	0.822	0.103	0.030	0.013	0.008	0.024
7	8.784	0.580	0.000	0.000	0.912	0.065	0.010	0.004	0.009
8	8.323	0.571	0.000	0.000	0.917	0.063	0.011	0.005	0.003
9	9.474	0.577	0.000	0.000	0.905	0.059	0.013	0.007	0.015
10	5.972	0.600	0.000	0.000	0.000	0.940	0.037	0.008	0.015
11	5.430	0.615	0.000	0.000	0.000	0.946	0.032	0.008	0.015
12	6.075	0.616	0.000	0.000	0.000	0.939	0.035	0.010	0.016
13	6.180	0.625	0.000	0.000	0.000	0.000	0.938	0.055	0.007
14	4.584	0.622	0.000	0.000	0.000	0.000	0.954	0.040	0.005
15	5.045	0.621	0.000	0.000	0.000	0.000	0.950	0.045	0.005
16	0.980	0.619	0.000	0.000	0.000	0.000	0.000	0.990	0.010
17	0.651	0.619	0.000	0.000	0.000	0.000	0.000	0.993	0.007
18	0.755	0.620	0.000	0.000	0.000	0.000	0.000	0.992	0.008

Table A20. Data for Gyratory Compaction Evolution of Natural Sand (1 kg = 2.2 lbs; 1 in = 25.4 mm)

Test #	Weight (kg)	Height of Aggregate Sample (mm) as a Function of Number of Gyrations											
		1	5	10	20	30	40	50	60	70	80	90	100
1	4.685	183.1	178.4	175.4	170.6	166.6	163.7	161.4	159.7	158.0	156.6	155.1	154.1
2	4.232	165.0	160.7	157.2	151.5	147.3	144.2	142.0	140.0	138.6	137.2	136.1	134.9
3	4.287	169.5	164.3	160.7	155.6	151.8	148.7	146.2	144.4	142.7	141.3	140.4	139.1
4	4.071	164.8	160.6	157.4	152.6	149.0	146.1	143.9	142.2	140.8	139.5	138.4	137.5
5	4.291	168.9	164.4	160.8	156.1	152.9	150.0	148.0	146.3	144.9	143.7	142.7	141.7
6	4.410	172.6	168.2	164.8	159.9	156.6	153.9	151.9	150.1	148.5	147.2	145.6	144.6
7	4.335	168.4	165.8	163.9	161.7	160.4	159.2	158.4	157.6	157.0	156.3	155.9	155.4
8	4.115	164.5	161.1	159.0	156.8	155.2	154.2	153.1	152.1	151.6	150.8	150.2	149.8
9	4.161	165.1	162.0	160.0	157.2	155.4	154.1	153.0	152.2	151.5	150.7	150.4	149.8
10	4.508	174.6	170.6	167.8	164.6	162.4	160.8	159.6	158.6	157.8	157.1	156.5	156.0
11	4.281	163.0	159.6	156.7	153.3	150.9	149.4	148.4	147.2	146.5	146.0	145.1	144.6
12	4.361	164.4	160.5	158.3	155.1	153.1	151.6	150.6	149.6	149.0	148.2	147.7	147.0
13	4.812	174.4	171.3	168.8	166.0	164.5	163.2	162.5	161.6	161.2	160.6	160.2	160.0
14	4.765	173.8	170.2	167.8	165.1	163.7	162.4	161.7	160.9	160.5	160.1	159.9	159.2
15	4.900	177.7	174.6	172.2	169.4	168.8	167.1	166.0	165.5	165.1	164.7	164.4	164.0
16	4.929	180.5	176.6	174.3	171.4	169.8	168.9	167.9	167.4	166.6	166.3	166.0	165.4
17	4.771	176.4	172.6	169.9	166.8	165.0	163.6	163.1	162.1	161.9	161.1	160.9	160.2
18	4.596	170.4	165.8	163.0	159.9	158.5	157.3	156.7	155.8	155.5	154.7	154.5	153.9

A.6 MANUFACTURED SAND

Table A21. Data from Vibrating Table Compaction of Manufactured Sand (1 in = 25.4 mm)

Test #	Broken Particles (%)	Experimental Packing Density	Volume Fraction of Aggregate Sieve Size (mm)						
			4.75	2.38	1.19	0.595	0.30	0.149	0.075
1	16.938	0.533	0.831	0.168	0.000	0.000	0.000	0.000	0.001
2	16.069	0.517	0.839	0.161	0.000	0.000	0.000	0.000	0.000
3	13.244	0.537	0.868	0.132	0.000	0.000	0.000	0.000	0.000
4	3.141	0.533	0.015	0.954	0.031	0.000	0.000	0.000	0.000
5	3.318	0.523	0.026	0.940	0.033	0.000	0.000	0.000	0.000
6	3.135	0.537	0.137	0.831	0.031	0.000	0.000	0.000	0.000
7	6.150	0.531	0.000	0.053	0.885	0.061	0.000	0.000	0.000
8	5.168	0.539	0.000	0.059	0.889	0.052	0.000	0.000	0.000
9	4.708	0.505	0.000	0.086	0.867	0.047	0.000	0.000	0.000
10	7.845	0.555	0.000	0.000	0.022	0.900	0.078	0.000	0.000
11	5.194	0.562	0.000	0.000	0.025	0.923	0.050	0.000	0.002
12	3.934	0.555	0.000	0.000	0.028	0.932	0.038	0.000	0.002
13	11.653	0.556	0.000	0.000	0.000	0.022	0.862	0.094	0.023
14	10.377	0.546	0.000	0.000	0.000	0.023	0.873	0.082	0.022
15	6.897	0.542	0.000	0.000	0.000	0.019	0.912	0.056	0.013
16	4.691	0.592	0.000	0.000	0.000	0.000	0.273	0.681	0.047
17	2.620	0.563	0.000	0.000	0.000	0.000	0.194	0.780	0.026
18	8.416	0.580	0.000	0.000	0.000	0.000	0.117	0.799	0.084
19	1.112	0.629	0.000	0.000	0.000	0.000	0.000	0.000	1.000
20	1.796	0.619	0.000	0.000	0.000	0.000	0.000	0.000	1.000
21	3.181	0.625	0.000	0.000	0.000	0.000	0.000	0.000	1.000

Table A22. Data from Modified Proctor Compaction of Manufactured Sand (1 in = 25.4 mm)

Test #	Broken Particles (%)	Experimental Packing Density	Volume Fraction of Aggregate Sieve Size (mm)						
			4.75	2.38	1.19	0.595	0.30	0.149	0.075
1	45.441	0.673	0.546	0.339	0.052	0.018	0.013	0.016	0.017
2	60.148	0.646	0.399	0.433	0.076	0.031	0.018	0.015	0.029
3	49.972	0.654	0.500	0.375	0.055	0.024	0.017	0.009	0.021
4	37.258	0.676	0.000	0.627	0.221	0.069	0.033	0.028	0.022
5	35.687	0.674	0.000	0.643	0.210	0.065	0.031	0.036	0.014
6	38.146	0.677	0.000	0.619	0.220	0.072	0.034	0.045	0.010
7	32.388	0.673	0.000	0.000	0.676	0.185	0.061	0.030	0.048
8	32.371	0.667	0.000	0.000	0.676	0.183	0.057	0.035	0.048
9	32.740	0.678	0.000	0.000	0.673	0.178	0.064	0.044	0.042
10	27.577	0.703	0.000	0.001	0.007	0.717	0.126	0.119	0.031
11	27.277	0.701	0.000	0.000	0.005	0.722	0.128	0.075	0.070
12	27.572	0.703	0.000	0.000	0.003	0.721	0.128	0.081	0.067
13	21.948	0.731	0.000	0.000	0.000	0.112	0.668	0.161	0.059
14	22.831	0.725	0.000	0.000	0.000	0.052	0.719	0.169	0.059
15	21.362	0.720	0.000	0.000	0.000	0.000	0.786	0.128	0.085
16	13.871	0.746	0.000	0.000	0.000	0.000	0.000	0.861	0.139
17	16.563	0.765	0.000	0.000	0.000	0.000	0.000	0.834	0.166
18	21.177	0.745	0.000	0.000	0.000	0.000	0.000	0.788	0.212
19	3.671	0.647	0.000	0.000	0.000	0.000	0.000	0.000	1.000
20	11.418	0.668	0.000	0.000	0.000	0.000	0.000	0.000	1.000
21	13.292	0.654	0.000	0.000	0.000	0.000	0.000	0.000	1.000

Table A23. Data from Gyratory Compaction of Manufactured Sand (1 in = 25.4 mm)

Test #	Broken Particles (%)	Experimental Packing Density	Volume Fraction of Aggregate Sieve Size (mm)						
			4.75	2.38	1.19	0.595	0.30	0.149	0.075
1	45.820	0.662	0.542	0.352	0.052	0.020	0.011	0.009	0.015
2	46.295	0.653	0.537	0.352	0.051	0.025	0.014	0.008	0.014
3	45.792	0.639	0.542	0.352	0.047	0.019	0.017	0.010	0.013
4	26.678	0.668	0.000	0.733	0.178	0.043	0.018	0.010	0.016
5	20.629	0.665	0.000	0.794	0.139	0.033	0.014	0.008	0.013
6	16.689	0.646	0.000	0.833	0.111	0.026	0.011	0.006	0.012
7	19.104	0.659	0.000	0.000	0.809	0.134	0.026	0.012	0.019
8	22.658	0.647	0.000	0.000	0.773	0.160	0.032	0.014	0.021
9	24.773	0.650	0.000	0.000	0.752	0.175	0.035	0.015	0.022
10	19.433	0.645	0.000	0.000	0.000	0.806	0.135	0.028	0.031
11	23.099	0.648	0.000	0.000	0.000	0.769	0.163	0.033	0.035
12	22.980	0.640	0.000	0.000	0.000	0.770	0.161	0.034	0.035
13	21.400	0.640	0.000	0.000	0.000	0.000	0.786	0.157	0.057
14	21.582	0.649	0.000	0.000	0.000	0.000	0.784	0.150	0.066
15	19.449	0.654	0.000	0.000	0.000	0.000	0.806	0.126	0.069
16	18.027	0.773	0.000	0.000	0.000	0.000	0.000	0.620	0.380
17	16.090	0.778	0.000	0.000	0.000	0.000	0.000	0.609	0.391
18	15.821	0.789	0.000	0.000	0.000	0.000	0.000	0.702	0.298
19	11.467	0.739	0.000	0.000	0.000	0.000	0.000	0.000	1.000
20	5.293	0.741	0.000	0.000	0.000	0.000	0.000	0.000	1.000
21	8.504	0.755	0.000	0.000	0.000	0.000	0.000	0.000	1.000

Table A24. Data for Gyratory Compaction Evolution of Manufactured Sand

(1 kg = 2.2 lbs; 1 in = 25.4 mm)

Test #	Weight (kg)	Height of Aggregate Sample (mm) as a Function of Number of Gyrations											
		1	5	10	20	30	40	50	60	70	80	90	100
1	3.969	152.3	146.8	142.6	137.2	134.0	131.8	129.9	128.6	127.2	126.3	125.3	124.5
2	4.399	169.8	165.5	161.6	156.1	152.1	149.2	146.9	145.1	143.4	142.2	141.1	139.9
3	4.492	183.9	176.3	171.9	165.1	160.5	157.2	154.7	152.3	150.5	148.7	147.3	146.1
4	3.877	156.2	150.0	144.8	136.9	131.9	128.8	126.5	125.0	123.5	122.2	121.2	120.5
5	4.101	156.5	151.4	147.7	142.4	138.5	135.9	134.0	132.3	131.1	130.0	129.2	128.1
6	4.398	172.3	166.7	162.9	157.3	153.6	150.6	148.5	146.6	145.2	143.7	142.4	141.4
7	3.957	155.0	148.7	144.6	138.8	134.8	132.2	130.1	128.5	127.3	126.1	125.3	124.7
8	4.361	173.0	167.1	163.0	156.9	152.9	149.9	147.8	145.8	144.2	142.5	141.3	140.0
9	4.227	168.8	162.1	157.7	151.5	147.4	144.5	142.3	140.3	139.0	137.3	136.0	135.0
10	4.314	168.7	163.4	159.2	152.9	149.1	146.4	144.4	143.0	141.6	140.7	139.7	139.0
11	4.304	171.4	164.0	159.0	152.9	148.8	146.2	144.1	142.4	141.0	139.8	138.9	138.0
12	4.316	172.1	165.8	161.8	156.0	152.3	149.5	147.1	145.1	143.5	142.1	141.0	140.0
13	4.270	164.7	158.3	154.3	149.6	146.6	144.4	142.8	141.9	140.9	140.0	139.3	138.6
14	4.374	167.3	162.3	158.6	153.4	150.0	147.5	145.6	144.0	142.8	142.0	141.0	140.1
15	4.263	164.8	158.2	154.4	149.1	145.8	143.4	141.4	139.8	138.5	137.3	136.4	135.5
16	3.617	112.9	107.8	104.6	101.3	99.9	99.1	98.6	98.2	97.8	97.6	97.4	97.2
17	4.003	124.6	119.6	116.6	112.6	111.0	109.9	109.2	108.7	108.3	108.0	107.7	106.9
18	3.816	118.0	112.3	108.8	105.8	104.4	103.4	102.6	101.6	101.4	100.9	100.7	100.5
19	3.271	107.1	102.9	99.8	97.2	95.1	94.4	93.9	93.1	92.8	92.4	92.2	92.0
20	3.818	124.4	118.7	115.8	112.4	111.1	109.8	109.2	108.8	108.5	107.5	107.2	107.0
21	3.350	106.3	101.8	99.0	96.8	95.1	94.3	93.7	93.2	92.8	92.4	92.3	92.2

APPENDIX B: MATLAB CODE

B.1 CODE FOR SPECIFIC CREEP MODEL FITTING

```
clear all; close all;

%import data
data = xlsread('specific_creep.xlsx');
time = data(:,1);
specific_creep = data(:,9);

%define specific creep model and parameters
x = [1 1 1]; %x(1) = J0, x(2) = J1, x(3) = T
F = @(x,xdata)x(1) + x(2)*(1-exp(-xdata/x(3)));

%initialize parameters
x0 = [1 1 1];

%perform model fit and plot
[x,resnorm,~,exitflag,output] = lsqcurvefit(F,x0,time,specific_creep);

figure;
plot(time,specific_creep,'k','Linewidth',2); hold on
plot(time,F(x,time),'r--','Linewidth',2);
legend('J(t) - Experimental','J(t) - Model');
xlabel('Loading Age (days)');
ylabel('Specific Creep (microstrain/MPa)');
```

B.2 CODE FOR DETERMINING TRANSVERSE RESONANCE FREQUENCY FROM ASTM C215 TESTING

```
clear all;

%Define signal variables.
data = xlsread('RCC5-1.xls');
time = data(:,1);
voltage = data(:,2);

%Perform Fast Fourier Transform.
L = length(time); %number of data points.
T = time(2)-time(1); %sampling period.
Fs = 1/T; %sampling frequency.
```

```
t = (0:L-1)*T;
n = 2^nextpow2(L);
FFT = fft(voltage,n); %imaginary and real components.
FFT_abs = abs(FFT/n);
f = Fs*(0:(n/2))/n; %frequency spectrum up to Nyquist frequency.
f1 = Fs*(1:n)/n; %full frequency spectrum.

%Plot results of Fast Fourier Transform.
plotlim = [0 10000]; %not interested in frequencies above 10 kHz for this specimen geometry.
plot(f,FFT_abs(1:n/2+1),'linewidth',2); hold on %only plot up to Nyquist frequency.
xlim(plotlim);
legend('237.2', '281.7', '326.2'); %cementitious contents.
ylabel('Amplitude (-)'); %non-dimensional parameter.
xlabel('Frequency, f (Hz)');

%Determine transverse resonance frequency.
[x,freq] = findpeaks(FFT_abs,f1); %determine peak amplitudes and corresponding indices.
[max_amp,I] = max(x); %define maximum of all peak amplitudes.
res_freq = freq(I) %resonance frequency.

%Verify resonance frequency on plot of amplitude vs. frequency.
```

APPENDIX C: GYRATORY AND MODIFIED PROCTOR COMPACTION CURVES

This appendix contains gyratory and modified Proctor compaction curves for the 17 mix designs presented in Appendix L.

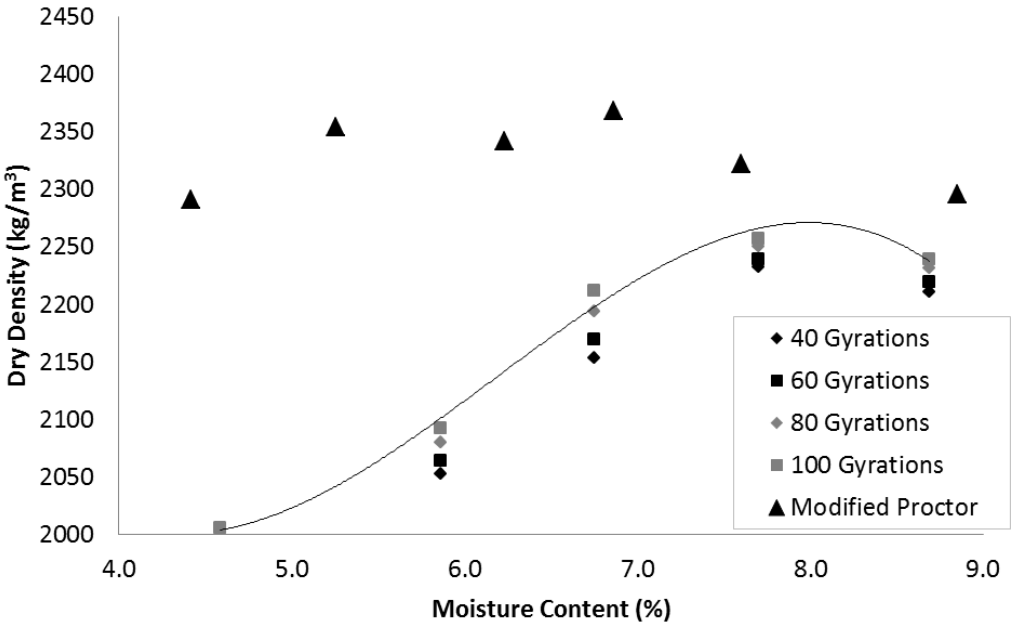

Figure C1. Gyratory and Modified Proctor Compaction Curves for Mix 1.
(1 kg/m^3 = 1.686 lb/yd^3)

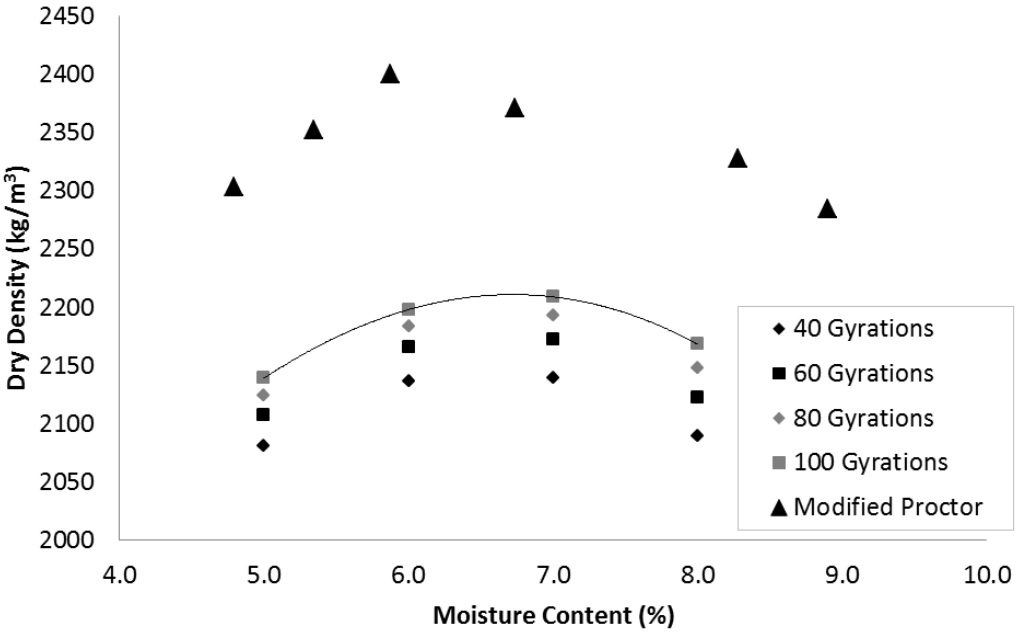

Figure C2. Gyratory and Modified Proctor Compaction Curves for Mix 2.
(1 kg/m^3 = 0.063 lb/ft^3)

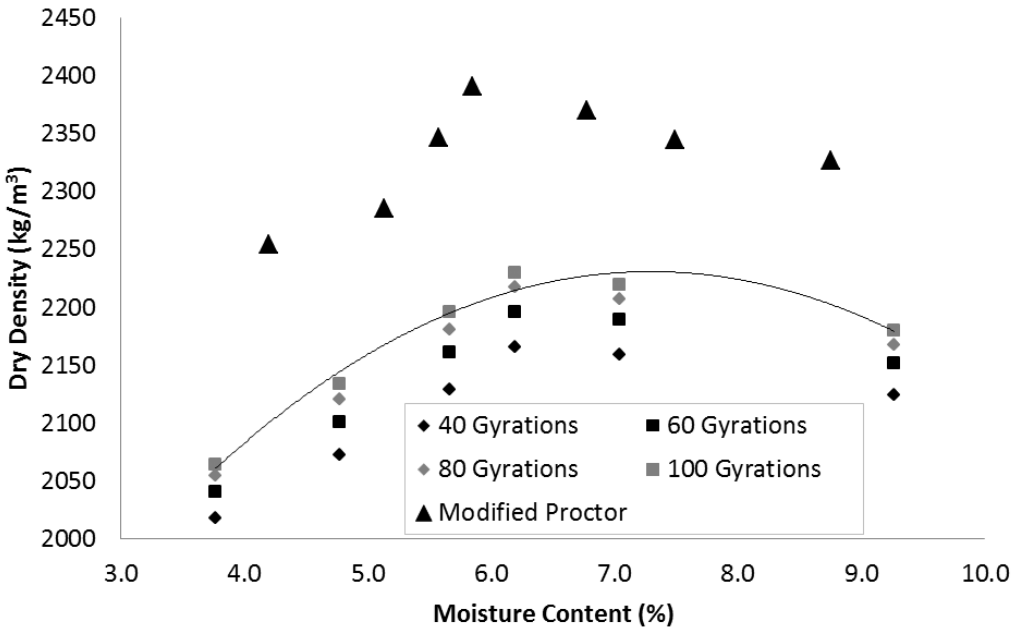

Figure C3. Gyratory and Modified Proctor Compaction Curves for Mix 3.
(1 kg/m^3 = 0.063 lb/ft^3)

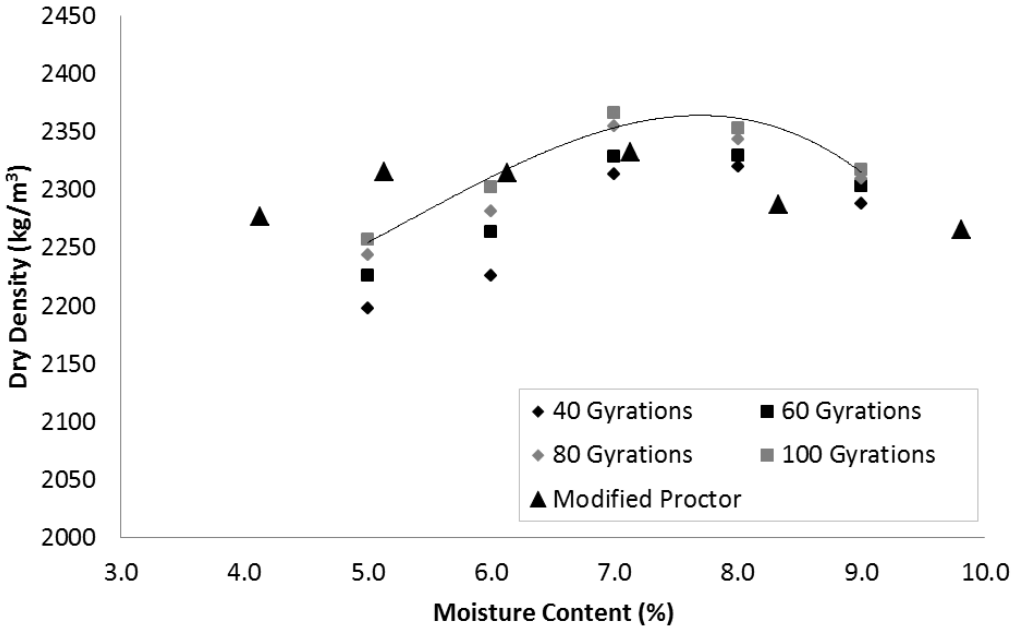

Figure C4. Gyratory and Modified Proctor Compaction Curves for Mix 4.
(1 kg/m^3 = 0.063 lb/ft^3)

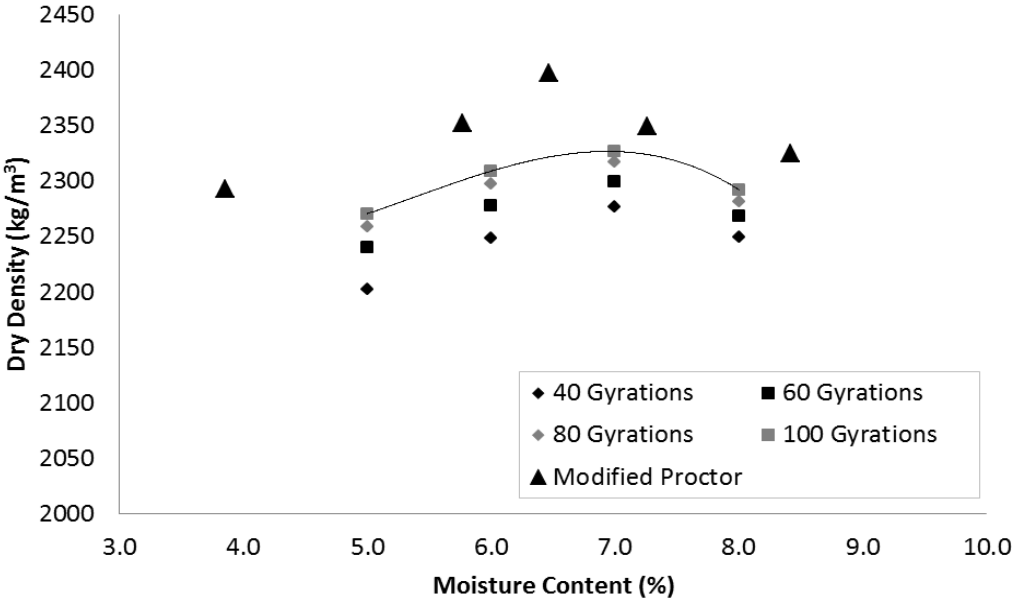

Figure C5. Gyratory and Modified Proctor Compaction Curves for Mix 5. (1 kg/m^3 = 0.063 lb/ft^3)

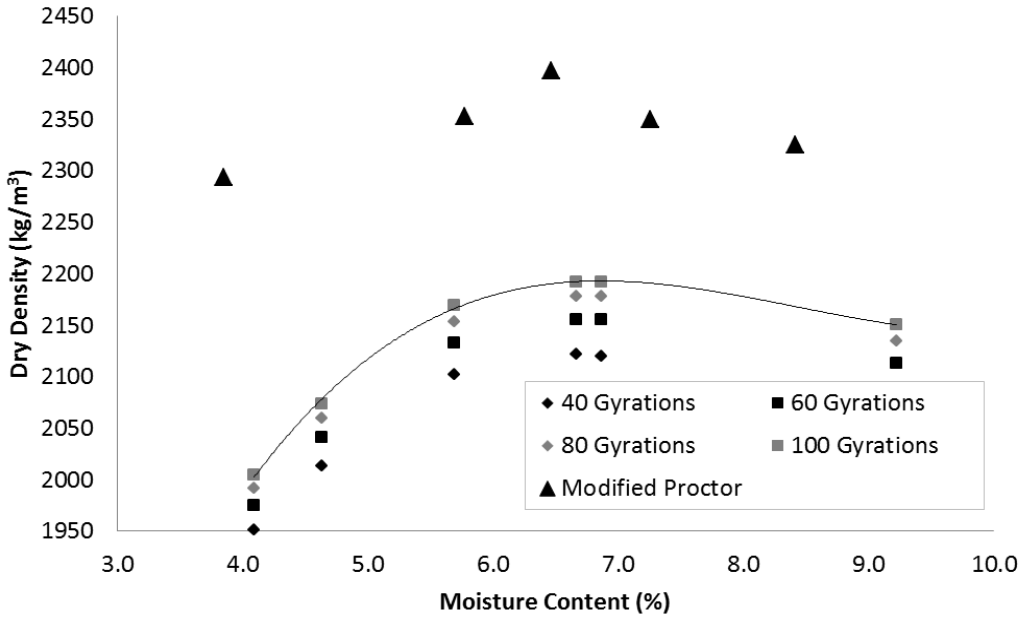

Figure C6. Gyratory and Modified Proctor Compaction Curves for Mix 6.
(1 kg/m^3 = 0.063 lb/ft^3)

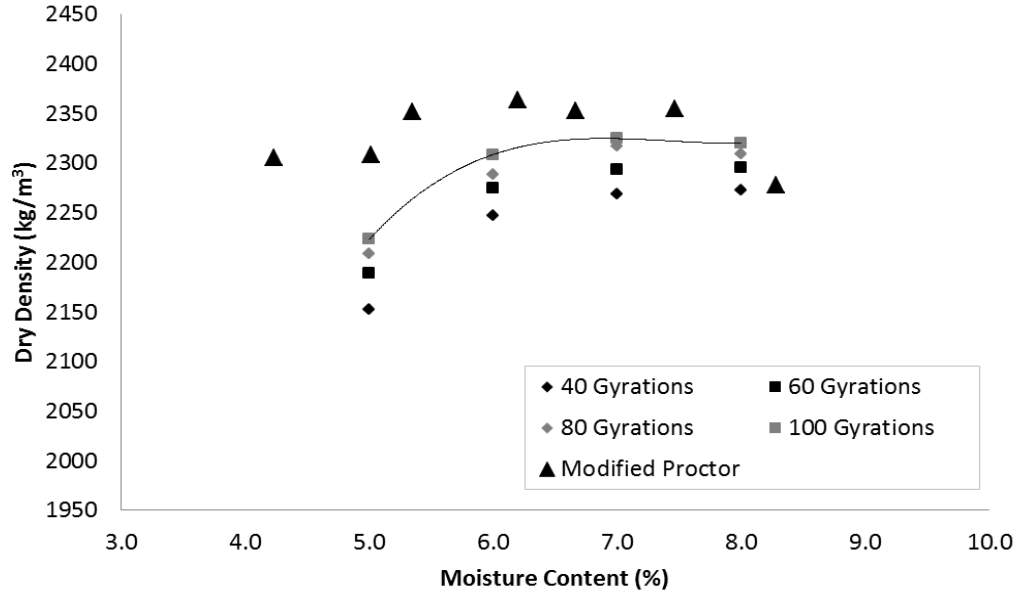

Figure C7. Gyratory and Modified Proctor Compaction Curves for Mix 7.
(1 kg/m^3 = 0.063 lb/ft^3)

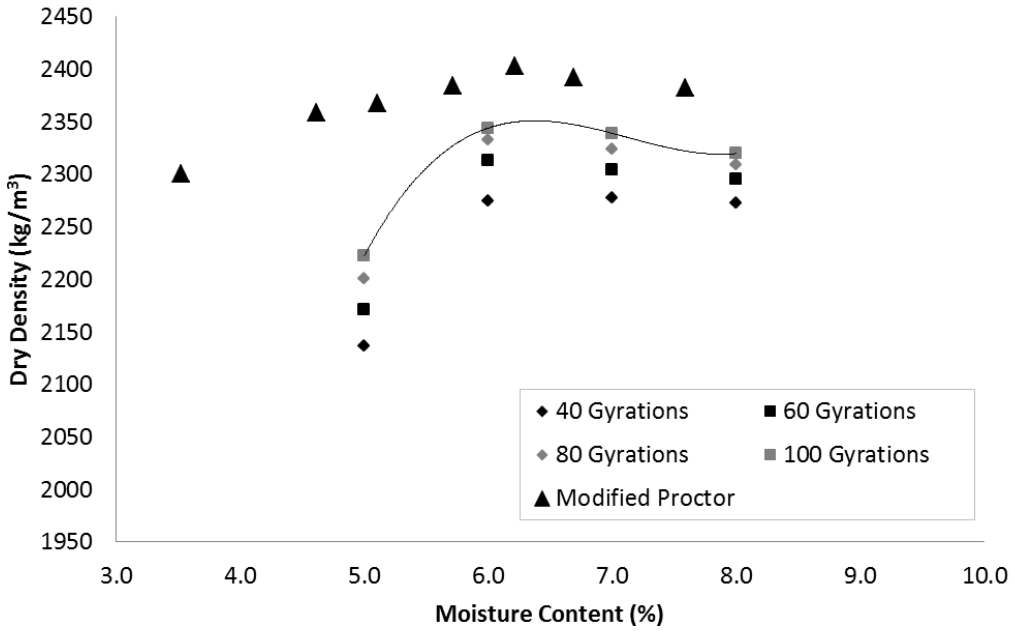

Figure C8. Gyratory and Modified Proctor Compaction Curves for Mix 8.
(1 kg/m^3 = 0.063 lb/ft^3)

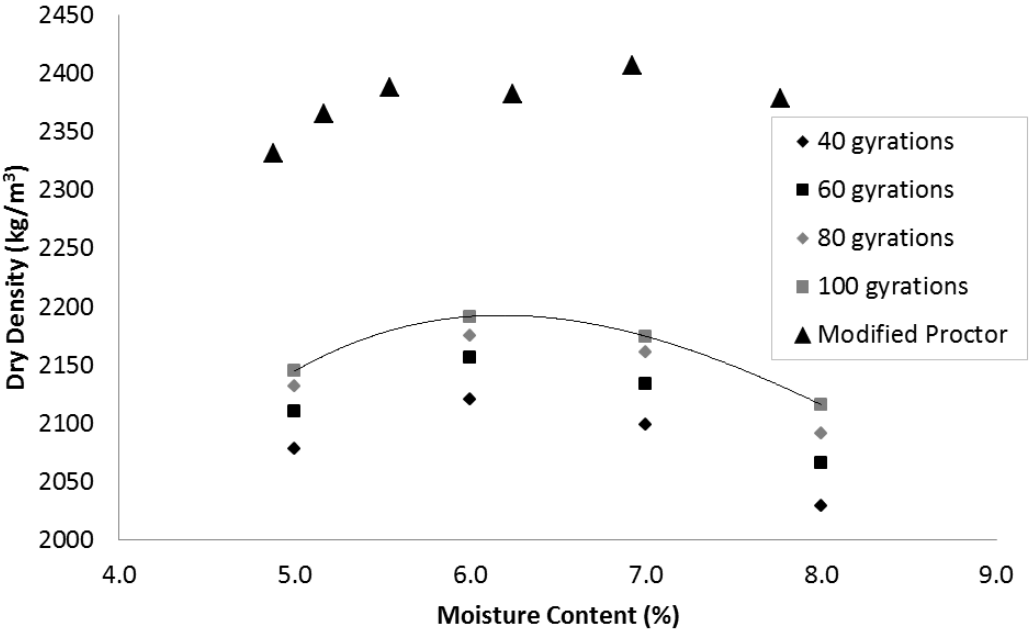

Figure C9. Gyratory and Modified Proctor Compaction Curves for Mix 9.
(1 kg/m^3 = 0.063 lb/ft^3)

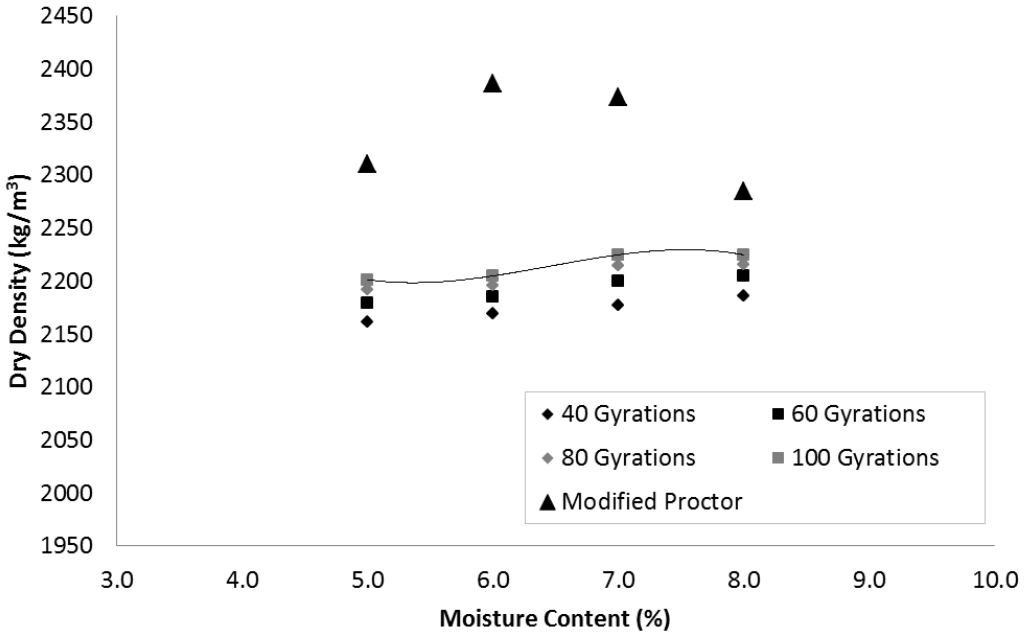

Figure C10. Gyratory and Modified Proctor Compaction Curves for Mix O.
(1 kg/m^3 = 0.063 lb/ft^3)

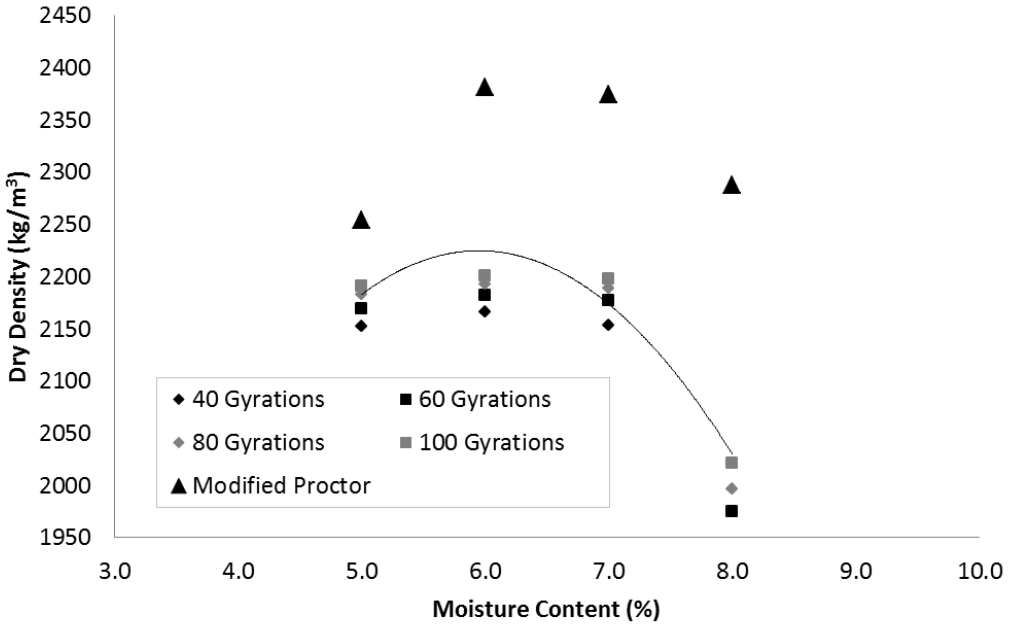

Figure C11. Gyratory and Modified Proctor Compaction Curves for Mix A.
(1 kg/m^3 = 0.063 lb/ft^3)

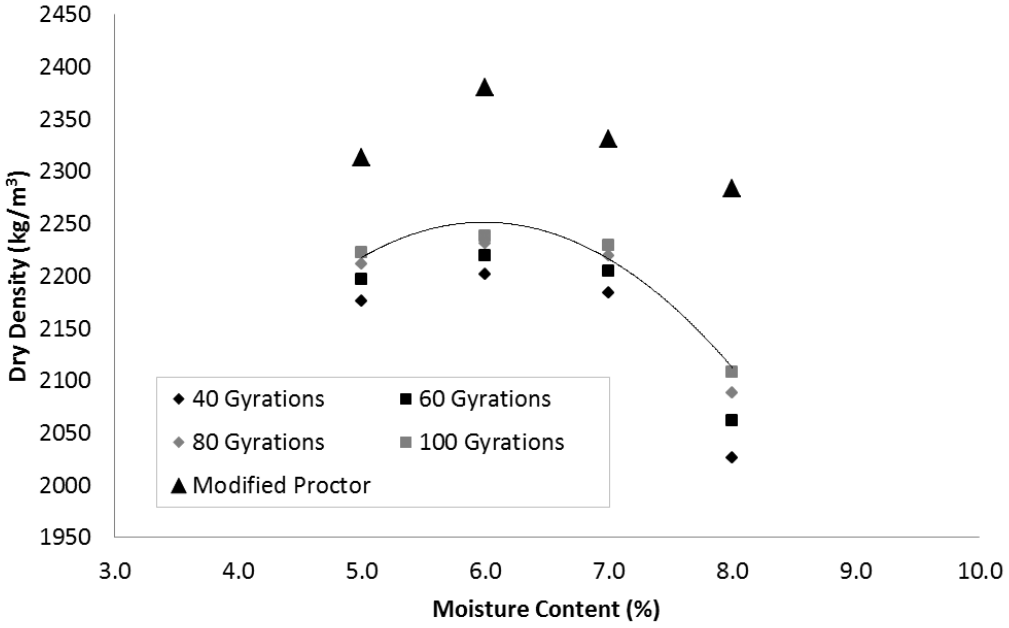

Figure C12. Gyratory and Modified Proctor Compaction Curves for Mix B.
(1 kg/m^3 = 0.063 lb/ft^3)

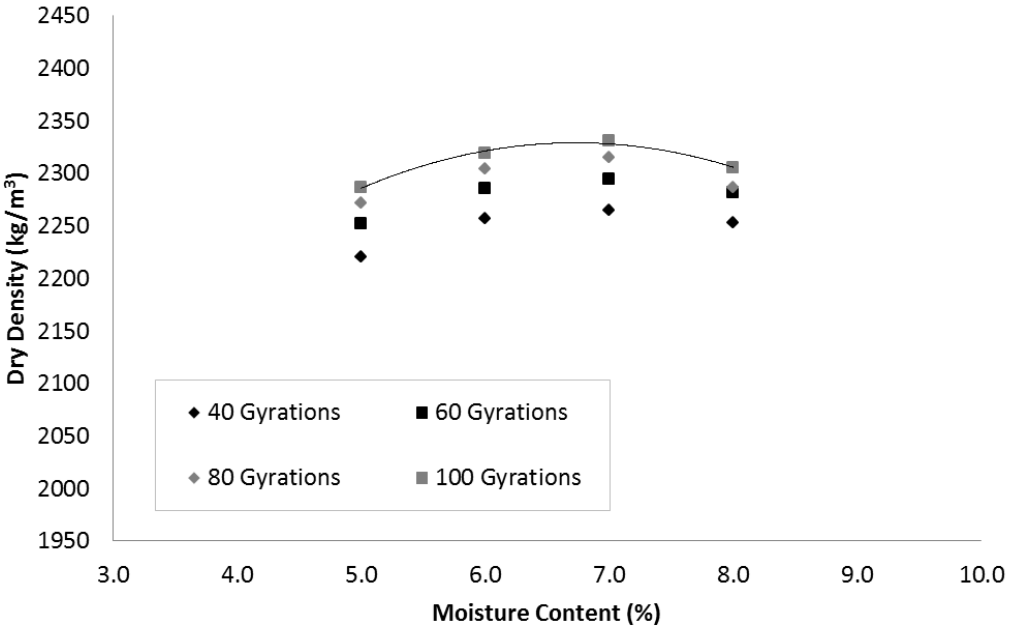

Figure C13. Gyratory Compaction Curves for Site B. (1 kg/m^3 = 0.063 lb/ft^3)

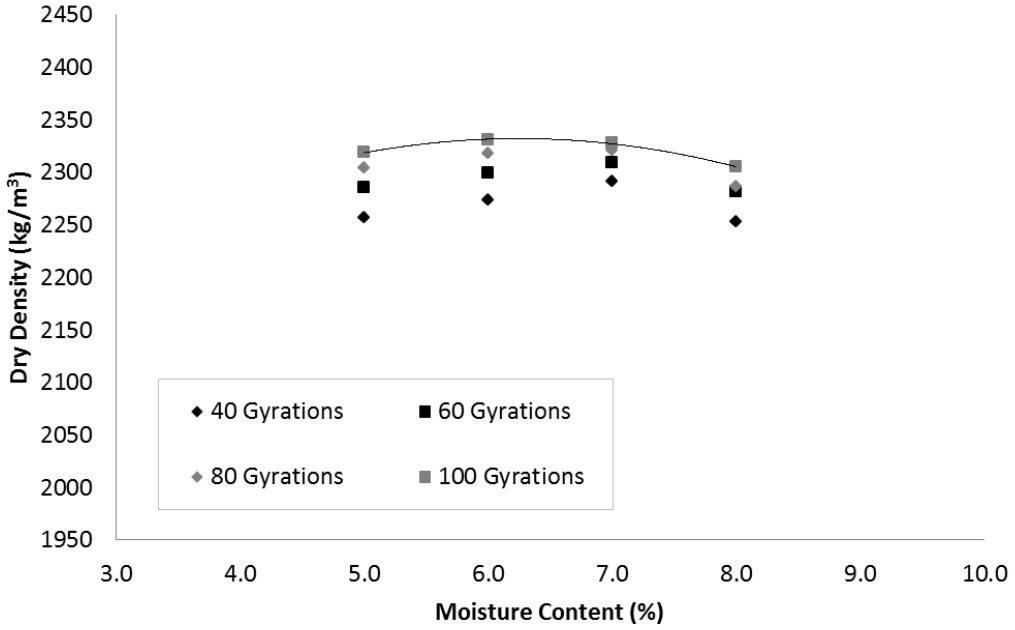

Figure C14. Gyratory Compaction Curves for Site C. (1 kg/m^3 = 0.063 lb/ft^3)

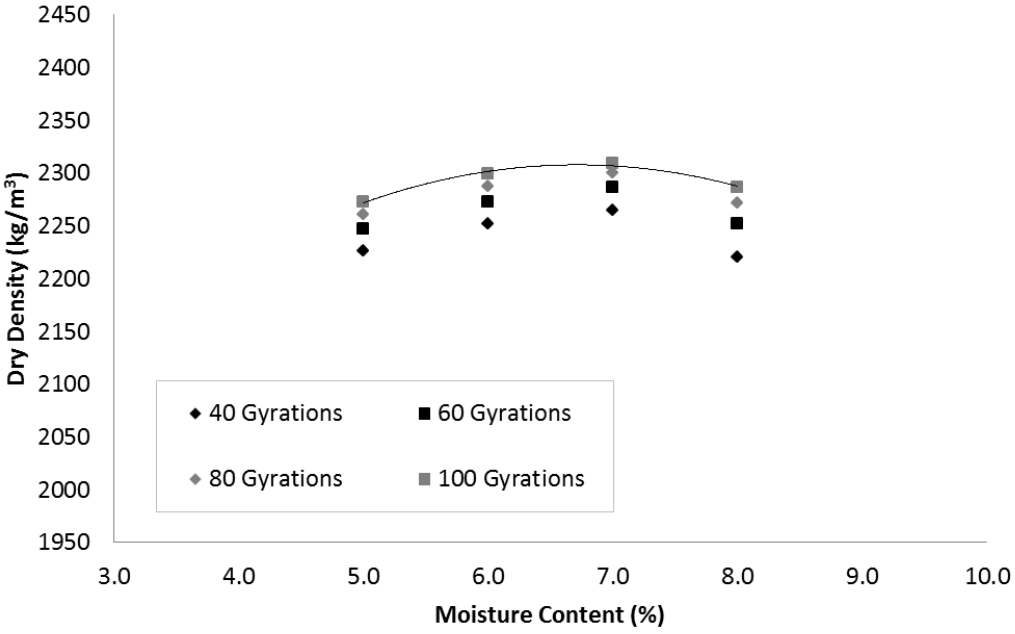

Figure C15. Gyratory Compaction Curves for Site D. (1 kg/m^3 = 0.063 lb/ft^3)

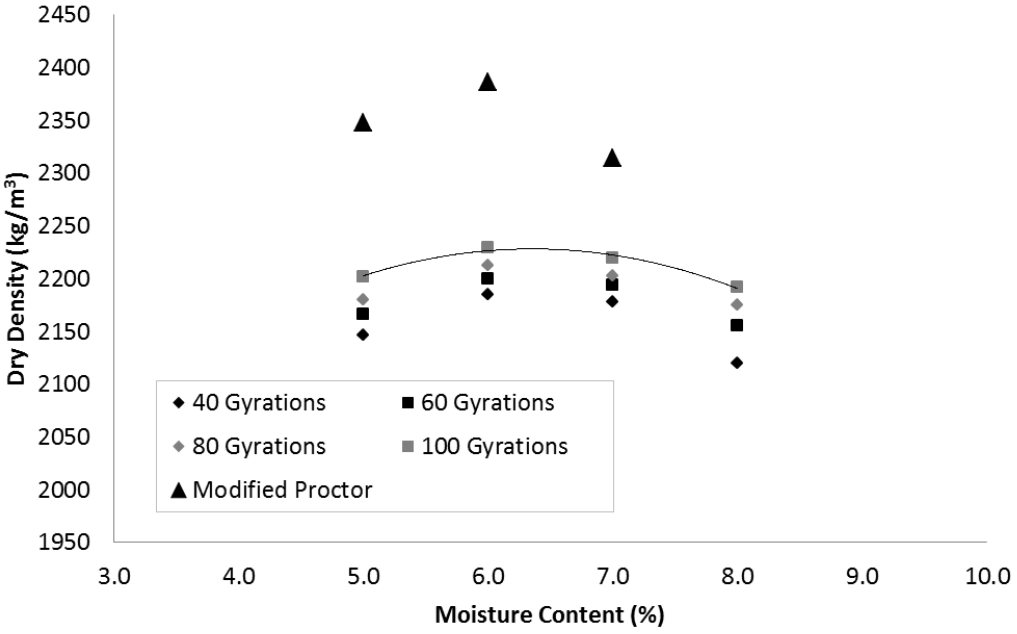

Figure C16. Gyratory and Modified Proctor Compaction Curves for Mix Trap Rock.
(1 kg/m^3 = 0.063 lb/ft^3)

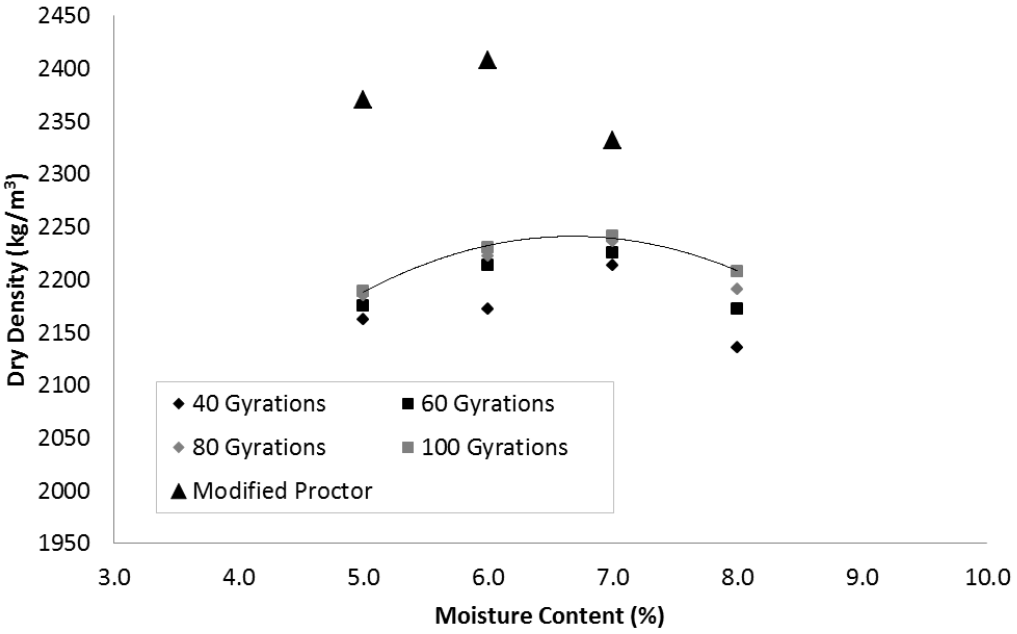

Figure C17. Gyratory and Modified Proctor Compaction Curves for Mix River Gravel.
(1 kg/m^3 = 0.063 lb/ft^3)

APPENDIX D: EXPERIMENTAL DESIGN DATA

This appendix contains the data used to develop the response data and contour plots in Chapter 4.

Table D1. Modified Proctor and Vebe Properties (1 kg/m^3 = 0.063 lb/ft^3)

Design Point Label	Maximum Dry Density (kg/m^3)	Optimum Moisture Content (%)	Vebe Time (sec)	Vebe Density (kg/m^3)
A	2391.6	6.59	12.5	2250.4
B	2364.1	6.26	17.8	2260.4
C	2394.2	5.95	17.0	2324.5
D	2382.7	6.44	15.8	2303.6
E	2387.2	6.23	12.9	2266.0
F	2324.4	6.64	20.1	2229.2
G	2301.5	6.84	13.0	2237.1
H	2411.5	6.31	11.0	2311.5
I	2319.9	6.52	11.6	2285.3
K	2358.7	6.57	13.9	2230.0
L	2358.8	6.24	18.5	2259.1
M	2390.5	6.55	13.2	2278.4
N	2383.2	6.38	14.6	2222.8
O	2390.5	6.39	13.7	2288.3
P	2407.0	6.00	15.0	2284.7
Q	2411.3	6.05	18.2	2342.5
R	2371.9	6.11	16.4	2246.3
S	2380.1	6.22	19.2	2274.1
T	2414.2	6.16	16.2	2271.7
U	2392.6	6.11	16.0	2210.8

Table D2. Compressive Strength (average of 3 replicates) (1 ksi = 6.89 MPa)

Design Point Label	1-Day Compressive Strength (MPa)	7-Day Compressive Strength (MPa)	28-Day Compressive Strength (MPa)
A	18.47	38.01	51.03
B	27.95	51.10	63.47
C	16.69	40.39	55.94
D	28.11	46.03	57.37
E	17.52	42.54	55.61
F	18.51	34.40	50.29
G	17.19	33.98	48.38
H	32.42	62.55	64.49
I	28.85	52.34	60.39
K	18.23	35.26	47.22
L	27.45	51.21	65.09
M	26.92	49.36	60.90
N	24.69	48.28	59.24
O	16.28	35.58	48.68
P	25.14	60.99	64.39
Q	24.13	43.67	62.36
R	17.03	39.35	60.71
S	25.25	48.35	63.35
T	25.29	47.60	58.37
U	21.91	45.02	60.76

Table D3. Split Tensile Strength (average of 3 replicates) (1 ksi = 6.89 MPa)

Design Point Label	1-Day Split Tensile Strength (MPa)	7-Day Split Tensile Strength (MPa)	28-Day Split Tensile Strength (MPa)
A	2.23	3.70	4.46
B	2.83	3.73	3.99
C	2.23	3.31	3.85
D	3.51	3.95	5.65
E	2.22	3.54	3.71
F	2.15	3.11	4.25
G	2.01	3.14	3.77
H	4.13	4.46	4.96
I	3.29	4.26	4.73
K	2.31	3.58	4.83
L	3.62	3.73	4.28
M	3.09	3.51	3.86
N	3.09	4.60	5.52
O	2.66	3.46	5.25
P	2.96	4.60	5.11
Q	3.16	3.92	4.47
R	2.23	3.73	4.18
S	2.97	3.69	4.57
T	2.92	4.00	4.83
U	2.71	3.66	4.27

Table D4. 28-Day Flexural Strength, Elastic Modulus, and Drying Shrinkage Strains (all measurements are averages of 3 replicates); (1 ksi = 6.89 MPa; 1 GPa = 145.03 ksi)

Design Point Label	28-Day Flexural Strength (MPa)	28-Day Elastic Modulus (GPa)	7-Day Drying Shrinkage Strain (με)	28-Day Drying Shrinkage Strain (με)
A	7.40	34.27	260.00	426.67
B	6.24	36.81	226.67	393.33
C	7.02	35.38	183.33	340.00
D	6.22	33.35	210.00	356.67
E	7.19	31.18	183.33	286.67
F	6.13	30.76	150.00	270.00
G	5.29	30.59	150.00	280.00
H	6.08	33.88	246.67	356.67
I	5.76	33.35	253.33	380.00
K	5.31	33.67	203.33	303.33
L	5.93	31.62	203.33	256.67
M	6.55	31.56	206.67	263.33
N	6.23	30.50	260.00	336.67
O	6.03	33.89	233.33	363.33
P	7.02	34.46	180.00	280.00
Q	6.79	33.84	170.00	283.33
R	6.88	34.68	163.33	263.33
S	6.98	31.11	166.67	253.33
T	6.74	31.68	163.33	246.67
U	6.65	32.11	233.33	306.67

APPENDIX E: GYRATORY RCC MIX DESIGN FRAMEWORK

The application of the Superpave Gyratory Compactor to RCC specimen preparation can lead to more consistent mixture design process. The gyratory compactor applies a kneading action for compaction of the RCC sample, which is more representative of the method that RCC is compacted for pavement applications in the same manner as for asphalt materials. Additionally, the gyratory applies a more consistent compactive effort. For example, in the compaction delay study, Appendix M, the gyratory compactor was found to be a better tool for assessing the effect of compaction delay on RCC because of the more precise results that arise from the consistent compactive effort. Appendix E summarizes work performed with the gyratory compactor for use in the mix design of RCC. This appendix is separated into a literature review, a summary of the work that has been performed throughout this report related to gyratory-based mix design of RCC, and finally a proposed framework for an RCC mix design method.

E.1 LITERATURE REVIEW

E.1.1 General Gyratory Compactor Information

The gyratory compactor can be adjusted to apply a varying amount of axial pressure at a range of selected angle of internal gyration. According to ASTM C1800, which summarizes a method to determine density of compacted samples of RCC using the gyratory compactor, the pressure should be 600 kPa and the internal angle of gyration should be 1.16 degrees. Additionally, the number of total gyrations is a parameter that must be determined. The gyratory compactor can either be used to compact to a certain number of gyrations or a certain density (fixed specimen height), given the initial mass of the material in the compactor. Previous research has reported that 50-75 gyrations best approximates field compaction (Amer et al., 2003).

E.1.2 Applying Gyratory Compactor in Mix Design for Moisture-Density Testing

The first general step of a mix design method using moisture-density testing is to determine the aggregate combination that will be used. Previous work has determined an optimal blend of aggregates using a gyratory compactor for packing density tests (Khayat and Libre, 2014). Other work, for example this report, has shown various aggregate gradations can result in acceptable mechanical properties. Williams (2013) concluded that aggregate gradations that are closer to the 0.45-power maximum density line yield RCC samples with a higher density. While other considerations should be made when considering the appropriate particle size distribution of aggregates for RCC, e.g., resistance to segregation and finishability, an optimum aggregate combination either from packing tests or from considering the maximum density gradation has been shown to be adequate (Williams, 2013; Khayat and Libre, 2014).

Cement content is the next parameter that must be selected in the mix design method. Khayat and Libre, 2014, indicate that a cement content as low as 250 kg/m^3 (420 lb/yd^3) could be used to achieve adequate mechanical properties. However, they recommend using a larger cement content (295 kg/m^3 (500 lb/yd^3) due to permeability and durability concerns (Khayat and Libre, 2014). Williams (2013) did not report the cement content used in their mixes, though it was kept constant.

Significant paste leakage in Williams' study indicates that the cement content likely was high. Ideally, the paste fraction in RCC is just sufficient to fill the voids in between aggregates, allow compaction to the specified density, and provide a durable surface. Excessive cement content will produce a less stable mixture and defeats one main objective of RCC pavements.

Given a selected aggregate gradation and proportion and cement content, the gyratory compactor is able to determine the RCC moisture-density relationship, optimum moisture content, and maximum dry density. Some previous research has indicated that moisture-density testing with the gyratory will not yield a true optimum moisture content because at higher moisture contents the gyratory compactor will squeeze excess paste out of the sample (Williams 2013). This has been seen to be true in this study when excessive water or cement is added to the RCC mixture proportions. However, under normal RCC mixture proportions this should not generally occur. Using an adjusted procedure to determine the optimum moisture content from gyratory compaction, Williams (2013) reported that OMC using the gyratory was typically 0.75% lower than the OMC using the modified Proctor. Additionally, the MDD from the gyratory was typically 75 kg/m^3 (4.7 lb/ft^3) higher than the MDD using the modified Proctor. Khayat and Libre (2014) did not observe the same behavior reported by Williams and a gyratory-based OMC existed like the modified Proctor test. Note, Khayat used an alternative gyratory compactor, called the Intensive Compaction Tester (ICT). Ultimately, it was recommended that a slightly higher optimum moisture content should be used for RCC mix design (relative to the Proctor) because the resulting mechanical properties are more sensitive to a decrease in water below optimum than an increase in water above optimum (Khayat and Libre, 2014).

E.1.3 Intensive Compaction Tester

As mentioned in the previous section, another gyratory compactor has been used by some researchers, called the Intensive Compaction Tester (ICT). While much work has focused on application of the Superpave Gyratory Compactor, this machine was not originally intended for application to RCC, and thus many have warned against damaging the Superpave Gyratory Compactor when using it for RCC (ASTM C1800, 2017; Williams, 2013; Käppi and Nordenswan, 2007). Käppi and Nordenswan (2007) describe their experience using the ICT for applications to no-slump concrete. They have been using this machine since the late 1980s, and they suggest that the ICT would be a good alternative to the Superpave Gyratory Compactor for use in aggregate packing and mixture optimization tests (Käppi and Nordenswan, 2007). Khayat and Libre (2014) successfully used the ICT for both optimization of packing density and determining OMC from moisture-density testing of RCC.

E.2 PROJECT REVIEW OF GYRATORY COMPACTOR RESULTS

Limited research directly related to using the gyratory compactor for RCC mix design was performed. Appendix F details the use of the gyratory compactor for dry aggregate packing tests, with the most notable result being that aggregate breakdown in the gyratory machine resulted in poor fit for the aggregate packing model. Breakdown of the aggregate was even worse for the modified Proctor compaction method. Most of the conclusions made with respect to the gyratory compactor for application to RCC mix design are related to moisture-density testing results. Appendix L describes the use of the gyratory compactor to determine OMC for the RCC mixture selected. An example

moisture-density plot is shown below in Figure E1. When comparing to the results from the modified Proctor compaction procedure, the gyratory compactor for these constituents and proportions typically resulted in similar OMC but lower MDD. To date, the use of the gyratory for mix design purposes has resulted in similar OMCs to the modified Proctor, indicating that it appears to be reliable for this task. Ultimately, further work needs to be performed to compare the densities obtained from various lab compaction methods and field compaction.

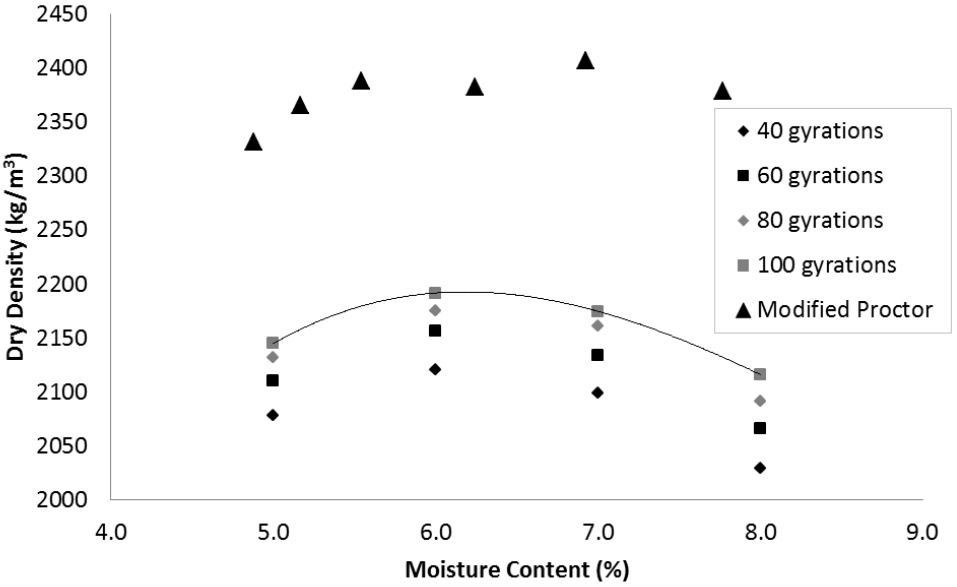

Figure E1: Comparison of Moisture-Density Results Using the Gyratory Compactor and Modified Proctor Procedure (from Appendix L). (1 kg/m^3 = 0.063 lb/ft^3)

E.3 PROPOSED GYRATORY MIX DESIGN PROCEDURE

E.3.1 Determine the Aggregate Gradation

The aggregate gradation should be inside the IDOT gradation limits, and ideally the gradation should be close to the 0.45-power maximum density line. Determination of what exact combination of aggregates is considered closest to the maximum density line can be performed using a minimization of the sum of square of error procedure for each sieve size. Ultimately, the gradation should allow for a dense packing of all aggregate sizes. An alternative procedure would be to conduct aggregate packing tests to determine what blend of aggregate combinations results in the highest density prior to selecting the cement content.

E.3.2 Determine the Cement Content

The cement content should be based on the IDOT minimum cement content, which is currently 320 kg/m^3 (540 lb/yd^3). This cement content is likely too high and an optimum cement content based on mechanical properties was identified in Chapter 4 as approximately 280 kg/m^3 (472 lb/yd^3). The

optimal cement content will depend on the desired surface characteristics, aggregate shape/texture, permeability, and durability requirements. More information can be found in Khayat and Libre (2014). Replacement of cement with a pozzolan such as fly ash can provide similar long-term mechanical and durability properties. However, a 20% fly ash replacement level, for example, may reduce the 1-day strength so this should be checked against the opening strength requirements.

E.3.3 Determine the Water Content from Moisture-Density Testing

From the selected constituents and proportions, from E.3.1-E.3.2, the water content of the mix should be based on the OMC from moisture-density testing with the gyratory compactor. Adjustments can be made considering other factors such as compaction delay. Additionally, the engineer could assess the effectiveness of the mix by comparing the maximum wet density with the theoretical maximum density (zero air void density), defined in ASTM C1800.

APPENDIX F: EXTENDING AGGREGATE PACKING MODEL FOR RCC

An aggregate packing model is extended for various RCC compaction methods and aggregate types in this chapter. Based on the new model parameters, RCC specimens were fabricated and tested to determine if trends observed in aggregate packing tests were manifested in improved hardened properties, namely strength (compressive, split tensile, and flexural), fracture properties (disk-shaped compact tension geometry), and drying shrinkage.

F.1 INTRODUCTION AND OBJECTIVES

There has been significant work in the literature on aggregate packing with both prescriptive models and optimized packing models based on packing tests. A lot of work has focused on optimizing the combined aggregate gradations for concrete pavements, self-consolidating concrete (SCC), ultra-high performance concrete (UHPC), unbound aggregate layers, and asphalt pavements. Many aggregate packing models have been published with one drawback being that they all assume that there is no aggregate degradation (no fracturing of aggregate particles), which may be a good assumption for most applications. With significant compaction energies imparted in laboratory compaction of RCC, there is a resultant breakdown of the initial aggregate gradation. The objective of this chapter is to create an aggregate packing model for commonly-used RCC compaction methods (modified Proctor, vibratory table with a surcharge, and the gyratory compactor) with the objective being to maximize density and/or predict the paste volume required to completely fill the voids in the aggregate structure.

F.2 DESCRIPTION OF AGGREGATE PACKING MODEL AND TESTS

Currently, the standard method of compaction for RCC mix design for pavements is the modified Proctor test (ASTM D1557), which compacts by means of vertical impact. Another method uses a vibrating table with a surcharge weight (i.e., the Vebe test), which is more common for RCC dams. The third method proposed by several past researchers (Amer et al. 2003; Amer et al. 2004; Delatte and Storey, 2005; Käppi and Nordenswan, 2007; Hazaree 2010; Williams 2013; Khayat and Libre, 2014) is the gyratory compactor which provides a combination of static compression and gyrating/shearing/kneading action to provide compactive effort. These three compaction methods were chosen to perform aggregate packing tests. After an extensive review of aggregate packing and particle packing literature, the model that showed the most promise with regards to aggregate packing for RCC was the Compressible Packing Model, termed CPM (De Larrard and Sedran, 2002). The main advantage of the CPM is that it has the capability of predicting packing density of poly-sized mixtures (multiple aggregate particle sizes) given multiple mono-particle densities, compaction energy, and compaction method (Lecomte, 2006).

The CPM uses the following three variables to calculate the combined aggregate packing density (φ) which is defined as the volume ratio of aggregate to total volume for a given aggregate type and gradation: packing index (K), virtual packing density when a particular aggregate size is dominant (γ_i),

volume fraction of the particular aggregate size (Y_i), and virtual packing density (i.e. maximum possible density) of a particular aggregate size (β_i) where subscript *i* corresponds to aggregate size (sieve-size) and the summation is over all aggregate (sieve) sizes (n). The relationship between K, γ_i, β_i, and φ is shown in Equation F1. The packing index (K) is a function of compaction method and compaction energy; therefore, this parameter will need to be calibrated for the three methods. Values of K for compaction on a vibrating table with a surcharge weight exist in the literature (Lecomte, 2006) however values of K for the modified Proctor or gyratory compactor do not currently exist. Equation F2 defines the relationship between γ_i, $\beta_{i\ or\ j}$, and two coefficients that account for the loosening effect (a_{ij}) and wall effect (b_{ij}). The coefficients a_{ij} and b_{ij} are defined by Equations F3 and F4, respectively, where d_i is the diameter of the particular aggregate size and subscripts *i* and *j* correspond to aggregate sieve size. Equation F5 defines β_i, which is a function of mono-sized particle virtual packing density (β_m), particle size (d_i), mold diameter (Θ), height of compacted aggregate (*h*), and a coefficient depending on particle shape (k_w), which is equal to 0.88 for rounded particles and 0.73 for crushed particles. The mono-sized particle virtual packing density (β_m) is defined in Equation F6.

$$K = \sum_{i=1}^{n} \frac{Y_i / \beta_i}{\frac{1}{\phi} - \frac{1}{\gamma_i}} \quad \text{(Eq. F1)}$$

$$\gamma_i = \frac{\beta_i}{1 - \sum_{j=1}^{i-1} Y_j \left[1 - \beta_i + b_{ij} \cdot \beta_i \left(1 - \frac{1}{\beta_j}\right)\right] - \sum_{j=i+1}^{n} Y_j \left[1 - a_{ij}\beta_i/\beta_j\right]} \quad \text{(Eq. F2)}$$

$$a_{ij} = \sqrt{1 - \left(1 - \frac{d_j}{d_i}\right)^{1.02}} \quad \text{(Eq. F3)}$$

$$b_{ij} = 1 - \left(1 - \frac{d_i}{d_j}\right)^{1.5} \quad \text{(Eq. F4)}$$

$$\beta_i = \frac{\beta_m}{1 - (1 - k_w)\left[1 - \left(1 - \frac{d_i}{\theta}\right)^2 \left(1 - \frac{d_i}{h}\right)\right]} \quad \text{(Eq. F5)}$$

$$\beta_m = \phi\left(1 + \frac{1}{K}\right) \quad \text{(Eq. F6)}$$

The unknowns in the above equations are K, φ, and β_m while all other parameters are constants or coefficients dependent on aggregate size (diameter), aggregate angularity/shape, dimensions of the

compaction mold, and the volume fraction of each aggregate size. The packing density (φ) is determined from the packing tests. In order to derive the two remaining unknown model parameters from packing tests, the packing densities of each individual particle size need to be measured for each compaction method (and aggregate type). Then, K and β_m can be iteratively solved. The remainder of the model coefficients from Equations F2 to F5 can be derived from the experimental data and knowing K and β_m.

In an attempt to calibrate the CPM over a range of aggregate types, six aggregate sources were sampled: coarse Dolomite, coarse trap rock, intermediate Dolomite, intermediate river gravel, natural sand, and manufactured sand. Two sources each of coarse, intermediate, and fine aggregates were sampled and shown in Figure F1. Coarse and intermediate Dolomite as well as natural sand are the most commonly used concrete aggregates in Illinois. Thus, an additional aggregate source for each size class (i.e. coarse, intermediate, and fine) was obtained to present a wider range of aggregate types. The trap rock is a stronger and stiffer aggregate than coarse Dolomite, while the river gravel is more rounded as compared to intermediate Dolomite, which is crushed and angular. Similarly, the manufactured sand is an angular fine aggregate with a higher fines content (amount passing the 0.074 mm (#200) sieve) than the rounded, natural sand. These combinations allow for comparison between a stiffer and more durable aggregate (trap rock) relative to a less hard aggregate (coarse Dolomite), as well as between crushed, angular aggregates and rounded, smooth aggregates.

Figure 21. Aggregates used in this Study. From left to right: Coarse Dolomite, Coarse Trap Rock, Intermediate Dolomite, Coarse River Gravel, Natural Sand, and Manufactured Sand.

In order to determine the parameter describing the packing ability of a particular compaction method, i.e., the packing index (K), packing tests were carried out on mono-sized aggregates as well

as the combined aggregate gradations for each aggregate type and each compaction method. Triplicate packing tests were carried out on each sieve-size fraction of each aggregate type, for each compaction method. This testing program resulted in approximately 320 packing tests. For a particular compaction method, aggregate type, and sieve-size fraction, 3 packing tests were carried out according to the compaction procedure for each compaction method (Table F1). After the compaction was completed and height and weight of the compacted aggregate sample were measured (as needed), a sieve analysis of the compacted aggregate sample was completed. The sieve analysis was performed to determine the amount of aggregate crushing that occurred during compaction and to determine the resulting volume fractions of each sieve-size, which was needed to calibrate the model. The raw data (aggregate packing density, particle size volume fractions, etc.) for all packing tests can be found in Appendix A.

Table F1. Compaction Procedures

Compaction Method	Procedure
Vibrating Table with Surcharge	Mold was filled with approximately 7 kg of aggregate, surcharge weight placed on top of aggregate, vibrated for 2 minutes (Lecomte 2006). The resulting height of the aggregate was measured.
Modified Proctor	Conducted according to ASTM D1557.
Gyratory Compactor	Approximately 7 kg (15.5 lbs) of aggregate was placed in the mold and compacted using 100 gyrations at 1.25 degree internal angle, and a compaction pressure of 600 kPa (87 lb/in^2).

F.3 PACKING MODEL CALIBRATION AND RESULTS

After completion of the packing test and determining the final aggregate gradation, the measured packing density and particle size volumes on each sieve size were used in the model to iteratively solve for K and β_m. This iterative process was continued until the sum of squared errors (SSE) between measured and predicted packing density was minimized (Figure F2). The end result of the iterative process is the value of K that produces the best model fit since all other parameters are a function of K, φ, and aggregate size volume fractions which are all known parameters now. Figure F2 also shows the predicted and experimental packing densities for all packing tests performed on a particular aggregate type using a particular compaction method. The value of K for each aggregate type and compaction method pair is shown in Table F2. There were some combinations of aggregate type and compaction method that did not converge to a solution. For these combinations, values of K were iterated to 100 however the error did not converge to a minimum for reasonable values of K (Figure F3). Therefore, the K value was considered not applicable and no model fit was proposed for that combination of aggregate type and compaction method. This is likely caused by significant

aggregate breakdown and the model was not able to compensate for this additional packing by simply increasing the packing index (K).

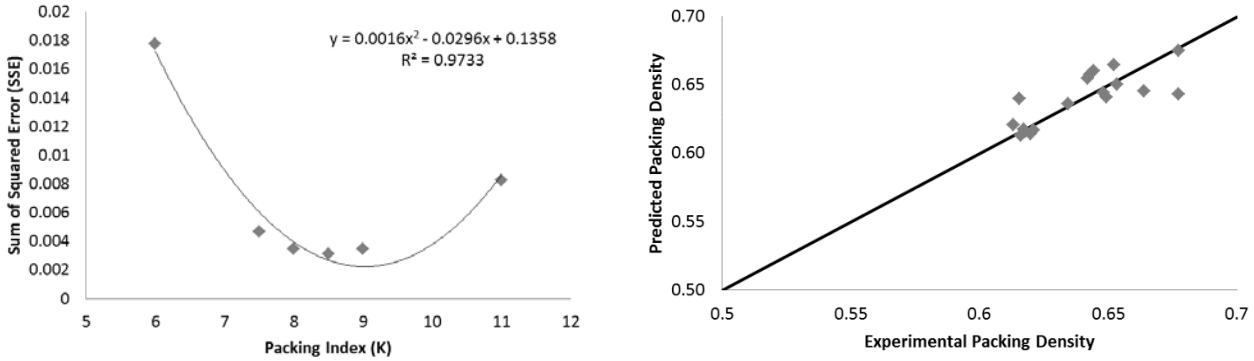

(a) **(b)**

Figure 22. Error vs. Packing Index for Given Aggregate Type and Compaction Method (a) and Predicted vs. Experimental Packing Densities at K-value that Minimizes SSE for Given Aggregate Type and Compaction Method (b).

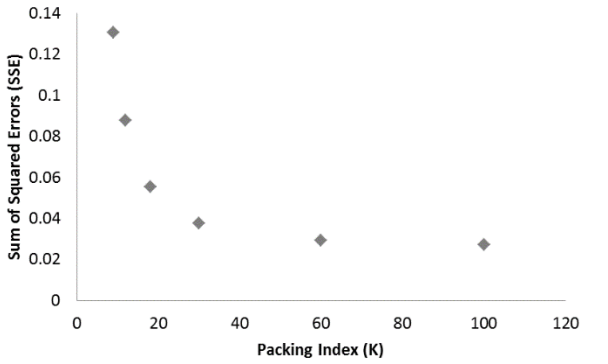

(a)

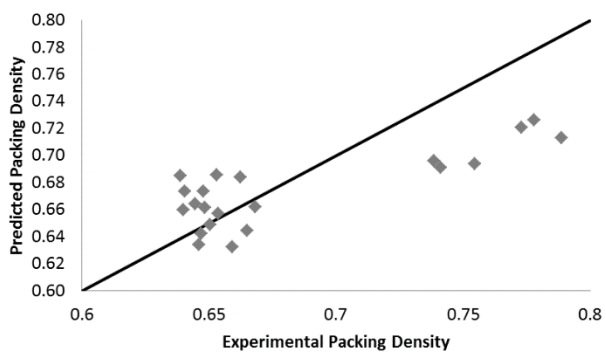

(b)

Figure 23. Error vs. Packing Index (a) and Predicted vs. Experimental Packing Density (b) at K=100 for Manufactured Sand compacted with Gyratory Compactor.

Table F2. Packing Index (K) as a Function of Aggregate Type and Compaction Method

Aggregate Type	Vibrating Table with Surcharge Weight	Modified Proctor	Gyratory Compactor
Coarse Dolomite	6.0	10.5	8.5
Trap Rock	4.3	7.5	7.1
River Gravel	7.1	15.8	7.5
Intermediate Dolomite	6.6	N/A*	9.0
Natural Sand	8.0	7.5	12.0
Manufactured Sand	6.7	N/A*	N/A*
Average	6.4	10.3	8.8

*N/A signifies that the error did not converge to a minimum and therefore no packing index value could be assigned. These values were excluded from the average K-value determination for each compaction method.

From Table F2, it can be seen that the modified Proctor method of compaction resulted in higher values of packing index than the gyratory compactor, while the vibrating table with the surcharge weight typically led to the lowest packing indices. When using the values of packing index in Table F2 to predict packing density of a particular aggregate type using a particular compaction method, the average packing density error (absolute value) was 0.016. Figure F4 compares the experimental and predicted packing densities for all 320 packing tests performed when the final aggregate gradation was known and the appropriate K-value (Table F2) was used for each aggregate type and compaction method pair. There is good agreement between the two for a wide range of packing densities, aggregate types, and compaction methods. The K values that minimized model error (Table F2) and the relationship between experimental and predicted packing densities (Figure F4) were developed based on the aggregate gradations after the packing tests were completed (called inverse model calibration here). Attempts were made to calibrate the model with the gradations before packing tests were conducted (Figure F5), which resulted in an average error (absolute value) in packing density of 0.031 (called forward model calibration here). The agreement between experimental and predicted packing densities in Figure F5 (correlation coefficient of 0.82) is not as good as that in Figure F4 (correlation coefficient of 0.96). The experimental and predicted packing densities for the vibrating table with surcharge method in Figure F5 show much better agreement than the other two compaction methods. The difference is likely related to the vibratory table breaks much less particles than the modified Proctor and gyratory compaction methods (Figure F6), and therefore results in a smaller change in the overall gradation. Broken particles (%) is defined as the percentage by weight of particles passing their initial sieve size (after compaction) to the initial weight of the aggregate sample. A higher value of broken particles indicates a greater weight change in aggregate gradation from pre-compaction to post-compaction.

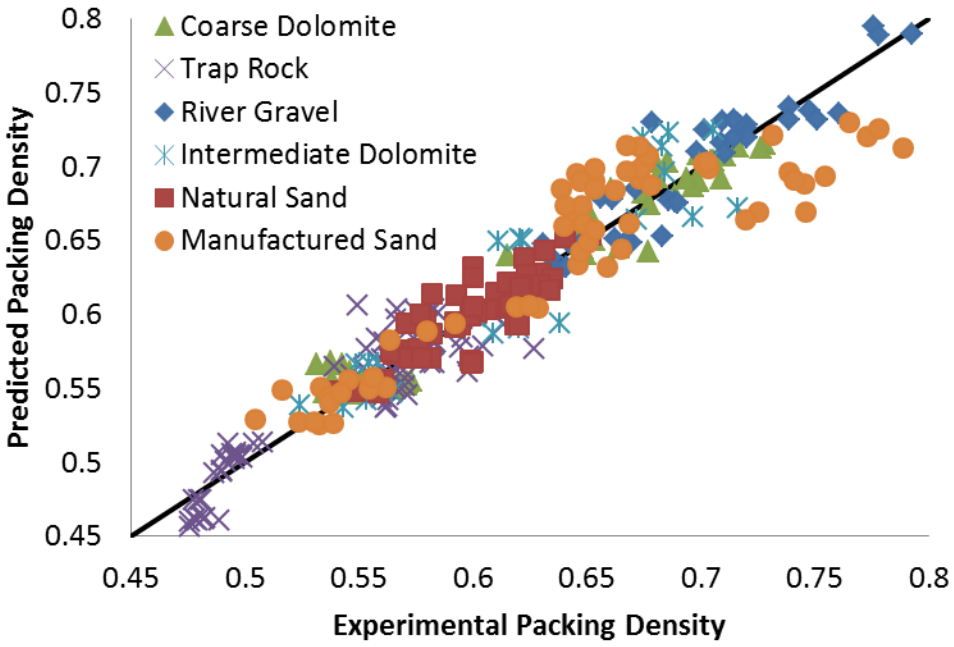

Figure 24. Comparison of All Predicted and Experimental Packing Densities based on Post-Packing Test Gradations.

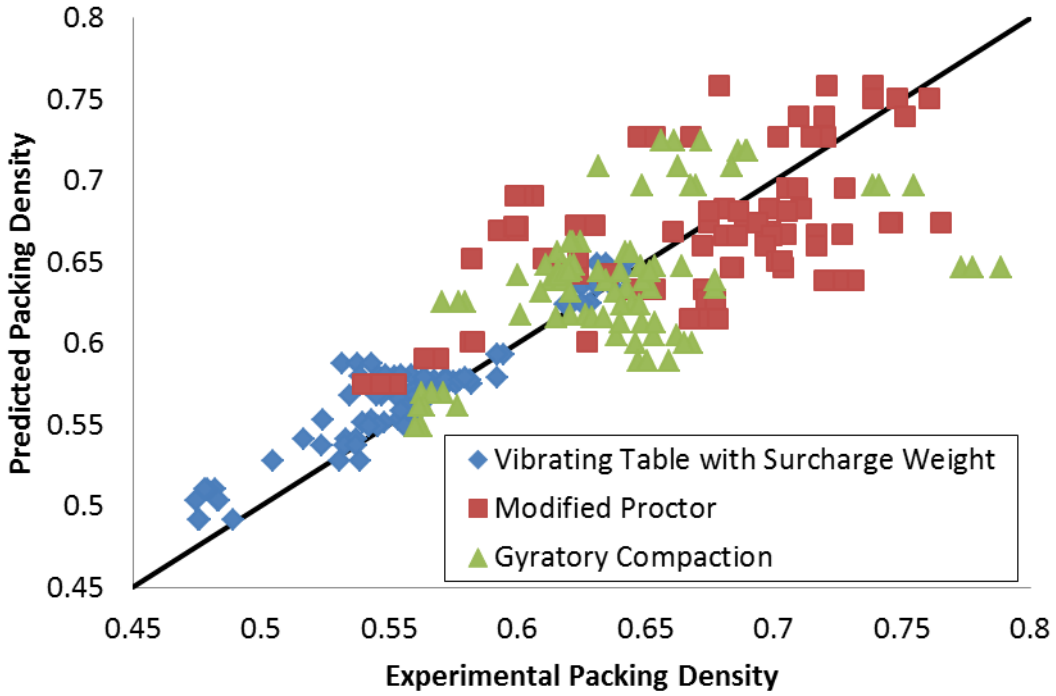

Figure 25. Comparison of All Predicted and Experimental Packing Density based on Initial Packing Test Gradations.

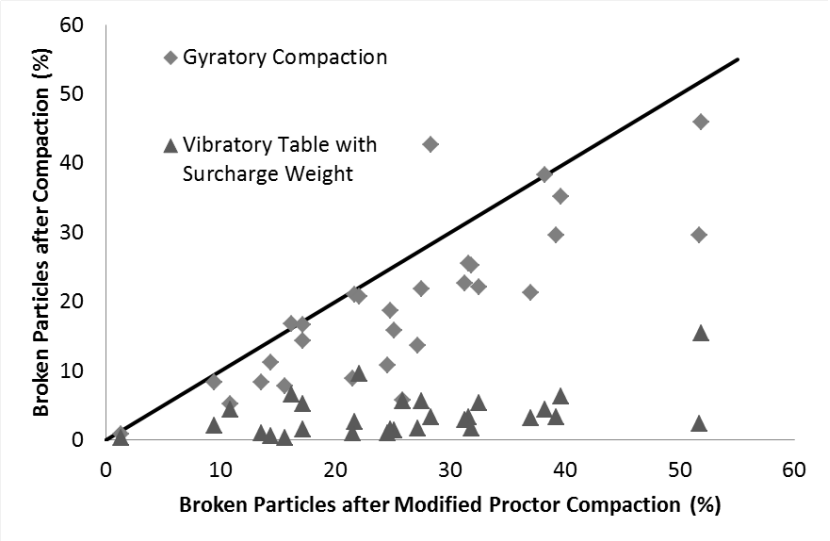

Figure 26. Comparison of Broken Particles from Three Compaction Methods.

The forward packing model (predicting packing density using initial gradation) is unable to account for significant aggregate breakage, since the final gradation is quite different from the initial gradation. However, using the inverse packing model (i.e. knowing the final, compacted gradation) produces much better results (Figure F4). Therefore, use of the model for forward prediction of aggregate packing for the gyratory and modified Proctor compaction methods was not reliable. Although the aggregate packing tests did not result in a comprehensive prediction model in its current functional form, they did reveal insight into the nature of aggregate packing in RCC compaction methods. Figure F6 shows that the modified Proctor compaction method breaks a significantly greater proportion of aggregates relative to the vibrating table and, to a lesser extent, the gyratory compactor. Both the gyratory compactor and modified Proctor compaction methods did result in greater packing densities than the vibrating table with surcharge weight (Figure F7). There was not a consistent trend in packing density between modified Proctor and gyratory compaction. From Table F3, it can be seen that coarse Dolomite had a higher packing density than trap rock which is likely a result of the fact that Dolomite is a weaker aggregate and therefore fractured more easily to fill in voids. The river gravel produced higher packing densities than the intermediate Dolomite because of the rounded nature of the river gravel that reduces friction and adjacent particle interlock. There was not a consistent and significant difference in packing density of the natural and manufactured sands. Note, all packing tests were done with the aggregate type in the dry condition which definitely led to more particle breakage than would be seen in compacted RCC with any of the 3 compaction methods.

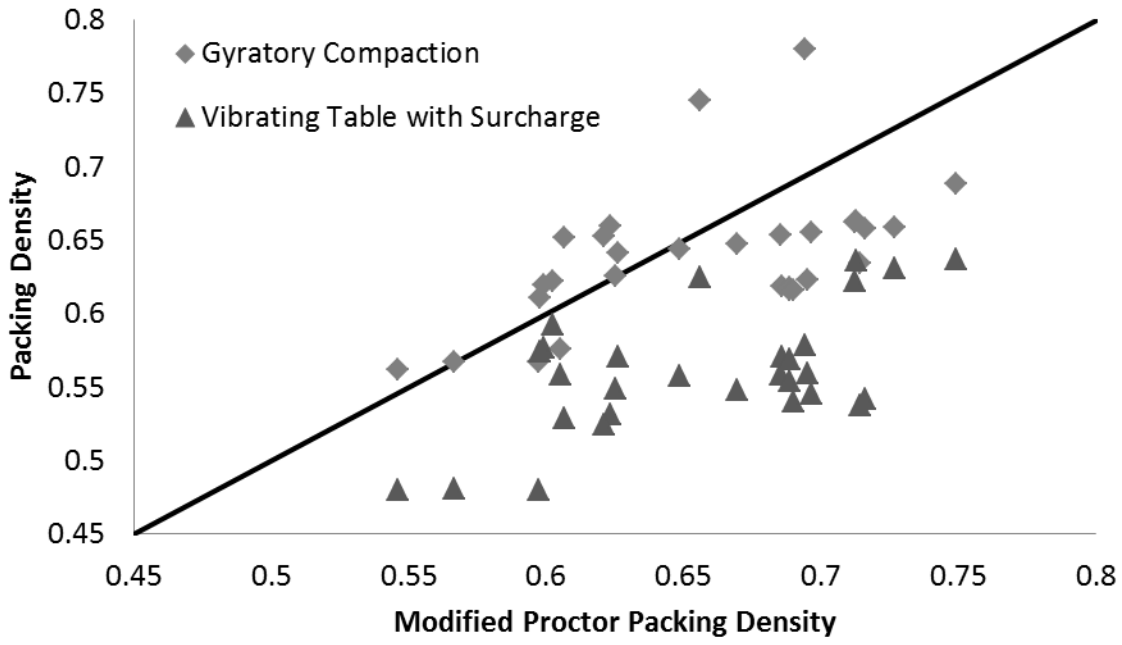

Figure 27. Comparison of Packing Density for each Compaction Method.

Table F3. Packing Density as a Function of Aggregate Type and Compaction Method

Aggregate Type	Vibrating Table with Surcharge Weight	Modified Proctor	Gyratory Compactor
Coarse Dolomite	0.55	0.70	0.64
Trap Rock	0.48	0.57	0.57
River Gravel	0.63	0.73	0.67
Intermediate Dolomite	0.55	0.69	0.62
Natural Sand	0.57	0.61	0.62
Manufactured Sand	0.56	0.65	0.68

F.4 MIX DESIGN AND FRESH PROPERTIES OF RCC WITH MULTIPLE AGGREGATE TYPES

Mix designs of RCC incorporating the aggregates used in the aggregate packing study were developed and specimens were cast in order to determine if aggregate type would have an impact on RCC fresh and hardened properties. A fixed gradation (Table F4) was obtained by sieving each aggregate source into individual sieve sizes and then recombining them in specific proportions to produce the desired combined gradation. The specific gravities of each aggregate were: 2.67 (coarse and intermediate Dolomite), 2.86 (trap rock), 2.53 (river gravel), and 2.64 (natural and manufactured sand). Four mixes were developed to determine the impact of the 6 aggregate types employed in the packing study. The control mixture (called Dolomite) consists of coarse and intermediate Dolomite as well as natural sand (these three aggregates comprise most RCC mix designs in this report: Chapters 2 and 4 and Appendices H, J, and K). The other three mix designs were obtained by replacing coarse Dolomite with trap rock (called Trap Rock), intermediate Dolomite with river gravel (called River Gravel), and natural sand with manufactured sand (called Manufactured Sand). A total cementitious content of 282 kg/m^3 (475 lb/yd^3)was fixed for all mixes with a 12.5% weight replacement with class C fly ash. The final RCC mix designs can be found in Table F5. The Vebe time for each mix was also measured with the river gravel mix producing the lowest Vebe time while the manufactured sand mix yielded the highest Vebe time. The river gravel mix also had the highest maximum dry density but the difference in MDD was less than one percent between the four mixes.

Table F4. Combined Aggregate Gradation (1 in = 25.4 mm)

Sieve Size (mm)	% Passing
19.0	100
12.7	77.4
9.51	73.1
4.76	50.0
2.38	38.2
1.19	35.8
0.595	24.5
0.30	2.9
0.15	0.2
0.075	0.0

Table F5. Oven-Dry Mix Designs (kg/m^3) (1 kg/m^3 = 1.686 lb/yd^3)

	Dolomite	Trap Rock	River Gravel	Manufactured Sand
Coarse Dolomite	791.6	-	525.9	693.8
Trap Rock	-	776.3	-	-
Intermediate Dolomite	417.7	430.7	-	366.1
River Gravel	-	-	787.7	-
Natural Sand	899.8	898.1	812.9	-
Manufactured Sand	-	-	-	1059.9
Cement	246.5	246.5	246.5	246.5
Fly Ash	35.2	35.2	35.2	35.2
Water	157.5	139.6	140.3	155.1
Vebe time (sec)	12.5	15.4	8.5	16.7
Maximum Dry Density	2390.8	2386.8	2408.2	2401.5
Optimum Moisture	6.6	5.8	5.8	6.5

F.5 RCC HARDENED PROPERTIES

Compressive and split tensile strength were determined on triplicate 100x200 mm (4x8 in) cylinders for each mix after 1, 7, 28, and 120 days of moist-curing. Flexural strength (MOR) was determined on triplicate 100x100x400 mm (4x4x16 in) beams after 28 days of moist-curing. Results of compressive strength are shown in Figure F8. Statistical analysis with the Tukey test was performed on 1 and 28 day compressive strengths with results shown in Table F6. All mixes easily met the typically specified 31 MPa (4.5 ksi) compressive strength at 28 days (ACPA, 2014) and 7 day strengths of 24 MPa (3.5 ksi). The 1-day compressive strength of the manufactured sand mix was statistically greater than all other mixes. The River Gravel mix yielded statistically similar compressive strengths at 1 and 28 days to the Dolomite mix. In conventional concrete, rounded aggregates typically result in lower strengths because of the reduced mechanical bond between aggregate and mortar (Guinea et al. 2002). The trap rock (i.e. higher quality rock) was more difficult to compact, as shown by lower packing densities, and therefore resulted in lower compressive strengths.

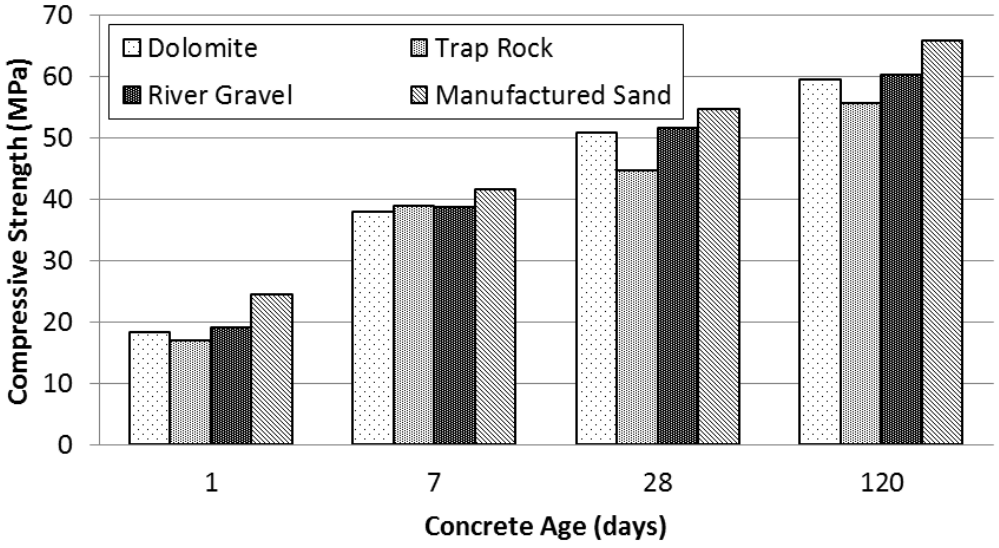

Figure 28. Average RCC Compressive Strength. (1 ksi = 6.89 MPa)

Table F6. Statistical Analysis of RCC Compressive Strength (1 ksi = 6.89 MPa)

Mix ID	1-Day Compressive Strength (MPa)	Statistical Grouping(s)		
Manufactured Sand	24.5	A		
River Gravel	19.2		B	
Dolomite	18.5		B	C
Trap Rock	17.1			C
	28-Day Compressive Strength (MPa)			
Manufactured Sand	54.7	A		
River Gravel	51.7	A		
Dolomite	51.0	A	B	
Trap Rock	44.8		B	

The results of split tensile strength testing are shown in Figure F9 along with statistical analysis results shown in Table F7. Similar to compressive strength, the 1-day split tensile strength of the Manufactured Sand mix was statistically greater than all other mixes. The Dolomite, Trap Rock, and River Gravel mixes all yielded statistically similar split tensile strengths at 1 and 28 days, suggesting that the effect of aggregate packing and aggregate surface characteristics on split tensile strength are less significant than compressive strength. Similar to split tensile strength, all four mixes resulted in statistically similar flexural strengths (Table F8). The split and flexural strengths produced the same strength rankings (i.e. the Dolomite mix had the highest split tensile and flexural strength, followed by the Manufactured Sand mix, etc.). Trap Rock yielded the lowest 28-day strength of all mixes in compression, split tension, and flexure. Trap Rock also had the lowest aggregate packing density from the packing tests (Table F3).

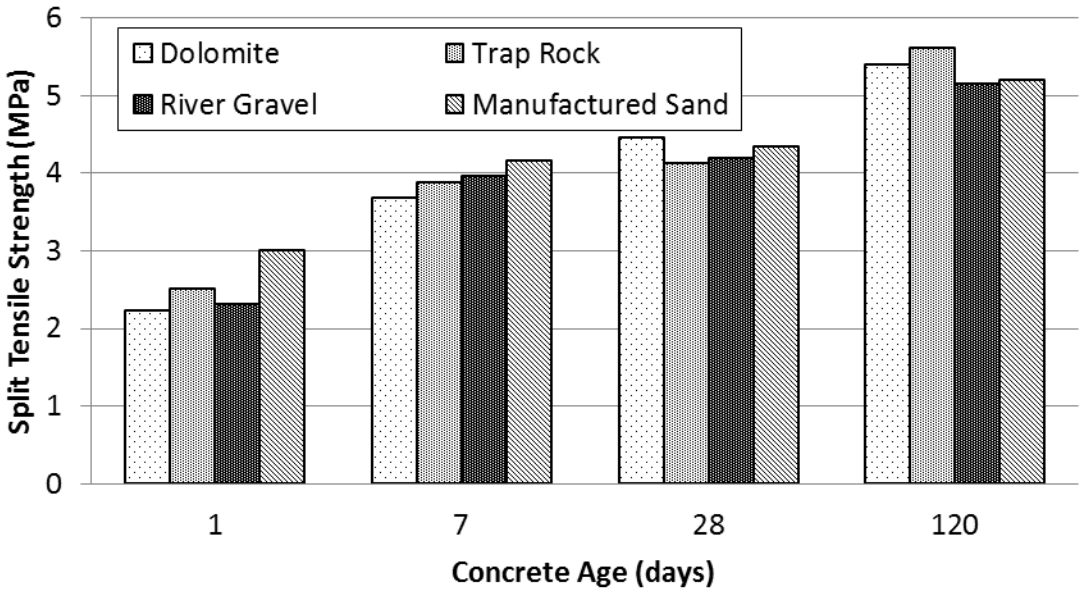

Figure 29. Average RCC Split Tensile Strength. (1 ksi = 6.89 MPa)

Table F7. Statistical Analysis of RCC Split Tensile Strength (1 ksi = 6.89 MPa)

Mix ID	1-Day Split Tensile Strength (MPa)	Statistical Grouping(s)	
Manufactured Sand	3.01	A	
Trap Rock	2.52		B
River Gravel	2.32		B
Dolomite	2.23		B
	28-Day Split Tensile Strength (MPa)		
Dolomite	4.46	A	
Manufactured Sand	4.35	A	
River Gravel	4.21	A	
Trap Rock	4.14	A	

*1 ksi = 6.89 MPa

Table F8. Statistical Analysis of RCC Flexural Strength (1 ksi = 6.89 MPa)

Mix ID	28-Day Flexural Strength (MPa)	Statistical Grouping(s)
Dolomite	7.40	A
Manufactured Sand	7.19	A
River Gravel	6.73	A
Trap Rock	6.49	A

Fracture properties of the four mixes were also tested at an age of 28 days with the DCT geometry (Amirkhanian et al. 2015). Results of fracture testing are shown in Table F9 while statistical analysis of critical stress intensity factor and total fracture energy is shown in Table F10. Trap Rock had the greatest total fracture energy despite having the lowest strengths. It has been shown that crushed aggregates lead to increases in fracture energy (Guinea et al. 2002; Chupanit and Roesler, 2005). The Trap Rock and River Gravel mixes had statistically lower critical stress intensity factors than the Manufactured Sand and Dolomite mixes, suggesting that the bond strength between the mortar and the trap rock and river gravel aggregates is less. The fracture properties for these different aggregate types are generally in agreement with fracture properties of RCC shown in Chapter 2.

Table F9. 28-Day Fracture Properties (COV, %); (1 MPa-$m^{1/2}$ = 0.910 ksi-$in^{1/2}$; 1 GPa = 145.03 ksi; 1 lb/in = 175 N/m)

Mix ID	Critical Stress Intensity Factor, K_{IC} (MPa-$m^{1/2}$)	Elastic Modulus, E (GPa)	Critical Crack Tip Opening Displacement, $CTOD_C$ (mm)	Initial Fracture Energy, G_f (N/m)	Total Fracture Energy, G_F (N/m)
Dolomite	1.43 (4.3)	35.5 (6.6)	0.0200 (14.8)	57.8 (11.8)	154.5 (11.9)
Trap Rock	1.25 (5.0)	34.3 (4.9)	0.0178 (12.7)	45.5 (13.8)	241.6 (17.2)
River Gravel	1.23 (11.8)	29.9 (7.9)	0.0179 (16.8)	51.4 (19.7)	186.8 (11.8)
Manufactured Sand	1.46 (5.2)	35.6 (4.3)	0.0196 (10.1)	60.2 (7.6)	134.6 (5.1)

Table F10. Statistical Analysis of Fracture Properties (1 MPa-$m^{1/2}$ = 0.910 ksi-$in^{1/2}$; 1 lb/in = 175 N/m)

Mix ID	Critical Stress Intensity Factor, K_{IC} (MPa-$m^{1/2}$)	Statistical Grouping(s)		
Manufactured Sand	1.46	A		
Dolomite	1.43	A		
Trap Rock	1.25		B	
River Gravel	1.23		B	
	Total Fracture Energy, G_F (N/m)			
Trap Rock	241.6	A		
River Gravel	186.8		B	
Dolomite	154.5		B	C
Manufactured Sand	134.6			C

Drying shrinkage measurements were conducted on the 4 mixes with drying beginning 24 hours after casting. The drying shrinkage strains over time are shown in Figure F10. It can be seen that the Dolomite and Manufactured Sand mixes had higher shrinkage strains than the River Gravel and Trap Rock mixes.

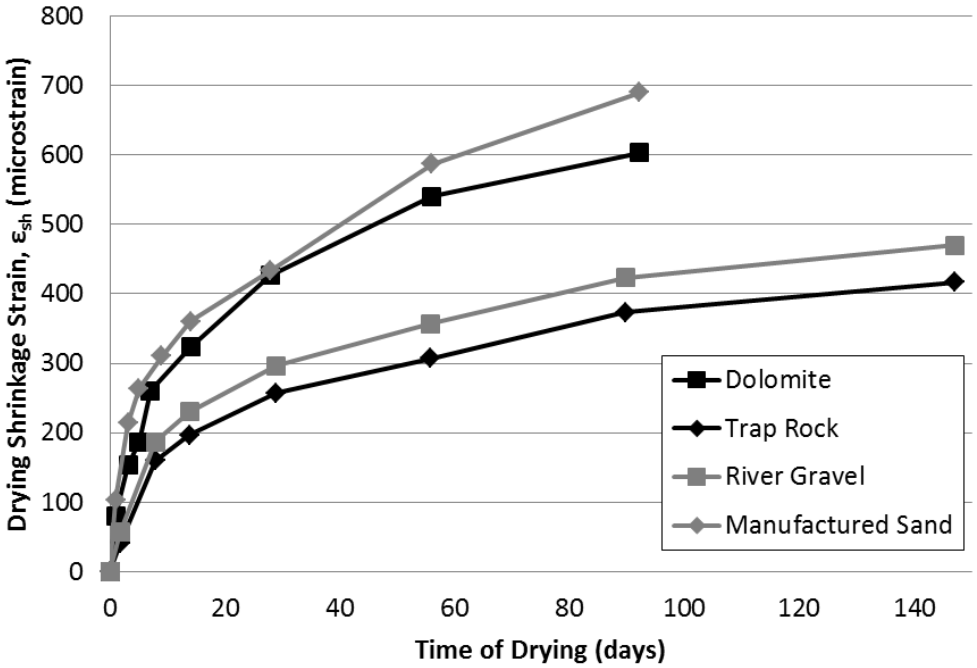

Figure F10. Drying Shrinkage Strains over Time

F.6 CONCLUSIONS

Oven-dry aggregate packing tests were conducted using the following three compaction methods utilized for RCC mix design and specimen fabrication: vibrating table with a surcharge weight, modified Proctor, and gyratory compaction. The packing tests were used to calibrate an aggregate packing model called the compressible packing model (CPM). The calibrated model had an average packing density error (absolute value) of 0.016 when the final compacted gradation was known. However, the absolute error increased to 0.031 when the initial gradation prior to compaction was used in the model calibration. Significant aggregate breakdown was observed for the modified Proctor and gyratory compactor compaction methods in the oven-dry aggregate condition, which led to the poor model fit when using the initial gradation before compaction. The gyratory compactor and modified Proctor compaction methods resulted in higher packing densities than the vibrating table with surcharge weight method because of the greater aggregate breakdown from those methods. The weaker coarse aggregate (Dolomite) had higher packing densities than the stronger, more durable coarse aggregate (trap rock) because of the trap rock's resistance to aggregate breakdown. The rounded, smooth river gravel resulted in higher packing densities than the intermediate limestone because of the river gravel's more favorable particle shape and texture for packing efficiency.

RCC mix designs were developed using the aggregates from the packing study with a fixed gradation. The mix incorporating river gravel as an intermediate aggregate produced the lowest Vebe time and greatest maximum dry density, however, neither of which were significantly different than the other

three RCC mixes. The mix with trap rock, the aggregate with the lowest packing density, resulted in the lowest compressive strengths. Drying shrinkage strains were shown to be affected by aggregate type with trap rock and river gravel aggregates yielding the two lowest shrinkage strains. In general, it was shown that aggregate shape and packing characteristics affected RCC compressive strength, fracture properties, and drying shrinkage strains but did not impact the maximum dry density, tensile and flexural strength, or Vebe times.

APPENDIX G: RECYCLED AGGREGATES IN ROLLER-COMPACTED CONCRETE

This chapter investigates the use of recycled aggregates in RCC pavement mix designs. The recycled aggregates used include: recycled concrete aggregate (RCA), reclaimed asphalt pavement (RAP), steel furnace slag fractionated RAP (SFSFRAP), and electric arc furnace (EAF) steel slag aggregates. Strength (compression, split tension, and flexure) and fracture properties were characterized for these mixes.

G.1 INTRODUCTION

The use of recycled materials, such as recycled concrete aggregate (RCA) and reclaimed asphalt pavement (RAP), as aggregate in concrete has been gaining interest as a result of growing interest in more sustainable pavement options. Many studies have shown the effects of such recycled materials on the fresh and hardened properties of conventional paving concrete (Van Dam et al. 2011; Gardiner and Komas 2013). However, there have been fewer studies on the use of recycled aggregates in roller-compacted concrete (RCC) with the majority published within the past six years (Haque and Ward 1986; Nanni 1988; Sobhan and Mashnad 2001; Sobhan and Mashnad 2002; Debieb et al. 2009; Courard et al. 2010; Albuquerque et al. 2011; Bilodeau et al. 2011, 2012; Sachet et al. 2011; Villena et al. 2011; Nguyen et al. 2012; Muscalu et al. 2013; Sachet et al. 2013; Ferrebee et al. 2014; Modarres and Hosseini 2014; Angelakopoulos et al. 2015). The most common recycled aggregate sources studied for use in RCC have been RAP and RCA, but there has also been some research on using other recycled, co-product, or waste material (RCWM), including rice husk ash (RHA), blast furnace slag sand, limestone tailings, and recycled masonry.

More recently, studies have been published concerning the performance or design of RCC with recycled materials. Accelerated pavement test (APT) sections of RCC with RAP and steel fibers were constructed in France with the material properties summarized by Bilodeau et al. (2011, 2012) and preliminary accelerated pavement testing results presented by Nguyen et al. (2012). Based on the APT results, Nguyen et al. (2012) developed a pavement design for their study and found that, as a base layer for a continuously reinforced concrete pavement, RCC with RAP needed to be 1-2 cm (0.4-0.8 in) thicker than RCC with limestone (virgin) aggregates.

Replacing virgin coarse aggregate with fractionated reclaimed asphalt pavement (FRAP), either as a partial or full replacement, in RCC was shown to reduce compressive strengths by approximately 40% (Courard et al. 2010; Ferrebee et al. 2014; Modarres and Hosseini 2014), flexural strengths by approximately 35% (Modarres and Hosseini 2014), and split tensile strengths by approximately 20% (Ferrebee et al. 2014). RAP also decreased the RCC elastic modulus by up to 50% (Bilodeau et al. 2011). The use of fine FRAP in RCC has proved to be more detrimental to the strength properties compared to the use of coarse FRAP (Modarres and Hosseini 2014). Fracture properties of RCC with 16% FRAP (by weight of total aggregate) were shown to be statistically similar to virgin RCC (Ferrebee et al. 2014), although Sachet et al. (2011) found that the use of RAP (50% by total aggregate volume) reduced the stress intensity factor of RCC. Modarres and Hosseini (2014) also demonstrated that RCC

with 100% RAP aggregates had a lower fatigue life compared with virgin RCC at stress ratios less than 0.70.

The addition of RCA to RCC has been shown to reduce its strength and elastic modulus (Debieb et al. 2009; Muscalu et al. 2013) with the magnitude of reduction dependent on the quality and source of the RCA. Angelakopoulos et al. (2015) showed that recycled masonry aggregates in RCC reduced strength by approximately 40% while high-quality RCA yielded similar strengths to a virgin aggregate RCC. Albuquerque et al. (2011) reported blast furnace slag sand reduced RCC strength and elastic modulus while having little effect on its fracture properties. The use of RHA (Villena et al. 2011) and limestone tailings (Nanni 1988) as aggregate replacements in RCC have yielded greater strengths than similar virgin RCC mixtures.

The literature for RCC containing recycled materials as aggregate have generally shown reductions in strength and modulus relative to virgin RCC with a few exceptions. None of the studies used a fixed gradation to compare the RCC properties produced by virgin or recycled aggregates even though aggregate gradation is known to affect the RCC properties (ACI 1995; LaHucik and Roesler 2015). Therefore, this study aims to compare the effects of various recycled materials on RCC properties, while maintaining the aggregate gradation and cement content, in order to better determine their feasibility for use in RCC pavements. For both recycled and virgin aggregate RCC mixtures, moisture-density relationship, strength (compression, split tension, and flexure), and fracture properties were measured in order to compare the various recycled material types and replacement amounts with the virgin RCC mixture.

G.2 MIXTURE DESIGN

Four types of recycled aggregates were included in this study: RAP, a fractionated reclaimed asphalt pavement that contained steel furnace slag aggregates (SFSFRAP), electric arc furnace slag aggregates (EAF), and RCA. A control mixture was also created using virgin dolomite and natural sand with a combined gradation typical of RCC (ACI, 1995). Extensive characterization of the EAF and SFSFRAP aggregates was performed by Brand and Roesler (2015a, 2015b). For one mix design of each recycled aggregate, the combined gradation was made equivalent to that of the virgin mix to make a direct comparison between all mixtures. For the fixed combined gradation mixtures, only the recycled aggregates coarse fraction (i.e., retained on 4.76 mm (#4) sieve) was used along with natural sand. In order to ensure that the combined gradations were equivalent between these mixtures, each aggregate was individually sieved and recombined. These mixtures are labeled by their type of recycled aggregate (RCA, EAF, RAP, and SFSFRAP) with all mixtures replacing 40% of total aggregate weight with recycled aggregate. Each recycled aggregate type also has at least one additional mix design where the recycled aggregate was used at its natural gradation and blended with the natural gradations of the virgin aggregates to minimize deviation from the 0.45-power curve. These mixes are labelled by their type of recycled aggregate followed by the percent replacement (by total aggregate weight) of virgin aggregate with recycled aggregate (i.e., RCA-25, RCA-40, etc.). For these mixes, the recycled aggregate gradation was used in its entirety, which includes any material passing the 4.76 mm (#4) sieve. The cement content was fixed at 282 kg/m^3 (475 lb/yd^3) for all mixes, using a Type I portland cement.

Three virgin aggregates (coarse dolomite, intermediate dolomite, and natural sand) were used in this study to obtain a dense gradation, following the recommended gradation for RCC by ACI (1995). The aggregate gradations, specific gravity, and absorption capacity for each virgin and recycled aggregate are shown in Table G1. The combined gradations for each mix design are shown in Figure G1 along with the maximum density line (0.45-power curve) and gradation limits suggested by the American Concrete Pavement Association (ACPA 2014). All of the RCC mixtures using recycled aggregates (RCA, RAP, SFSFRAP) in their stock gradations have similar combined gradations, which are also quite similar to the mixtures where the gradation was held constant by sieving and recombining, at least until the 0.3 mm (#50) sieve. Modified Proctor testing according to ASTM D1557 (2012) was performed to determine the optimum moisture content (OMC) and maximum dry density (MDD) of each mixture. The final mixture proportions (Table G2) were determined by knowing the MDD, OMC, aggregate blends, and cement content for each mix. The EAF mixes yielded greater values of MDD (relative to the control) as a result of the higher specific gravity of the EAF aggregates while the RCA mixes yielded greater values of OMC (relative to the control) because of the high absorption capacity of the RCA as noted in Table G1 and Table G2.

Table G1. Stock Aggregate Gradations and Physical Properties (1 in = 25.4 mm)

	Coarse Dolomite	Intermediate Dolomite	Natural Sand	RAP	SFSFRAP	EAF	RCA
Sieve Size (mm)	Cumulative Percent Passing (%)						
25.4	100.0	100.0	100.0	98.3	100.0	100.0	91.0
19	76.8	100.0	100.0	95.0	100.0	100.0	74.4
12.7	30.9	99.8	100.0	88.2	99.9	99.9	53.3
9.51	13.5	93.8	100.0	81.9	83.7	83.3	43.9
4.76	2.1	33.6	96.0	53.2	13.3	24.1	28.8
2.38	0.5	3.6	83.2	30.1	3.9	4.7	20.4
1.19	0.4	1.2	66.6	15.3	2.8	2.2	14.6
0.595	0.4	0.9	46.3	2.0	2.5	1.9	4.0
0.297	0.4	0.8	12.4	0.2	2.2	1.6	1.2
0.149	0.3	0.7	1.3	0.0	1.7	1.3	0.2
0.074	0.3	0.6	0.4	0.0	0.8	0.9	0.1
Absorption Capacity (%)	2.95	3.00	1.38	2.12	2.00	1.75	7.34
Oven-Dry Specific	2.49	2.45	2.50	2.40	2.63	3.64	2.42

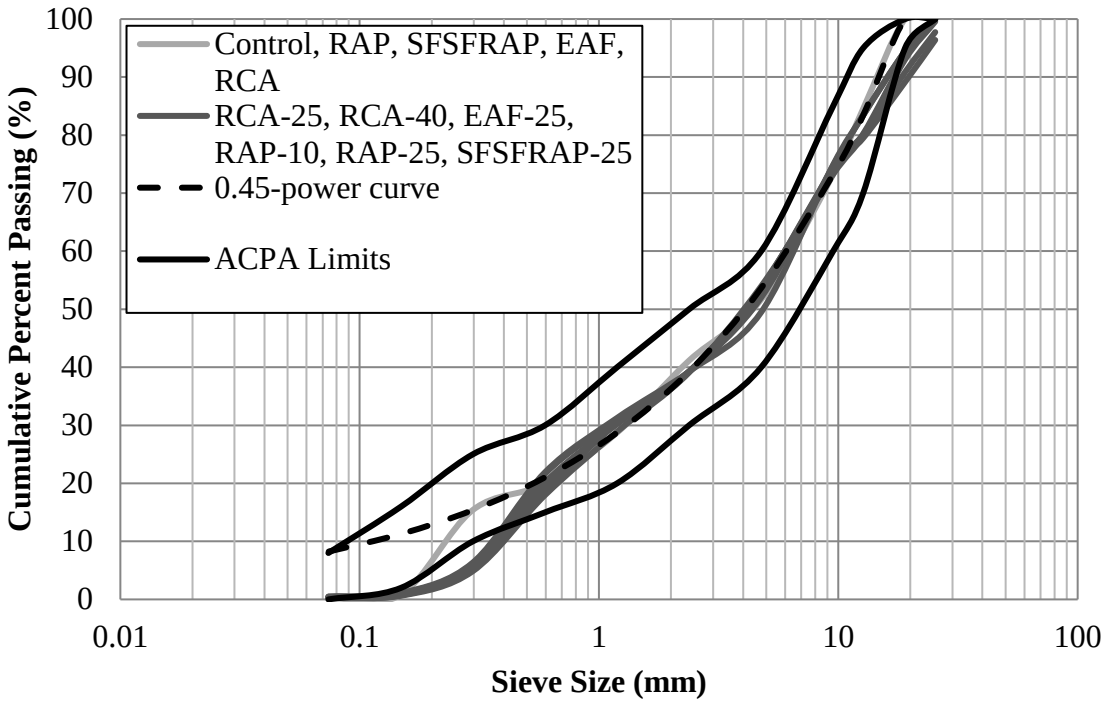

Figure G1. Combined Aggregate Gradations. (1 in = 25.4 mm)

Table G2. Mixture Proportions and Modified Proctor Results (1 kg/m^3 = 1.68 lb/yd^3)

Mixture	Modified Proctor Results		Mixture Proportions (kg/m^3)		
	MDD (kg/m^3)	OMC (%)	Total Aggregate	Cement	Water
Control	2351	6.43	2070	282	151.2
RCA	2262	8.52	1980	282	192.7
RCA-25	2375	7.06	2094	282	167.7
RCA-40	2342	7.94	2060	282	185.9
EAF	2641	6.80	2360	282	179.6
EAF-25	2540	5.99	2259	282	152.2
RAP	2311	6.75	2030	282	156.0
RAP-10	2382	6.06	2100	282	144.3
RAP-25	2375	6.20	2094	282	147.3
SFSFRAP	2404	5.90	2123	282	141.9
SFSFRAP-25	2382	6.14	2100	282	146.3

G.3 SPECIMEN PREPARATION

All specimens were mixed in a pan mixer according to ASTM C192 (2013) using the mixture proportions from Table G2. Virgin aggregates were mixed in an oven dry condition while RAP, SFSFRAP, and EAF were mixed in an air dry condition to avoid altering aggregate characteristics via oven drying. The RCA was mixed at approximately 80% of its saturated surface dry condition according to recommendations by Brand et al. (2015). For fracture testing via the disk-shaped compact tension (DCT) geometry, 150x300 mm (6x12 in) cylinders were cast according to ASTM C1435 (2008). For strength testing (compression and split tension), 100x200 mm (4x8 in) cylinders were cast in a similar manner to ASTM C1435 (2008) with the differences being the size of the tamping plate (88 mm (3.5 in) diameter), number of lifts (three), and cylinder size (100 by 200 mm vs. 150 by 300 mm, 4x8 in vs 6x12 in). Flexural strength beams measuring 100x100x400 mm (4x4x16in) were cast in two layers using a vibrating hammer with an 88x88 mm (3.5x3.5 in) tamping plate attached to a vibrating hammer. Each layer was compacted for 5 seconds at the following locations: the ends, the middle, and between each end and the middle for a total of 25 seconds per layer. All specimens were cured in a fog room at 100% relative humidity and 20°C (68°F) until the time of testing

G.4 RESULTS

G.4.1 Compressive Strength

Compressive strength testing was conducted according to ASTM C39 (2012) at ages of 7, 14, and 28 days. Triplicate specimens were tested at each age for all mixes. Results of compressive strength testing are shown in Figure G2. In order to analyze the statistical significance of these results, Tukey's significant difference (TSD) test was performed piecewise with 95% confidence to compare which mean values were statistically similar (Mason et al. 2003). The TSD is essentially a piecewise t-test that compares the statistical significance of the results for each mix to those of every other mix. By doing this, the statistical significance of results for all mixes can be grouped to show which mixes are similar or different to each other. Results of the TSD test for only the 28-day compressive strength are shown in Table G3.

The EAF-25 mixture yielded statistically greater 28-day compressive strength relative to the RCC control while the EAF and RCA coarse aggregate replacement mixes had statistically similar strength to the virgin RCC. The two RCA mixtures that contained the entire RCA gradation (i.e., RCA-25 and RCA-40) as well as all mixtures containing RAP and SFSFRAP yielded statistically lower 28-day compressive strengths than the control. Comparing the RCA mix (which has 40% replacement of virgin aggregate with coarse RCA) with RCA-40, it can be seen that the inclusion of the fine fraction of the RCA led to a significant reduction in strength (ignoring slight differences between the two combined gradations). Compressive strength was also shown to decrease with increasing RAP content, which agreed with the findings by Brand and Roesler (2015c) for slip-form paving concrete. Mixtures with SFSFRAP and RAP yielded statistically similar 28-day compressive strengths, for the same replacement levels, which was also reported by Brand and Roesler (2014, 2015b) for slip-form paving concrete. Overall, the recycled aggregate gradations for EAF, RAP, and RCA were shown to

impact the RCC compressive strength like it was shown for virgin aggregates (LaHucik and Roesler 2015)

The ACPA (2014) suggests minimum 28-day compressive strengths of 31 and 28 MPa (4.5 and 4 ksi) for RCC in areas with and without freeze-thaw conditions, respectively. Thus, in a freeze-thaw susceptible climate, the only mixture containing RAP or SFSFRAP that meets this requirement is RAP-10, and all mixtures containing RCA or EAF, as well as the control, would be acceptable for this strength requirement. The guidelines set forth by ACPA (2014) are for RCC when used as a wearing course. If RCC were to be used lower in the pavement structure, such as a base material, compressive strength requirements would likely be reduced and mixtures such as RAP-25, RAP, SFSFRAP-25, and SFSFRAP could have acceptable strengths.

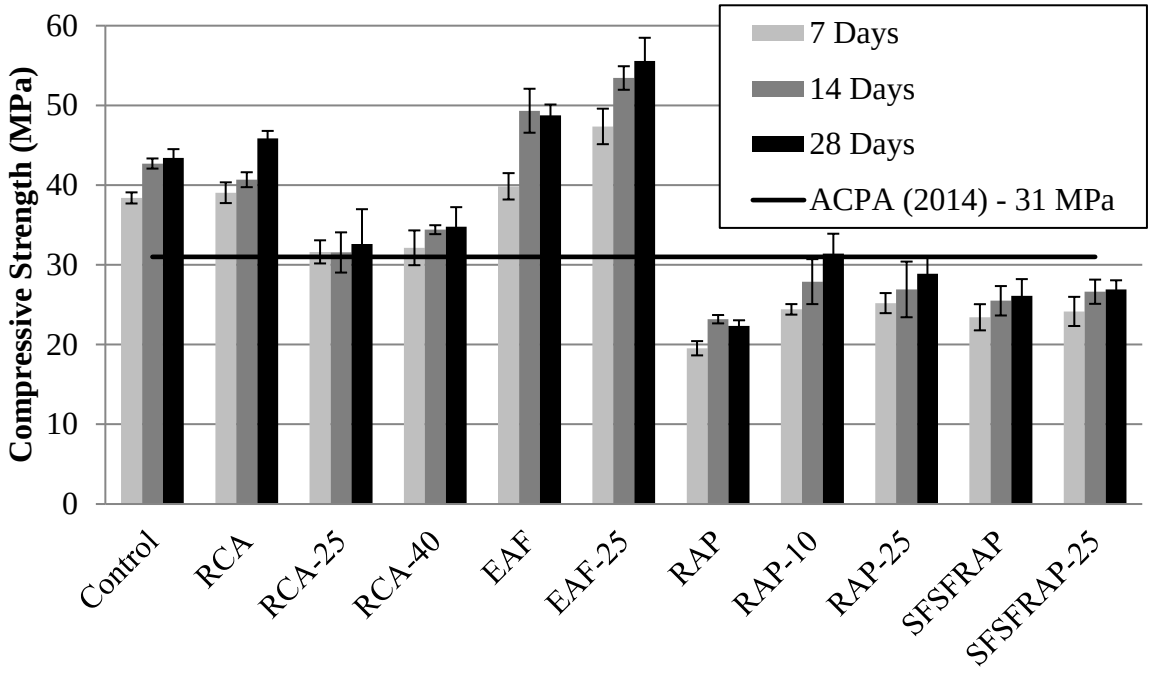

Figure G2. Compressive Strength Results (error bars indicate +/- one standard deviation).
(1 ksi = 6.89 MPa)

Table G3. Statistical Groupings for 28-Day Compressive Strength based on the TSD Test Results
(1 ksi = 6.89 MPa)

Tukey Grouping*						Mean (MPa)	Standard Deviation (MPa)	Mixture
A						55.6	2.9	EAF-25
	B					48.7	1.4	EAF
	B					45.8	1.0	RCA
	B					43.4	1.1	Control
		C				34.8	2.4	RCA-40
		C	D			32.6	4.4	RCA-25
		C	D	E		31.4	2.5	RAP-10
		C	D	E		28.9	2.1	RAP-25
			D	E	F	26.9	1.1	SFSFRAP-25
				E	F	26.1	2.1	SFSFRAP
					F	22.3	0.7	RAP

*Means with the same letter are not significantly different.

G.4.2 Split Tensile and Flexural Strengths

Split tensile strength testing was performed in accordance with ASTM C496 (2011) at an age of 28 days. Flexural strength testing (third-point loading) was performed on 100x100x400 mm (4x4x16) beams in accordance with ASTM C78 (2010) at an age of 28 days. For each test type, triplicate specimens were tested for each mix. Results of split tensile and flexural strength testing are shown in Figure G3 with the results of the TSD tests shown in Table G4. In addition to the TSD tests, t-tests (with a 95% confidence interval) comparing split tensile and flexural strengths for each mixture were conducted. Of the 11 mixtures, four mixtures yielded statistically different split tensile and flexural strengths (control, EAF, RAP, and SFSFRAP). Brand et al. (2014) showed that flexural strength measured on 150x150x530 mm (6x6x21 in) beams yielded consistently greater strengths than split tensile tests conducted on 100x200 mm (4x8 in) cylinders for virgin aggregate concrete as well as concrete with FRAP and RCA. As seen from Table G4, all mixtures yielded statistically similar split tensile strengths relative to the control. For RCC flexural strength, only mix EAF was statistically similar to the RCC control mix with all other mixtures statistically lower. Split tensile strength results show similar trends as 28-day compressive strength (i.e., EAF mixes had greater strengths than RCA mixes, which were greater than RAP and SFSFRAP mixes). Mixtures with SFSFRAP and RAP, for the

same replacement levels, yielded statistically similar flexural strengths as well as split tensile strengths. Brand and Roesler (2014, 2015b) showed statistically similar split tensile strengths but statistically different flexural strengths when comparing slip-form paving mixtures containing SFSFRAP and RAP.

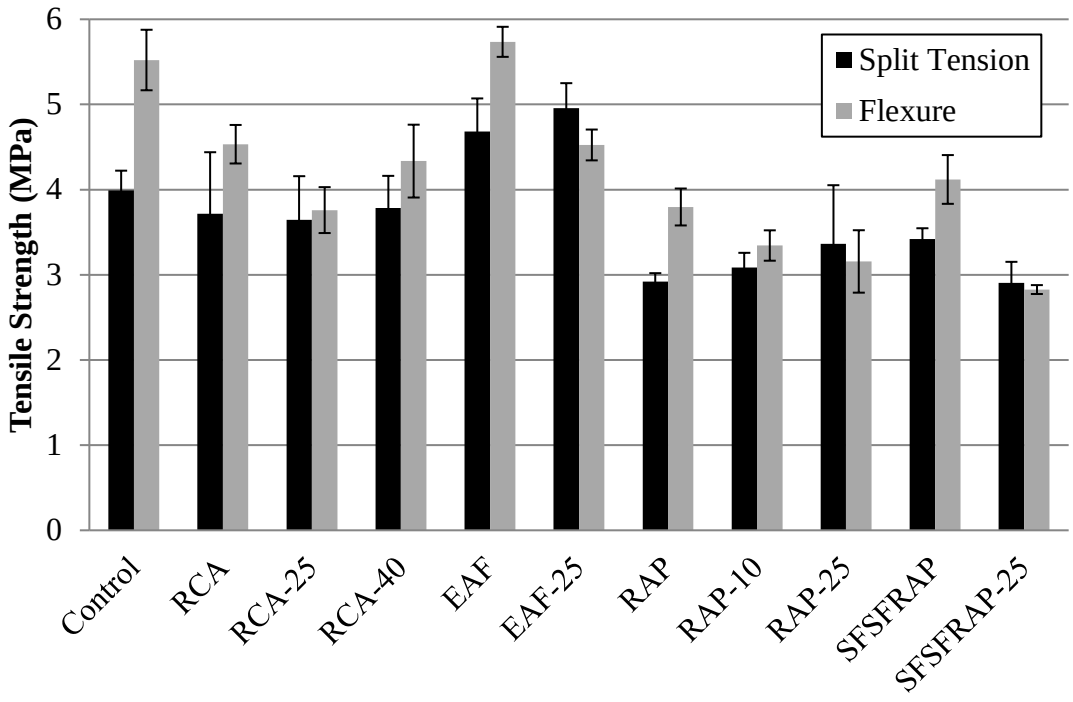

Figure G3. Split Tensile and Flexural Strength Results at 28-Days Age (error bars indicate +/- one standard deviation). (1 ksi = 6.89 MPa)

Table G4. Statistical Groupings for 28-Day Split Tensile and Flexural Strength based on the TSD Test Results (1 ksi = 6.89 MPa)

Tukey Grouping*					Mean (MPa)	Standard Deviation (MPa)	Mixture
Split Tensile Strength							
A					4.96	0.29	EAF-25
A	B				4.68	0.39	EAF
A	B	C			3.99	0.23	Control
A	B	C			3.79	0.38	RCA-40
	B	C			3.72	0.72	RCA
	B	C			3.65	0.51	RCA-25
		C			3.42	0.13	SFSFRAP
		C			3.36	0.69	RAP-25
		C			3.09	0.17	RAP-10
		C			2.92	0.10	RAP
		C			2.91	0.25	SFSFRAP-25
Flexural Strength							
A					5.74	0.18	EAF
A					5.52	0.36	Control
	B				4.53	0.23	RCA
	B				4.52	0.18	EAF-25
	B				4.34	0.43	RCA-40
	B	C			4.12	0.29	SFSFRAP
	B	C	D		3.80	0.22	RAP
	B	C	D		3.76	0.27	RCA-25
		C	D	E	3.34	0.18	RAP-10
			D	E	3.16	0.37	RAP-25
				E	2.83	0.05	SFSFRAP-25

*Means with the same letter are not significantly different.

G.4.3 Fracture Properties

RCC fracture testing was conducted on DCT samples (Figure G4 fabricated from 150x300 mm (6x12 in) cylindrical specimens according to Amirkhanian et al. (2015). The RCC fracture parameters are derived based on the Jenq and Shah (1985) two-parameter fracture model (TPFM) and work of fracture method (Hillerborg 1985), with five replicates tested per mix. The main benefits of fracture testing are provisions for both size dependent (total fracture energy) and size independent properties (critical stress intensity factor and critical crack tip opening displacement) as well as useful parameters for the structural design of concrete pavements (Ioannides et al. 2006; Gaedicke et al. 2012; Brand et al. 2014). These benefits allow for a more in-depth comparison of the performance of the various mixtures presented in this paper. The derived fracture properties are the critical stress intensity factor (K_{IC}), elastic modulus (E), critical crack tip opening displacement ($CTOD_C$), initial fracture energy (G_f), and total fracture energy (G_F). Results of fracture testing are shown in Table G5 along with their coefficients of variation (COV). Table G6 shows results of the TSD tests on critical stress intensity factor and total fracture energy.

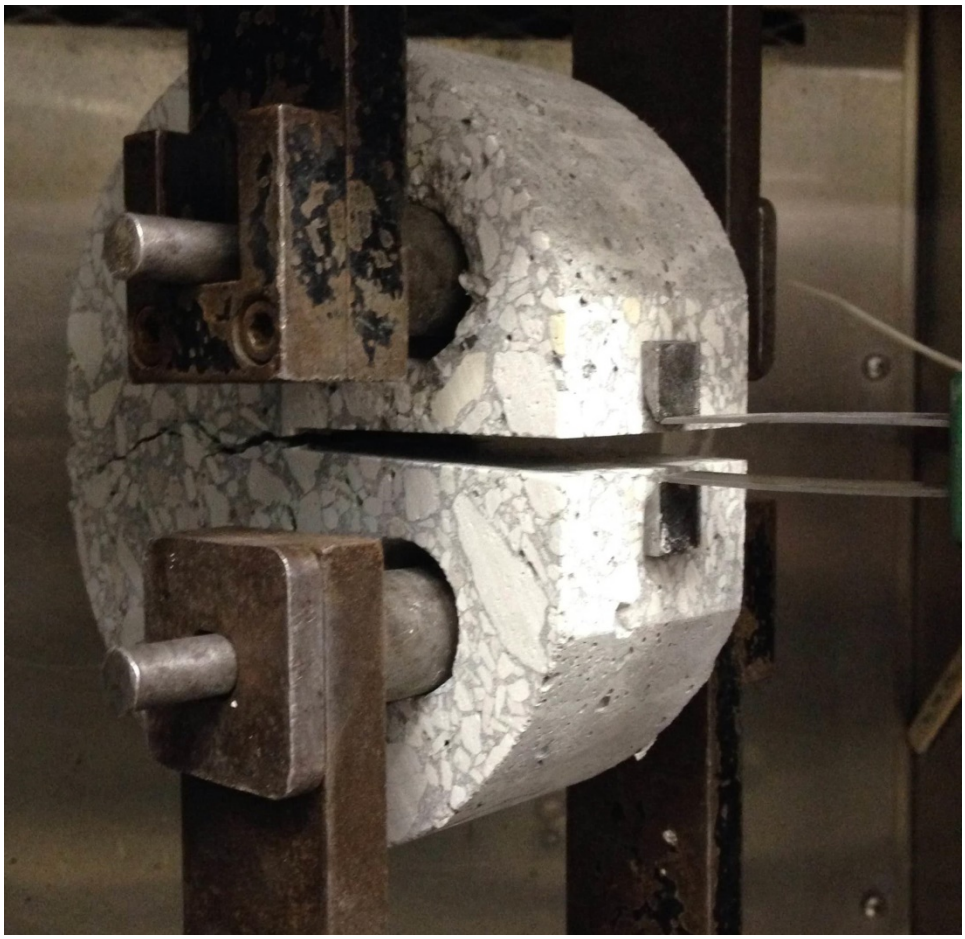

Figure G4. DCT Specimen Loaded in Tension with Clip Gauge (right) Measuring Crack-Mouth Opening Displacement (CMOD).

According to Table G6, all RCC mixtures had statistically similar or better K_{IC} and G_F relative to the control. Mixture EAF-25 produced statistically greater K_{IC} and G_F than the virgin RCC mix. Previous researchers (Montgomery and Wang 1992; Brand and Roesler 2015a) have reported improved fracture properties for concrete containing steel furnace slag aggregates relative to virgin aggregate concrete. Likewise, the similarity of fracture properties with concrete containing RAP, SFSFRAP, or RCA aggregates relative to virgin aggregate concrete have been previously presented in the literature (Amirkhanian 2012; Brand et al. 2014; Brand and Roesler 2015b, 2015c).

Brand et al. (2014) tested strength and fracture properties of paving concrete with recycled aggregates (RCA and RAP) in addition to conducting slab tests on the same mixtures. They found that the concrete with recycled aggregates resulted in lower strength and elastic modulus values (relative to virgin aggregate concrete) while the fracture parameters and slab testing results demonstrated that the concrete with recycled aggregates performed similarly or slightly better compared to the virgin concrete. Given the strength and fracture properties of RCC mixtures containing virgin or recycled aggregates and previous literature on concrete slab testing, it is likely that RCC slabs containing recycled aggregates would have a similar flexural capacity to RCC with virgin aggregates. Flexural slab capacity testing needs to be conducted to prove or disapprove this hypothesis for RCC materials.

Table G5. Fracture Testing Results (COV, %); (1 MPa-m$^{1/2}$ = 0.910 ksi-in$^{1/2}$; 1 GPa = 145 ksi; 1 in = 25.4 mm; 1 lb/in = 175 N/m)

Mixture	K_{IC}, MPa-m$^{1/2}$	E, GPa	$CTOD_C$, mm	G_f, N/m	G_F, N/m
Control	1.07 (6.6)	29.0 (7.2)	0.017 (29.3)	40.0 (18.1)	131.0 (9.7)
RCA	1.04 (9.3)	28.5 (13.9)	0.016 (9.6)	38.3 (9.8)	118.6 (11.3)
RCA-25	0.88 (8.6)	22.5 (8.7)	0.022 (20.8)	34.6 (15.4)	122.1 (17.0)
RCA-40	1.16 (10.5)	35.5 (8.3)	0.016 (18.5)	37.9 (14.1)	149.9 (13.9)
EAF	1.43 (10.5)	42.8 (7.6)	0.017 (18.3)	48.3 (17.8)	170.2 (13.1)
EAF-25	1.40 (8.9)	35.6 (9.5)	0.019 (24.0)	56.5 (25.4)	191.0 (5.7)
RAP	0.86 (17.3)	20.9 (3.1)	0.022 (29.7)	36.5 (32.5)	158.1 (22.3)
RAP-10	0.87 (13.8)	24.7 (15.0)	0.019 (31.2)	31.3 (24.9)	140.3 (6.8)
RAP-25	0.97 (4.1)	21.6 (11.1)	0.021 (10.6)	43.7 (9.3)	157.9 (5.9)
SFSFRAP	1.03 (10.8)	29.0 (6.8)	0.016 (20.9)	37.0 (23.9)	261.1 (12.2)
SFSFRAP-25	1.14 (6.2)	31.4 (6.6)	0.018 (11.6)	41.2 (7.5)	195.3 (16.1)

Table G6. Statistical Groupings for 28-Day Critical Stress Intensity Factor and Total Fracture Energy based on the TSD Test Results; (1 MPa*m$^{1/2}$ = 0.910 ksi*in$^{1/2}$)

Tukey Grouping			Mean	Standard Deviation	Mixture
K_{IC}			MPa*m$^{1/2}$	MPa*m$^{1/2}$	
A			1.43	0.151	EAF
A			1.40	0.124	EAF-25
	B		1.16	0.122	RCA-40
	B		1.14	0.070	SFSFRAP-25
	B	C	1.07	0.071	Control
	B	C	1.04	0.097	RCA
	B	C	1.03	0.111	SFSFRAP
	B	C	0.97	0.040	RAP-25
		C	0.88	0.076	RCA-25
		C	0.87	0.120	RAP-10
		C	0.86	0.149	RAP
G_F			N/m	N/m	
A			261.1	31.7	SFSFRAP
	B		195.3	31.4	SFSFRAP-25
	B		191.0	11.0	EAF-25
	B	C	170.2	22.2	EAF
	B	C	158.1	35.2	RAP
	B	C	157.9	9.3	RAP-25
	B	C	149.9	20.8	RCA-40
		C	140.3	9.6	RAP-10
		C	131.0	12.7	Control
		C	122.1	20.8	RCA-25
		C	118.6	13.4	RCA

*Means with the same letter are not statistically different.

G.5 CONCLUSIONS

The effect of partial replacement of virgin aggregates with recycled aggregates on the moisture-density, strength, and fracture properties of roller-compacted concrete (RCC) was examined. The recycled aggregates utilized for this study were recycled concrete aggregate (RCA), electric arc furnace (EAF) steel slag aggregate, reclaimed asphalt pavement (RAP), and steel furnace slag fractionated reclaimed asphalt pavement (SFSFRAP). All mixes contained the same source of virgin aggregates and cement content. The MDD for the mixes varied with the specific gravity of the blended aggregates while the OMC for all mixtures ranged from 5.9% to 8.5% and depended on the porosity of the recycled aggregate.

The compressive strength of RCC mixes with partial replacement of virgin aggregates with RCA, RAP, and EAF aggregates were impacted by which particle sizes were replaced, i.e., coarse fraction or part of the coarse and fine aggregates. However, increasing the replacement level of a given recycled aggregate did not have a statistically significant effect on strength or fracture properties. RCC mixes with EAF aggregates produced similar to greater compressive strengths relative to the control mix, while RCC mixes with RCA had similar or lower compressive strengths. RCC mixes containing RAP and SFSFRAP led to consistently lower compressive strengths relative to the virgin aggregate, RCC control mix. The split tensile strength of all recycled aggregate RCC mixtures were similar to the control while the flexural strength results produced statistically lower flexural strengths to the control except EAF aggregates.

Fracture properties for RCC mixes were derived from disk-shaped compact tension (DCT) testing. All mixtures containing recycled aggregates yielded similar or greater values of critical stress intensity factor and total fracture energy relative to the RCC control mixture. Previous literature has shown that fracture properties are more indicative of flexural capacity of concrete slabs with recycled aggregates than strength testing of cylinders or beams. Therefore, it is hypothesized that the slab flexural capacity of RCC mixtures containing these recycled aggregates is similar to that of the RCC mixture with virgin aggregates.

APPENDIX H: MECHANICAL PROPERTIES OF ROLLER-COMPACTED CONCRETE WITH MACRO-FIBERS

This chapter investigates the use of macro-fibers (steel and synthetic) on the properties of roller-compacted concrete. Properties measured include: strength (compressive, split tensile, and flexural), fracture properties, flexural toughness, and residual strength testing.

H.1 INTRODUCTION

Due to the method of construction, RCC does not allow for the conventional placement of dowel bars. Therefore, load transfer across contraction joints in an RCC pavement may be a concern (Nanni and Johari, 1989) especially at higher traffic levels. Structural macro-fibers may provide improved shear load transfer and residual strength in RCC as noted for conventional PCC pavement (Bordelon and Roesler, 2009). Macro-fibers have been added to PCC pavement to reduce slab thickness, control crack width and decrease crack deterioration rates, increase joint spacing, and increase fracture properties (Roesler et al. 2004; Altoubat et al. 2008; Bordelon and Roesler, 2009; Bordelon et al. 2009; Roesler et al. 2012). By reducing the crack width at a joint, the shear mechanism of aggregate interlock is enhanced (Millard and Johnson, 1984; Soroushian et al. 1988), thereby increasing load transfer and potentially reducing the slab's critical tensile stresses.

Previous studies of fiber-reinforced RCC (Nanni and Johari, 1989; Kokubun and Kagaya, 2001; Sobhan and Mashnad, 2001; Sobhan and Mashnad, 2002; Achilleos et al. 2011; Bilodeau et al. 2011; Neocleous et al. 2011; Yandong et al. 2011; Graeff et al. 2012; Madhkhan et al. 2012; Nguyen et al. 2012; Muscalu et al. 2013; Jafarifar et al. 2015; Yazici et al. 2015) have primarily explored steel macro-fibers, with exception of one study (Madhkhan et al. 2012) that utilized synthetic fibers, and reported varying mechanical property results. A summary of the impact of fibers on RCC mechanical properties from the literature is shown in Table H1. The addition of fibers to RCC has been shown to increase or decrease strength, elastic modulus, fracture energy, density, and fatigue life relative to RCC without fibers. Clearly, the type of fiber (steel or synthetic), geometric properties of the fiber (aspect ratio, length, shape, and surface texture), and fiber dosage affect the mechanical properties of a given fiber-reinforced concrete mixture (Gopalaratnam et al. 1991; Johnston and Zemp, 1991; Johnston and Skarendahl, 1992; Cha et al. 1998; Roesler et al. 2004). In this study, the effect of fiber type, geometry, and dosage level on the mechanical and fracture properties of RCC will be determined for a fixed set of constituents, i.e., aggregate type and gradation; cement type and content.

Table H1. Effects of Fibers on RCC Mechanical Properties Relative to Non-Fiber RCC from Literature
(values in % indicate volume dosage of fibers used)

	Increase	No Effect	Decrease	Variable
Split Tensile Strength	Nanni and Johari (1989): 0.58%; Kokubun and Kagaya (2013): 0.25 – 0.75%			Sobhan and Mashnad (2001): 0.25 and 0.5%
Compressive Strength	Nanni and Johari (1989): 0.58%; Muscalu et al. (2013): 3%; Madhkhan et al. (2012): 0.4 – 0.8% (steel) and 0.1% (synthetic)	Kokubun and Kagaya (2013): 0.25 – 0.75%	Sobhan and Mashnad (2001): 0.25 and 0.5%; Neocleous et al. 2011: 1 and 2%	
Elastic Modulus	Nanni and Johari (1989): 0.58%		Muscalu et al. (2013): 3%	
Flexural Strength	Kokubun and Kagaya (2013): 0.5 and 0.75%; Muscalu et al. (2013): 3%		Kokubun and Kagaya (2013): 0.25%	Sobhan and Mashnad (2001): 0.25 and 0.5%; Madhkhan et al. (2012): 0.4 – 0.8% (steel) and 0.1% (synthetic)
Fatigue Life	Graeff et al. (2012): 2 and 6% for stress ratios < 0.7		Graeff et al. (2012): 2 and 6 % for stress ratios > 0.7	
Fracture Energy	Yandong et al. (2011): 0.5 and 1%			
Maximum Dry Density (MDD)	Neocleous et al. (2011): 1 and 2%	Nanni and Johari (1989): 0.58%		

H.2 OBJECTIVES

The addition of macro-fibers to plain concrete has provided enhanced structural and functional benefits to concrete pavements especially for concrete overlays in recent years (Bordelon and Roesler, 2011). There have been limited studies on macro-fibers, especially synthetic fibers, on the strength, toughness, and fracture properties of RCC. The objectives of this study are to characterize fiber-reinforced RCC strength, elastic modulus, fiber-reinforced concrete (FRC) toughness parameters, and disk-shaped compact tension (DCT) fracture parameters for a variety of fiber type, geometries and dosage given a fixed RCC mix design for pavements.

H.3 METHODOLOGY

H.3.1 Mixture Design

Aggregate type and gradation is one of the key factors in the mixture design of RCC, which has been shown to impact its fresh and mechanical properties (ACI, 1995; Qasrawi et al. 2005; Harrington et al. 2010; Williams, 2013; LaHucik and Roesler, 2015). Three aggregate sources, coarse dolomite (19 mm, ¾ in, nominal maximum size), dolomite chips (9.5 mm, 3/8 in, nominal maximum size), and natural sand (fineness modulus = 2.74), were proportioned to target a combined aggregate gradation that approached the 0.45 power maximum density curve. The chosen aggregate gradation has previously been shown to provide sufficient strengths for an RCC pavement with the same cement content used in this study (LaHucik and Roesler, 2015). All aggregates were sieved into individual sizes and re-combined to yield the target gradation. Aggregates were also brought to an oven-dry condition to limit between batch aggregate moisture variability.

For this study, twelve RCC mixtures (Table H2) were developed using a volumetric method: a control mixture without fibers, six mixtures with a fiber dosage of 0.4% by volume, and five mixtures with a fiber dosage of 0.2% by volume. The geometry and material properties of the six fibers are shown in Table H3 while pictures of each fiber are shown in Figure H1. The fiber nomenclature in Table H3 uses a fiber description, e.g., surface texture or fiber feature followed by length of fiber (mm), and finally fiber dosage level. For example, Emboss-48-0.4 represents a fiber with embossing, a length of 48 mm (2 in), and a dosage of 0.4% by volume. All RCC mixtures had a constant cement content of 281.8 kg/m^3 (475 lb/yd^3).

Table H2. RCC Mixture Proportions (kg/m³); (1 kg/m³ = 1.686 lb/yd³)

Mixture ID	Type I/II Portland Cement	Aggregate (Oven Dry)	Water	Fibers
Control	282	2093	154	N/A
Emboss-48-0.2	282	2169	156	1.8
Emboss-48-0.4	282	2168	156	3.6
Emboss-50-0.2	282	2142	170	1.8
Emboss-50-0.4	282	2140	170	3.6
Smooth-40-0.2	282	2132	172	1.8
Smooth-40-0.4	282	2130	172	3.6
Smooth-58-0.2	282	2155	155	1.8
Smooth-58-0.4	282	2154	155	3.7
Helical-25-0.4	282	2099	178	31.4
Hook-60-0.2	282	2125	172	15.7
Hook-60-0.4	282	2109	172	31.4

Table H3. Fiber Material Properties (1 ksi = 6.89 MPa; 1 GPa = 145 ksi; 1 in = 25.4 mm)

Fiber Label	Material	Aspect ratio	Length (mm)	Deformation	Tensile Strength	Elastic Modulus
Emboss-48	Synthetic macro fiber (modified olefin)	67	48	Continuously embossed	640	10
Smooth -40	Synthetic macro fiber (polypropylene/polyethyle	90	40	Smooth	620	9.5
Emboss-50	Synthetic macro fiber (polypropylene)	75	50	Surface deformation	550	7
Smooth -58	Synthetic macro fiber (modified olefin)	-	58	Smooth	620	7
Hook-60	Steel Fiber (made from cold-drawn wire)	55	60	Hooked end	1500	207
Helical-25	High carbon Steel (electroplated zinc coating)	50	25	Helical shape	1700	-

		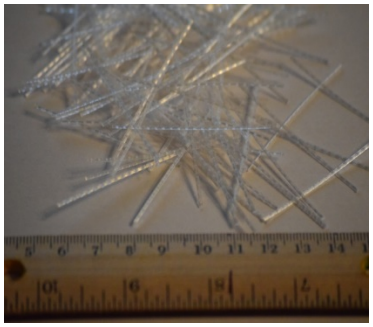
Emboss - 48	**Smooth - 40**	**Emboss - 50**
	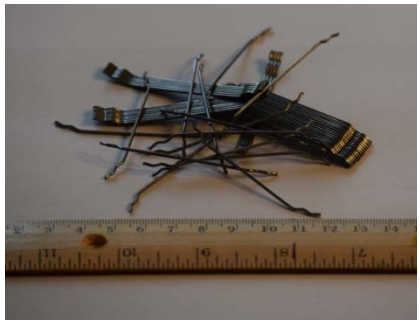	
Smooth - 58	**Hook - 60**	**Helical - 25**

Figure H1. Macro-Fibers used in this study.

Modified Proctor tests were performed according to ASTM D1557 (ASTM, 2012) to determine the moisture-density relationship for a given fiber type. Five point modified Proctors were performed at nominal moisture contents varying from 5% to 9% to obtain the maximum dry density (MDD) and optimum moisture content (OMC) as is listed in Table H4. Modified Proctor testing was only performed for RCC mixtures with 0.4% fiber volume. It was assumed there would be negligible difference in OMC for the lower fiber volume of 0.2%. In general, macro-fibers produced similar or slightly greater values of OMC for the RCC mixtures, relative to the control, as shown in Table H4. The MDD of each mixture with fibers was greater than that of the RCC control mixture (Table H4), which was also found by Neocleous et al. (2011) for higher volumes of steel fibers than were used in this study. In order to determine if the fiber weight was the primary reason for the increased MDD, the weight of fibers per cubic meter of RCC was subtracted from the MDD as shown in Table H4. The results in Table H4 clearly demonstrate that addition of any synthetic macro-fiber aided in compaction of the RCC, whereas steel fibers had only a limited impact on the MDD, i.e., Helical-25 and Hook-60. On average, synthetic fiber mixes increased the MDD by 55 kg/m^3 (3.4 lb/ft^3) or 2.3% relative to the control mixture, whereas steel fibers only increased the MDD by 11 kg/m^3 (0.7 lb/ft3)

or 0.5%. The proposed mechanism for the increased MDD in RCC containing synthetic fibers was a reduction in the internal friction between the aggregates provided by the polymeric fiber.

Table H4. Results of Modified Proctor Testing (1 kg/m^3 = 0.062 lb/ft^3)

Mixture ID	MDD (kg/m^3)	OMC (%)	MDD - Fiber Weight (kg/m^3)	Percent Difference in MDD relative to control (kg/m^3)*
Control	2374	6.5	N/A	N/A
Emboss-48-0.4	2453	6.4	2449	3.2% (74.9)
Emboss-50-0.4	2425	7.0	2422	2.0% (47.3)
Smooth-40-0.4	2416	7.1	2412	1.6% (37.5)
Smooth-58-0.4	2439	6.4	2435	1.8% (60.9)
Helical-25-0.4	2412	7.4	2381	0.3% (6.3)
Hook-60-0.4	2422	7.1	2391	0.7% (16.2)

*Value in parenthesis represents difference of MDD, in kg/m^3, between fiber and control mix.

H.3.2 SPECIMEN MIXING, FABRICATION, AND TESTING

All specimens were mixed in a pan mixer according to ASTM C192 (ASTM, 2013) using the final mixture proportions in Table H2 and were moist cured in a fog room until testing. Fiber balling was evident for those mixes containing synthetic fibers that had little to no flexural rigidity (i.e. smooth-40 and smooth-58), particularly for the higher fiber dosage (0.4%). Fibers did not have a noticeable impact on RCC workability. For compressive, split tensile, and elastic modulus testing, 100 by 200 mm cylinders were compacted with a vibratory hammer similar to ASTM C1435 (ASTM, 2008) with the differences being the size of the tamping plate (88 mm diameter), number of lifts (three), and cylinder size (100x200 vs. 150x 300 mm or 4x8 vs. 6x12 in). Three replicate cylinders were made for each strength and modulus test. Elastic modulus, compressive strength, and split tensile strength testing were conducted according to ASTM C469 (ASTM, 2010), ASTM C39 (ASTM, 2012), and ASTM C496 (ASTM, 2011), respectively. All tests were conducted at 28 days with additional compressive strength testing at 7 days.

In addition to the standard strength tests, fracture specimens were cast. The benefit of fracture testing is that the parameters, such as the critical stress intensity factor (K_{IC}) and critical crack tip opening deflection ($CTOD_C$), are size and specimen independent properties (Jenq and Shah, 1985), which allows comparison with other published data. The disk-shaped compact tension (DCT) geometry (Figure H2) was chosen because RCC specimens can be fabricated from 150 by 300 mm (6x12 in) cylinders, which can be created by a standardized method (ASTM, 2008), as opposed to

previous studies that utilized a nonstandard compaction method for testing fracture properties of RCC beams (Ferrebee et al. 2014). For fracture property testing with the DCT geometry, one 150 by 300 mm (6x12 in) cylinder was cast according to ASTM C1435 (ASTM, 2008) from which five specimens were cut, prepared, tested, and characterized according to process outlined by Amirkhanian et al. (2015). The resultant fracture properties reported are the critical stress intensity factor (K_{IC}), critical crack tip opening displacement ($CTOD_C$), initial fracture energy (G_f), total fracture energy (G_F), and fracture energy to reach a CMOD of 5 mm (0.2 in) (G_{F5}).

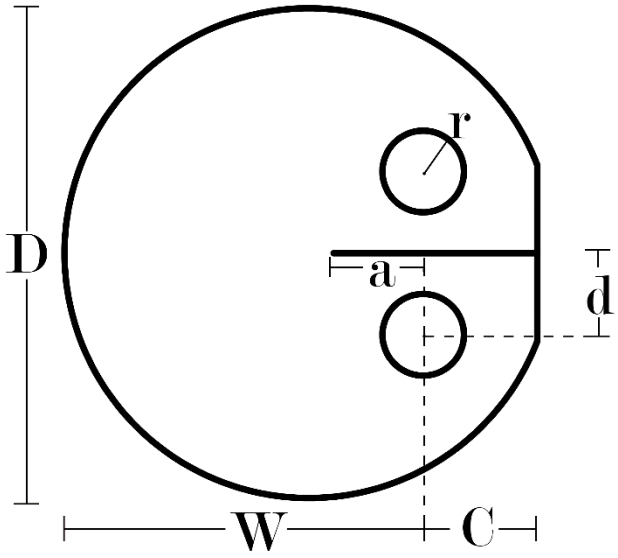

Figure H2. Schematic of the DCT Specimen where *D* is 150mm, *W* is 110mm, *C* is 35mm, *d* is 25mm, *a* is 27.5mm, and *r* is 12.5mm (Amirkhanian et al. 2015). (1 in = 25.4mm)

For flexural beam testing according to ASTM C1609 (ASTM, 2010), five replicate beams (150 by 150 by 525 mm) were cast using an ASTM draft standard for casting RCC beam specimens. Simply supported-beams were tested under four point (third-point) loading using a closed-looped, servo-hydraulic load frame and unlimited travel rollers (Bernard, 2014). The deflection-based loading rates suggested in ASTM C1609 (ASTM, 2010) have been shown to cause premature failure of specimens (Banthia and Islam, 2013), particularly higher strength beams and therefore modified deflection rates suggested by Banthia and Islam (2013) were employed.

Residual loads at net deflection values of L/600 (0.75 mm or 30 mil) and L/150 (3 mm or 118 mil), were used to compute the residual strengths, F_{600} and F_{150}. The thickness design of fiber-reinforced concrete pavements has employed the residual strength, F_{150}, of FRC materials to modify the concrete's flexural strength (Bordelon and Roesler, 2009; Bordelon and Roesler, 2011; Vandenbossche et al. 2016). In addition, the area under the load-deflection curve was computed up to a net deflection of L/150, which produces the toughness, T_{150} (N-m), of the specimen. The residual

flexural strengths (F_{600} and F_{150}) are calculated using Equation H1 where P is the load (N) at a given deflection, i.e. L/600 or L/150 for F_{600} and F_{150}, respectively, L is the span length (450 mm or 18 in), b is the width (150 mm or 6 in), and d is the depth (150 mm or 6 in). The equivalent flexural strength ratio ($R_{T,150}$), which takes into account the toughness, is calculated using Equation H2 where MOR represents the peak flexural strength (MPa). Figure H3 shows a representative load-deflection curve from each RCC mix design.

$$F_{150\ or\ 600} = \frac{P \cdot L}{b \cdot d^2} \quad \text{(Eq. H1)}$$

$$R_{T,150} = \frac{150 \cdot T_{150}}{MOR \cdot b \cdot d^2} \cdot 100\% \quad \text{(Eq. H2)}$$

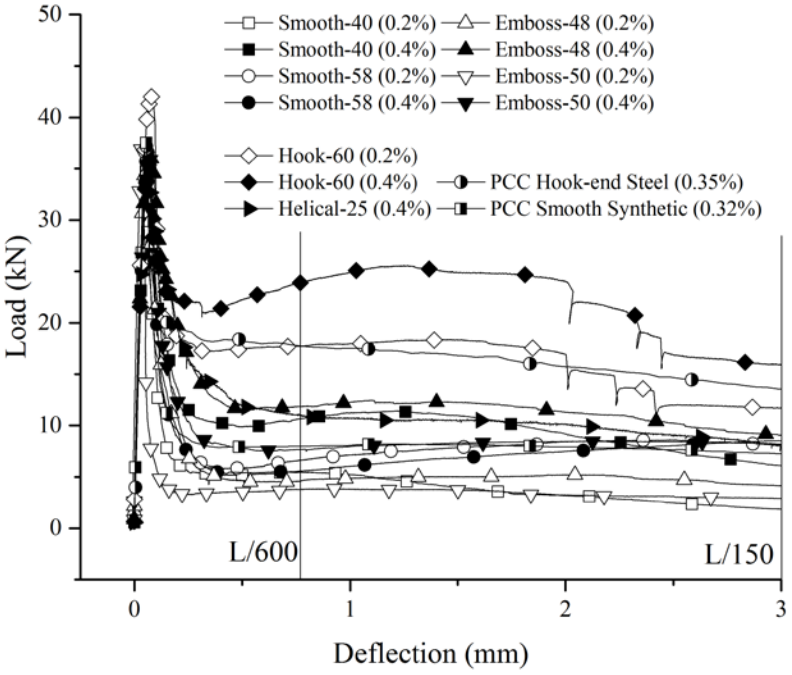

Figure H3. Load vs. Deflection for Fiber-Reinforced RCC Beams. Hollow Symbols indicate 0.2% Fiber Dosage and Filled Symbols indicate 0.4% Fiber Dosage. (1 kN = 224.8 lbf; 1 in = 25.4 mm)

H.4 STRENGTH AND ELASTIC MODULUS RESULTS

The average of three samples for strength and modulus are presented in Table H5 along with the coefficient of variation (COV). The 7 and 28 day compressive strengths for all mixes are much higher than typical RCC specifications requiring 24 MPa (3.5 ksi) and 31 MPa (4.5 ksi), respectively (ACPA, 2014). The RCC fiber mixes that resulted in the greatest compressive strengths were also the RCC mixes with the largest MDD. Synthetic fiber mixes produced greater compressive strength gains from 7 to 28 days than the control whereas steel fiber mixes yielded similar strength gains to the control. All fibers, with the exception of Helical-25, produced greater average 28-day compressive strengths than the control mixture but only 4 of the 11 fiber mixes were statistically greater (according to a t-test with 95% confidence interval). The four statistically greater RCC mixes all contained synthetic fibers. Previous research has reported similar findings that inclusion of synthetic or steel fibers in concrete increased compressive strengths without providing a mechanism for this observed behavior (Nanni and Johari, 1989; Sahin and Köksal, 2011; Muscalu et al. 2013; Peng et al. 2015). Increasing the fiber dosage from 0.2% to 0.4% yielded a statistical increase in compressive strength for only one fiber type (Smooth-40) while none of the remaining fibers had statistically different compressive strengths when only changing the fiber dosage.

Table H5. Compressive Strength, Split Tensile Strength, and Elastic Modulus Results (COV, %)*

(1 ksi = 6.89 MPa; 1 GPa = 145 ksi)

Mixture ID	7 Day Compressive Strength (MPa)	28 Day Compressive Strength (MPa)	28 Day Split Tensile Strength (MPa)	28 Day Elastic Modulus (GPa)
Control	40.5 (4.3)	46.7 (4.3)	4.00 (5.5)	31.6 (2.2)
Emboss-48-0.2	42.7 (0.8)	**52.3 (3.0)**	5.30 (15.0)	33.0 (6.6)
Emboss-48-0.4	42.0 (4.7)	**56.6 (5.6)**	**5.35 (2.4)**	29.0 (7.4)
Emboss-50-0.2	41.7 (3.8)	51.0 (3.1)	**5.25 (7.9)**	31.8 (6.4)
Emboss-50-0.4	40.0 (2.1)	48.2 (7.1)	**4.85 (3.8)**	28.8 (8.0)
Smooth-40-0.2	38.1 (3.0)	47.2 (1.7)	4.25 (8.3)	30.2 (7.0)
Smooth-40-0.4	37.2 (4.7)	**54.5 (2.8)**	4.25 (8.5)	30.4 (1.7)
Smooth-58-0.2	40.1 (5.6)	49.9 (1.8)	**4.80 (2.9)**	30.8 (2.5)
Smooth-58-0.4	42.0 (6.1)	**53.9 (4.5)**	4.45 (2.7)	32.6 (1.8)
Helical-25-0.4	**34.9 (4.1)**	**41.1 (3.8)**	**5.90 (8.5)**	-
Hook-60-0.2	43.2 (0.3)	50.3 (1.6)	**6.75 (12.9)**	32.0 (2.7)
Hook-60-0.4	39.4 (2.9)	46.3 (5.9)	**6.30 (11.1)**	30.8 (2.8)

*Bold values represent statistical difference from control. (-) signifies that results are not available for this test due to material constraints of that specific fiber.

Relative to the RCC control mixture, all fiber mixtures had higher average 28-day split tensile strength, which has been shown in the literature for steel fibers (Nanni and Johari, 1989; Sahin and Köksal, 2011; Kokubun and Kagaya, 2001; Peng et al. 2015) with 7 out of 11 RCC fiber mixes yielding statistically greater split tensile strengths (represented by bold values in Table H5). Of the four fiber mixes without statistical difference in split tensile strength compared to the RCC control, three were smooth synthetic fibers that likely had reduced interfacial bonding between the fiber and paste. The three steel fiber mixtures produced the greatest increase in split tensile strength with the Hook-60-0.2 mixture increasing the split tensile strength by 68% over the control. The inclusion of fibers had no statistical effect on the RCC's elastic modulus similar to Sahin and Köksal (2011) despite other literature showing that the elastic modulus can increase (Nanni and Johari, 1989) or decrease (Muscalu et al. 2013) with steel fibers.

H.5 FLEXURAL PERFORMANCE TESTING

The experimental load-deflection curves from ASTM C1609 testing are shown in Figure H3 while the resulting flexural performance parameters are listed in Table H6. The addition of fibers produced statistically lower flexural strengths, compared to the control RCC mix for 7 of the 11 RCC fiber mixes. RCC flexural strength values of 4.3 to 5.7 MPa (0.62 to 0.83 ksi) can be expected based on the literature (ACI, 1995) for saw-cut beams from RCC pavements. The lower flexural strengths of all RCC mixes in this study are likely attributed to the difficulty associated with RCC beam compaction and lack of a standardized method.

Table H6. Flexural Performance Testing Results for RCC and PCC (COV, %)*

(1 ksi = 6.89 MPa; 1 N-m = 8.85 lb-in)

Mixture ID	MOR (MPa)	F_{600} (MPa)	F_{150} (MPa)	T_{150} (N-m)	$R_{T,150}$ (%)
RCC Control	4.65 (4.0)	N/A	N/A	N/A	N/A
Emboss-48-0.2	**4.15 (2.5)**	0.70 (18.6)	0.40 (16.4)	18.5 (10.2)	17.4 (11.2)
Emboss-48-0.4	4.35 (3.2)	1.45 (19.4)	1.05 (15.6)	36.5 (16.7)	32.5 (14.7)
Emboss-50-0.2	**4.10 (6.5)**	0.55 (36.9)	0.50 (43.6)	16.0 (32.5)	15.4 (35.5)
Emboss-50-0.4	4.00 (14.1)	1.05 (29.4)	1.05 (34.8)	30.0 (28.7)	29.2 (23.1)
Smooth-40-0.2	**3.95 (4.1)**	0.60 (16.0)	0.25 (22.9)	14.5 (15.9)	14.2 (16.3)
Smooth-40-0.4	**4.00 (4.9)**	1.15 (16.1)	0.55 (22.7)	26.0 (15.9)	25.7 (17.7)
Smooth-58-0.2	**4.25 (3.7)**	0.50 (45.9)	0.60 (45.3)	17.5 (38.5)	16.1 (37.0)
Smooth-58-0.4	**4.25 (5.8)**	0.85 (20.9)	1.05 (12.1)	25.5 (13.6)	23.5 (10.3)
Helical-25-0.4	**4.15 (6.3)**	1.20 (10.8)	0.75 (17.4)	31.0 (10.7)	29.3 (6.5)
Hook-60-0.2	5.05 (1.0)	2.00 (9.7)	1.35 (2.5)	47.0 (10.9)	36.6 (11.5)
Hook-60-0.4	4.50 (5.3)	3.10 (7.8)	1.95 (14.2)	68.5 (8.4)	59.8 (10.3)
PCC Hook-End Steel 0.35% (Altoubat et al. 2008)	4.70	2.10	1.60	51.0	42.8
PCC Smooth Synthetic 0.32% (Altoubat et al. 2008)	4.70	0.95	0.85	26.0	21.8
PCC Smooth Synthetic 0.48% (Altoubat et al. 2008)	4.80	2.00	1.55	48.4	39.5

*Bold values indicate statistical difference from RCC control.

For a fixed fiber volume fraction, mixture Hook-60-0.4 had the highest residual strengths and equivalent flexural strength ratio of all RCC fiber mixes, which confirms a similar trend for conventional concrete shown by Altoubat et al. (2008). Buratti et al. (2011) had also reported higher

toughness values for hooked-end steel fibers relative to synthetic fibers with load vs. CMOD plots similar to those shown in Figure H3. As the fiber dosage increased, the values of residual strength (F_{600} and F_{150}) and flexural toughness (T_{150}) increased for each fiber type, which is consistent with FRC literature (Altoubat et al. 2008; Bordelon and Roesler, 2009; Buratti et al. 2011; Neocleous et al. 2011). The results in Table H6 demonstrated all RCC mixtures containing fibers did produce residual strengths that would be acceptable for use in concrete pavements with the magnitude of the residual strength dependent on the fiber type, geometry, and dosage, as expected.

RCC with hooked-end steel fibers can result in residual strengths similar to conventional fiber-reinforced Portland cement concrete (FRC), e.g., 1.60 MPa (230 lb/in^2) for F_{150} at 0.35% (Bordelon and Roesler, 2009), whereas RCC containing synthetic fibers at the same volume fraction as steel produce lower residual strengths. In general, like conventional FRC, increased volume fractions of synthetic fibers may be required to obtain similar residual strength to certain steel fiber types. The RCC compaction method deforms the steel fiber in a way that can increase the residual strength and toughness for certain steel fibers relative to synthetic fibers. This fiber deformation during compaction also occurs for synthetic fibers and actually produces the noted increases in strength in Table H5, but this mechanism likely results in a decrease in the residual strength of RCC with fibers because more fibers rupture during loading rather than pulling out.

H.6 FRACTURE TESTING

The results of the fracture testing as well as comparisons to literature are shown in Table H7. Generally, the K_{IC} for the RCC control and fiber mixtures were statistically the same. Macro-fibers at these volume fractions for RCC or PCC don't influence the development of micro- and macro-cracks in laboratory-sized specimens. All RCC fiber mixtures had statistically greater fracture energies at a 5 mm CMOD (G_{F5}) relative to the RCC control mixture, with fracture energy increasing with fiber dosage, as expected (Sahin and Köksal, 2011; Yandong et al. 2011). Similar to the beam flexural toughness tests (ASTM C1609) hooked-end steel fiber mixtures (Hook-60-0.2 and Hook-60-0.4) produced the greatest fracture energies. Comparing the RCC fracture results with those of an FRC paving mix in Figure H4 (PCC Smooth-40-0.4) and a PCC paving mix (Roesler et al. 2007) shown in Table H7, RCC (plain and fiber-reinforced) has statistically greater fracture properties (K_{IC} and G_F or G_{F5}) than the PCC or PCC Smooth-40-0.4 paving mix (for the same fiber dosage), respectively. Additionally, the PCC Smooth-40-0.4 mix in Table H7 and Figure H4 was tested at an age of 220 days and still had lower fracture parameters than the RCC mixtures with fibers that were tested at 28 days.

Table H7. DCT Fracture Testing Results for RCC and PCC with and without Macro-Fibers (COV, %)*.

(1 MPa*m$^{1/2}$ = 0.910 ksi*in$^{1/2}$; 1 GPa = 145 ksi; 1 in = 25.4 mm; 1 lb/in = 175 N/m)

Mixture ID	K_{IC} (MPa-m$^{1/2}$)	E (GPa)	$CTOD_C$ (mm)	G_f (N/m)	G_{F5} (N/m)
RCC Control	1.29 (4.1)	28.7 (4.4)	0.0217 (9.5)	57.7 (4.6)	165 (11.7)**
Emboss-48-0.2	**1.49 (3.1)**	33.4 (5.5)	0.0296 (16.7)	66.7 (11.0)	**787 (20.3)**
Emboss-48-0.4	1.39 (8.4)	29.9 (4.9)	0.0247 (17.3)	65.7 (13.1)	**1058 (20.8)**
Emboss-50-0.2	1.32 (8.6)	34.5 (5.5)	0.0206 (22.5)	51.0 (15.6)	**527 (18.7)**
Emboss-50-0.4	1.30 (8.0)	29.5 (4.4)	0.0203 (14.0)	57.8 (15.5)	**703 (22.7)**
Smooth-40-0.2	1.57 (14.8)	33.9 (7.6)	0.0299 (17.1)	73.2 (23.4)	**582 (8.8)**
Smooth-40-0.4	1.42 (11.3)	30.5 (5.7)	0.0230 (16.8)	66.5 (17.3)	**1011 (33.0)**
Smooth-58-0.2	1.23 (8.4)	32.6 (6.0)	0.0172 (12.2)	46.9 (15.1)	**356 (9.5)**
Smooth-58-0.4	1.14 (10.3)	26.5 (4.1)	0.0233 (7.8)	49.8 (19.8)	**652 (29.8)**
Helical-25-0.4	1.38 (11.1)	30.8 (3.1)	0.0219 (19.3)	62.4 (19.7)	**1212 (33.4)**
Hook-60-0.2	1.51 (7.3)	35.4 (5.0)	0.0245 (24.8)	65.0 (18.1)	**1480 (5.7)**
Hook-60-0.4	1.48 (17.0)	30.1 (2.6)	0.0255 (35.9)	75.0 (40.7)	**1481 (34.9)**
PCC Paving Mix (Roesler et al. 2007)	1.01	N/A	0.016	38.3	120**
PCC Smooth-40-0.4	1.09 (5.7)	36.8 (3.4)	0.0134 (4.0)	32.2 (9.6)	629 (14.0)

*Bold values represent statistical difference from control for K_{IC}, G_f, and G_5. N/A signifies that the value was not available.

**These mixtures did not contain fibers and therefore these values are their total fracture energy (i.e. fracture energy required to fail the specimen) and not fracture energy for a CMOD of 5 mm (0.2 in).

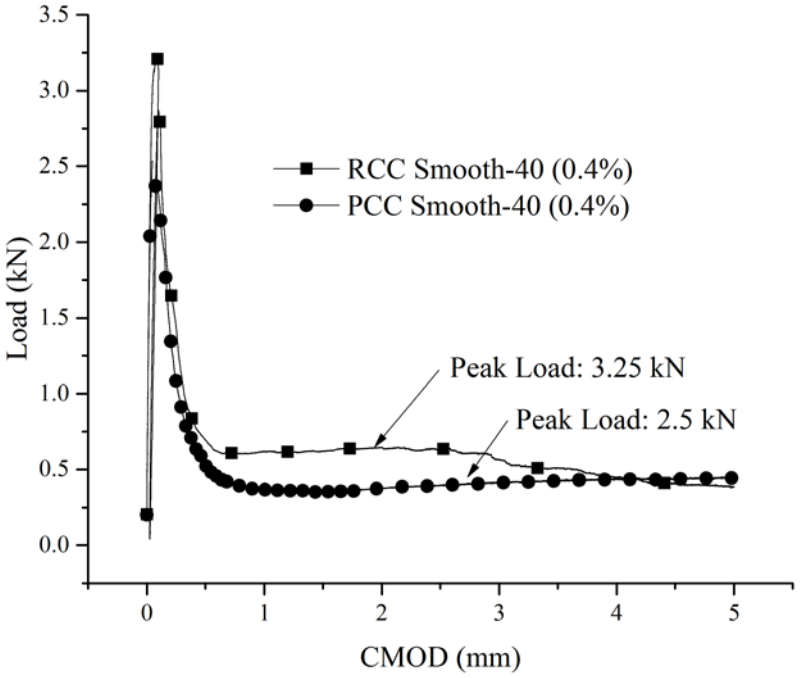

Figure H4. Comparison of DCT Load vs. CMOD Plots from Smooth - 40 RCC Mixture and an Equivalent Smooth - 40 PCC Mixture. (1 kN=224.8 lbf)

H.7 APPLICATION TO RCC PAVEMENT DESIGN

Currently, few concrete pavement design methods utilize the residual strength values from fiber-reinforced concrete (Altoubat et al. 2008; Bordelon and Roesler, 2009; Bordelon and Roesler, 2011). It has been shown that the residual strength from ASTM C1609 (ASTM, 2010) can be used to enhance the thickness design of PCC pavements with structural fibers (Altoubat et al. 2008; Roesler et al. 2012; Bordelon and Roesler, 2011) resulting in reduced thicknesses for a similar fatigue life. Altoubat et al. (2008) showed that for an equivalent flexural strength ratio of 30%, slab thicknesses were reduced by approximately 15%. Wu and Mahdi (2015) showed that the fatigue life of even plain RCC is much greater than that predicted by the Portland Cement Association's (PCA) thickness design procedure for RCC. With the addition of macro-fibers, the fatigue life can possibly be extended further because of the improved fracture properties as shown in Table H7 as well as the possibility of increased strength with certain fiber types. In summary, properly design macro-fibers in RCC may lead to thickness reductions, reduced crack widths for enhanced aggregate interlock joints/cracks, and reduced crack deterioration rates (Roesler et al. 2012).

H.8 CONCLUSIONS

This research addressed the impact of fiber type, four macro-synthetic and two steel fibers at two dosages (0.2% and 0.4% by volume), on the strength, elastic modulus, fiber reinforced concrete (FRC) toughness, and fracture parameters for a fixed roller-compacted concrete (RCC) mixture. Several RCC mixes containing synthetic fiber types had significant increases in MDD and compressive strength relative to the RCC control mixture. In terms of split tensile strength, the steel fibers tested increased the RCC control strength greater than synthetic fibers. There was no statistical difference between the elastic modulus of any fiber mix and the control.

Flexural toughness and residual strengths for RCC mixes with fibers, according to ASTM C1609, increased with higher fiber dosages, as expected. For the same volume fraction and fibers tested in this study, the hooked-end steel fiber had greater flexural toughness and residual strength values relative to the synthetic fibers in RCC. The flexural performance tests showed that fiber-reinforced RCC can produce acceptable flexural toughness and residual strength values for pavement applications but these values are either similar or lower than the toughness and residual strengths derived from conventional FRC depending on the fiber type and dosage.

Fracture testing indicated that RCC (plain and fiber-reinforced) exhibited greater fracture properties than conventional concrete paving mixes (plain and fiber-reinforced) from the literature, suggesting that RCC, if properly constructed, has similar or better fatigue resistance relative to PCC. The addition of fibers further improved the fracture properties relative to the control RCC mixture with the largest improvement being the increase in fracture energy. Due to these increases in strength and fracture properties, RCC with fibers should increase the overall fatigue resistance and service life of RCC pavements.

APPENDIX I: ROLLER COMPACTED CEMENT TREATED BASES CONTAINING RECLAIMED ASPHALT PAVEMENT, QUARRY BYPRODUCTS, AND FIBERS

This chapter investigates the use of quarry byproducts, reclaimed asphalt pavement, and macro-synthetic fibers in a lightly cement-treated aggregate base. Properties tested include: strength (compressive and split tensile), elastic modulus, flexural performance (toughness and residual strength), as well as fracture properties.

I.1 INTRODUCTION

Aggregate quarry processes such as blasting, crushing and screening of coarser grade aggregates produce byproduct mineral fine materials, at approximately 8% of the mined aggregate, commonly known as quarry waste or quarry dust. Depending upon the resulting gradation, quarry byproducts can be used as a manufactured sand. Quarry waste fines or byproducts (QB) are typically less than ¼ in. (6 mm) in size and consist of coarse, medium, fine sand particles, and a varying amount of fines passing the No. 200 sieve (0.075 mm). Current economic conditions and an increased emphasis in the construction industry on sustainability and recycling require production of virgin aggregate gradations with lower dust and smaller maximum aggregate sizes. These new production limitations have "unbalanced" the aggregates production stream, mostly because of the demand for cleaner aggregates with smaller top sizes in fine-graded asphalt concrete mixes, resulting in an overall increase in energy use and waste fines. Research that leads to making more beneficial use of QB in conjunction with locally-available, acceptable materials, marginal aggregate materials, or recycled materials is urgently needed.

NCHRP Synthesis 445 (Tutumluer, 2013) clearly emphasized the need for pavement projects to be sustainable and cost-effective by (i) making more effective use of locally available and marginal aggregate materials; (ii) increasing use of recycled aggregate products, such as recycled concrete aggregate (RCA) and reclaimed asphalt pavement (RAP), in pavement construction; and (iii) targeting long life and improvement in pavement performance.

The use of RAP in hot mix asphalt concrete is becoming common practice since virgin binder contents can be reduced because of the binder present in the RAP. In order to gain the maximum amount of binder from the RAP, asphalt producers use a proportion of the fine fraction of RAP (i.e. passing the 4.75 mm, No. 4 sieve) resulting in large stockpiles of coarse RAP (i.e. fractionated reclaimed asphalt pavement, FRAP). The coarse FRAP generally consists of particle sizes greater than 4.75 mm (No. 4 sieve size). A similar trend is observed for stone QB with large stockpiles being created continually each year because few applications permit use of QB. The use of RAP or QB in pavement layers has previously been studied by many researchers (Schroeder 1994; Garg and Thompson, 1996; Taha et al. 2002; Puppala et al. 2012; Rezende et al. 2014; Hoppe et al. 2015; Mohammadinia et al. 2015; Mwumvaneza et al. 2015). However, the use of either of these recycled/marginal materials in cement-treated foundation layers has been somewhat limited, especially the use of QB.

An International Center for Aggregates Research study tested the acceptability of high fines content in aggregate pavement layers and reported that aggregate systems with higher fines benefited considerably from low percentages (1-2%) of cement stabilizer (Ashtiani and Little, 2007). The study found that with the proper design of fines content, cement content and moisture, the performance of the stabilized systems with high fines content could perform equivalent to or even better than systems with standard fines content. Cement treated quarry fines were also used as a pavement base material on SH-360 in Arlington, Texas, as part of a research project (Puppala et al. 2008). The study reported that the unconfined compressive strength of cement treated quarry fines was adequate and that field monitoring indicated low permanent deformation during service. A recent Iowa DOT study also focused on road construction utilizing admixture stabilized limestone fines and found that stabilized fines could perform satisfactorily as a structural layer in road construction (Rupnow et al. 2010). In their study, unconfined compression, freezing and thawing, and wet-dry durability test results showed that cement kiln dust (CKD) was not an acceptable stabilizer because of poor durability performance but mixtures of class C fly ash and CKD were determined to be acceptable.

While cement treated foundation layers increase strength, stiffness, and reduce rutting potential, relative to unbound aggregates, they also increase the brittleness of the material. This increased brittleness leads to shrinkage cracking, fatigue cracking from mechanical loading, and potentially other cracking from environmental distresses (i.e. freezing and thawing). It is well known that reflective cracking of hot mix asphalt (HMA) is a common issue when paved on top of a cement treated layer (Mushota et al. 2014). The use of fibers in cement treated layers has been shown to maintain tighter crack widths (Grilli et al. 2013); fibers have also been shown to reduce cracking severity of concrete pavements (Roesler et al. 2011). By maintaining tighter crack widths and reducing the severity of cracking, fiber-reinforced cement treated layers have the potential to reduce the severity of reflective cracking. In addition to reducing cracking severity, fibers have also been shown to increase the fatigue life of cement treated layers as well as concrete pavements (Johnston and Zemp, 1991; Matsumoto and Li, 1999; Cervantes and Roesler, 2009; Sobhan and Krizek, 1999).

I.2 OBJECTIVES

The main objective of this study was to determine the feasibility of using a recycled aggregate (FRAP) and quarry byproduct material (QB), in combination with synthetic macro-fibers, as a sustainable alternative to produce lightly cement-stabilized foundation layers that can be used for sustainable pavement alternatives, such as in the case of inverted pavements (Syed and Scullion, 2001; Tutumluer, 2013) or as a stronger, more durable base course. The addition of macro-fibers is also studied to add ductility, increase crack shear capacity, and resist crack propagation in the stabilized base course. Six mixture designs were developed for this study in order to investigate how cement content, combining QB with FRAP or virgin aggregates, and the use of macro-synthetic fibers would affect strength and stiffness characteristics of the CTB material. Since compressive strength is typically used as a construction specification and elastic modulus is a required input for mechanistic pavement analysis, strength (compression and split tension) and elastic modulus were measured in this study.

I.3 MATERIALS AND MIXTURE DESIGN

The two main aggregates studied were coarse fractionated reclaimed asphalt pavement (coarse FRAP) and quarry byproducts (QB). In this study, QB were essentially a manufactured sand, derived from a dolomitic limestone, with a relatively high fines content. Extensive characterization of the FRAP and QB used in this study can be found in Mwumvaneza et al. (2015) and Brand and Roesler (2015c), respectively. Two other aggregates, coarse and intermediate dolomite, were used to replace the coarse FRAP as the control mixture, i.e., virgin aggregate. The gradation curve for each aggregate can be found in Figure I1. The oven-dry (OD) specific gravity of each aggregate is: 2.53, 2.64, 2.67, and 2.66 for FRAP, QB, coarse dolomite, and intermediate dolomite, respectively. The synthetic macro-fiber used in this study was a 50 mm (2 in) embossed polymeric fiber with an elastic modulus of 7 GPa (1015 ksi) and tensile strength of 550 MPa (80 ksi). This fiber geometry was initially selected because of its length (50 mm, 2 in) which was recommended by Sobhan and Mashnad (2001) as being the optimal with respect to the desired mechanical properties of a cement treated base course.

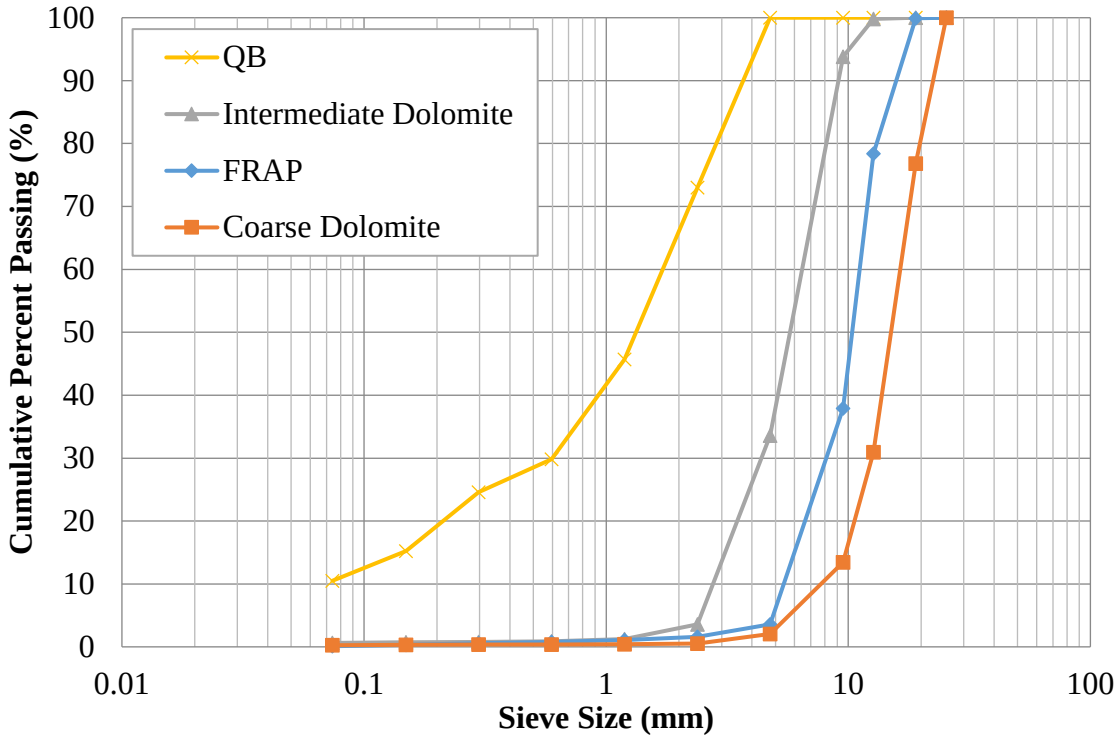

Figure I1. Aggregate Gradation Curves. (1 in = 25.4 mm)

I.3.1 Aggregate Packing Tests

Six mixtures of FRAP and QB were used to perform packing density tests according to ASTM Standard C29 (ASTM, 1997) which served the purpose of determininig the minimum void content, or maximum packing density, of the blended aggregate to use in the mix design. It was assumed that minimizing the void content of the aggregate would translate to less required cement content to fill those voids. Because packing tests were performed in the dry condition, the effect of lubrication from cement paste was not considered. The percent volume of QB for each mixture was increased in increments of 5% from 55% to 80% with the remainder of the aggregate being FRAP. As shown in Figure I2, to achieve the maximum density (minimum void content) for a mixture of FRAP and QB, the optimal volume fraction of QB is 70% with a corresponding FRAP volume fraction of 30%. In Figure I2, packing density refers to the compliment of void content, i.e., one minus packing density. At 70% QB by volume, void content was approximately 23 to 24%.

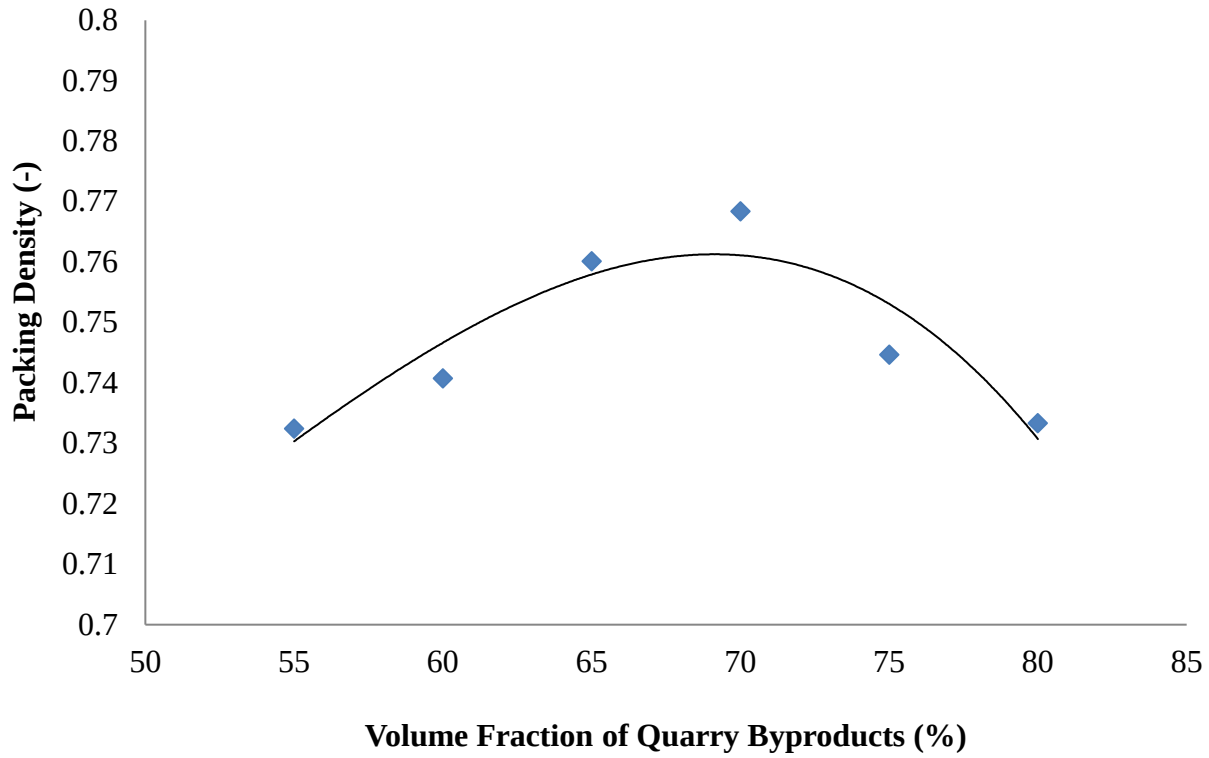

Figure I2. Aggregate Packing Density of QB and and FRAP.

To validate the results of the aggregate packing tests, two trial mix designs were prepared at different percentages of QB relative to the combined aggregate gradation. Thus, 55% QB - 45% FRAP and 70% QB - 30% FRAP mixtures were chosen as the two trial mixtures. The 55% QB – 45% FRAP blend was chosen because it represents a combined gradation closer to the maximum density curve and follows typical gradation limits for dense-graded base course materials. Moisture-density tests following the modified Proctor test procedure (ASTM D1557, 2012) were performed to determine the optimum water content to use for each trial mix design. The only difference between the two mix designs is the

combined aggregate gradation and the water content while cement content by volume (4%) and fiber dosage (0.4%) were held constant. The cement content of 4% was chosen for the initial study in order to avoid potentially greater variability with lower cement contents. Twelve 100 by 200 mm cylinders were then fabricated for strength testing to compare the compressive and split tensile strengths of the two different combined gradations. The compressive and split tensile strengths of 70% QB – 30% FRAP were both statistically greater (95% confidence limit) than those of 55% QB – 45% FRAP as seen in Table I1. As a result, the 70% QB – 30% FRAP mixture fraction was selected as the combined gradation for the remainder of the study. For the virgin aggregate mixtures, the FRAP was replaced with coarse and intermediate size dolomite particles. The coarse and intermediate dolomite aggregates were blended such that their combined gradation was equal to that of the FRAP. The optimal packing density of the QB and virgin dolomite was not determined for these mixtures.

Table I1. Strength Results from Aggregate Packing Validation Tests

	55% QB – 45% FRAP	70% QB – 30% FRAP
7 Day Compressive Strength		
Average in MPa (psi)	9.03 (1,309)	11.01 (1,596)
Standard Deviation in MPa (psi)	0.45 (65.3)	0.35 (50.8)
Statistically Different at 95% Confidence Limit?	YES	
7 Day Split Tensile Strength		
Average in MPa (psi)	1.51 (219.0)	1.72 (249.4)
Standard Deviation in MPa (psi)	0.05 (7.3)	0.11 (16.0)
Statistically Different at 95% Confidence Limit?	YES	

I.3.2 Mixture Design Nomenclature

A three-character name was given to each of the six mixtures for this study. The first character is a number which represents the cement content in total volume percentage (2, 3, or 4%). The second character is a letter which denotes whether the coarse aggregate used is recycled FRAP (R) or virgin (V). The third character is a letter which denotes whether the mixture has fibers (F) or none (N). All mixtures had the same weight content and gradation of QB aggregates. The following six mix designs were considered in this study:

- 2RF: 2% cement, FRAP, QB, fibers
- 3RF: 3% cement, FRAP, QB, fibers

- 4RF: 4% cement, FRAP, QB, fibers
- 4RN: 4% cement, FRAP, QB, No fibers
- 4VF: 4% cement, Virgin Coarse Aggregate, QB, fibers
- 4VN: 4% cement, Virgin Coarse Aggregate, QB, No fibers

I.3.3 Moisture-Density Tests and Final Mixture Proportions

Modified Proctor moisture-density tests (ASTM, 2012) were performed to determine the optimum moisture content (OMC) and maximum dry density (MDD) for each of the six mixtures. The moisture contents considered ranged from 4% to 8% (by total dry weight of aggregate and cement). Table I2 lists the MDD and OMC values which did not vary significantly between mixtures. Maximum dry densities ranged between 2,291 – 2,377 kg/m^3 (143 – 148.4 lb/ft^3) while optimum moisture contents were quite consistent ranging between 6.2 – 6.6%. Table I2 also presents the mixture design proportions used in this study. For the fiber mixtures, a dosage of 0.4% by volume was chosen.

Table I2. Oven - Dry Mixture Proportions and Moisture - Density Results (1 kg/m^3 = 1.686 lb/yd^3)

	2RF	3RF	4RF	4RN	4VF	4VN
Fibers (kg/m^3)	3.64	3.64	3.64	-	3.64	-
Cement (kg/m^3)	62.9	94.3	125.8	125.8	125.8	125.8
FRAP (kg/m^3)	647.9	648.5	638.4	647.3	-	-
Coarse Dolomite (kg/m^3)	-	-	-	-	471.7	474.0
Intermediate Dolomite (kg/m^3)	-	-	-	-	202.3	203.5
QB (kg/m^3)	1,577.0	1,578.2	1,554.4	1,575.2	1,565.1	1,574.0
Water (kg/m^3)	151.9	148.3	152.5	147.1	154.9	148.3
Maximum Dry Density (kg/m^3)	2,291	2,324	2,323	2,348	2,369	2,377
Optimum Moisture Content (%)	6.6	6.4	6.6	6.3	6.5	6.2

I.3.4 Specimen Fabrication

Cylinders for compressive strength, split tensile strength, and elastic modulus tests were compacted according to ASTM C1435 (ASTM, 2008) with a slight difference; 100 x 200 mm (4 in. x 8 in.) cylinders were made instead of 150 x 300 mm (6 in. x 12 in.) cylinders to reduce the volume of material required. All specimens were cured in a moist room at 100% relative humidity and 20 degrees Celsius until the time of testing.

I.4 COMPRESSIVE AND SPLIT TENSILE STRENGTH PROPERTIES

Unconfined compressive strength (UCS) tests, as seen in Figure I3, were performed according to ASTM C39 (ASTM, 2012) on 100 x 200 mm (4 in. x 8 in.) cylinders at ages of 7, 14, and 28 days for each mixture. The average compressive strengths of three replicate specimens for each mix design at ages of 7, 14, and 28 days are shown in Figure I4, where the error bars represent one standard deviation. As expected, the average UCS increased with cement addition and was found to be statistically significant (95% confidence limit) using the Tukey significant difference test (Mason et al. 2003). In addition, after doubling the cement content (from 2RF to 4RF) the average UCS increased by a factor of 3.5 at the age of 28 days. Further strength gain after 7 days was noted for all mixes. Mixes without fibers (4RN or 4VN) were not statistically different than mixes with fibers (4RF or 4VF). The virgin aggregate mix with fibers (4VF) had a statistically different UCS relative to recycled aggregate mix with fibers (4RF), but there was no statistical difference between virgin and recycled mixes without fibers (4VN and 4RN).

Figure I3. Failure of Unconfined Compressive (left) and Split Tensile Strength (right) Specimens.

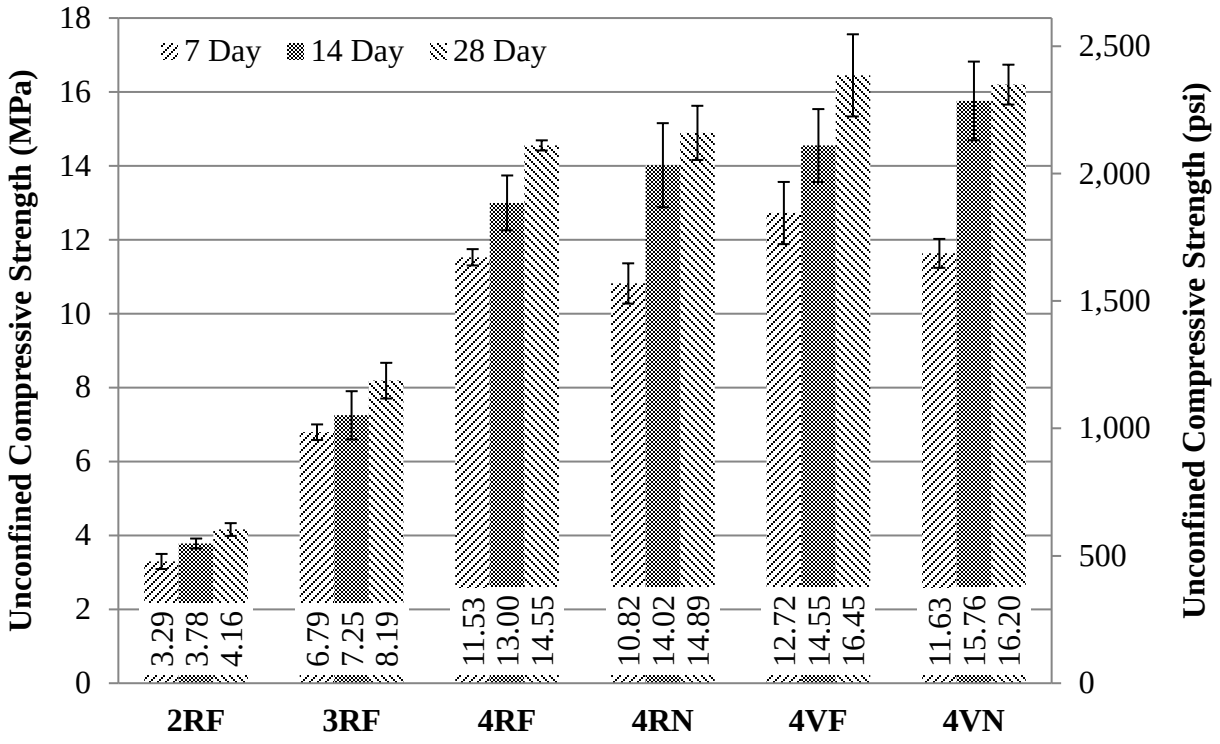

Figure I4. Unconfined Compressive Strength Results (error bars indicate +/- one standard deviation). (1 ksi = 6.89 MPa)

Mix 2RF produced a 28-day compressive strength of 4.16 MPa (603 psi) which classifies as a cement treated base materials (Halsted et al. 2006). All 4% cement mixes produced an average 28-day UCS exceeding 14 MPa (2,030 psi) with the highest average UCS achieved with the 4VF mix. Mix 3RF with 3% cement had a 28-day compressive strength of 8.19 MPa (1,188 psi) similar to lean concrete base materials (Greene et al. 2011). The 4% cement mixes presented in this study resulted in significantly greater compressive strengths than that of the lean concrete or econocrete base types (4.66 MPa, 0,67 ksi, at 28 days) with a similar cement content (Greene et al. 2011).

Splitting tensile strength tests were performed according to ASTM C496 (ASTM, 2011) on 100 x 200 mm (4 in. x 8 in.) cylinders (see Figure I3) at ages of 7, 14, and 28 days with 3 replicates tested per age for each mix. As shown in Figure I5, split tensile strengths increase with the addition of cement (statistically significant per the Tukey test at a 95% confidence limit). At 7 days, several mixes with fibers yield greater split tensile strengths than mixes without fibers. However, mixtures containing fibers had little to no tensile strength gain after 7 days, whereas mixtures without fibers continued to gain strength after 7 days. For the mixes where the 28-day split tensile strength was lower than at 14 days, the differences were not statistically significant. Figure I5 also indicates that the virgin aggregate mix without fibers (4VN) produced a greater split tensile strength than the FRAP mix without fibers (4RN). After doubling the amount of cement (2RF to 4RF), the split tensile strength increases by a factor of 2.15 at an age of 28 days. The 4% cement (126 kg/m^3, 212 lb/yd^3) mixes

produced 28-day split tensile strengths greater than 1.8 MPa (261 psi) which exceeds all of the econocrete mixes presented by Greene et al. (2011) with split tensile strengths less than or equal to 1.7 MPa (250 psi).

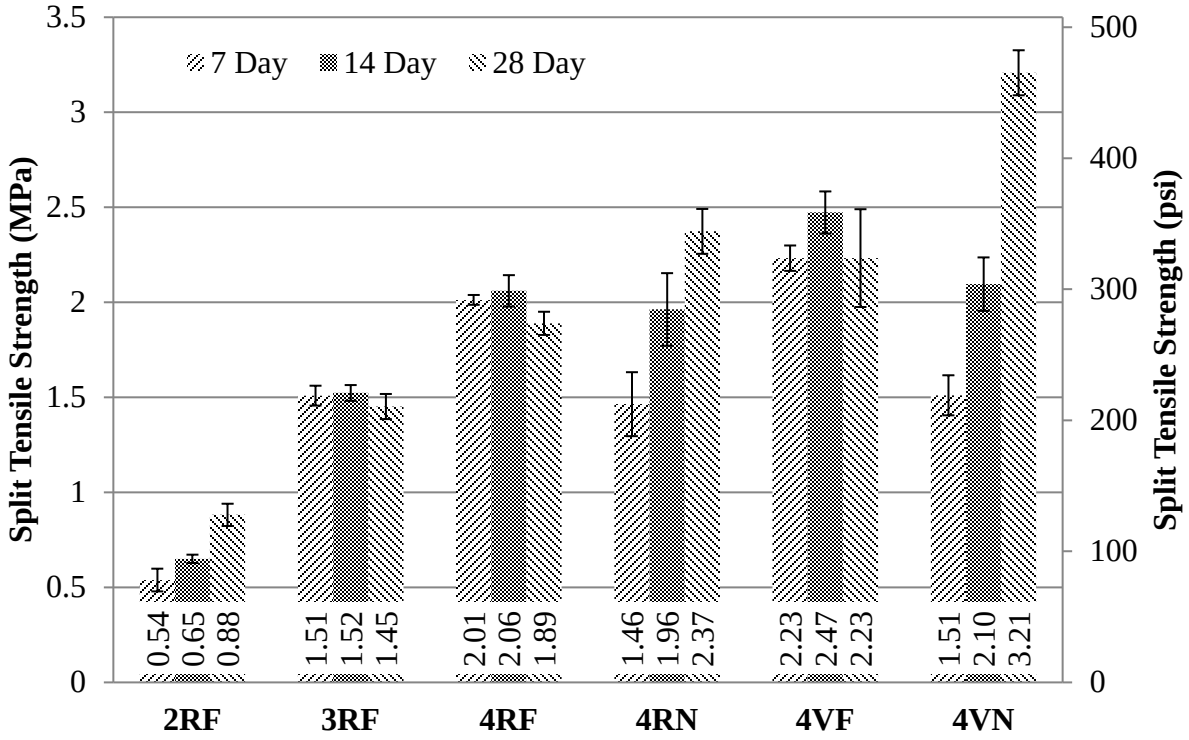

Figure I5. Split Tensile Strength Results (error bars indicate +/- one standard deviation).

I.5 ELASTIC MODULUS PROPERTIES

Modulus of elasticity tests were performed according to ASTM C469 (ASTM, 2010) on 100 x 200 mm (4 in. x 8 in.) cylinders after 28 days of moist curing with 3 replicates tested for each mix. Figure I6 shows an initial stress-strain plot from each mix. The average, 28-day elastic modulus values obtained for each mix are shown in Figure I7. Similar to the unconfined compressive strength and split tensile strength results, elastic modulus increases with cement content and is statistically significant at 95% confidence limit. The elastic modulus of the CTB material with FRAP and fibers increase by a factor of 2.7 from 2% to 4% cement. As expected, CTB materials with virgin aggregate had larger elastic modulus than with FRAP aggregates. Given the same cement content, fibers did not impact the elastic modulus values for the CTB material. Relative to elastic moduli of econocrete mixes presented by Greene et al. (2011) of 8.9 to 15.2 GPa (1.3 to 2.2 ksi), all 4% cement mixes presented in this study were stiffer.

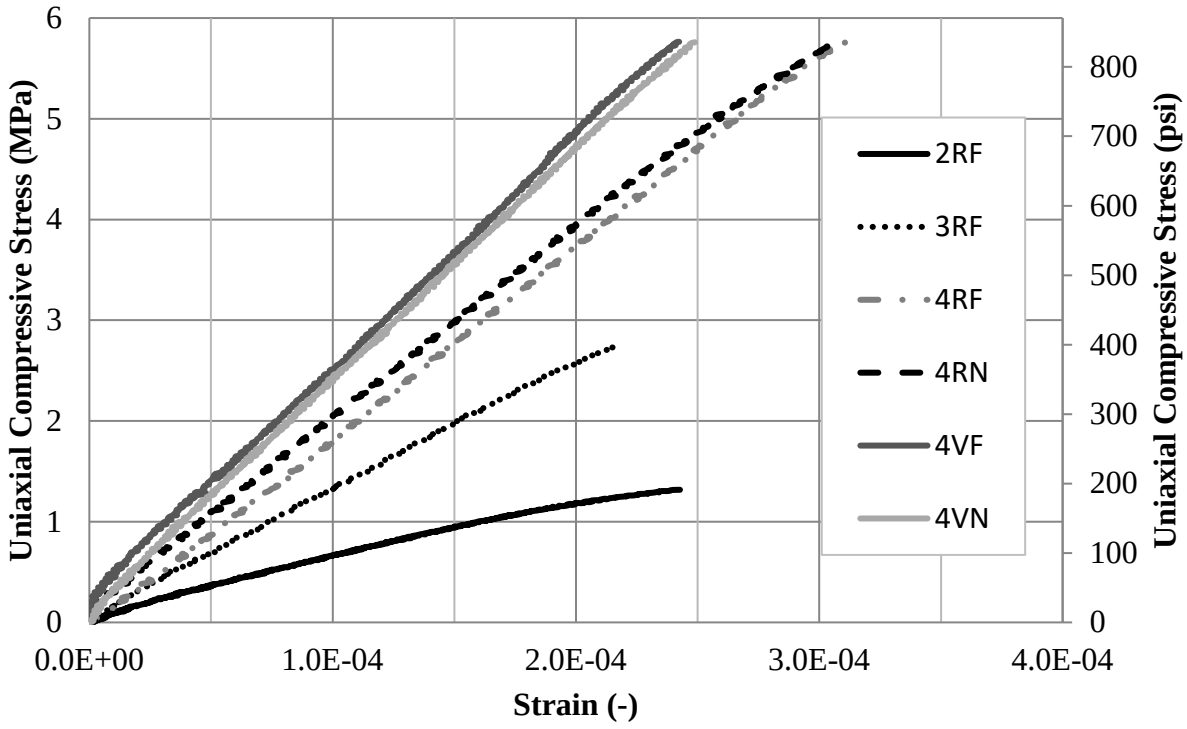

Figure I6. Stress - Strain Curves from Elastic Modulus Tests at 28 Days.

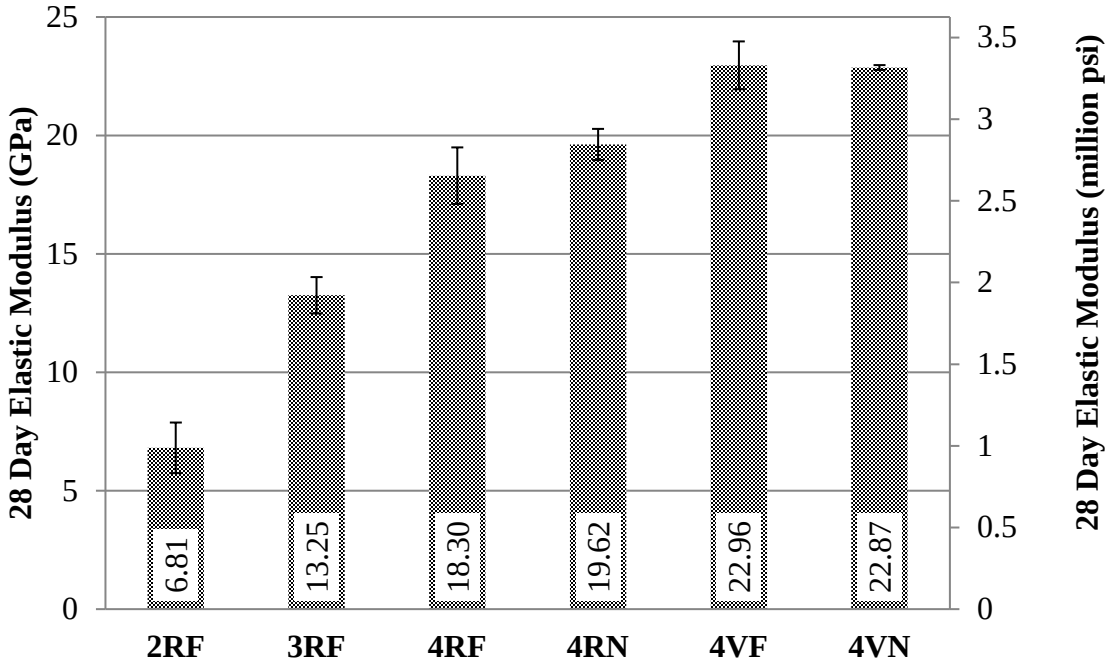

Figure I7. Elastic Modulus Results (error bars indicate +/- one standard deviation).

I.6 FLEXURAL PERFORMANCE TESTING

Flexural performance testing, according to ASTM C1609 (2010), was performed at an age of 14 days on 150 x 150 x 525 mm (6 x 6 x 21 in.) beam specimens. The beams were tested in four point (third-point) bending using a closed-loop servo-hydraulic load frame along with unlimited travel rollers to reduce friction between the beam and the rollers. The test setup for flexural performance testing is shown in Figure I8. The deflection rates suggested by ASTM C1609 (2010) have been shown to cause premature failure (Banthia and Islam, 2013) and thus modified (slower) deflection rates suggested by Banthia and Islam (2013) were used. Using a linear variable differential transformer (LVDT) to measure vertical deflection, the tests were run in deflection control up to a net deflection of 3 mm (0.12 in) which corresponds to L/150 where L represents the span length (450 mm, 18 in).

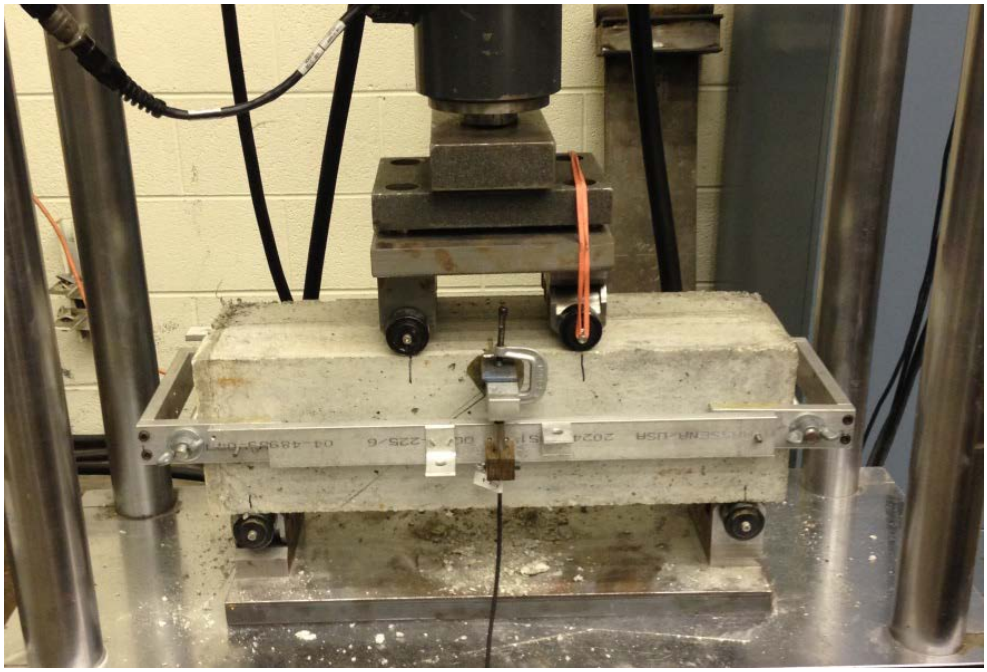

Figure I8. Flexural Performance Test Setup.

The reported properties from the flexural performance testing are peak flexural strength (*MOR*, MPa), residual flexural strengths corresponding to loads at deflections of L/600 and L/150 (F_{600} and F_{150}, MPa), respectively, flexural toughness (T_{150}, N-m), and equivalent flexural strength ratio ($R_{T,150}$, %). The peak flexural strength or modulus of rupture, *MOR*, is computed using Equation I1.

$$MOR = \frac{P \cdot L}{b \cdot d^2} \qquad \text{(Eq. I1)}$$

where *P* represents the peak load (N), *L* represents the span length (mm), *b* represents the width of the beam (mm), and *d* represents the depth of the beam (mm). Residual flexural strengths, F_{600} and F_{150}, are also calculated using Equation I1 by replacing the peak load with the load corresponding to deflections of L/600 and L/150, respectively. Flexural toughness is calculated by integrating the area under the load-deflection curve up to a deflection of 3 mm (0.12 in). The equivalent flexural strength ratio takes into account flexural toughness and is calculated using Equation I2.

$$R_{T,150} = \frac{150 \cdot T_{150}}{MOR \cdot b \cdot d^2} \cdot 100\% \qquad \text{(Eq. I2)}$$

Figure I9 shows load-deflection curves for each mix containing fibers; mixes without fibers are not shown since deflection was not measured due to catastrophic failure of the specimens upon reaching their peak loads which would have caused damage to the LVDT. From Figure I9, the inclusion of fibers produces a quasi-brittle response with measurable flexural toughness. Note that virgin and FRAP mixtures yield similar load-deflection curves.

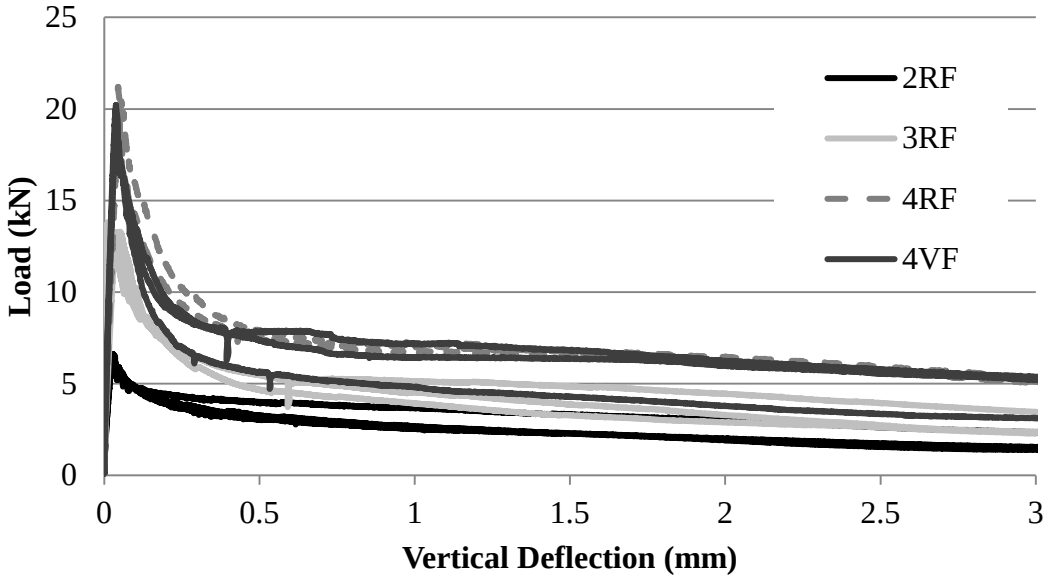

Figure I9. Load vs. Deflection Curves from Fiber-Reinforced Mixtures.
(1 kN = 224.8 lbf; 1 in = 25.4 mm)

Results, along with coefficients of variation (COV), from flexural performance testing are presented in Table I3 with the values given as averages of the three beam specimens tested. Increasing cement content led to significantly greater values of peak flexural strength, residual flexural strength, and flexural toughness. And, cement content did not have a statistically significant effect on equivalent flexural strength ratio. As expected, the inclusion of fibers did not have a significant effect on the peak flexural strength. Virgin and FRAP mixtures yielded similar peak and residual strengths, toughness values, and equivalent flexural strength ratios. The peak flexural strengths of the 4% cement mixtures were similar to those from Greene et al. (2011) for lean concrete bases.

Table I3. Flexural Performance Testing Results (1 ksi = 6.89 MPa; 1 N-m = 8.85 lb-in)

	MOR, MPa	F_{600}, MPa	F_{150}, MPa	T_{150}, N-m	$R_{T,150}$, %
2RF	0.75 (4.0)	0.35 (13.9)	0.20 (22.0)	8.5 (15.5)	43.7 (18.4)
3RF	1.75 (1.8)	0.60 (8.2)	0.35 (19.8)	13.5 (11.0)	32.5 (11.6)
4RF	2.40 (1.7)	0.85 (0.8)	0.60 (1.9)	21.5 (1.2)	34.3 (2.0)
4RN	2.45 (5.8)	N/A	N/A	N/A	N/A
4VF	2.30 (1.2)	0.75 (15.3)	0.55 (23.1)	19.0 (16.1)	31.7 (17.8)
4VN	2.85 (4.8)	N/A	N/A	N/A	N/A

Since all layers in a pavement structure experience tensile stresses as a result of loading and/or environmental conditions (Huang, 2004), flexural strength is a key parameter for the design of rigid (i.e. concrete) pavements and cement-treated layers. It has been shown in this study and in the literature that the flexural strength is not statistically increased by the inclusion of fibers, therefore suggesting that the use of fibers is not beneficial. However, it has been shown that the inclusion of fibers in concrete and cement-treated layers has led to improved fatigue life (Johnston and Zemp, 1991; Matsumoto and Li, 1999; Cervantes and Roesler, 2009; Sobhan and Krizek, 1999) as well as improved slab capacities for concrete pavements (Roesler et al, 2004). Therefore, the use of an adjusted flexural strength (effective modulus of rupture, *MOR'*) has been suggested to account for the increase in fatigue life with the inclusion of fibers (Bordelon and Roesler, 2009; Altoubat et al, 2006). The effective modulus of rupture (*MOR'*, MPa) takes into account the equivalent flexural strength ratio, which also accounts for the flexural toughness, and is calculated using Equation I3 as follows:

$$MOR' = MOR \cdot \left(1 + \frac{R_{T,150}}{100}\right) \quad \text{(Eq. I3)}$$

For the pavement design example given by Altoubat et al. (2006), a concrete thickness reduction of 17% was observed when using a fiber type/dosage that yielded an equivalent flexural strength ratio of 30%; all of the fiber-reinforced mixtures presented in this study yielded equivalent flexural strength ratios greater than 30%. Therefore, the inclusion of fibers in this cement-treated layer will either: (1) reduce required thickness for a design fatigue/service life, or (2) increase the fatigue/service life for a similar thickness to a non-fiber mixture.

I.7 FRACTURE TESTING

Fracture testing was performed at an age of 28 days according to the procedure set forth by Amirkhanian et al. (2015) for the disk-shaped compact tension (DCT) geometry. Specimens were fabricated from a 150 x 300 mm cylinder which was compacted according to ASTM C1435 (ASTM, 2008). Due to insufficient strength to withstand the saw-cutting and coring required for DCT specimen preparation, mix 2RF was not tested. In general, specimens were loaded at a crack-mouth opening displacement (CMOD) rate of 0.06 mm/min (2.36 mil) until the specimen reached a peak load after which the specimen was unloaded. Upon unloading to the original seating load, the specimen was reloaded at the initial CMOD rate until failure. For specimens without fibers (i.e. 4RN and 4VN), failure was defined as reaching a load of 0.1 kN (22.5 lbf) or breaking of the specimen whereas specimens containing fibers (i.e. 3RF, 4RF, and 4VF) were unable to reach this load within the constraints of the test setup. The clip gauge used to measure CMOD has a maximum opening of 6.35 mm (1/4 in); therefore the test was stopped at a CMOD of 5 mm (0.2 in) for specimens with fibers. The test setup for DCT fracture testing is shown in Figure I10. The fracture properties reported are: critical stress intensity factor (K_{IC}), critical crack tip opening displacement ($CTOD_C$), initial fracture energy (G_f), and total fracture energy (G_F). Figure I11 and Figure I12 show the load-CMOD curves from the fiber and non-fiber mixtures, respectively. Fracture testing results, which represent an average of four or five specimens, are shown in Table I4 along with their coefficients of variation (COV).

Figure I10. DCT Fracture Test Setup.

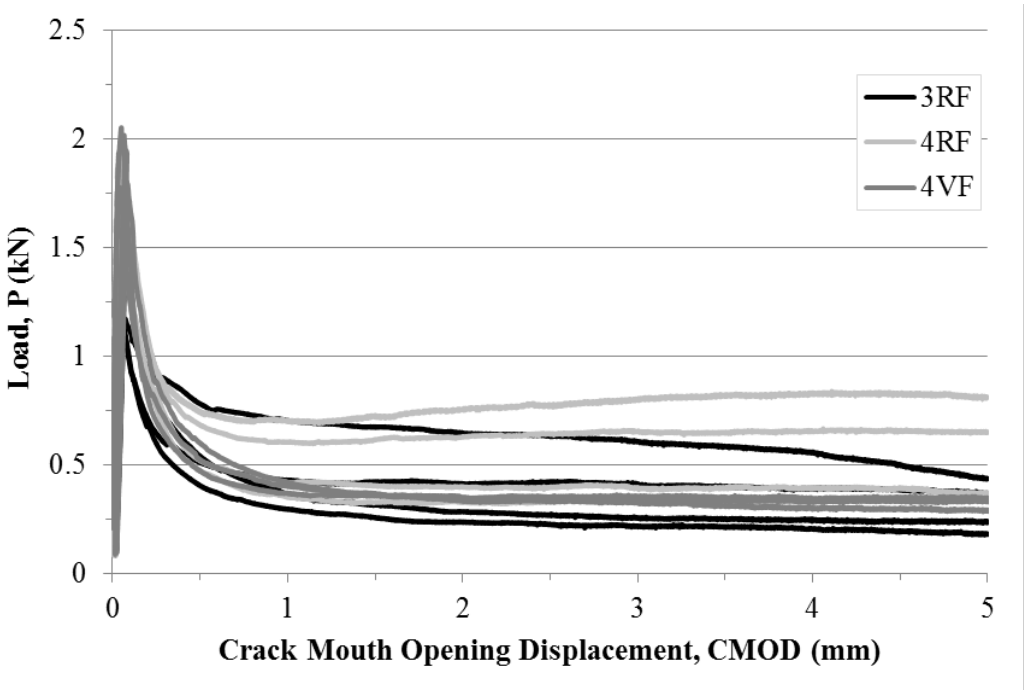

Figure I11. Load vs. CMOD Plots from DCT Testing of Fiber-Reinforced Mixtures. (1 kN=224.8 lbf)

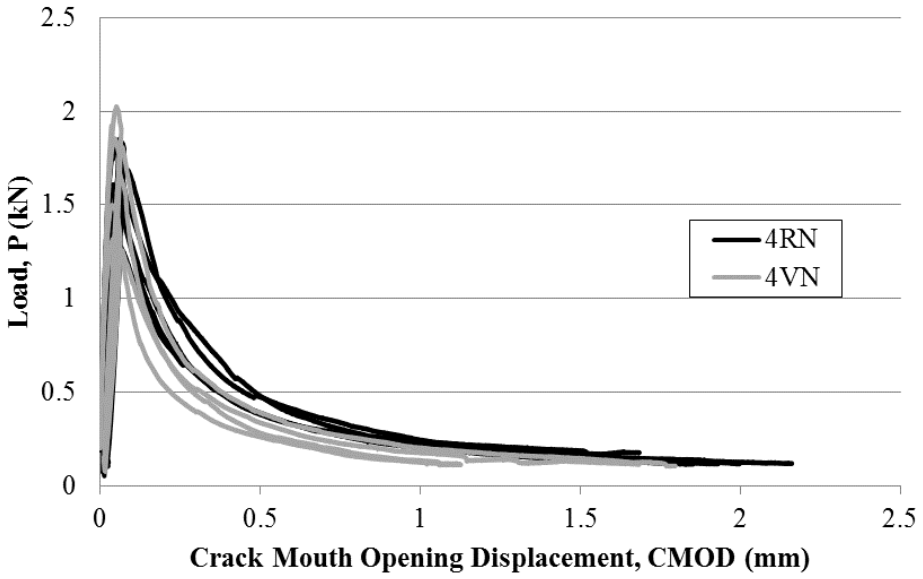

Figure I12. Load vs. CMOD Plots from DCT Testing of Non-Fiber Mixtures. (1 kN=224.8 lbf)

Table I4. Fracture Testing Results (COV, %) (1 MPa*m$^{1/2}$ = 0.910 ksi*in$^{1/2}$; 1 GPa = 145 ksi; 1 in = 25.4 mm; 1 lb/in = 175 N/m)

	K_{IC}, MPa-m$^{1/2}$	$CTOD_C$ (mm)	G_f (N/m)	G_F (N/m)*
3RF	0.581 (12.1)	0.0145 (16.1)	17.5 (21.3)	515.5 (38.0)
4RF	0.813 (10.6)	0.0159 (16.8)	25.2 (17.9)	698.4 (33.1)
4RN	0.752 (13.9)	0.0147 (17.3)	22.9 (23.2)	178.5 (12.5)
4VF	0.965 (13.8)	0.0195 (20.6)	34.1 (25.3)	522.8 (3.9)
4VN	0.847 (12.3)	0.0189 (12.6)	28.4 (18.7)	131.6 (23.8)

*Total fracture energy for fiber-reinforced mixtures represents fracture energy for a CMOD of 5 mm, (0.2 in).

From Figure I11 and Figure I12 it can be seen that the two non-fiber mixes yielded similar load-CMOD plots while mix 4RF showed a better post-peak load response than mix 4VF. Figure I11 indicates that none of the fiber mixes have reached a load of 0.1 kN (22.5 lbf) even after 5 mm (0.2 in) of CMOD. The critical stress intensity factor (K_{IC}), which is a measure of a material's initial cracking resistance, for each of the mixes containing 4% cement was statistically greater (confidence limit of 95%) than that of the mix containing 3% cement. Hou et al. (2011) showed the opposite trend for K_{IC} (i.e. increasing cement content reduced K_{IC}) of cement treated aggregate at cement contents greater than 4% and a testing age of 60 days. Virgin and FRAP mixes yielded statistically similar values of K_{IC} which has also been shown by Brand and Roesler (2015c) for concrete containing FRAP. Increasing cement content from 3% to 4% did not result in a statistical increase in total fracture energy (G_F). As shown by Brand and Roesler (2015c), the virgin and FRAP mixtures did not yield statistically different values of G_F. The inclusion of fibers did not produce statistically different values of K_{IC}, G_f, or $CTOD_C$ which has been shown by Roesler et al. (2007). The inclusion of fibers yielded statistically greater values of G_F compared to non-fiber mixes which is supported by fiber-reinforced concrete literature (Harris et al., 1972; Cha et al., 1997; Roesler et al., 2007).

I.8 CONCLUSIONS

This study investigated the beneficial use of stone quarry byproducts (QB) mixed with fractionated reclaimed asphalt pavement (FRAP), i.e. 100 % waste and recycled materials, in an effort to construct a more sustainable cement treated base course. The addition of synthetic macro-fibers was also considered as well as varying the cement contents (2, 3, and 4% by volume). Aggregate packing tests determined that the QB and FRAP aggregate proportions to minimize the combined aggregate void content (and greatest packing density) for their respective aggregate gradations required 70% QB and 30% FRAP by volume. Six separate mixtures were produced with a combination of 70% QB; virgin or FRAP aggregates; cement content of 2, 3, or 4%; and fibers or none.

As expected, compressive and split tensile strengths increased with additional cement content. On average, increasing cement from 2% to 4% increased 28-day compressive strengths by a factor of 3.5, increased 28-day split tensile strengths by 2.15, and elastic modulus by 2.7. Statistically, there was not a consistent difference between strengths (compressive and split tensile) of virgin and recycled aggregate mixtures with QB (i.e. FRAP vs. dolomite) except virgin aggregate mixes had statistically greater elastic moduli than FRAP mixtures. The addition of fibers did not produce statistically different compressive strengths, elastic moduli, or have a consistent trend on split tensile strengths. The mix designs of QB and FRAP presented in this study produced 28-day compressive strengths similar to cement treated base course requirements (mix 2RF) and were much greater than econocrete base material strength specifications (3% and 4% cement mixes). Therefore, the use of recycled and waste materials (FRAP and quarry byproducts, respectively) as aggregate for lightly cement treated foundation layers is feasible for at least no-freeze zones.

Flexural performance testing showed that the inclusion of fibers resulted in a quasi-brittle response with measurable flexural toughness and significantly greater fracture energy than non-fiber mixtures. Virgin and FRAP mixtures yielded similar flexural and fracture properties. In general, fracture and flexural performance properties improved as cement content increased. Regardless of cement content and aggregate type (i.e. FRAP vs. virgin), all fiber-reinforced mixtures in this study yielded equivalent flexural strength ratios greater than 30%. The inclusion of fibers yields residual shear capacity which will maintain load transfer across joints or cracks as well as improved fatigue resistance. These results show that use of macro-synthetic fibers with recycled and by-product aggregates (FRAP and QB, respectively) for lightly cement treated layers not only increases the fatigue life, but will also maintain tighter cracks which can reduce reflective cracking of overlying pavement layers.

APPENDIX J: SUPPLEMENTARY CEMENTITIOUS MATERIALS IN ROLLER-COMPACTED CONCRETE

This chapter investigates the impact of supplementary cementitious materials (SCMs) on roller-compacted concrete (RCC) fresh and hardened properties. Fresh properties measured include moisture-density relationship from the modified Proctor test and compactibility from the Vebe test. Hardened properties quantified were strength (compressive, split tensile, and flexural), fracture properties with the disk-shaped compact tension geometry, and free drying shrinkage.

J.1 INTRODUCTION

The use of supplementary cementitious materials (SCMs) in RCC has been studied by previous researchers with the focus mostly being on fly ash. Some researchers have investigated the other common SCMs (silica fume and ground granulated blast furnace slag) but to a lesser extent than fly ash. The use of SCMs in concrete have many potential benefits such as refined pore structure because of the pozzolanic reaction, increases in strength and durability properties, as well as reduction in the quantity of cement. Incorporating SCMs into a RCC mix design makes sense as long as the resulting mix properties meet the original intended application.

A review of the literature regarding use of fly ash in RCC was conducted (Table J1) and in general, the strength properties were lower than a reference RCC mix without fly ash. Compressive strength was more sensitive to the use of fly ash than flexural strength, however most studies found a reduction in compressive and flexural strength, especially at earlier ages (less than 28 days). As expected, this finding is dependent on the type of fly ash (class F, class C, or non-standard) as well as the dosage. Of the limited studies that looked at durability of RCC incorporating fly ash, there was good agreement that fly ash reduced the physical durability (resistance to freeze-thaw and salt scaling) even at dosages as low as 20%. Additionally, other researchers (Delagrave et al. 1997; Gao et al. 2006; Yerramala and Babu, 2011; Pavan and Rao, 2014) have incorporated fly ash in RCC but are not included in Table J1 since a control (i.e. RCC without fly ash) mix was not included in the respective studies.

A review of the literature regarding use of ground granulated blast furnace slag (GGBFS) and silica fume in RCC was conducted (Table J2). Significantly fewer studies have investigated the effect of GGBFS or silica fume on RCC relative to fly ash. GGBFS reduced compressive strengths at ages less than 7 days however, there was conflicting data regarding compressive strengths after 28 days. The use of silica fume was shown to increase compressive strength at any age. Silica fume was shown to increase durability (resistance to freeze-thaw and salt scaling) at dosages of 8% and 10%. In addition, there have also been studies investigating the use of non-traditional cementitious additives and natural pozzolans. Circulating fluidized bed combustion ash, coal waste, and limestone powder have all been successfully used in RCC with resulting mechanical properties being at least equivalent to control RCC mixes (Chi and Huang, 2014; Hesami et al. 2016). Researchers have also used natural pozzolans in RCC with the results typically showing reductions in mechanical and durability properties (Vahedifard et al. 2010; Nili and Zehari, 2011; Madhkhan et al. 2012).

Table J1. Literature Review of Fly Ash Effects (relative to RCC without fly ash) on RCC Properties

	Decrease	No Effect	Increase
Compressive Strength – Early Age (< 28 days)	Tangtermsirikul et al. (2004): 20-80% Nili and Zaheri (2011): 20% Mardani and Ramyar (2013): 20-60% Atis (2005): 50-70% Cao et al. (2000): 39-72%		
Compressive Strength – Later Age (> 28 days)	Tangtermsirikul et al. (2004): 20-80% Mardani and Ramyar (2013): 20-60% Atis (2005): 70% Cao et al. (2000): 60-72%		Nili and Zaheri (2011): 20% Atis (2005): 50% Cao et al. (2000): 39-53%
Split Tensile Strength – 28 Days	Mardani and Ramyar (2013): 20-60% Atis (2005): 70%		Atis (2005): 50%
Flexural Strength – 28 Days	Mardani and Ramyar (2013): 20-60% Atis (2005): 70% Cao et al. (2000): 72%	Atis (2005): 50% Cao et al. (2000): 53-60%	Cao et al. (2000): 39-46%
Sorptivity	Mardani et al. (2013): 20-60%		
Freeze-thaw Resistance	Mardani et al. (2013): 20-60%		
Deicer Salt Scaling Resistance	Nili and Zaheri (2011): 20%		
Vebe Time	Nili and Zaheri (2011): 20%		

Table J2. Literature Review of Silica Fume and Ground Granulated Blast Furnace Slag (GGBFS) Effects (relative to RCC without silica fume or GGBFS) on RCC Properties*

	Decrease	No Effect	Increase
Compressive Strength – Early Age (< 28 days)	**Rao et al. (2016): 0-10% (for < 7 days age)**		*Nili and Zaheri (2011): 8%* *Vahedifard et al. (2010): 10%*
Compressive Strength – Later Age (> 28 days)	**Karimpour (2010): 25-75%**		*Nili and Zaheri (2011): 8%* *Vahedifard et al. (2010): 10%* **Rao et al. (2016): 10-60%**
Absorption			**Karimpour (2010): 50%**
Freeze-thaw Resistance			*Vahedifard et al. (2010): 10%*
Deicer Salt Scaling Resistance			*Nili and Zaheri (2011): 8%*
Vebe Time		*Nili and Zaheri (2011): 8%*	

*Bold indicates studies using GGBFS and italicized indicates studies using silica fume.

J.2 RCC MIX DESIGNS WITH SCMS

A total of 7 mix designs were developed to quantify the effects of class C fly ash, silica fume, and GGBFS on RCC properties. Two mix designs were developed for each SCM (two replacement dosages) with the final mix design being a control, PC-100, (i.e. straight cement). Typically reported values for specific gravity of fly ash (2.3), silica fume (2.2), and GGBFS (2.2) were assumed (Mindess et al. 2003). The replacement dosages (weight % of total cementitious) were determined from a guide on RCC (Harrington et al. 2010) as well as a review of construction specifications related to RCC pavements (Chapter 3). Based on Harrington et al. (2010), the maximum recommended weight replacement of cement is 25% for fly ash and 8% for silica fume. Therefore, these two replacement levels were adopted (FA-25 and SF-8, respectively) while replacement levels corresponding to half of the maximums were also used (FA-12.5 and SF-4). Since Harrington et al. (2010) did not give guidance on GGBFS, the maximum replacement level was taken from a review of RCC construction specifications (Chapter 3) and found to be 40% (SLG-40). Half of the maximum GGBFS replacement level was also

used (SLG-20). The GGBFS used in this study is Grade-100 and the fly ash is class C. The aggregate gradation (Table J3) and total cementitious content of all mixtures (281.7 kg/m^3 or 475 lb/yd^3) were kept constant to limit influencing factors. The mix designs were developed after performing modified Proctor testing and determining the maximum dry density (MDD) and optimum moisture content (OMC) as shown in Table J4. The mix designs and corresponding Vebe times are also shown in Table J4. All Vebe times were below 20 seconds, the suggested maximum Vebe time from ACI (1995).

Table J3. Combined Aggregate Gradation (1 in = 25.4mm)

Sieve Size (mm)	% Passing
19.0	100
12.7	77.4
9.51	73.1
4.76	50.0
2.38	38.2
1.19	35.8
0.595	24.5
0.30	2.9
0.15	0.2
0.075	0.0

Table J4. Oven-Dry Mix Designs (kg/m^3), Moisture-Density Relationship, and Vebe Times
(1 kg/m^3 = 1.686 lb/yd^3)

	PC-100	FA-12.5	FA-25	SF-4	SF-8	SLG-20	SLG-40
Total Aggregate	2100	2109	2089.3	2104	2104	2085.8	2101.8
Cement	281.7	246.5	211.3	270.4	259.1	225.3	169
Fly Ash	-	35.2	70.4	-	-	-	-
Silica Fume	-	-	-	11.3	22.5	-	-
GGBFS	-	-	-	-	-	56.3	112.7
Water	153.5	157.5	144.9	155.1	155.1	149.4	154.5
MDD (kg/m^3)	2381.7	2390.7	2371	2385.7	2385.6	2367.4	2383.5
OMC (%)	6.4	6.6	6.1	6.5	6.5	6.3	6.5
Vebe Time (sec)	15.8	12.5	16.4	18.4	18.5	12.9	14.1

J.3 STRENGTH RESULTS

Compressive and split tensile strengths were measured on 100x200 mm (4x8 in) cylinders at ages of 1, 7, and 28 days with triplicate specimens per age. Flexural strength was measured on 100x100x400 mm (4x4x16 in) beams at an age of 28 days with triplicate specimens per mix. Compressive strength results are shown in Figure J1 while statistical analysis of the results (Tukey test) is shown in Table J5. As anticipated from the literature review (Table J1 and Table J2), fly ash and GGBFS have a negative impact on compressive strength at early ages (1 and 7 days) compared to later ages (28 days) relative to the 100% cement control mix. At an age of 1 day the silica fume mixes yielded statistically greater compressive strengths than the control mix (PC-100) while all other mixes produced statistically lower compressive strengths than PC-100. After 28 days of curing, only SLG-40 had a statistically lower compressive strength than PC-100 which agrees with Karimpour (2010). All mixes meet a 7-day compressive strength of 24 MPa (3.5 ksi) (See Chapter 3) and the 28-day, 31 MPa (4.5 ksi) compressive strength requirement by the American Concrete Pavement Association (2014). A review of RCC pavement construction specifications (Chapter 3) found that minimum compressive strengths for determining the age at which the pavement could be opened to traffic were at most 21 MPa (3 ksi). The silica fume mixes and control mix (PC-100) all met this requirement after only 1 day however, the other RCC mixes might require an additional day or two of curing.

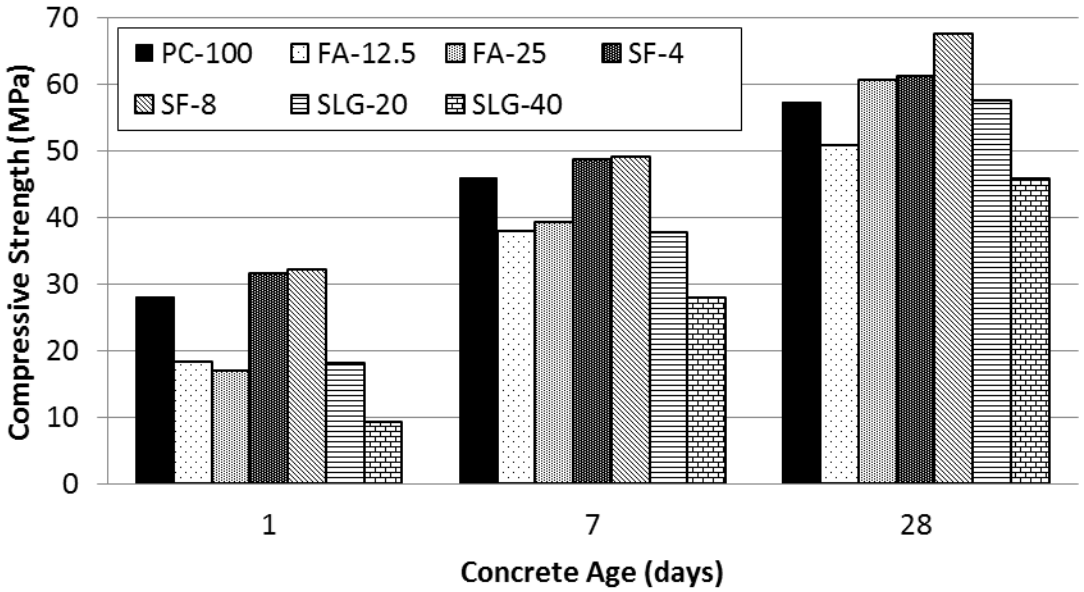

Figure J1. Average RCC Compressive Strength over Time with SCMs. (1 ksi = 6.89 MPa)

Table J5. Statistical Analysis of RCC Compressive Strength Results (1 ksi = 6.89 MPa)

Mix ID	1-Day Compressive Strength (MPa)	Statistical Grouping(s)			
SF-8	32.3	A			
SF-4	31.6	A			
PC-100	28.1		B		
FA-12.5	18.5			C	
SLG-20	18.2			C	
FA-25	17.0			C	
SLG-40	9.3				D
Mix ID	28-Day Compressive Strength (MPa)	Statistical Grouping(s)			
SF-8	67.7	A			
SF-4	61.4	A	B		
FA-25	60.7	A	B		
SLG-20	57.7		B	C	
PC-100	57.4		B	C	
FA-12.5	51.0			C	D
SLG-40	45.9				D

Elastic modulus was tested at an age of 28 days according to ASTM C469 (ASTM, 2010) using 100x200 mm (4x8 in) cylinders. Results from elastic modulus testing are shown in Table J6 with the reported values being an average of 3 specimens.

Table J6. 28-Day Elastic Modulus Results (1 GPa = 145 ksi)

Mix ID	Elastic Modulus (GPa)	Coefficient of Variation, COV (%)
PC-100	33.3	7.0
FA-12.5	34.3	2.1
FA-25	34.7	5.2
SLG-20	34.3	3.6
SLG-40	30.7	1.4
SF-4	33.8	3.9
SF-8	33.7	5.4

Results of split tensile strength testing are shown in Figure J2 and statistical analysis of split tensile strength results is shown in Table J7. Similar to compressive strength results, the fly ash and GGBFS mixtures had statistically lower split tensile strengths at 1 day relative to the control mix (PC-100) with the same trend also seen at 28 days. The silica fume mixtures also had statistically lower split tensile strengths than PC-100 at 28 days. This unexpected result could be because of self-desiccation (Loukili et al. 1999) from the silica fume that resulted in incomplete hydration of cementitious products and poor tensile bond properties or it could simply be cylinder artifacts. Regardless, the 28-day split tensile strengths of the silica fume mix were unexpected. Unlike split tensile strength, flexural strengths of all mixes were statistically similar to PC-100 with the exception of SF-8 which was statistically greater (Table J8). Discrepancies between split tensile strength and flexural strength of RCC have been well-documented throughout this report as well as in the literature for conventional concrete (Brand et al. 2014).

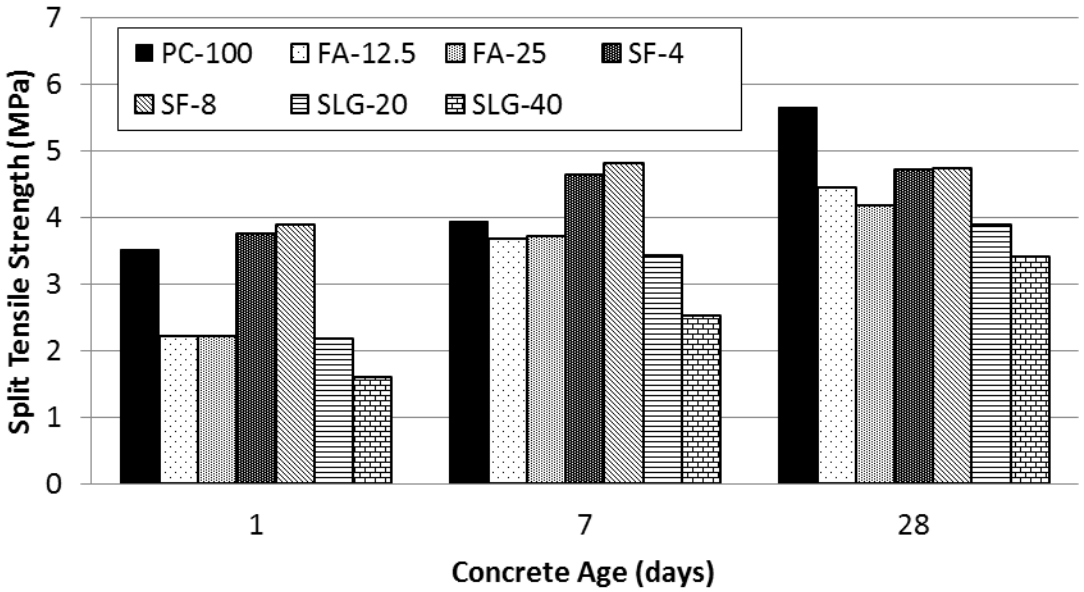

Figure J2. Average RCC Split Tensile Strength over Time. (1 ksi = 6.89 MPa)

Table J7. Statistical Analysis of RCC Split Tensile Strength Results (1 ksi = 6.89 MPa)

Mix ID	1-Day Split Tensile Strength (MPa)	Statistical Grouping(s)		
SF-8	3.90	A		
SF-4	3.76	A		
PC-100	3.51	A		
FA-25	2.23		B	
FA-12.5	2.23		B	
SLG-20	2.19		B	C
SLG-40	1.60			C
Mix ID	28-Day Split Tensile Strength (MPa)	Statistical Grouping(s)		
PC-100	5.65	A		
SF-8	4.75		B	
SF-4	4.72		B	
FA-12.5	4.46		B	
FA-25	4.18		B	C
SLG-20	3.90		B	C
SLG-40	3.42			C

Table J8. Statistical Analysis of RCC Flexural Strength Results (1 ksi = 6.89 MPa)

Mix ID	28-Day Flexural Strength (MPa)	Statistical Grouping(s)	
SF-8	7.78	A	
FA-12.5	7.40	A	B
SF-4	7.06	A	B
FA-25	6.88	A	B
SLG-20	6.56	A	B
PC-100	6.22		B
SLG-40	6.21		B

J.4 FRACTURE PROPERTIES

Fracture properties were determined at an age of 28 days using the disk-shaped compact tension (DCT) geometry according to Amirkhanian et al. (2016). Results of fracture testing are shown in Table J9. Fracture properties for the two silica fume mixes were not obtained. It can be seen that all of the mixes in Table J9 result in similar fracture properties at a testing age of 28 days. Akkaya et al. (2007) showed reduced critical stress intensity values (by approximately 25%) for mixes containing 20% fly ash when tested at young ages (less than 14 days). Fly ash undergoes a pozzolanic reaction which takes time to activate (Mindess et al. 2003) which explains why fly ash might have a negative impact at early ages (less than 14 days) but not much of an impact at 28 days. Fracture results in Table J9 show a smaller range than those found in Chapters 2 or Appendix F suggesting that aggregate gradation and type have a more significant effect on fracture properties than the SCMs and dosages considered here.

Table J9. Results of 28-Day Fracture Testing (COV, %) (1 MPa-$m^{1/2}$ = 0.910 ksi-$in^{1/2}$; 1 GPa = 145 ksi; 1 in = 25.4 mm; 1 lb/in = 175 N/m)

Mix ID	Critical Stress Intensity Factor, K_{IC} (MPa-$m^{1/2}$)	Elastic Modulus, E (GPa)	Critical Crack Tip Opening Displacement, $CTOD_C$ (mm)	Initial Fracture Energy, G_f (N/m)	Total Fracture Energy, G_F (N/m)
PC-100	1.38 (13.2)	38.7 (9.2)	0.0192 (21.9)	49.2 (17.5)	148.7 (8.1)
FA-12.5	1.43 (4.3)	35.5 (6.6)	0.0200 (14.8)	57.8 (11.8)	154.5 (11.9)
FA-25	1.42 (8.2)	39.1 (8.4)	0.0162 (10.7)	51.3 (10.2)	154.2 (7.3)
SF-4	N/A	N/A	N/A	N/A	N/A
SF-8	N/A	N/A	N/A	N/A	N/A
SLG-20	1.36 (4.2)	37.5 (4.4)	0.0164 (6.9)	49.8 (10.5)	145.7 (10.1)
SLG-40	1.23 (4.9)	33.2 (4.0)	0.0164 (12.8)	45.8 (9.8)	147.9 (2.9)

J.5 DRYING SHRINKAGE

Drying shrinkage measurements were conducted on triplicate specimens from each mix with drying beginning 24 hours after casting. The specimens were stored in a 50% relative humidity and 23 degrees Celsius environment beginning at 24 hours after casting. Average drying shrinkage strains for each mix are shown in Figure J3 as a function of time. It can be seen that the mixes with relatively high SCM dosages (FA-25, SLG-20, and SLG-40) had the lowest drying shrinkage strains after 28 days of drying. Kar et al. (2013) also found that dosages of 35% GGBFS and 25% fly ash resulted in lower drying shrinkage strains than a control concrete mixture with no SCMs. The two silica fume mixes (4 and 8%) resulted in drying shrinkage strains similar to mix PC-100 which was also found by Kar et al. (2013) for a 10% dosage of silica fume. The 12.5% fly ash mix (FA-12.5) resulted in slightly higher drying shrinkage strains relative to the rest of the mixes in Figure J3. In general, the use of silica fume did not have a significant effect on drying shrinkage while higher dosages of fly ash and GGBFS resulted in lower drying shrinkage strains relative to the control (PC-100) mix.

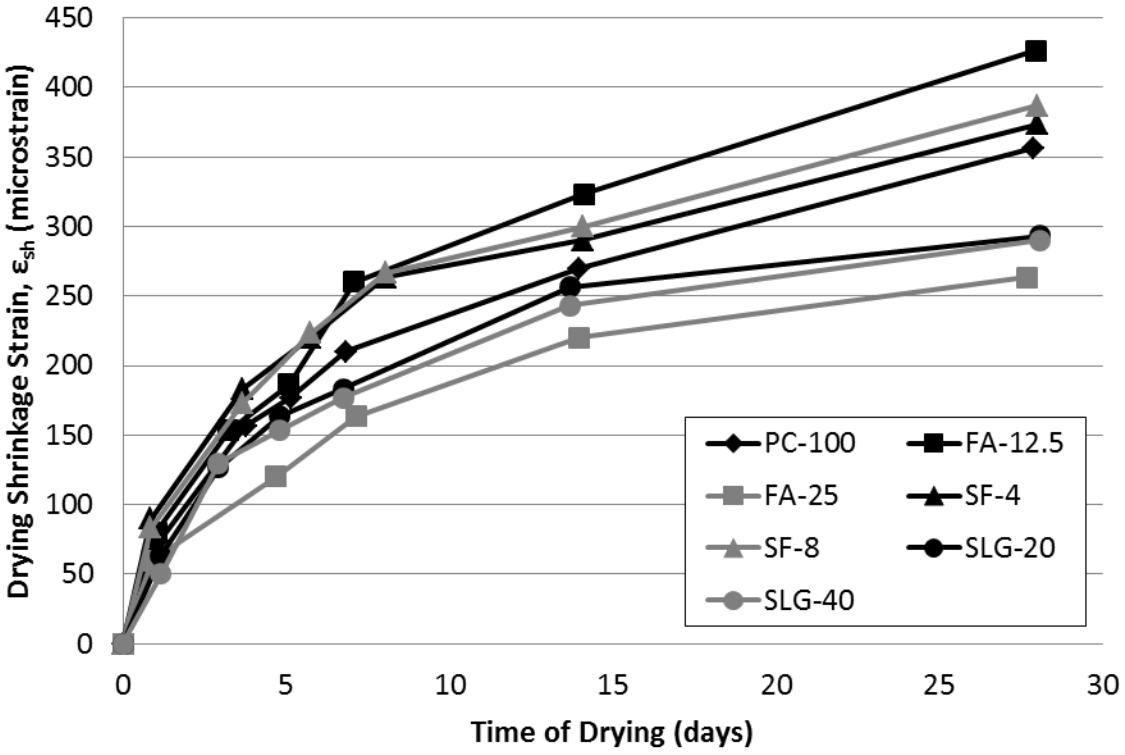

Figure J3. RCC Drying Shrinkage Strains with SCMs over Time.

J.6 CONCLUSIONS

A total of 7 mix designs were developed to investigate the effects of fly ash (class C), silica fume, and Grade-100 ground-granulated blast furnace slag (GGBFS) on RCC properties. Two dosages of each supplementary cementitious material (SCM) were used based on their maximum recommended dosages with one dosage being the maximum recommended and the second dosage being half of the maximum. None of the SCMs had a significant effect on compactability according to the Vebe test. The SCM type and age of the RCC specimen impacted the compressive strength of the mix relative to the control. Silica fume produced a similar or greater compressive strength relative to a control mix (100% Portland cement) at all ages while fly ash and GGBFS mixes had statistically lower strengths at early ages (1 day) but similar strengths at 28-days relative to a control mix. The silica fume mixes and control mix met the typical opening strength requirement (21 MPa, 3 ksi, compressive strength) at 1 day while all mixes met a 7-day requirement of 24 MPa (3.5 ksi) and 28-day specification of 31 MPa (4.5 ksi).

In general, all mixes had similar 28-day flexural strengths while all mixes with SCMs resulted in lower 28-day split tensile strengths relative to the RCC control. High dosages of fly ash (25%) and GGBFS (20% and 40%) resulted in reduced drying shrinkage strains whereas silica fume resulted in similar drying shrinkage strains relative to the control. In general, the three SCMs investigated had negligible or beneficial effects on RCC properties, especially at later ages (28 days and greater). The main drawback to using fly ash or GGBFS (especially at relatively high dosages) is the slower rate of strength gain at very early ages. Therefore fly ash or GGBFS might delay opening to traffic by a day or a few days and could cause strength gain issues if paving in colder temperatures. Long-term strengths of RCC incorporating fly ash or GGBFS are not expected to be an issue.

APPENDIX K: EARLY-AGE CREEP PROPERTIES OF ROLLER-COMPACTED CONCRETE

This chapter investigates the early-age (24 hours and 7 days) creep properties of a roller-compacted concrete (RCC) pavement mix. Compressive and tensile creep were measured at both curing ages. Drying and basic creep measurements were taken for each creep mode (compressive and tensile) as well as each curing duration (1 and 7 days). The free drying shrinkage and strength properties of the same RCC mix design were also measured.

K.1 MOTIVATION

Tensile creep mechanisms (Lange and Shin, 2001; Lee et al. 2011; Yeon et al. 2012) can significantly reduce stresses (by up to 60%) caused by environmental loading of concrete pavements, i.e., drying shrinkage, temperature curling, moisture curling, etc. Creep has been shown to significantly reduce corner deflections (by approximately 50%) and maximum principal stress at the center of the slab (by approximately 67%) resulting from moisture curling (Lee et al. 2011). Since RCC is typically opened to traffic earlier than conventional concrete pavements (in some cases RCC is opened to car traffic within hours of paving), the effects of creep at early ages might prove quite beneficial in reducing the overall stresses experienced by the pavement. If the tensile stresses are kept below the RCC's tensile strength, unplanned cracking is unlikely to occur. While creep is unlikely to reduce the stresses resulting from moving wheel loads, it can help reduce stresses because of environmental effects that are more sustained with respect to time. The effects of creep at early ages (i.e. within the first few days after construction) can help reduce the internal residual stresses at the time when the concrete pavement is still gaining tensile strength.

K.2 REVIEW OF PREVIOUS RESEARCH

The research on compressive creep of RCC for dams is scarce. Creep of RCC mixes for dams, which typically have low total cementitious contents but a higher supplementary cementitious material (SCM) replacement levels, has shown that RCC exhibits higher specific compressive creep than conventional concrete (Kogan, 1991). Compressive creep of RCC for dams was also studied by Xie et al. (2011) who found lower values of specific creep than Kogan (1991). There was no research found on the creep of RCC for pavement applications. Literature of creep of conventional concrete (i.e. PCC) is rather abundant.

Traditionally creep of concrete is measured by two methods: basic creep and total creep. Basic creep is measured on specimens that are sealed (typically with aluminum tape) while total creep is measured on specimens that are left exposed to the environmental conditions present during testing. There are many factors that affect the magnitude of creep (Figure K1) which makes comparing one creep study to another difficult since it is rare that researchers use the same environmental conditions, loading configurations and stress levels, time of loading and loading duration, etc. The age of concrete at the time of initial loading is one of the most significant factors affecting creep (Figure K2) as shown by Atrushi (2003). Creep is relatively high at early ages (Figure K2) which is beneficial for

concrete pavements since this is when the concrete strength is the weakest and is also when the pavement is being exposed to relatively high tensile stresses from drying shrinkage, temperature differentials (both along the pavement length and through the depth), moisture curling, and possibly autogeneous shrinkage and/or mechanical loading. Therefore, early age creep of RCC was investigated for its relevance to pavements; specifically the ability of a pavement to relax stresses through creep at early ages after casting.

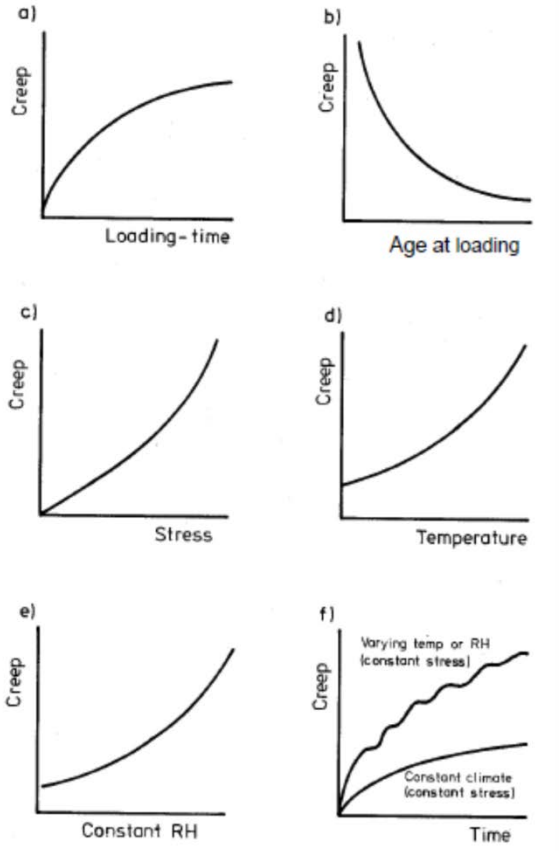

Figure K1. General Factors Affecting Concrete Creep (Atrushi, 2003).

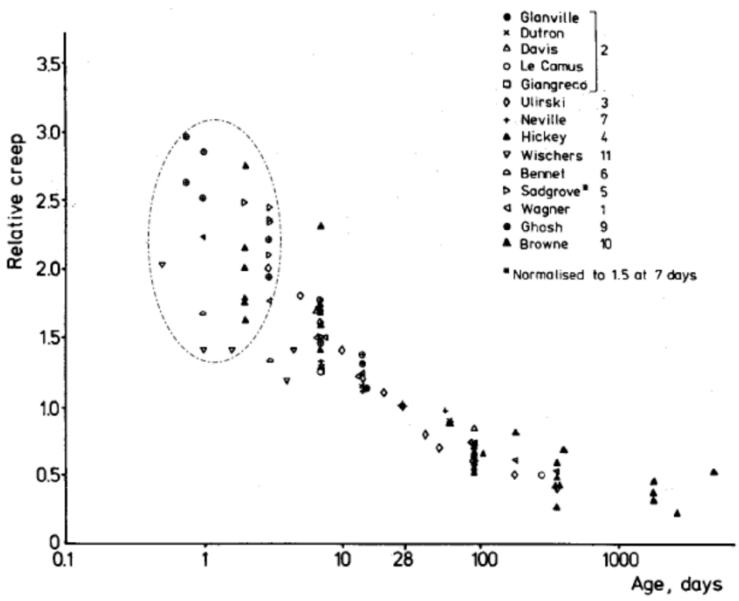

Figure K2. Effect of Age at Loading on Creep (Atrushi, 2003). Relative creep is the ratio of creep at a particular age to creep at 28 days.

K.3 RCC MIXTURE DESIGN

A typical RCC mix design for pavements was utilized for this creep study. The mix design consisted of 281.7 kg/m^3 (475 lb/yd^3) of cementitious materials with a 12.5% cement replacement (by weight) with class C fly ash . The gradation was chosen by combining three aggregates (coarse and intermediate dolomite as well as natural sand) such that their combined gradation followed the 0.45-power curve (i.e. maximum density curve) as closely as possible while also remaining within the recommended gradation limits by ACPA (2014). The gradation is shown in Table K1. Modified Proctor testing was performed to determine the maximum dry density (MDD) and optimum moisture content (OMC) which are required to determine the final mix proportions. Results of the modified Proctor testing as well as the final mix proportions are shown in Table K2.

Table K1. Combined Aggregate Gradation (1 in = 25.4mm)

Sieve Size (mm)	% Passing
19.0	100
12.7	77.4
9.51	73.1
4.76	50.0
2.38	38.2
1.19	35.8
0.595	24.5
0.30	2.9
0.15	0.2
0.075	0.0

Table K2. Modified Proctor Results and Final Mix Proportions (1 kg/m^3 = 1.686 lb/yd^3)

Maximum Dry Density (kg/m^3)	2391
Optimum Moisture Content (%)	6.59
Cement, Type I/II (kg/m^3)	246.5
Class C Fly Ash (kg/m^3)	35.2
Combined Aggregate, oven-dry (kg/m^3)	2109.0
Water (kg/m^3)	157.5

K.4 CREEP TESTING METHODOLOGY

Compressive creep testing was conducted according to ASTM C512 (2015) on 100x200 mm (4x8 in) cylinders with 2 replicates for each testing age and specimen configuration. Two replicates were sealed with aluminum tape to prevent moisture loss while two replicates were left unsealed and exposed to drying. The sealed specimens were used to determine basic creep and the unsealed specimens were used to determine total creep. The testing ages were 24 hours after casting (0 days of moist curing) and 7 days after casting, i.e., 6 days of moist curing. Compressive creep specimens

were loaded to 40% of their compressive strength at the time of loading as determined by companion specimens. Due to the method of RCC cylinder compaction, the use of internal strain gauges is not possible. Therefore, surface mounted strain gauges of 90 mm (3.5 in) length (Tokyo Sokki Kenkyujo PL-90-11-1L) were used. Triplicate strain gauges were attached longitudinally to each cylinder with the strain gauges being located 120 degrees apart from each other. The strain gauges were attached to the cylinders with a thin film of epoxy. For the specimens that were sealed with aluminum tape, a thin membrane was placed over the strain gauge so that the aluminum tape would not provide any restraint. Figure K3 shows a strain gauge mounted on a compressive creep cylinder.

In order to facilitate rapid commencement of data acquisition upon bringing the creep specimens into the environmentally-controlled room, an Ethernet patch panel configuration was employed. Due to the early ages at which these specimens were being loaded (some just 24 hours after casting) along with the multitude of strain gauges, it was essential that the specimens could be loaded as soon as possible upon introducing them to the drying environment. Therefore, each strain gauge was soldered to one end of Ethernet cable with the other end being terminated with an Ethernet connector. The cable connected to a patch panel that in turn was permanently connected to the data acquisition system. This allowed the strain gauges to be directly connected to an Ethernet patch panel instantaneously rather than installing three wires per strain gauge, into a screw terminal after exposing the specimens to the drying environment. The second process (use of the screw terminal as opposed to an Ethernet patch panel) would have taken hours and valuable data about initial moisture loss and resulting creep effects would have been lost. Figure K4 shows the setup of all creep specimens along with the Ethernet cords (from the strain gauges) leading to the patch panels which are connected to a data acquisition system. The setup of the patch panels is shown in Figure K5 and the connection of the patch panels to the DAQ (via screw terminal boxes) is shown in Figure K6.

Similar to compressive creep specimens, the tensile creep specimens had 3 external strain gauges each located 120 degrees apart from each other. Previous research in this area utilized screws that were embedded into tensile creep specimens during concrete casting and after demolding, these screws were attached to a plate to which the load is applied (Amirkhanian 2016). This setup is not possible in RCC because of the method of compaction. Therefore, a new technique for applying tensile creep load was devised. Steel pipe end caps with a diameter slightly greater than 100 mm (4 in) were used to transmit load to the tensile specimens. Two holes were drilled into the top of the end caps through which a steel cable was threaded. This cable would later be attached to the tensile creep frame and would apply load to the steel caps which would then transmit the load to the cylinder. The steel caps were affixed to the cylinder ends by means of a high-strength anchoring epoxy that is typically used for embedding steel reinforcement (dowel bars, tie bars, etc.) into concrete. It was crucial that the epoxy have a rapid final cure time because of the early-age of the specimens at loading. The epoxy used had a cure time of 4 hours which was sufficient. It was also important that the strain gauges be located between the extent of the steel caps to avoid being restrained by the steel end caps and/or the epoxy and also to prevent measurement of any creep because of the epoxy. By ensuring that the strain gauges were located within the extent of the steel end caps, all strains measured were solely due to length change of the concrete. Figure K7 shows an example of a prepared tensile creep specimen.

Two replicates were sealed with aluminum foil and two replicates were left exposed per testing age for tensile creep testing. Tensile creep specimens were tested at the same ages as compressive creep specimens (after 0 and 6 days of moist curing). Unlike compressive creep, there is no standardized procedure or loading regime for tensile creep. Therefore, a cantilevered dead load frame was used to apply uniaxial tensile loads to the specimens with loads corresponding to 10% of the split tensile strength at the time of loading as determined by companion specimens (D'Ambrosia, 2011; Lee et al. 2011; Amirkhanian 2016). All creep specimens were kept in an environmentally controlled room at 50% relative humidity (RH) and 23°C (73.4°F). Strain measurements were recorded approximately twice per minute for 28 days after commencement of loading. The arrangement of all creep specimens and their corresponding load frames is shown in Figure K4. The compressive and tensile creep test setup schematics are shown in Figure K8 and Figure K9, respectively (Lee et al. 2011).

Figure K3. Attachment of Strain Gauge to Compressive Creep Cylinder.

Figure K4. Compressive and Tensile Creep Testing Setup in Environmentally-Controlled Room.

Figure K5. Patch Panels for Ethernet Connection.

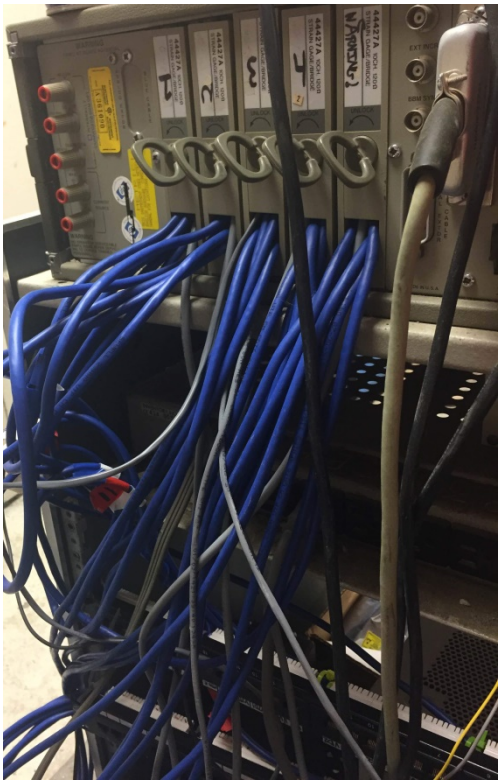

Figure K6. Connection of Patch Panels to DAQ Screw Terminals.

Figure K7. Tensile Creep Specimen Loaded in Cantilevered Dead Load Frame.

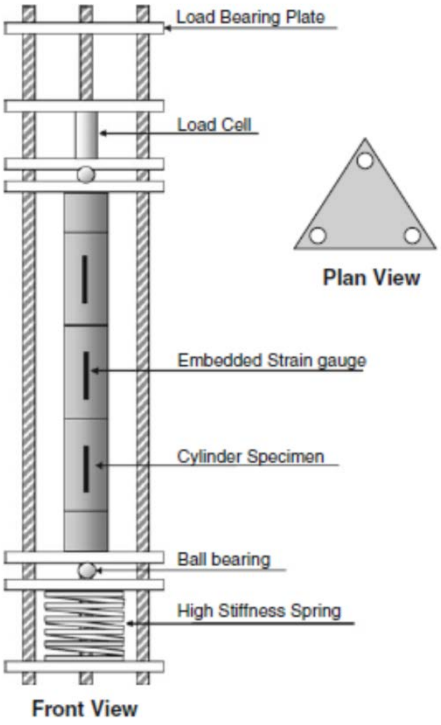

Figure K8. Schematic of Compressive Creep Frame (Lee et al. 2011).

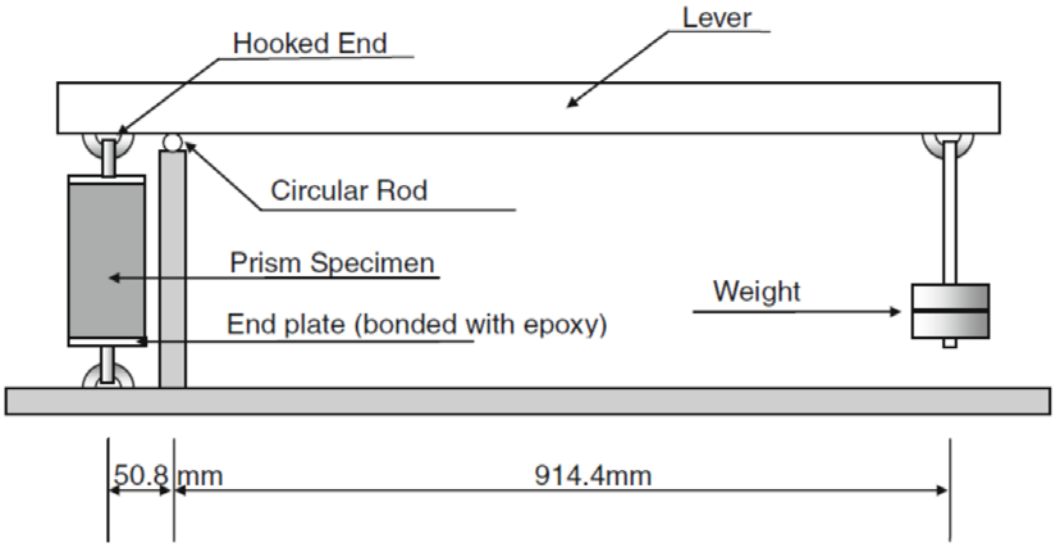

Figure K9. Schematic of Tensile Creep Frame (Lee et al. 2011).

K.5 DRYING AND SEALED SHRINKAGE

In order to analyze the creep data, drying shrinkage measurements were required. A total of 12 companion shrinkage prisms were made using the procedure described in Chapter 2. Six of the prisms were moist cured for 6 days upon demolding and the other six were exposed to drying 24 hours after casting. For each set of 6 shrinkage prisms, 3 were sealed with aluminum foil to prevent moisture loss and 3 were left exposed in order to promote drying (Figure K10). The resulting shrinkage strains are shown in Figure K11 with each curve being an average of three shrinkage specimens. The specimens that were moist cured for 6 days had lower values of shrinkage, both drying and sealed, than the specimens that did not receive any moist curing. The specimens that were sealed experienced some initial expansion (i.e. negative shrinkage strains) at early ages. Jingfu et al. (2009) also showed slight expansion of RCC shrinkage specimens at early ages. The mechanism for expansion at early ages can be explained by the continued hydration of cement (hydration products are greater in volume than their initial components) since the specimens are sealed and not exposed to drying. Therefore, sufficient water is available to continue the hydration process. After a few days, the hydration process slows down rapidly as it has consumed most of the available water in the RCC.

Figure K10. Sealed (left) and Drying (right) RCC Shrinkage Specimens.

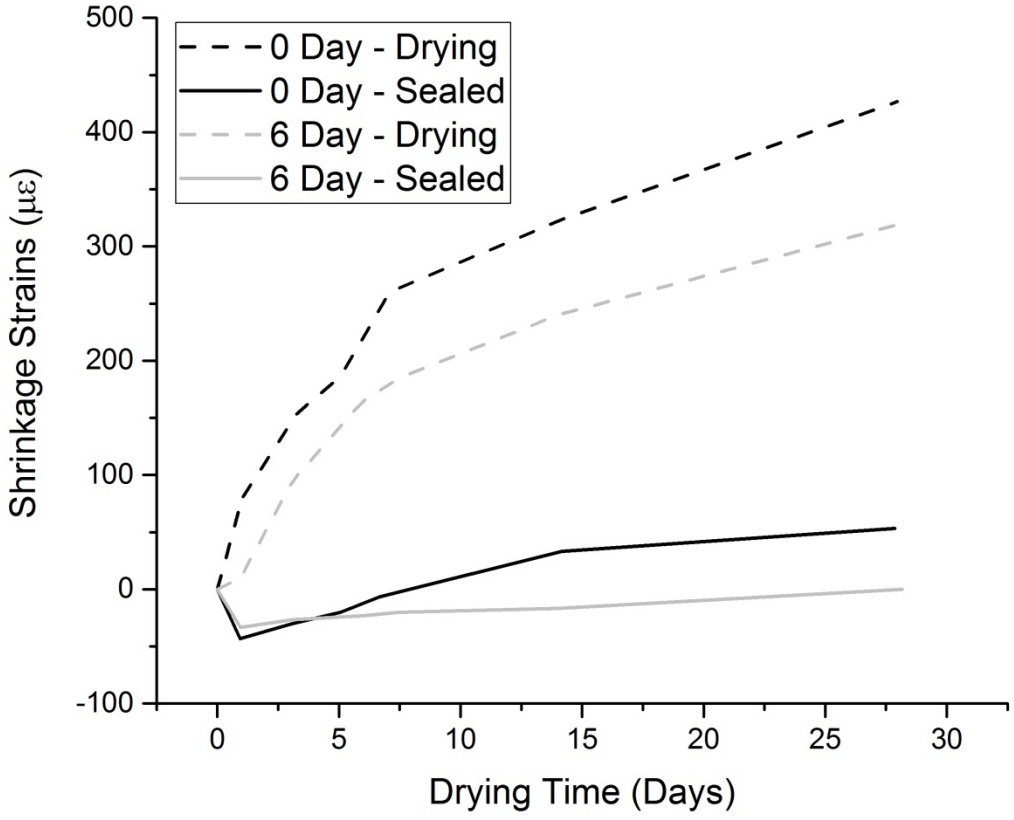

Figure K11. Shrinkage Strains of RCC Companion Specimens.

K.6 MECHANICAL PROPERTIES

The compressive and split tensile strengths of the RCC mix were measured in order to determine the proper loads to apply for creep testing. Strength testing was performed on 100x200 mm (4x8 in) cylinders at ages of 1, 3, 7, 28, and 120 days with triplicate specimens at each age for compression (ASTM C39, 2012) and split tension (ASTM C496, 2011). Results of strength testing are shown in Table K3. A hyperbolic model fit was applied to the strength data to determine a relationship between strength and time. Equations K1 and K2 are the resultant equations for predicting compressive strength (σ_c, MPa) and split tensile strength (σ_{sp}, MPa) as a function of time (t, days) for this RCC mixture design.

Table K3. Compressive and Split Tensile Strengths (COV, %); (1 ksi = 6.89 MPa)

Age, days	Compressive Strength, MPa	Split Tensile Strength, MPa
1	18.5 (4.3)	2.23 (1.8)
3	27.6 (0.6)	2.89 (5.2)
7	38.0 (0.6)	3.70 (5.9)
28	51.0 (6.5)	4.46 (7.1)
120	59.6 (0.7)	5.41 (7.7)

$$\sigma_c = \frac{58.6t}{3.17 + t} \quad \text{(Eq. K1)}$$

$$\sigma_{sp} = \frac{5.04t}{1.86 + t} \quad \text{(Eq. K2)}$$

K.7 RCC EARLY-AGE CREEP RESULTS

The measured creep strains for compressive and tensile creep are shown in Figure K12 where each curve represents the average of two cylindrical specimens with each cylinder being the average of 3 strain gauge readings. In general, creep specimens exposed to drying yielded higher strains than basic creep (sealed) specimens as expected. The 0-day total compressive creep specimen exhibited a decrease in strain after the instantaneous, elastic strain from load application. This decay of strain was not expected for a fixed load. It was hypothesized that the relatively high stress-strength ratio (40%) along with the young age of the concrete (24 hours after casting) and the introduction to a rapid-drying environment induced surface microcracking and/or localized cracking that interfered with the strain measurement. Because the total compressive creep was not as expected at 0-day, it will not be considered in further analysis.

While the compressive creep specimens exhibit a large initial strain upon loading, this is not evident in the tensile specimens (Figure K12) and is likely a result of the relatively low stress-strength ratio (10%) used for tensile creep setup. The relationship between stress-strength ratio and loading age is shown in Figure K13. It can clearly be seen that although all specimens were initially loaded to a stress-strength ratio of 40% (compressive) or 10% (tensile), this ratio decreases rapidly for specimens that did not receive any moist curing (0-day specimens). The specimens moist cured for 6 days also showed decreasing stress-strength ratios with loading time but they were not as significant as the 0-day specimens which was still hydrating and aging.

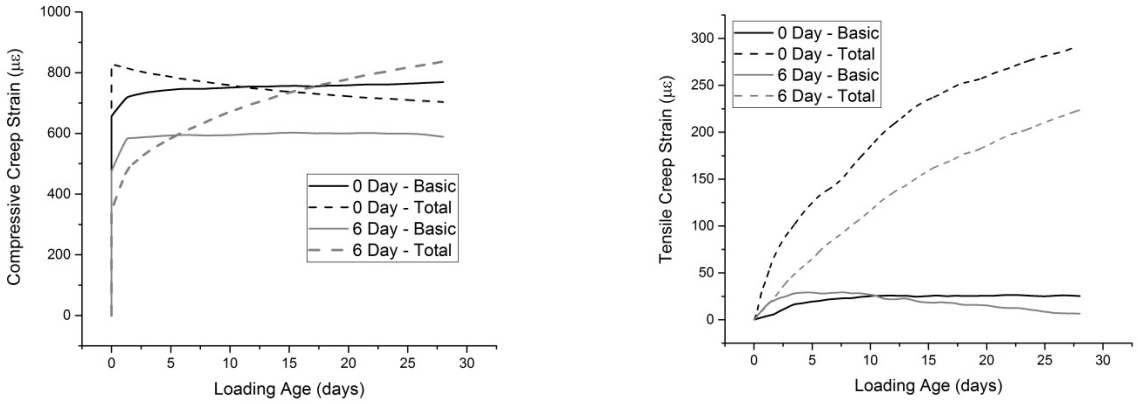

Figure K12. Total and Basic Compressive and Tensile Creep Strains for RCC.

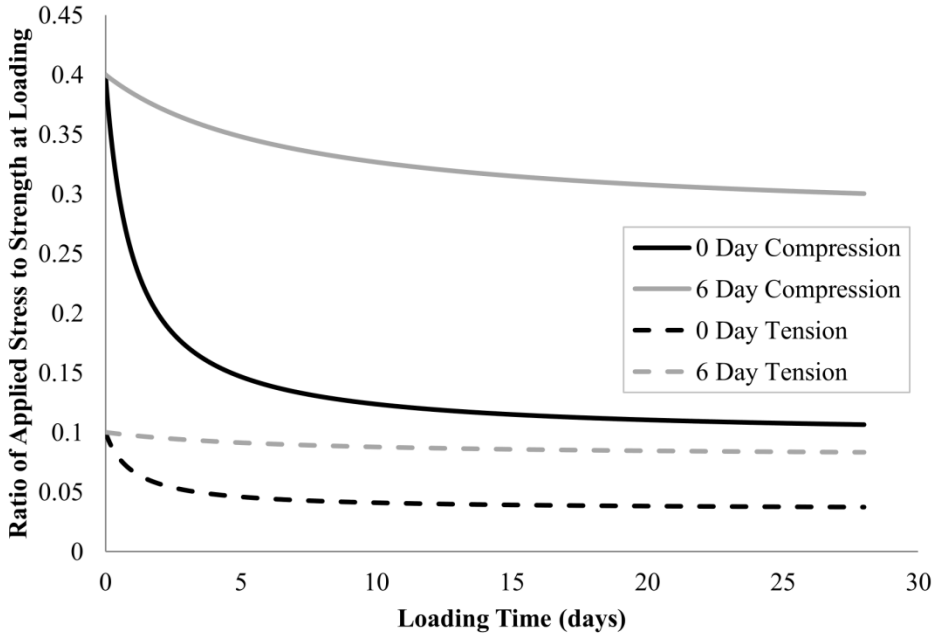

Figure K13. Stress - Strength Ratio as a Function of Loading Time.

The specific creep, $J(t)$, with units of (με/MPa) was calculated knowing the creep strains (με), $\epsilon_{creep}(t)$, and the constant applied stress, $\sigma_{applied}$ (MPa) from Equation K3. The specific creep data (shown in Figure K14) was also fitted using the three-parameter solid model (Amirkhanian, 2016) shown in Equation K4 as a function of time (t). The initial compliance is quantified by J_0 while the time dependent compliance is quantified by the J_1 and τ terms. The MATLAB code used to perform

the model fitting is shown in Appendix B. Model fitting parameters for the three parameter solid model are shown in Table K4. In order to capture the goodness of fit for the models, the residual sum of squares (SSE_{res}) was calculated from Equation K5. The model fits for compressive and tensile specific creep data are shown in Figure K15 and Figure K16, respectively. The three-parameter solid model for specific creep fits the compressive specific creep data well (Figure K15), with the exception of the 0-day total compressive creep specimens which likely had errors with strain/load measurement. Only the 0-day basic tensile specific creep showed a good model fit (Figure K16).

$$J_{experimental}(t) = \frac{\epsilon_{creep}(t)}{\sigma_{applied}} \quad \text{(Eq. K3)}$$

$$J_{model}(t) = J_0 + J_1\left(1 - exp^{-t/\tau}\right) \quad \text{(Eq. K4)}$$

$$SSE_{res} = \sum\left(J_{experimental}(t) - J_{model}(t)\right)^2 \quad \text{(Eq. K5)}$$

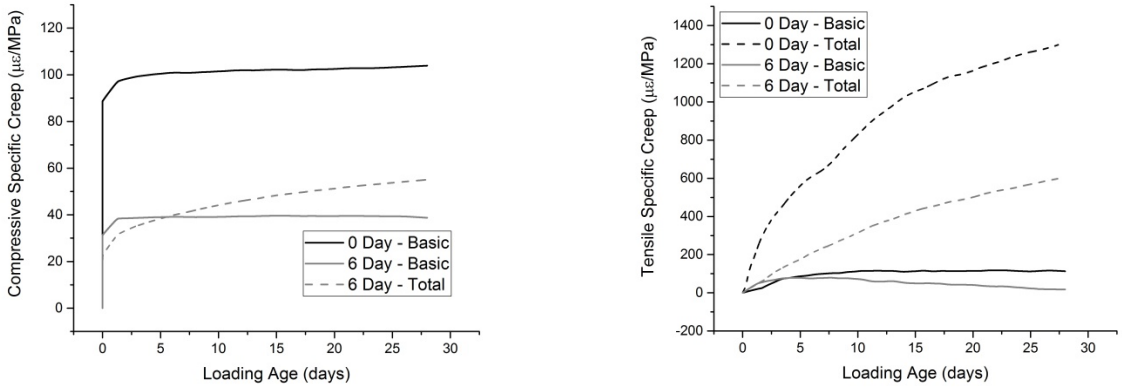

Figure K14. Specific Creep.

Table K4. Specific Creep Model Fit Parameters* (1 ksi = 6.89 MPa)

	J_0 (με/MPa)	J_1 (με/MPa)	τ (days)	Residual Sum of Squares
0 Day - Compressive - Basic	79.3	22.1	0.09	3.4×10^5
0 Day - Tensile - Basic	-14.3	130.3	3.42	5.9×10^5
0 Day - Tensile – Total**	n/a	n/a	n/a	2.4×10^{10}
6 Day - Compressive - Basic	30.7	8.7	0.82	4.5×10^3
6 Day - Compressive - Total	27.7	29.4	11.94	3.6×10^4
6 Day - Tensile – Total**	n/a	n/a	n/a	1.0×10^9

*No model fit parameters are shown for the 0 Day - Compressive - Total or 6 Day - Tensile – Basic conditions since their specific creep values decrease as a function of time after some period of time (chosen model form incapable of modeling this phenomenon).

**Poor model fit obtained (shown by residual sum of squares), therefore model fit parameters not shown.

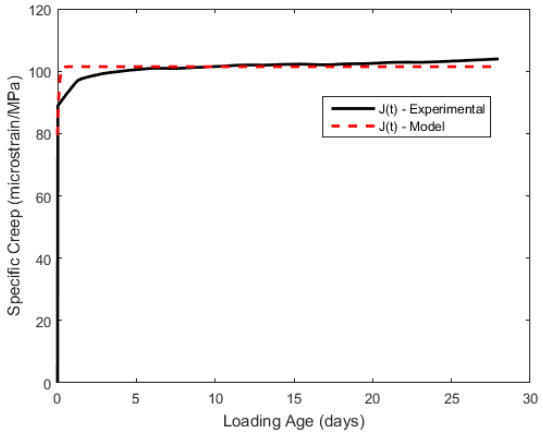

0-Day Basic

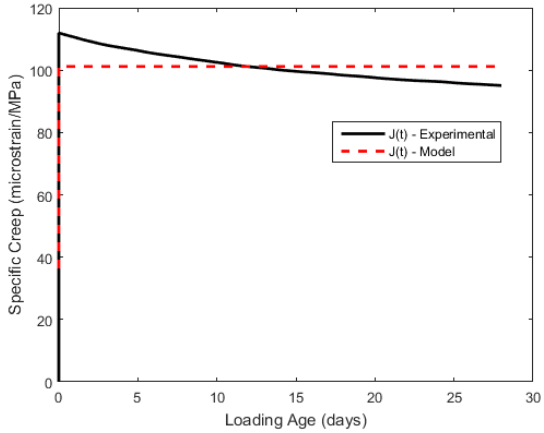

0-Day Total

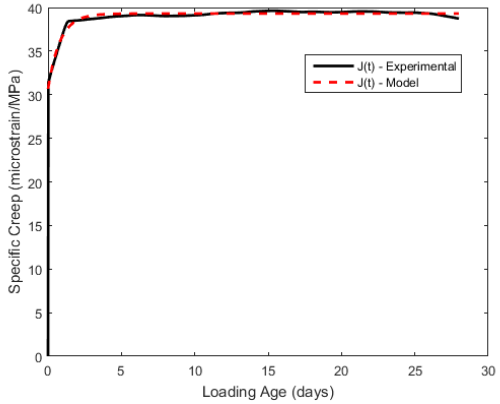

6-Day Basic

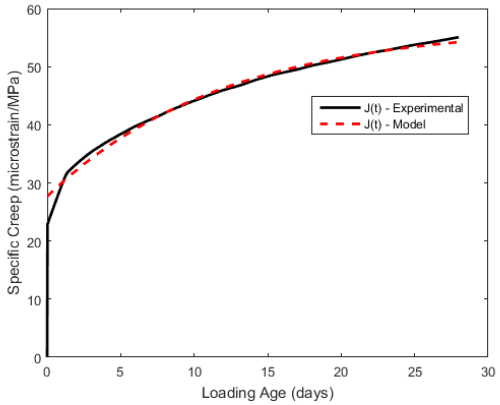

6-Day Total

Figure K15. Compressive Specific Creep Model Fits. (1 ksi = 6.89 MPa)

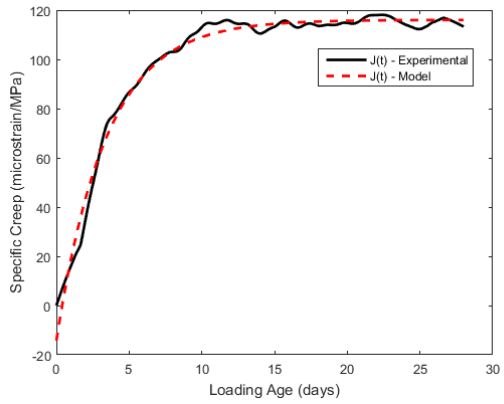

0-Day Basic

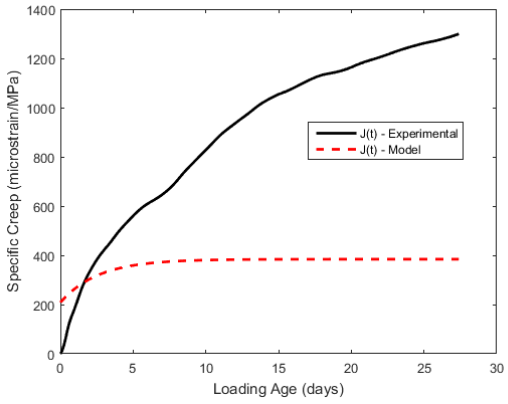

0-Day Total

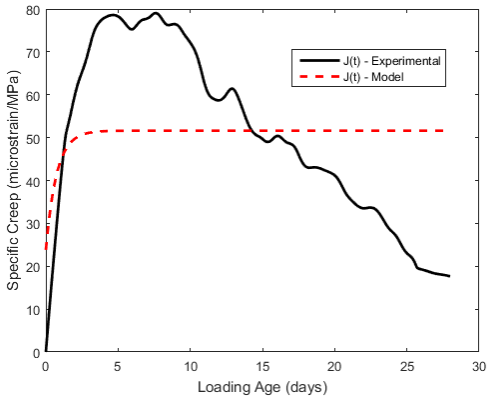

6-Day Basic

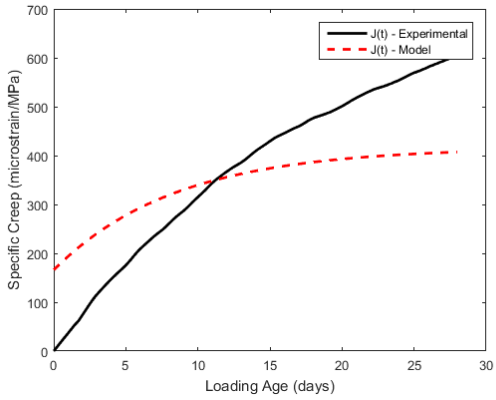

6-Day Total

Figure K16. Tensile Specific Creep Model Fits. (1 ksi = 6.89 MPa)

Compared to Amirkhanian (2016), who tested basic and total creep of tensile and compressive conventional concrete specimens after 0 and 6 days of moist curing, RCC exhibits lower compressive and tensile specific creep. Brooks and Johari (2001) measured compressive creep (basic and total) at 20% of the compressive strength for conventional concrete after 28 days moist curing with the resulting specific creep being approximately 16.5 με/MPa and 11.9 με/MPa for the total and basic conditions after 28 days of loading. These specific creep values do not account for the initial, elastic strain observed upon loading. If the initial, elastic strains are removed from the compressive creep measurements shown in Figure K12 then it can be seen that RCC basic compressive specific creep, at a higher stress-strength ratio and at much earlier ages, is lower than that found by Brooks and Johari (2001). Rossi et al. (2012) performed basic tensile and compressive creep measurements on concrete at a stress-strength ratio of 50% and 64 days curing with the basic tensile and compressive specific

creep values being lower than those shown in Figure 67. Østergaard et al. (2001) performed early-age basic tensile creep measurements (Figure K17) on large, dog-bone shaped specimens at stress ratios of 0.2-0.45 and found results similar to those shown in Figure K14.

Brooks and Neville (1977) tested compressive and tensile creep (basic and total) at an approximate stress ratio of 0.25 after 28 days curing (results shown in Figure K18) with the compressive specific creeps (basic and total) being greater than those in Figure K14. The total tensile specific creeps measured by Brooks and Neville (1977) were significantly less than those found for RCC (Figure K14) however the basic tensile specific creeps were relatively similar. Bissonnette and Pigeon (1995) measured total tensile creep of conventional concrete at ages of 1 and 7 days (Figure 72) and found significantly lower specific creep values than those in Figure K14. Table K5 provides a summary of RCC creep results with respect to the literature and it is apparent that there is not much agreement in terms of the relationship between RCC creep and creep of conventional concrete for the above studies. However, all studies that measured total compressive specific creep reported higher values than found for RCC. It is generally accepted that creep of concrete occurs in the paste fraction and is exacerbated under drying conditions (Acker and Ulm, 2001), therefore, it is of no surprise that RCC exhibits less total compressive creep since RCC contains less paste and less water than conventional concrete.

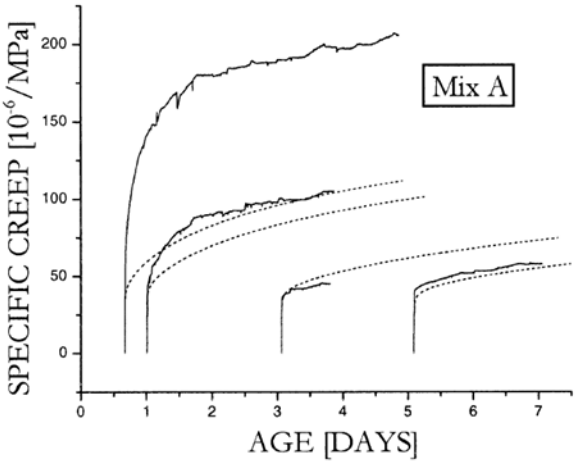

Figure K17. Basic Tensile Specific Creep from Østergaard et al. (2001).

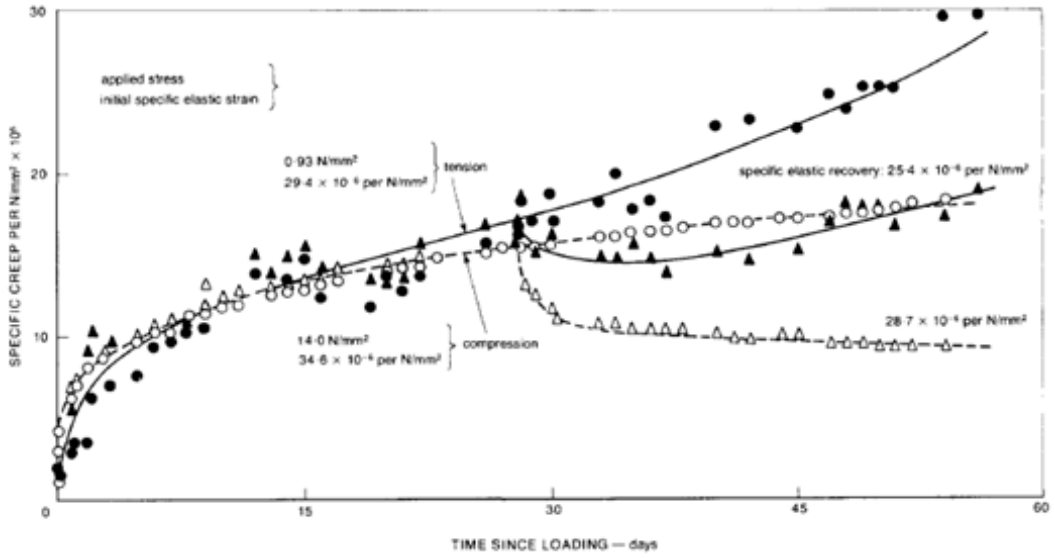

(a)

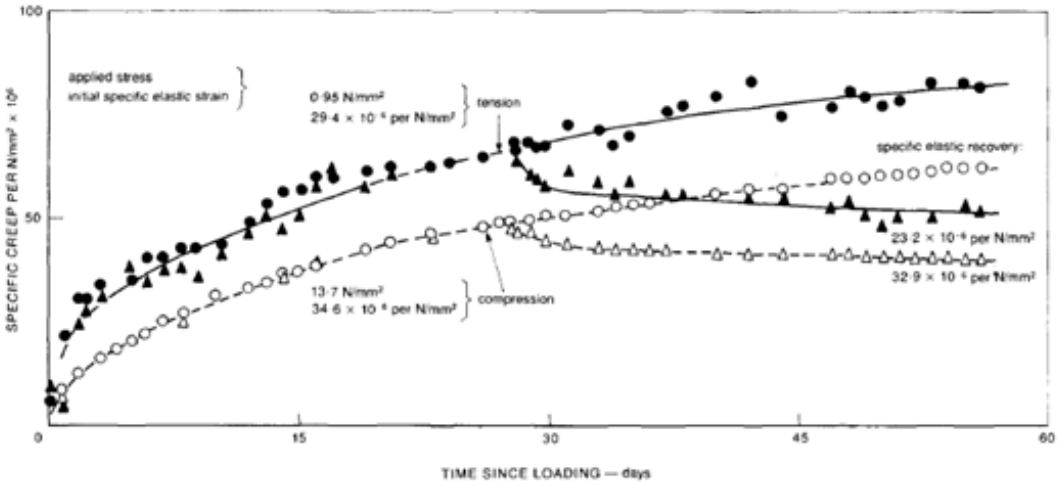

(b)

Figure K18. Basic (a) and Total (b) Specific Creep in Tension and Compression from Brooks and Neville (1977).

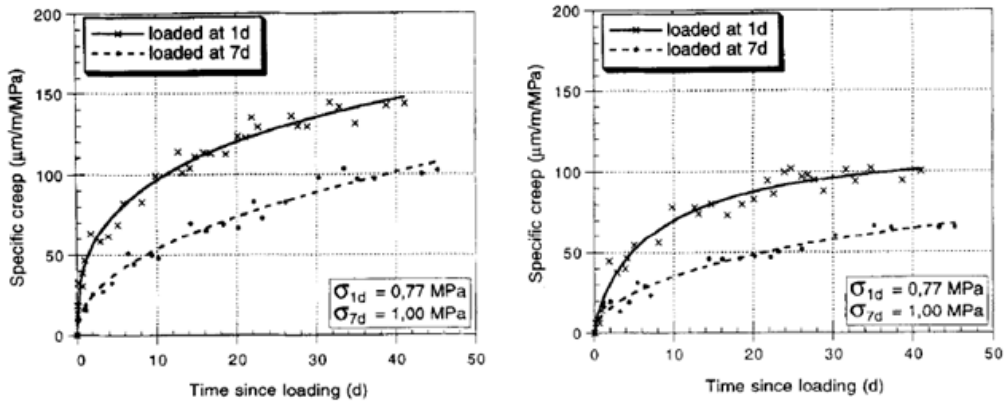

Figure K19. Total Tensile Specific Creep of Two Mixtures from Bissonnette and Pigeon (1995).

Three studies on creep of conventional concrete in compression and tension were found in the literature (Atrushi, 2003; Ji et al. 2013; Ranaivomanana et al. 2013) that had similar testing conditions to those used in this study. Atrushi (2003) measured basic tensile and compressive creep at early ages for a range of environmental conditions, stress/strength ratios, and loading ages. A direct comparison between basic compressive creep of RCC determined in this study and basic compressive creep measured by Atrushi (2003) was possible since all testing parameters were equivalent (i.e. loading ages, 0.4 stress/strength ratio, and relative humidity/temperature). RCC basic compressive creep was similar that found by Atrushi (2003) as shown in Figure K20. The stress/strength ratio used for tensile creep by Atrushi (2003) was much higher than the 0.1 stress/strength ratio used for RCC tensile creep, however, Atrushi (2003) showed similar specific creep in tension relative to that found for RCC in this study (Figure K20).

When comparing results of RCC creep testing presented here with results of conventional concrete early-age basic creep testing (Ji et al. 2013) with relatively high mineral admixture dosages (at least 25%), RCC exhibits relatively similar basic compressive and tensile specific creep values. Comparison with data from Ranaivomanana et al. (2013), who moist-cured specimens for 28 days before loading, also shows that RCC exhibits similar basic compressive creep. Ranaivomanana et al. (2013) loaded tensile specimens at 30, 40, and 50% of their tensile strength and still found lower basic tensile creep than RCC. The shape of the basic tensile creep curves from Ranaivomanana et al. (2013), i.e. increasing specific creep until a maximum and then continuous decrease in specific creep with time, is similar to the basic tensile creep curves observed for RCC (Figure K14). For the three studies discussed in this section which had similar environmental and loading conditions to this study it can be seen that there is better agreement on the relationship between basic creep of RCC and conventional concrete (Table K5). It was found that RCC exhibits similar basic compressive specific creep and similar or greater basic tensile specific creep relative to conventional concrete.

Table K5. Comparison of RCC Specific Creep Results with Literature*

Researcher(s)	Type of Creep Measured	Specific Creep Values Relative to RCC
Amirkhanian (2016)	Basic and Total (tensile and compressive)	Greater
Brooks and Johari	Basic and Total (compressive)	Greater
Rossi et al. (2012)	Basic (compressive and tensile)	Less
Østergaard et al. (2001)	Basic tensile	Similar
Brooks and Neville (1977)	Basic and Total (compressive)	Greater
	Basic and Total (tensile)	Similar (basic) and Less (total)
Bissonnette and Pigeon (1995)	Total tensile	Less
Atrushi (2003)	**Basic (tensile and compressive)**	**Similar**
Ji et al. (2013)	**Basic (tensile and compressive)**	**Similar**
Ranaivomanana et al. (2013)	**Basic (tensile and compressive)**	**Similar (compressive) and Less (tensile)**

*Bold signifies similar testing and environmental conditions to this study.

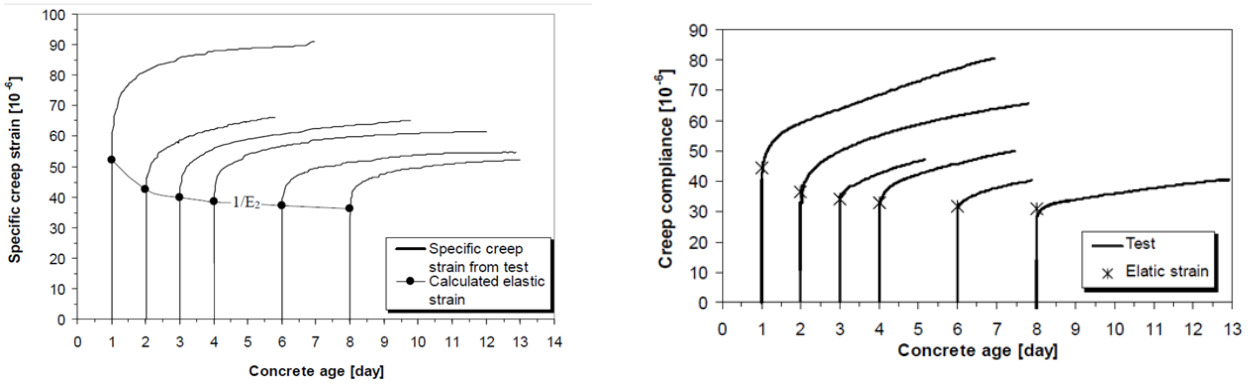

(a) **(b)**

Figure K20. Basic Compressive (a) and Tensile (b) Specific Creep of Early-age Concrete from Atrushi (2003).

Relative to previous RCC creep studies on dam mixes, basic compressive creep of 7-day old specimens was similar to that found in this study with the same applied stress ratio of 0.4 (Kogan, 1991). The other study on creep of RCC dams (Xie et al. 2011) measured compressive creep to be lower than that found in this study. However, the stress ratio used was not stated nor was it stated whether the compressive creep measured was total or basic creep.

K.8 CONCLUSIONS

Early-age creep properties of RCC were measured in order to quantify the potential for creep to relax early-age stresses in RCC pavements. Compressive and tensile creep were measured for two moist-curing durations (0 and 6 days) and two environmental conditions: specimens exposed to 50% relative humidity (total creep) and sealed specimens (basic creep). Compressive creep cylinders were loaded instantaneously to 40% of their compressive strength. Tensile creep cylinders were loaded using a cantilevered dead-load frame to 10% of their split tensile strength at commencement of loading. Strains were measured using three external strain gauges (per cylinder) with a 120 degree radial spacing. Creep strain measurements were accompanied by shrinkage strain measurements and strength testing.

Specific creep decreased as the moist-curing duration increased from 0 days to 6 days for all creep specimen combinations as expected. Tensile creep showed significant differences between sealed specimens and specimens exposed to drying whereas compressive creep for sealed and un-sealed specimens was relatively similar. With respect to conventional concrete (PCC) creep literature, there is strong agreement that total compressive creep of RCC is less than that of conventional concrete which is likely a result of the reduced paste content in RCC. For PCC creep literature that had similar environmental and loading conditions to this study, basic compressive specific creep of RCC and PCC were relatively similar while basic tensile specific creep of RCC was similar or greater than that of PCC. Basic compressive specific creep of RCC presented here was similar to a previous RCC dam creep study that employed similar loading conditions.

APPENDIX L: COMPARISON OF RCC LABORATORY COMPACTION METHODS

This chapter adapts and extends previous research on the use of the gyratory compactor for RCC and then compares compactability, density, strength, and fracture properties of RCC mix designs developed from the following three compaction methods: modified Proctor test procedure, modified Vebe table, and gyratory compactor. Density and strength properties were compared between specimens compacted with the modified Vebe table, gyratory compactor, and vibratory hammer while fracture properties were compared between the gyratory compactor and the vibratory hammer.

L.1 INTRODUCTION

Current RCC mix design procedures either employ the modified Proctor test (pavement applications) or the Vebe test (dam applications). The modified Proctor test is a well understood and most commonly run test but is very labor intensive and subject to operator error which may influence the selected maximum dry density (MDD) and optimum moisture content (OMC). The Vebe test is a subjective approach to quantifying the compactibility (i.e. workability) of an RCC mix. The Vebe test is used for RCC dam mix design, i.e., to determine mix proportions for a specified Vebe time, whereas for RCC pavement mixes the Vebe test is only used to measure compactibility. For RCC pavements, the modified Proctor test is conducted in order to determine the OMC and MDD of an RCC mix. The modified Proctor test compacts specimens through a vertical impact energy, which is significantly different than how RCC pavements are compacted [combination of vertical pressure, vibratory forces, and kneading (shear) at the surface]. In order to enhance the RCC pavement mix design process to better replicate field conditions, systematically adjust mix design parameters, and be more repeatable, the gyratory compactor was explored as an alternative.

There has been limited research on the use of the gyratory compactor with respect to RCC mix design, but extensive research and practical applications of the gyratory compactor for asphalt materials have been completed over the past 25 years. In addition to the use of the gyratory compactor for pavement materials, there has been limited research on using the gyratory compactor for geo-materials, i.e., aggregate base courses, clay, sands, etc. Previous research on applicability of the gyratory compactor to RCC mix design has focused on comparing gyratory densities to modified Proctor testing (Amer et al. 2004; Williams 2013), comparing gyratory densities to field cores (Amer et al. 2003), or effects of other mix design parameters on gyratory compaction and mechanical properties of resultant specimens (Delatte and Storey, 2005; Käppi and Nordenswan, 2007; Hazaree 2010; Khayat and Libre, 2014).

Amer et al. (2004) showed that gyratory compactor specimens had higher densities (3-5%) than specimens compacted via the modified Proctor test. However, the modified Proctor specimens were only compacted at one moisture content and it was not known if this was the optimum moisture content. Williams (2013) compacted specimens using the gyratory compactor and modified Proctor procedures while varying aggregate gradation, aggregate type, and moisture content. By varying

moisture content, moisture-density relationships were generated for each mix and from both compaction methods. Due to paste leakage from the gyratory compactor molds, the typical parabolic relationship between density and moisture content that is produced from modified Proctor testing was not seen for the gyratory compactor specimens. Rather, the moisture-density relationship of the gyratory specimens became asymptotic at a moisture content that typically coincided with the optimum moisture content from the modified Proctor testing (Figure L1). Williams (2013) defined the maximum dry density of gyratory specimens as the dry density of the specimen that achieved the highest density. Using this definition of maximum dry density from the gyratory compactor, Williams (2013) found that all mix designs yielded greater maximum dry densities when compacted with the gyratory compactor compared to the modified Proctor procedure.

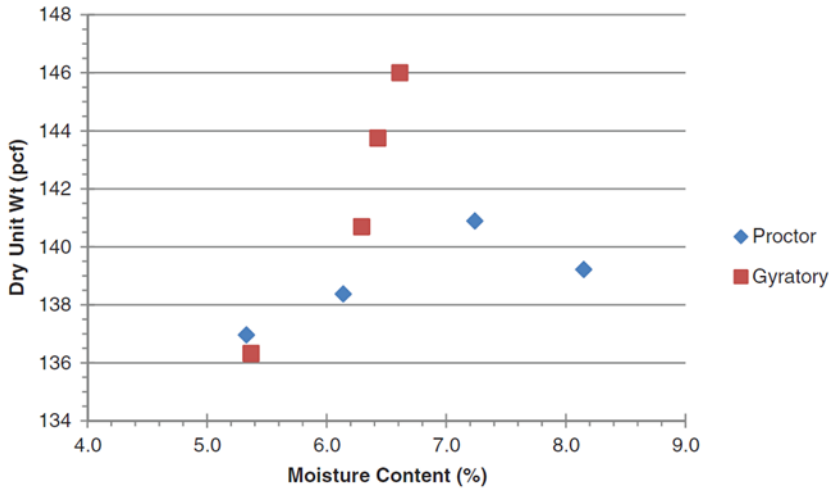

Figure L1. Comparison of Moisture-Density Relationships from Gyratory and Modified Proctor Compaction Methods (Williams 2013). (1 lb/ft^3 = 16 kg/m^3)

Amer et al. (2003) performed a comparison study between gyratory compaction and field compaction from two RCC pavement projects. Using the same mix designs as the field projects, companion RCC specimens were fabricated using the gyratory compactor and tested for density and strength (compressive and split tensile). Gyratory specimens were compacted using 50-100 gyrations. The density of the gyratory specimens and field cores agreed well. The gyratory specimens had densities that were 1.3% higher than the densities obtained in the field. The differences in compressive strength between the field and gyratory compaction methods for the two projects were less than 5% while the differences in split tensile strength were less than 2%. For the two project sites and their respective mix designs, Amer et al. (2003) found that gyratory specimens compacted to between 50-60 gyrations provided the best agreement with field properties.

The gyratory compactor has also been used to fabricate RCC specimens for testing of mechanical and durability properties as well as determining optimum aggregate blends. Delatte and Storey (2005)

used the gyratory compactor to produce RCC specimens (pavement and dam mixes) for freeze-thaw testing. One of the variables in the study was the number of gyrations (50 vs. 90). Although the specimens that received 90 gyrations had slightly higher densities (approximately 1% higher) than the specimens with 50 gyrations, there was not a significant difference in mass loss because of freezing and thawing between the two sets of specimens. Due to the smaller surface to volume ratio of the freeze-thaw specimens compacted with the gyratory, fundamental transverse frequency was not obtained and damage was done based only on mass loss and visual inspection. Specimens for strength testing have been fabricated with the gyratory compactor and were shown to produce sufficient strengths that satisfied the typical strength requirement of 31 MPa (4.5 ksi) at 28 days (Amer et al. 2004; Käppi and Nordenswan, 2007; Hazaree 2010; Khayat and Libre, 2014). Amer et al. (2004) found that as the water-cement (w/c) ratio decreased, the effect of number of gyrations increased (i.e., lower w/c ratio led to larger density differences between 50 and 90 gyrations). Käppi and Nordenswan (2007) found that increasing cement content and/or w/c ratio led to increased workability (decreased number of gyrations to achieve specified density). The gyratory compactor was used by Hazaree (2010) as well as Khayat and Libre (2014) to determine optimal aggregate blends for maximizing laboratory density of RCC.

L.2 RCC MIXTURE CONSTITUENTS AND COMPACTION PROCEDURES

The RCC mix constituents, aggregate gradations, and proportions chosen for this study were taken from Chapters 2, 3, and 4 and Appendix F. The 17 RCC mixtures used in this study, along with their original motivation, are shown in Table L1. The mix designs reported in the respective chapters in Table L1 represent the final mix designs used for compacting specimens via the modified Proctor, modified Vebe, and vibrating hammer methods. The mix constituents and proportions are shown in Table L2 based on the range of mix designs shown in Table L1. In this chapter, the same constituents and aggregate gradations are utilized to develop final mix proportions (MDD, OMC, and total aggregate) from the gyratory compactor similar to the modified Proctor test procedure.

Table L1. Mix Design Motivations

Mix Design ID's	Chapter Mix Design Appears	Motivation
1-9	2	Various aggregate gradations
A, B, O	4	Range of cementitious contents
Trap Rock and River Gravel	Appendix F	Different aggregate types
Field Sites B, C, and D	3	Compare results to field cores. Also have various gradations, cementitious contents and materials, and different aggregates.

Table L2. Oven-Dry Mixture Proportions for Modified Proctor, Vibrating Hammer, and Modified Vebe (kg/m³); (1 kg/m³ = 1.686 lb/yd³)

Mix Design	Aggregate	Water	OMC (%)	Type I/II Cement	Fly Ash (Class C)	Slag (Grade 100)
1	2068.7	151.1	6.4	281.7	-	-
2	2104	145.3	6.1	281.7	-	-
3	2084.8	159.3	6.7	281.7	-	-
4	2046.3	156.4	6.7	281.7	-	-
5	2089.6	152	6.4	281.7	-	-
6	2153.6	174.1	7.2	281.7	-	-
7	2083.1	158.2	6.7	281.7	-	-
8	2112	156.8	6.6	281.7	-	-
9	2118.4	161.3	6.7	281.7	-	-
A	2110.0	157.5	6.6	246.5	35.2	-
B	2037.9	147.9	6.3	285.4	40.8	-
O	2153.3	152.8	6.4	207.6	29.7	-
Site B	2028.8	154.2	6.5	326.2	-	-
Site C	2058.5	138.7	5.9	177.9	59.3	59.3
Site D	1979.0	139.2	6.0	237.2	100.8	-
Trap Rock	2105.1	139.6	5.8	246.5	35.2	-
River Gravel	2126.5	140.3	5.8	246.5	35.2	-

A total of four compaction methods were investigated in this chapter: modified Proctor (ASTM D1557), vibratory hammer (ASTM C1435), modified Vebe (ASTM C1170 and ASTM C1176), and the gyratory compactor. For the modified Proctor procedure, specimens were compacted according to the ASTM procedure. The specimens compacted with the vibratory hammer were either compacted according to the ASTM procedure (150x300 mm, 6x12 in cylinders) or a similar procedure outlined in Chapter 2 (100x200 mm, 4x8 in cylinders). Modified Vebe time was measured according to ASTM

C1170 (ASTM, 2008) and specimens for strength testing were cored from the resulting compacted specimen. Figure L2 shows the apparatus used for Vebe testing.

Figure L2. Modified Vebe Test Apparatus.

Gyratory compactor specimens were compacted using a portable gyratory compactor (Figure L3) with resultant specimen dimensions being 150 mm (6 in) in diameter and approximately 150-175 mm (6-7 in) in height. Gyratory parameters were adapted from SuperPave compaction procedures for asphalt concrete (Huber et al. 1994). The compaction pressure was fixed at 600 kPa (87 lb/in^2) and the angle of gyration was set at 1.25 degrees. Contact pressures of vibratory rollers for asphalt compaction have been shown to be approximately 600-700 kPa (87-100 lb/in^2) (Delgadillo and Bahia, 2008). The angle of gyration has been shown to have a significant effect on density and by reducing angle of gyration from 1.25 degrees to 1 degree reduced the percent compaction by almost 2% (Swami et al. 2004). Typically, asphalt concrete gyratory specimens are not compacted beyond 100 gyrations since this would not represent field core conditions. For this study, specimens were compacted to 100 gyrations while fixing the pressure and angle noted above.

Figure L3. Portable gyratory compactor used for RCC mixes.

L.3 DEVELOPMENT OF GYRATORY COMPACTOR RCC MIX DESIGNS

RCC mix designs were developed based on the gyratory compactor similarly to the modified Proctor compaction procedure (ASTM D1557) where the same mix constituents and proportions are compacted at various moisture contents to determine the moisture-density relationship for a particular mix design. The resultant parameters from the moisture-density relationship derived from the gyratory are the maximum dry density (MDD) and the corresponding optimum moisture content (OMC). These two parameters are used to determine the final RCC mixture proportions. A minimum of four different moisture contents were tested for each gyratory mix design to develop the corresponding moisture-density relationship. Since the gyratory compactor outputs the height of the specimen at each gyration, a compaction evolution curve can be generated with a known specimen weight. Example compaction evolution curves developed for the moisture-density relationship of mix 9 are shown in Figure L4. There are two main prominent stable regions of compaction: initial compaction rate, i.e., 0-10 gyrations, and the long-term stable compaction rate, i.e., 20-100 gyrations, where the rate of compaction/gyration is significantly lower. These compaction evolution curves are similar to those shown in the field by comparing density to number of roller passes (Pittman, 1989).

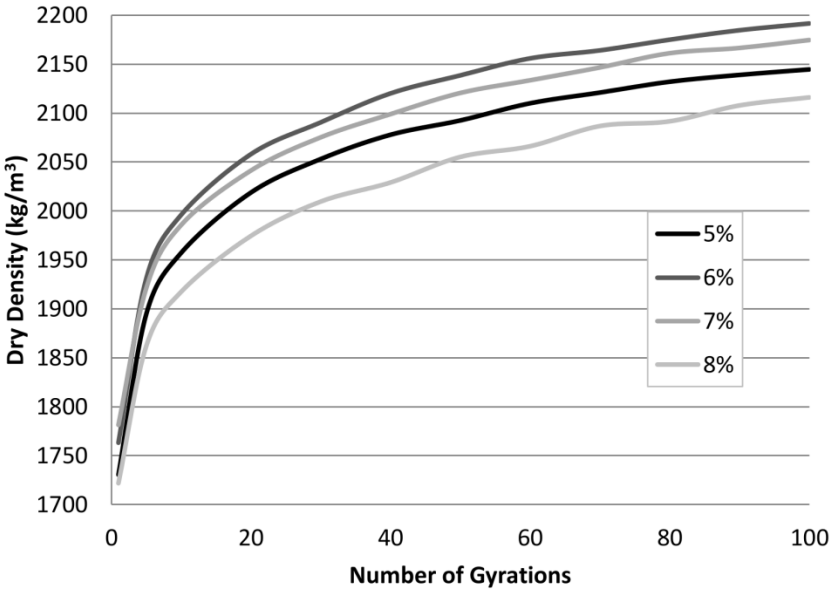

Figure L4. RCC Gyratory Compaction Evolution Curves as a Function of Moisture Content.
(1 kg/m^3 = 0.062 lb/ft^3)

In order to determine the MDD and OMC, the density at a particular number of gyrations was plotted against moisture content. Densities at 40, 60, 80, and 100 gyrations were plotted against moisture content (Figure L5) with the MDD and OMC being determined based on the densities at 100 gyrations. The rest of the compaction curves comparing gyratory and modified Proctor moisture-density relationships can be found in Appendix C. The number of gyrations (100) was chosen since it was noticed that densities below 100 gyrations were not agreeing with their respective densities from the modified Proctor. In addition, using more than 100 gyrations would be unrealistic since asphalt mix designs typically use a maximum of 100 gyrations. Despite the MDD decreasing as the number of gyrations is reduced, the OMC remains approximately the same. Upon completing the moisture-density relationships for each of the 17 RCC mixtures investigated in this study, the final RCC mix designs (proportions) were developed based on the MDD and OMC corresponding to 100 gyrations. The final RCC gyratory mixture proportions are shown in Table L3.

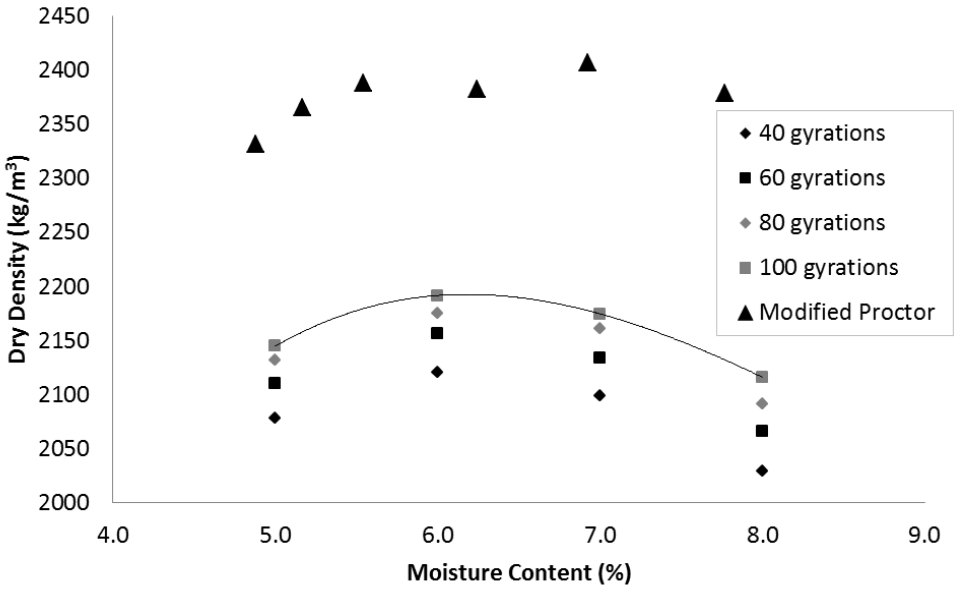

Figure L5. Moisture-Density Relationship for Gyratory Compactor Mix Design and Modified Proctor Mix Design. (1 kg/m^3 = 1.686 lb/yd^3)

Table L3. Oven-Dry Gyratory Mix Proportions (kg/m^3) (1 kg/m^3 = 1.686 lb/yd^3)

Mix Design	Aggregate	Water	OMC (%)	Type I/II Cement	Class C Fly Ash	Grade 100 Slag
1	1988.1	181.4	8.0	281.7	-	-
2	1927.4	144.5	6.5	281.7	-	-
3	1948.7	163.0	7.3	281.7	-	-
4	2075.2	176.7	7.5	281.7	-	-
5	2044.2	161.4	6.9	281.7	-	-
6	1924.0	163.3	7.4	281.7	-	-
7	2049.8	167.4	7.2	281.7	-	-
8	2074.7	152.2	6.5	281.7	-	-
9	1904.3	148.6	6.8	281.7	-	-
A	1918.2	134.6	6.1	246.5	35.2	-
B	1912.2	141.0	6.3	285.4	40.8	-
O	1986.6	155.7	7.0	207.6	29.7	-
Site B	2003.5	165.4	7.1	326.2	-	-
Site C	2033.1	139.8	6.0	177.9	59.3	59.3
Site D	1969.2	150.0	6.5	237.2	100.8	-
Trap Rock	2105.2	139.6	5.8	246.5	35.2	-
River Gravel	1959.0	154.2	6.9	246.5	35.2	-

L.4 COMPARISON OF COMPACTION METHOD DENSITIES

Typical specifications for density are written relative to a laboratory compaction method (i.e. modified Proctor), therefore, it is essential that the laboratory compaction method mimic field compaction. This idea is the underlying basis for the development of the SuperPave gyratory compactor from the Strategic Highway Research Program (SHRP) for asphalt concrete during the 1990's (Huber et al. 1994). In order to replicate field compaction, the gyratory compactor imparts both static compression and gyrating/kneading action on the specimen by means of eccentric loading (Figure L6). Values of MDD from three compaction methods (modified Proctor, modified Vebe, and the gyratory compactor), for the same RCC mix constituents listed in Table L3, were compared.

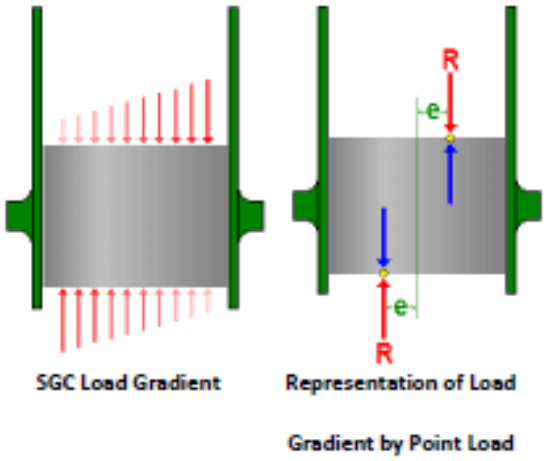

Figure L6. Loading Conditions on Gyratory Specimen (FHWA, 2010).

MDDs from the gyratory compactor and modified Proctor compaction are compared in Figure L7, while those from the modified Vebe and modified Proctor compaction are shown in Figure L8. The number of mix designs presented in Figure L8 is 45 and consists of mixes from Chapters 2, 3, and 4 and Appendices F and J. The densities resulting from the three methods for the 17 different mix designs in this study are shown in Table L4. The gyratory compactor does produce a wider range of MDD relative to the modified Proctor (Figure L7). The modified Proctor compaction method results in significantly higher MDD's and is likely a combination of higher compaction energy, dynamic compaction method, and breaking of aggregates (Appendix F). The Vebe densities are consistently much lower than the modified Proctor MDDs (Figure L8). From Figure L9, it can be seen that the gyratory compactor generally resulted in higher optimum moisture contents than the modified Proctor. Higher moisture contents indicate that more paste volume is required to sufficiently lubricate the mix to achieve maximum packing.

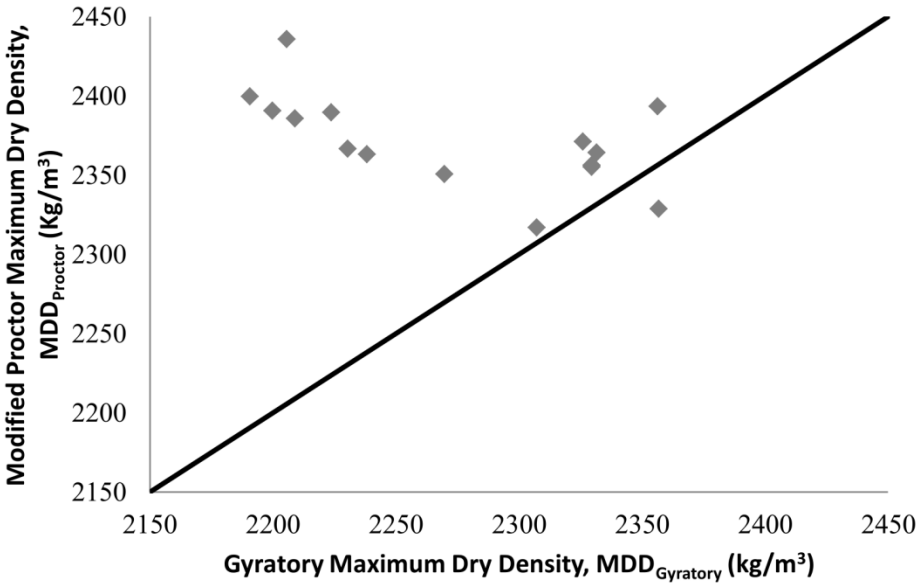

Figure L7. Comparison of Modified Proctor and Gyratory Maximum Dry Density.
(1 kg/m^3 = 0.062 lb/ft^3)

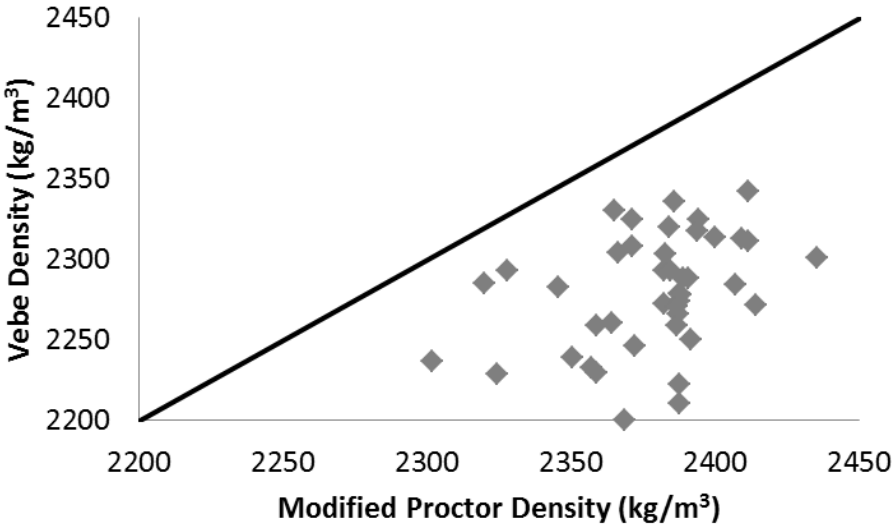

Figure L8. Comparison of Modified Proctor and Vebe Densities. (1 kg/m^3 = 0.062 lb/ft^3)

Table L4. Density Values from Modified Proctor, Gyratory Compactor, and Modified Vebe (kg/m^3)*

(1 kg/m^3 = 0.062 lb/ft^3)

Mix Design	Modified Proctor	Gyratory	Modified Vebe
1	2350.4	2269.7	2238.4
2	2385.8	2209.0	2335.2
3	2366.4	2230.5	2303.3
4	2328.6	**2356.8**	**2291.7**
5	2370.9	**2325.9**	2306.9
6	2435.9	2205.7	2300.0
7	2364.2	**2331.5**	**2329.0**
8	2393.5	**2356.3**	2316.6
9	2399.6	2190.6	2312.9
A	2389.5	2223.8	2250.4
B	2390.6	2199.9	2260.4
O	2363.1	2238.3	2288.3
Site B	2356.0	**2329.6**	**2338.1**
Site C	2355.2	**2329.6**	**2309.5**
Site D	2316.8	**2307.2**	**2285.6**
Trap Rock	2386.8	2229.3	2276.7
River Gravel	2408.2	2240.6	2312.1

*Bold values indicate that density is at least 98% of modified Proctor density.

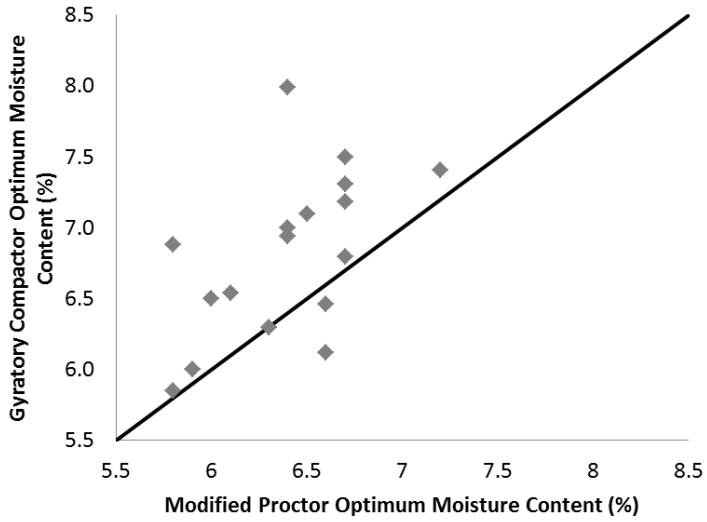

Figure L9. Comparison of Gyratory and Modified Proctor Optimum Moisture Contents.

Of the 17 mix designs tested, 7 had gyratory densities that were at least 98% of the modified Proctor density, while the remaining mixtures had lower densities (Figure L7). Figure L10 clearly shows the difference in appearance between specimens that achieved the 98% density threshold and those that did not. Of these 7 mix designs that were greater than 98% of the MDD, 4 were from the study on aggregate gradation effects (Chapter 2) while the other 3 were the mixes from the field site visits (Chapter 3). These results indicate that the relative density between the gyratory compactor and the modified Proctor compaction method is a function of aggregate gradation, aggregate type, and/or cementitious content/type. Since only 4 of the 9 mix designs from the aggregate gradation study achieved 98% compaction from the gyratory, it can be concluded that aggregate gradation plays a large role especially since the cement content (282 kg/m^3 or 475 lb/yd^3) and aggregate type for all these mix designs was fixed. All three mix designs from the field site visits achieved 98% compaction and all three mix designs used different aggregate sources, aggregate gradations, as well as cementitious contents and types. Figure L11 shows the aggregate gradations of the 17 mix designs as a function of their compactibility, i.e., whether or not the gyratory densities were at least 98% of the modified Proctor densities). In general, those mix designs with aggregate gradations containing at least 30% passing the 1.19 mm (#16) sieve had densities of at least 98% relative to the modified Proctor method. Mix designs with aggregate gradations containing between 20% and 30% passing the 1.19 mm (#16) sieve did not meet the 98% density threshold.

Figure L10. Specimens Compacted with Gyratory Compactor. Specimen on left (mix 9) did not meet 98% Compaction Requirement while Specimen on right did (site B mix).

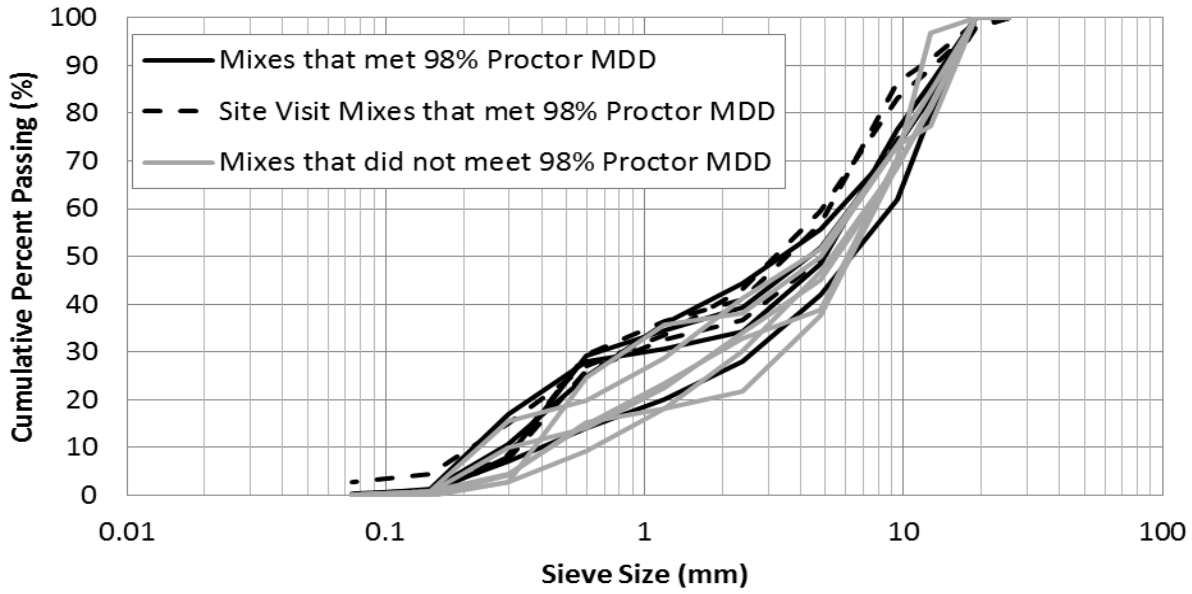

Figure L11. Combined Aggregate Gradations and RCC Densities. (1 in = 25.4 mm)

The densities from modified Vebe compaction in Figure L8 are always lower than those of the MDD from the modified Proctor, which was previously shown by Tayabji and Okamoto (1987). Of the 17 mix designs in this study, only 5 had Vebe densities that were at least 98% of the modified Proctor density (Table L4). Those 5 mix designs also had gyratory compactor densities that were at least 98% of the modified Proctor density. Comparing the densities from the gyratory compactor and the Vebe test in Figure L12, there is approximately an even amount of data points above the line of unity relative to those below the line of unity. Therefore, the gyratory compactor and modified Vebe densities appear to be good indicators of compactibility of an RCC mix relative to the proctor MDD for the range of aggregates and proportions used in this research.

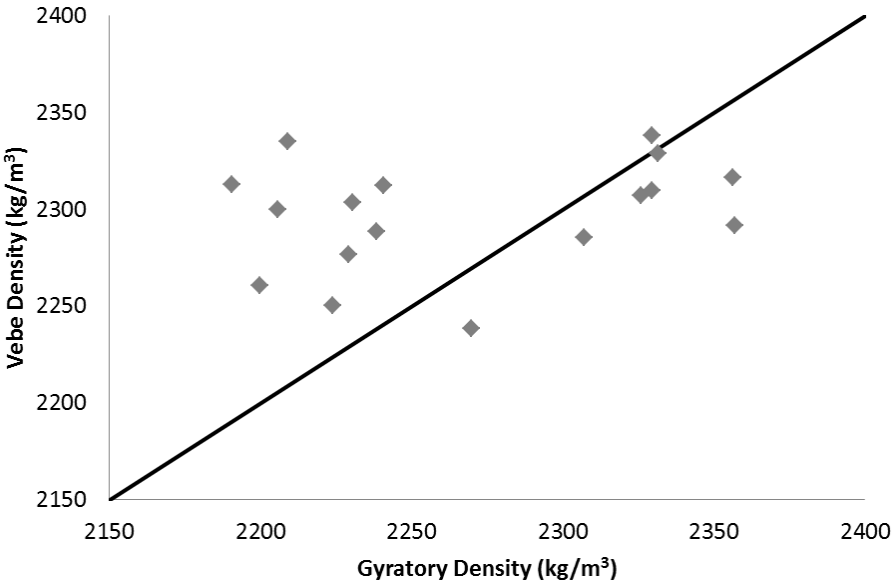

Figure L12. Comparison of Vebe and Gyratory Densities for RCC. (1 kg/m^3 = 0.062 lb/ft^3)

L.5 COMPARISON OF RCC STRENGTH PROPERTIES

Strength properties were measured on 75x150mm (3x6 in) cores from specimens compacted with the vibratory hammer, gyratory compactor, and modified Vebe methods (Figure L13). The 75x150mm (3x6 in) core size was chosen since this is the largest, standard size cylinder (i.e. height-to-diameter ratio of 2:1) that could be cored from specimens of all three compaction methods. Compressive strength testing was conducted on the cored specimens from the three compaction methods at 28 days age with triplicate specimens per mix per compaction method. Likewise split tensile strength testing was conducted at 28 days on the vibratory hammer and gyratory compacted specimens with triplicate specimens per mix and compaction method. The hardened Vebe specimen was not large enough to yield cores for compressive and split tensile strength. Compressive and split tensile strengths from the various compaction methods are shown in Table L5 and Table L6, respectively.

(a) **(b)** **(c)**

Figure L13. Cores (75x150 mm) from Vebe (a), Gyratory (b), and Vibratory Hammer (c).

Table L5. Compressive Strengths (MPa) from Three Compaction Methods - 28-Day Core (75x150mm) (1 ksi = 6.89 MPa; 1 in = 25.4 mm)

Mix Design[a]	Vibratory Hammer	Gyratory[b,c]	Vebe[b,c]
1	45.7	**54.9**	50.0
3	57.9	**45.3**	53.6
4	51.4	41.0	56.0
5	64.8	**49.7**	**59.0**
6	44.9	44.9	48.3
7	58.2	50.4	62.4
8	57.7	63.7	52.9
Site B	57.0	64.5	64.7
Site C	54.3	**84.0**	53.0
Site D	61.9	**76.8**	54.5

[a] Italicized values indicate that the density of the gyratory specimens were at least 98% of the modified Proctor density.

[b] Bold values indicate statistical difference (t-test, 95% confidence) from vibratory hammer core compressive strength.

[c] Underlined values indicate statistical difference (t-test, 95% confidence) between gyratory and Vebe compressive strengths.

Table L6. Split Tensile Strengths (MPa) from Vibratory Hammer and Gyratory Compaction Methods - 28-Day Core (75x150mm) (1 ksi = 6.89 MPa; 1 in = 25.4 mm)

Mix Design[a]	Vibratory Hammer	Gyratory[b]
3	4.40	**3.62**
4	4.04	3.99
5	4.51	3.91
6	3.66	4.54
7	4.21	3.86
8	4.38	3.62
Site B	5.41	**4.58**
Site C	3.92	**5.75**
Site D	4.70	5.42

[a] Italicized values indicate that the density of the gyratory specimens were at least 98% of the modified Proctor density.

[b] Bold values indicate statistical difference (t-test, 95% confidence) from vibratory hammer core split tensile strength.

All compressive strengths from Vebe specimens are statistically similar to the vibratory hammer cores except for one mix (#5), which yielded a statistically lower compressive strength from the Vebe specimen (Table L5). The Vebe density of mix 5 was also less than 98% of the modified Proctor MDD. Comparing compressive strengths (average of 3) of all cores (mix designs from Chapters 2, 3, and 4 and Appendix F) from Vebe and vibratory hammer specimens suggests that the two compaction methods produce relatively similar strengths (Figure L14).

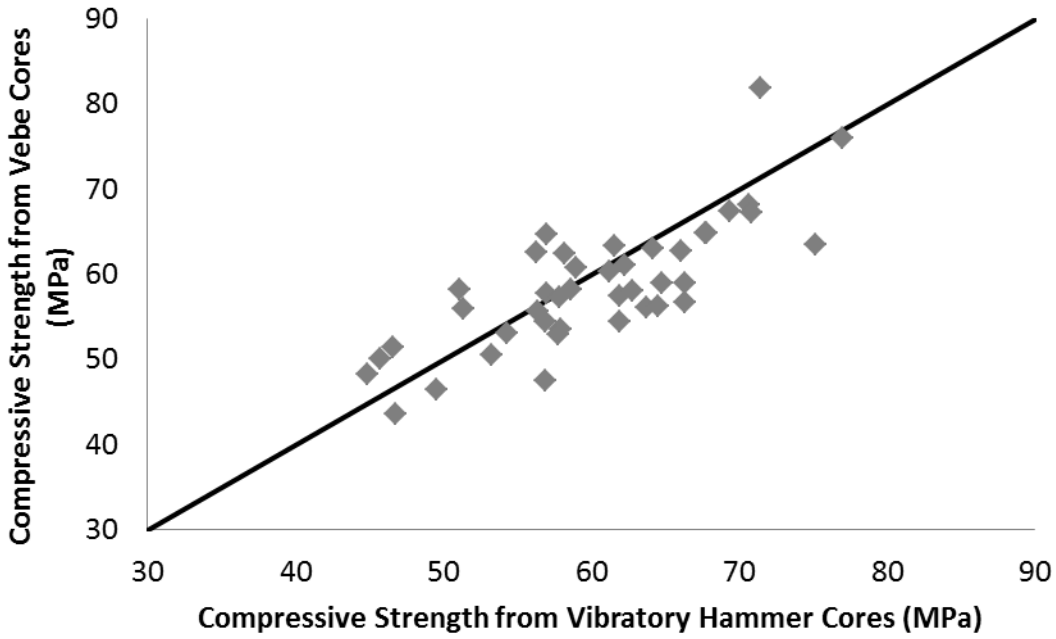

Figure L14. Comparison of Laboratory Compressive Strength from Vebe and Vibratory Hammer Cores. (1 ksi = 6.89 MPa)

When comparing gyratory specimen cores and vibratory hammer cores (Figure L13), 5 had statistically similar compressive strengths, 3 gyratory mixes had statistically greater strengths, and 2 had statistically lower compressive strengths. For the 7 mix designs that had gyratory densities greater than or equal to 98% of the modified Proctor MDD, 4 had statistically similar compressive strengths, 2 had statistically greater compressive strengths with gyratory compaction, and only one had statistically lower compressive strengths from gyratory compaction. One observation from these results is that meeting the 98% modified Proctor density generally produces statistically similar or greater compressive strength. However, overall there does not appear to be a clear trend relating compressive strength of cores compacted from the two methods. Several reasons are that the gyratory induces a more constant total energy of compaction whereas the vibratory hammer is operator and mix dependent. Gyratory specimens were also compacted at different optimum moisture contents, which were not necessarily equal to the optimum moisture content from the modified Proctor testing and subsequent fabrication of the vibratory hammer specimens. Gyratory specimens tended to be compacted at higher OMCs (Figure L9). The two gyratory mix designs that had statistically lower compressive strengths than their respective vibratory hammer specimens also had higher moisture contents (Table L3) than their vibratory hammer specimens.

The majority of the RCC mix designs have statistically similar split tensile strengths when comparing vibratory hammer and gyratory cores (Table L6): 6 out of 9 have statistically similar strengths, 2 out of 9 have statistically lower gyratory specimen strengths, and 1 has a statistically higher gyratory strength. The two mix designs which had statistically lower split tensile strengths from gyratory

specimens relative to vibratory hammer specimens also had higher OMC (See Table L3) relative to the vibratory hammer specimens (modified Proctor).

Comparing the gyratory compressive and split tensile strengths of the three field mixes (sites B, C, and D) to their respective field core strengths (Chapter 3), the gyratory strengths are always statistically greater. This is primarily a result of the field core densities not meeting the 98% modified proctor compaction requirement.

Figure L15 shows failure surfaces of gyratory split tensile strength specimens. There does not appear to be any visible voiding or aggregate segregation throughout the cross section of the specimens. One limitation of the gyratory cylinder geometry is that flexural strength specimens cannot be fabricated and therefore, established correlations between compressive or split tensile strength and flexural strength must be utilized or compaction with a vibratory hammer must be employed.

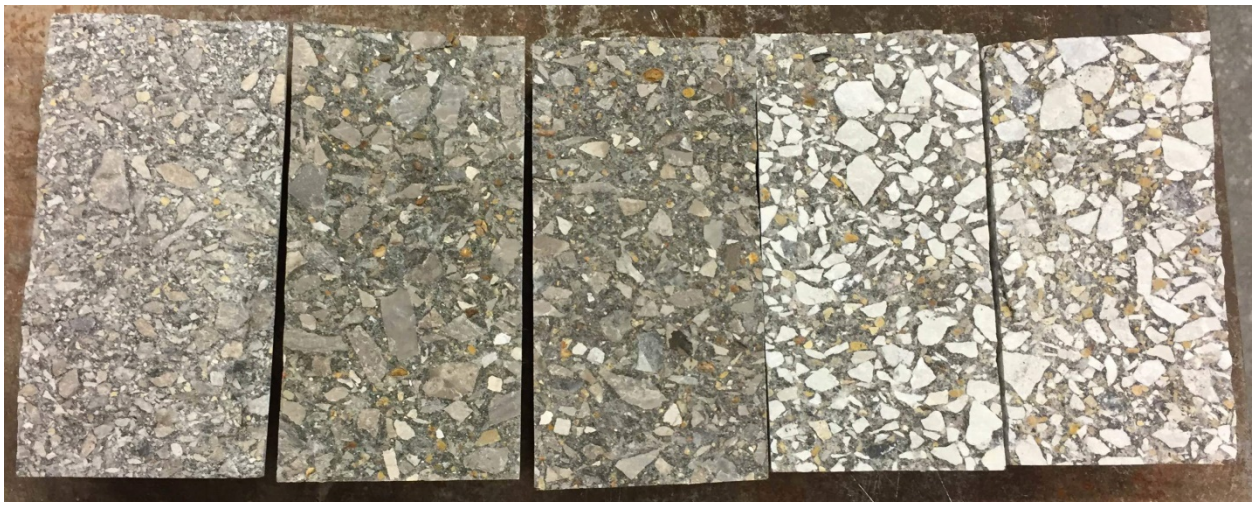

Figure L15. Failure Surfaces of Split Tensile Strength Specimens Compacted with the Gyratory Compactor. Mixes (from left to right): Site B, Site C, Site D, #7, and #8

L.6 COMPARISON OF RCC FRACTURE PROPERTIES FROM VIBRATORY AND GYRATORY COMPACTION

Fracture properties were compared between the vibratory hammer and gyratory specimens. Fracture properties were tested using the disk-shaped compact tension (DCT) geometry according to Amirkhanian et al. (2015). Fracture testing was conducted at 28 days age with a minimum of 5 replicates per mix per compaction method. Fracture results from gyratory specimens, along with their statistical significance to those from the vibratory hammer specimens, are shown in Table L7. Fracture results from the vibratory hammer-prepared specimens can be found in their respective chapters. Fracture properties reported include: critical stress intensity factor (K_{IC}), elastic modulus (E), critical crack tip opening displacement ($CTOD_C$), initial fracture energy (G_f), and total fracture energy (G_F).

Three mix designs were chosen to determine if there are any effects of specimen location (i.e. depth into the gyratory specimen) on fracture properties. For the three chosen mix designs (mixes 1, 3, and 6), five replicate cylinders were made. Three DCT specimens were obtained from each cylinder; one specimen from the top, middle, and bottom of the cylinder. Therefore, five replicates for each depth and each mix design were tested. Figure L16 shows the critical stress intensity factor and total fracture energy as a function of depth for each mix with the fracture properties measured at all three depths being statistically similar to each other. This suggests that density remains uniform with depth because density has been shown to be related to the mechanical properties of RCC (Tayabji and Okamoto, 1987; Pittman, 1989; Shihata, 2000; Delatte and Storey, 2005; Harrington et al. 2010). The constant fracture properties with depth support the qualitative observations on the gyratory split tensile failure surfaces (Figure L15).

Table L7. 28-Day Fracture Properties Measured on Gyratory RCC Specimens (1 MPa-$m^{1/2}$ = 0.910 ksi-$in^{1/2}$; 1 GPa = 145 ksi; 1 in = 25.4 mm; 1 lb/in = 175 N/m)

Mix Design	K_{IC}, MPa-$m^{1/2}$	E, GPa	CTODc, mm	G_f, N/m	G_F, N/m
1	1.15	28.9	0.0189	46.4	**183.4**
2	1.27	**29.9**	0.0215	54.4	187.2
3	1.24	**35.2**	**0.0144**	**44.1**	**204.3**
4	1.25	32.0	0.0196	48.6	180.8
5	1.23	32.8	0.0175	46.4	229.2
6	**1.43**	**37.3**	**0.0167**	54.8	**194.7**
7	1.26	32.6	0.0197	49.1	**206.5**
8	1.32	**32.8**	0.0212	52.9	**205.0**
9	**1.20**	29.5	0.0191	49.2	**205.0**
A	**1.08**	**29.2**	0.0203	**40.3**	**199.9**
B	1.16	32.0	0.0177	42.7	**206.9**
O	**1.16**	**33.8**	**0.0165**	**40.2**	191.1
Site B	1.49	42.3	0.0170	53.2	174.9
Site C	**1.69**	**48.4**	0.0189	**59.8**	190.9
Site D	**1.55**	**45.5**	**0.0189**	**53.1**	198.5
Trap Rock	1.44	34.7	0.0248	60.4	**367.3**
River Gravel	1.42	**35.3**	0.0216	57.4	234.0

*Bold values indicate statistical difference (t-test, 95% confidence) from fracture properties measured on vibratory hammer specimens.

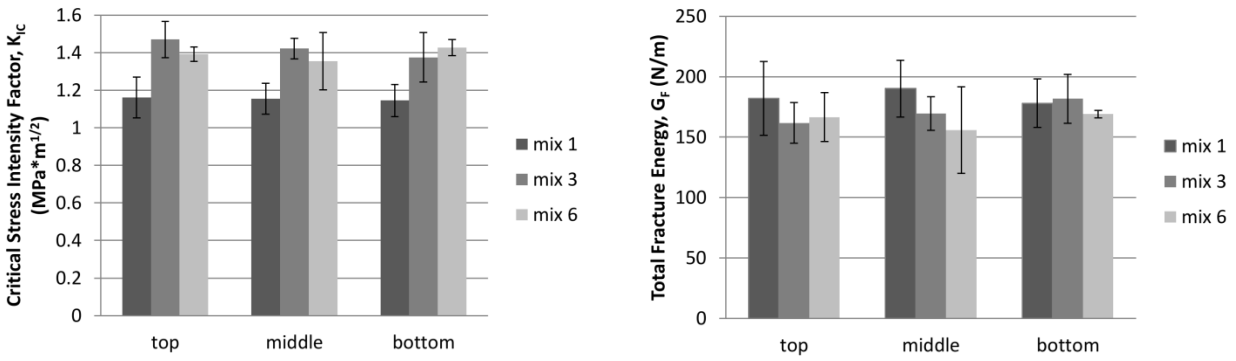

Figure L16. Gyratory Fracture Properties as a Function of Depth (error bars indicate +/- one standard deviation). (1 MPa-m$^{1/2}$ = 0.910 ksi-in$^{1/2}$; 1 lb/in = 175 N/m)

It can be seen from Table L7 that there is not consistent agreement between fracture properties determined on gyratory compacted specimens and specimens compacted via the vibratory hammer. Of the 17 mixes, 14 had at least one statistically different fracture property between the two compaction methods. All of the mix designs that had gyratory densities that were at least 98% of the modified Proctor maximum density resulted in gyratory fracture properties statistically similar or greater than those from the vibratory hammer. For the remainder of the mix designs (i.e. those that didn't achieve the 98% density specification), lower density did not guarantee reduced fracture properties. Figure L17 compares fracture properties (K_{IC} and G_F) between gyratory and vibratory hammer compacted specimens, where the gyratory compactor always yields higher values of total fracture energy. The greater total fracture energies from the gyratory compactor relative to the vibratory hammer are likely related to less aggregate breakage in the gyratory compactor as shown in Appendix F. Less aggregate breakage would suggest that more aggregate interlock is maintained which would assist in deflecting propagating cracks. The relationship between fracture properties and compressive strength for the two compaction methods is shown in Figure L18. For the critical stress intensity factor, it can be seen that there is a good, positive relationship between critical stress intensity factor and compressive strength for gyratory specimens, but there is no relationship for vibratory hammer specimens. Total fracture energy does not appear to correlate well with compressive strength for either compaction method.

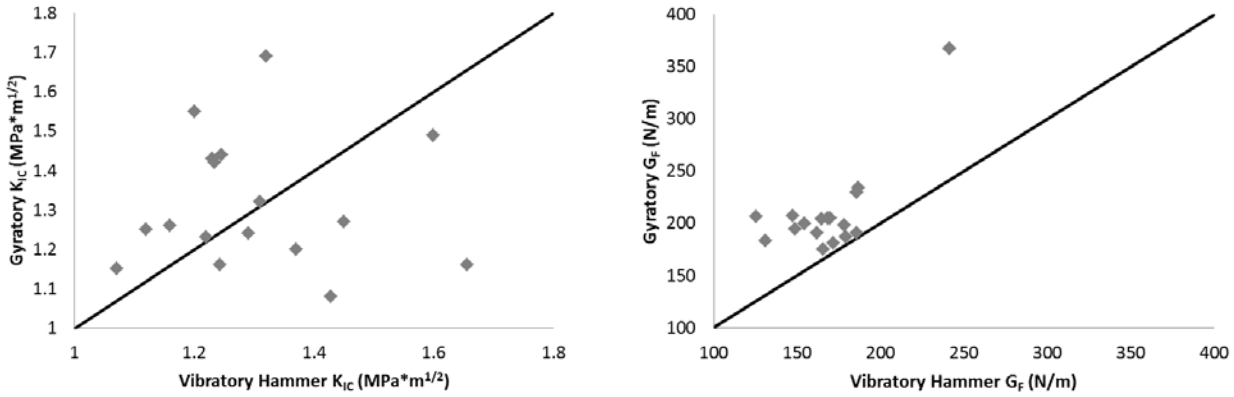

Figure L17. Comparison of Fracture Properties between Gyratory and Vibratory Hammer Specimens. (1 MPa*m$^{1/2}$ = 0.910 ksi*in$^{1/2}$; 1 lb/in = 175 N/m)

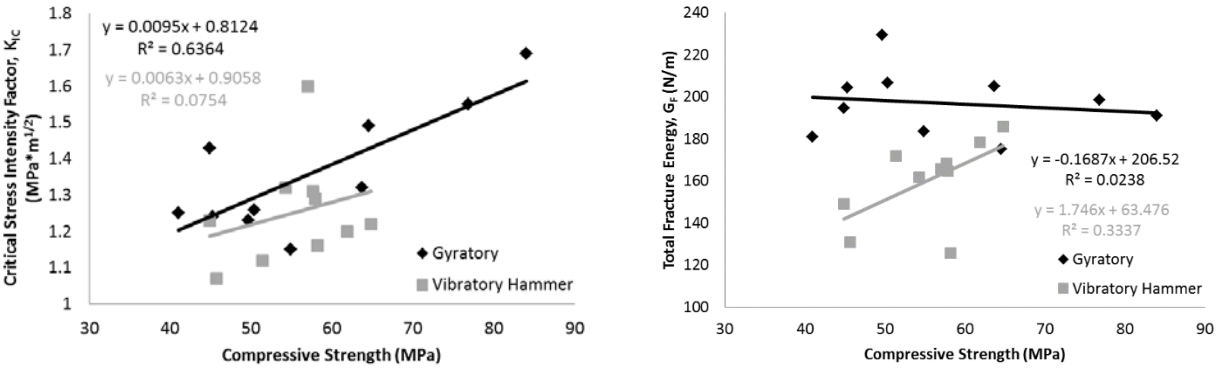

Figure L18. Relationship between Fracture Properties and Compressive Strength. (1 MPa*m$^{1/2}$ = 0.910 ksi*in$^{1/2}$; 1 lb/in = 175 N/m; 1 ksi = 6.89 MPa)

L.7 CONCLUSIONS

The gyratory compactor was introduced for asphalt mix design during the strategic highway research program (SHRP) since it replicated field compaction better than the Marshall hammer. Since RCC materials are constructed similarly to asphalt pavements, utilizing the gyratory compactor should produce more realistic field to lab correlations and be more sensitive to changes in mix design constituents and proportions than the modified Proctor hammer. Gyratory compactor and modified Vebe densities do not always agree with densities from the modified Proctor compaction method and both are generally lower than the Proctor method. The mixes that did not achieve the 98% density threshold would be expected to pose difficulties with compaction in the field since the compaction mechanisms in the field are well mimicked by the gyratory compactor and, to a lesser extent, by the Vebe test. Thus, the use of the gyratory compactor for selecting mix designs (particularly aggregate gradations and aggregate sources) that would likely lead to acceptable density in the field (i.e. 98% of

modified Proctor density) is recommended. The gyratory compactor could also be used for field verification of a mix immediately prior to paving and rolling.

Gyratory compaction of RCC mixes was found to achieve statistically similar, greater, or lower strengths than the vibratory hammer. For the statistically lower strengths, the gyratory mix designs had higher moisture contents than the vibratory hammer specimens and thus, the reduced strengths may be attributed to higher water contents. In general, the mix designs that had gyratory densities greater than or equal to 98% of the modified Proctor maximum density produced statistically similar or greater mechanical properties (strength and fracture) relative to specimens compacted with the vibratory hammer. Comparison of fracture properties as a function of depth in the gyratory specimens showed no statistical differences. Therefore, the gyratory compactor provides a more uniform specimen compaction with depth. The gyratory compactor shows significant promise for mix design, specimen fabrication, and field quality assurance/quality control of RCC because of its consistent compaction energy, lower operator error, and similarity to the field compaction mechanism.

APPENDIX M: EFFECT OF COMPACTION DELAY ON EARLY AGE PROPERTIES OF ROLLER-COMPACTED CONCRETE

M.1 INTRODUCTION

Roller-compacted concrete (RCC) for pavement applications has been shown to offer benefits in terms of cost, sustainability, constructability, and early opening to traffic. The cement content of RCC pavements required to achieve strengths equivalent to those of conventional Portland cement concrete (PCC) pavements is lower. The practice of RCC paving makes it a very attractive technology because it is cost effective as compared to conventional concrete and asphalt pavements as labor costs and opening times to traffic are reduced while the construction productivity is increased (ACI 1995, Lamond and Pielert 2006, Luhr 2004).

For projects where an onsite continuous batch plant, i.e., a pugmill, is not used, a central batch plant mixes the RCC, and dump trucks transport RCC to the project site. The American Concrete Pavement Association (ACPA) specification for RCC (American Concrete Pavement Association 2014) suggests that for long hauls these trucks must be equipped with retractable covers, as environmental factors such as temperature, humidity, and wind can enhance evaporation of the moisture from the RCC material. Existing specifications recommend that the compaction of RCC pavements be completed within 60 minutes of mixing (American Concrete Pavement Association 2014, Portland Cement Association 2004) and adjusted to 30 or 45 minutes if hot weather is expected (Halsted 2009). Wet density and moisture measurements are performed as quality control requirements, where density has to be at least 98% of the laboratory maximum wet density determined from the modified Proctor test.

Limited research has been performed on the impact of compaction delay on fresh and hardened properties of RCC. However, compaction delay of soil-cement has been extensively studied. Brooks et al. (2009) performed Proctor compaction, unconfined compressive strength (UCS), and swell tests on cement kiln dust stabilized clays. They found that differences between samples at 1 hr and 3 hr of compaction delay were statistically insignificant, but were significant at 72 hr. Generally, it was concluded that the UCS values decreased as the delay time increased. Guthrie et al. (2009) examined the effects of environmental factors such as wind speed, air temperature, relative humidity, and delay time on the strength of soil-cement layers and showed that a decrease in relative humidity, and increases in wind speed, air temperature, and compaction delay time resulted in lower strengths compared to control samples.

With respect to RCC compaction delay, Dasmeh et al. (2000) analyzed how delaying compaction in the modified Proctor test (ASTM D1557, 2012) by 15, 45, 60, 90, 120, and 150 minutes affected the properties of ten RCC mixes; however, no clear relationship between delay times and strength could be found. Gharavi (2003) studied the optimum delay time between mixing and placing/compacting of RCC. Eight mixes, including six with pozzolans, were prepared at optimum moisture using the modified Proctor procedure at delay times varying from 15 to 120 minutes. The use of pozzolans helped increase allowable working times with RCC. Most recently, Karimpour (2010) studied the

effects of changing the time between mixing and compaction of RCC with Ground Granulated Blast Furnace Slag (GGBFS). Mix designs with varying total cementitious content and slag replacement levels were developed, and specimens were cast after compaction delay times of up to 180 minutes. The mixes with straight cement showed a decrease in strength as the delay time increased, while the mixes with slag generally showed similar results throughout all delay times tested.

There has been extensive research and application of the Superpave gyratory compactor for asphalt materials over the past 25 years, but research on the applicability of this equipment for specimen preparation of RCC has been limited. The gyratory compactor has promising features, such as kneading compaction and consistent compactive energy. Amer et al. (2003) compared gyratory densities and mechanical properties to field cores of two industrial pavement projects, using the same mix designs and source materials. It was concluded that the gyratory compactor could be utilized to more precisely assess RCC properties by compacting to a specific target density, usually corresponding with approximately 50-75 gyrations to best represent field densities. Amer et al. (2004) later proposed a mix design procedure utilizing the number of gyrations to compact samples with varying mix proportions to varying densities. Most recently, Williams (2013) compared the gyratory compactor and modified Proctor as methods to determine the optimum moisture content for RCC mix design. Below optimum moisture contents, the two methods yielded similar moisture-density results. Above optimum moisture contents, the gyratory compactor resulted higher densities due to paste leakage from the equipment. Both methods did result in feasible mix designs, though these mix designs were not necessarily equivalent. Thus, further research was proposed to determine which method best represents field compaction.

M.2 OBJECTIVES

Given that all specifications put a maximum time limit for RCC material placement after mixing and limited studies having been completed on the effects of RCC compaction delay on early-age properties (Dasmeh et al. 2000, Gharavi 2003, Karimpour 2010), the objectives of this study are to create a test methodology and quantify the impacts of temperature conditions and compaction delay with respect to workability, density, early-age strength, and fracture properties for several RCC mixtures. RCC mixes investigated include a control mix at two temperatures, a mix with a retarding admixture, and a mix containing saturated fine lightweight aggregates. Additionally, the effect of compaction method is analyzed by comparing samples prepared with the vibratory hammer and gyratory compactor, as shown in Figure M1.

Figure M1. Vibratory Hammer (left) and Portable Gyratory Compactor (right).

M.3 EXPERIMENTAL SETUP AND TEST METHODOLOGY

An experimental plan and testing protocol was developed to assess compaction delay and temperature impacts on early-age RCC properties. Modified Proctor compaction was used to establish moisture density relationships for selecting the optimum moisture content. Specimens were prepared with the gyratory compactor and vibratory hammer (see Figure M1) at compaction delay times of 0, 45, 90, 135, and 180 minutes from the start of mixing. The gyratory compactor was also used to assess the compactability as a percentage of the initial wet density achieved at 100 gyrations for a given delay time. Early-age strength and fracture testing at 7-days was performed on cylinder and DCT specimens, respectively. The details of the constituent materials, mix proportions, and specimen preparation and testing will be described in the next section.

M.3.1 Material Constituents

Four different aggregate types were used: coarse dolomite, intermediate dolomite, natural sand, and fine lightweight aggregate (FLWA) manufactured from expanded shale. Aggregates were oven dried and then dry sieved as per ASTM C136 (2014). The specific gravity and absorption capacity were determined according to ASTM C127 (2015) and C128 (2015), respectively. The physical properties and the average gradation of three replicate samples for each aggregate type are shown in Table M1. The combined aggregate blend closely approximated the 0.45-power maximum density curve for all sieves except passing 0.297 mm (#50) and finer. Portland cement type I/II was used in all RCC mixes. A chemical admixture, with both retarding and rheology-modifying effects, was used in one of the mixes.

Table M1. Aggregate Gradation and Physical Properties (1 in = 25.4 mm)

	Percent Passing			
Sieve Size (mm)	Coarse Dolomite	Intermediate Dolomite	Natural Sand	Fine LWA
25.4	100	100	100	100
19.0	88.8	100	100	100
12.7	49.0	100	100	100
9.51	28.9	95.1	100	100
4.76	9.04	32.0	100	100
2.38	3.11	5.77	83.2	74.2
1.19	2.12	2.36	66.6	47.0
0.595	1.83	1.71	46.3	29.8
0.297	1.66	1.44	12.4	19.0
0.149	1.51	1.33	1.26	13.0
0.074	0.87	1.02	0.38	9.01
Specific Gravity (SSD)	2.67	2.66	2.64	1.63
Absorption Capacity	2.95%	3.0%	1.38%	14.3%

M.3.2 Mix Design

The following three RCC mix designs (Table M2) were developed using the volumetric method: a control mix at 21.1°C (70°F) and 35°C (95°F) (labeled CT and HT, respectively), the control mix with the addition of a retarding and rheology-modifying admixture (RT) at 35°C (95°F), and the control mix with partial replacement of sand with FLWA (LW) at 35°C (95°F). For mix designs CT/HT and RT, the aggregates were blended in a 25/45/30 weight ratio of coarse dolomite, natural sand, and intermediate dolomite, respectively. For the LW mix design, the same aggregate blend was employed except FLWA replaced the natural sand by 25% volume. All mix designs had 13% cement by weight of dry aggregates.

Modified Proctor tests as per ASTM D1557, 2012 method C, were performed for each of the mix designs with six moisture contents ranging from 5% to 8% batched to determine the optimum moisture content (OMC) and maximum dry density (MDD) of each mix. Prior to conducting the moisture-density tests, the FLWA were soaked and then prepared to be mixed at saturated-surface dry (SSD) condition. The MDD and OMC for each mix is shown in Table M2. The wet and dry moisture-density relationships at 21.1°C (70°F) are shown in Figure M2. The MDD and OMC curves for the CT and RT mixes had similar shapes except that the RT mix had a higher OMC. For the LW mix, the FLWA held onto part of the mix water and thus the MDD was maintained over a larger moisture content range than the other mixes.

Table M2. RCC Mixture Constituents, Proportions, and Maximum Dry Density (kg/m^3)*

Mixture ID	Aggregate (Oven Dry)	Type I/II Portland Cement	Water	Admixture (ml/100 kg cement)	MDD	OMC (%)
CT	2030.2	263.9	146.8	N/A	2277.9	6.4
HT	2030.2	263.9	146.8	N/A	2277.9	6.4
RT	1993.4	259.1	162.2	650	2276.8	7.2
LW	1957.1	254.4	143.7	N/A	2227.2	6.5

*1 kg/m^3 = 1.686 lb/yd^3; N/A signifies “not applicable.”

*1 fl.oz/cwt = 65 mL/100 kg

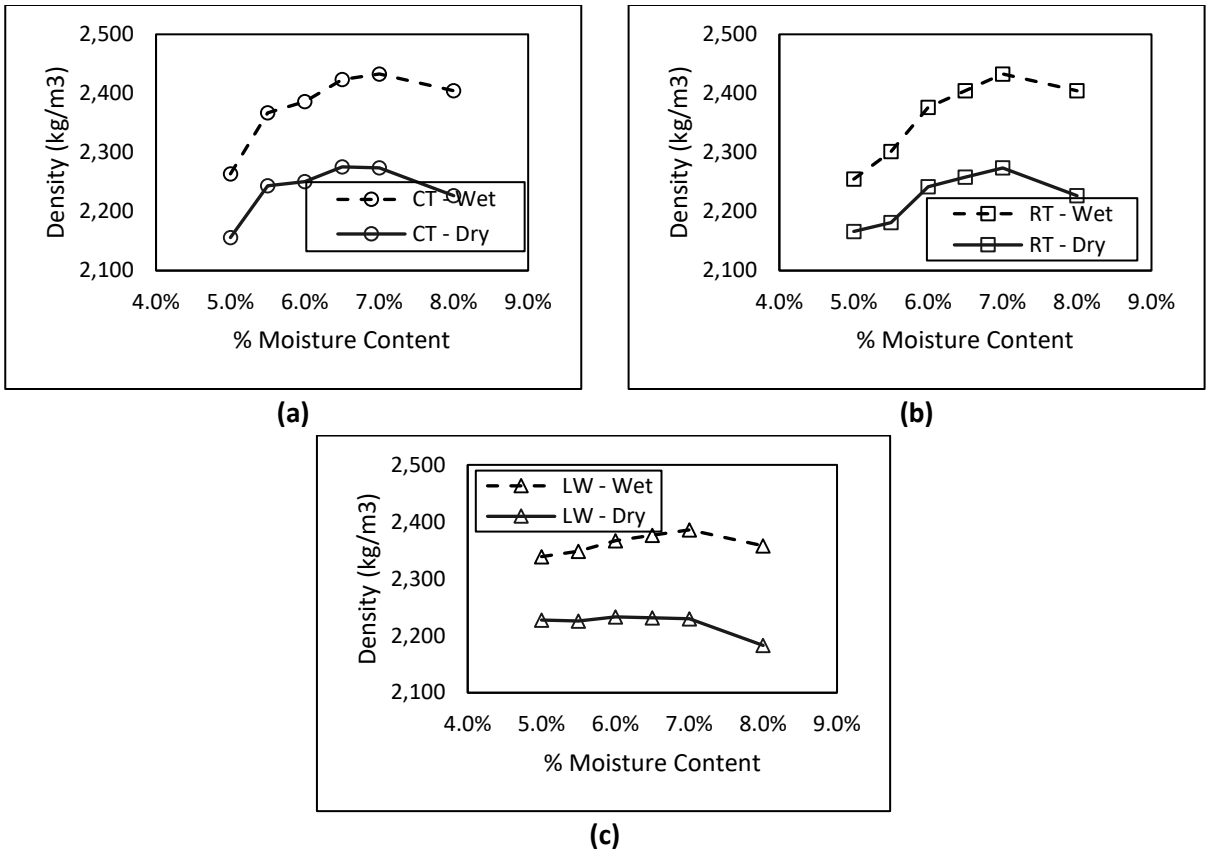

Figure M2. Wet density (dashed) and dry density (solid) curves for RCC mixes (a) CT (b) RT, and (c) LW. (1 kg/m^3 = 0.062 lb/ft^3)

M.3.3 Testing Protocol and Specimen Preparation

With the objective of simulating delayed compaction and hot weather field conditions (high mix temperature at the plant, during hauling, and at placement), a high temperature mixing procedure (Popovics et al. 2011) was adopted. Of the four mixes from Table M2, only mix CT was kept at ambient room temperature of 21.1°C (70°F) during compaction delay. Mixes HT, RT, and LW were stored after batching inside a thermally insulated area at an elevated temperature of approximately 35°C (95°F) (Figure M3), which was large enough to accommodate five 0.0708 m3 (2.5 ft^3) mixing pans and three portable space heaters to maintain the elevated temperature.

For the high temperature evaluation (mixes HT, RT, and LW), all of the dry components were oven-heated to about 35°C (95°F) along with preheating the mixing pans in the thermally-insulated area. The dry components were then mixed with hot water at 35°C (95°F) for three minutes of initial mixing, three minutes of rest, and a final two minutes of mixing.

Figure M3. Thermally-controlled area for high temperature compaction delay times.

At each of the compaction delay times, moisture content was determined by microwave oven drying (AASHTO T 318-02, 2011), and Vebe consistency tests (ASTM C1170, 2008) were performed. Three 100 x 200 mm (4 in. x 8 in.) cylindrical samples for compressive strength testing were molded with a vibratory hammer as described in LaHucik and Roesler (2016). Likewise, three samples were fabricated with a gyratory compactor for 100 gyrations at a constant vertical pressure of 600 kPa and an internal angle of gyration of 1.16°. Of the three gyratory samples, one sample was prepared for DCT fracture testing in accordance to Amirkhanian et al. (2015), and the two other gyratory samples were cored to extract a total of two 75 x 150 mm (3 in. x 6 in.) cylindrical samples for compressive strength testing (ASTM C39, 2012). From the height data of the gyratory compactor output per gyration and the measured weight of each sample, the density per gyration was computed.

After 24 hours from casting, the samples were demolded and moist cured in a temperature-controlled room at 23°C (73°F). All DCT fracture and compressive strength specimens were tested at an age of 7 days.

M.4 RESULTS

M.4.1 Workability

The Vebe consistency times for each mix with respect to compaction delay times are shown in Table M3. After 45 minutes delay time, Vebe times increased with delay time and were above accepted standard of 40 seconds (ACI 325.10R-95, 1995) with mix RT being the exception. The time at which the mortar ring forms between the plastic plate and mold is highly subjective. Alternatively, plots of gyrations versus wet density as seen in Figure M4 can be compiled to establish acceptable limits on field density and delay times. The wet density versus number of gyration data could be a much better measure of workability relative to the Vebe consistency test, as described in Käppi and Nordenswan (2007).

Table M3. Vebe Consistency times (sec) for each RCC mix and compaction delay time (min)

Mixture ID	Vebe Time (s)				
	t = 0	t = 45	t = 90	t = 135	t = 180
CT	33	47	>60	>60	>60
HT	48	>60	52.6	>60	>60
RT	25	32	45.4	59	>60
LW	21	42	>60	53	>60

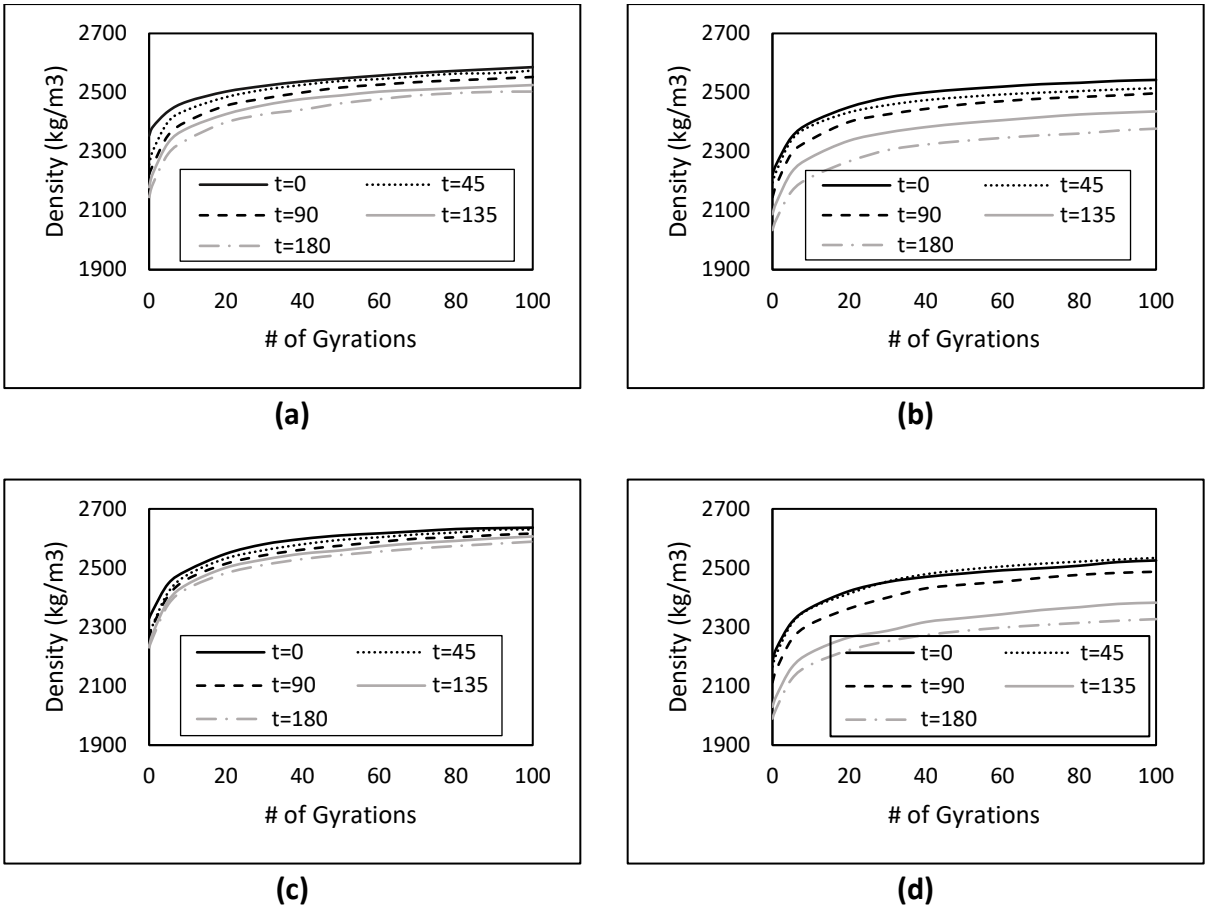

Figure M4. Compaction Delay effect on the Evolution of Wet Density for mixes (a) CT, (b) HT, (c) RT, and (d) LW. (1 kg/m^3 = 0.062 lb/ft^3)

M.4.2 Gyratory Moisture and Density

To compare the relative compactability of each mix over delay time, the gyratory compactor was used to add consistent compaction energy across all RCC mixes. The relative gyratory wet density was defined as the ratio of gyratory wet density at any delay time to the initial gyratory wet density after mixing (t=0 minutes). As expected, the wet densities of all mixes decreased as compaction delay time increased, as demonstrated in Figure M5. Mix RT showed the smallest decrease in relative wet density (98.2%) of all mixes at 180 minutes compaction delay followed by mix CT, mix HT, and mix LW. After 90 minutes, all mixes showed an approximately linear decrease in density with mix LW having the greatest rate of relative density loss. Based on the laboratory results, all mixes were above 98% relative gyratory wet density at 90 minutes despite guide specifications (American Concrete Pavement Assocation 2014, Portland Cement Association 2004) that state RCC must be compacted within 60 minutes of initial mixing or be rejected. However, this allowable delay time can significantly vary with climatic conditions during mixing, hauling, and placement.

The effect of compaction delay on total moisture loss, based on microwave drying test, is plotted in Figure M6. Mixes CT and HT had the largest percentage of moisture loss, while mix LW and RT had an initial moisture loss but little to no significant moisture loss after 90 minutes. The initial moisture loss likely occurred at the exposed surface of the RCC material. The RCC mix with the retarding admixture and the mix with FLWA maintained the internal moisture of the RCC batch. The mix at room temperature (mix CT) showed an initial higher moisture loss than the mix (HT) in the high temperature chamber because of a higher relative humidity within the insulated chamber as compared with the ambient laboratory conditions (Topçu and Elgün 2004).

The relationship between moisture loss and relative gyratory wet density was also analyzed. For mixes CT and HT, an increase in moisture loss corresponded with a proportional decrease in percent maximum wet density. In contrast, the relative gyratory wet density of the LW mix decreased significantly after 90 minutes of compaction delay without any further moisture loss. In this case, the decrease in density is attributed to an uneven distribution of water between the paste and the saturated aggregate. The water in the saturated aggregate does not contribute to the compactibility of the RCC mix, leading to a large decrease in density of the LW mix between 90 and 135 minutes of compaction delay. Additionally, the effective water to cement ratio in the paste of the LW mix was lower, leading to more resistance to compaction in the gyratory compactor. For the RT mix, the retarding and rheology-enhancing admixture limited the moisture loss and enabled the RCC mix to maintain 98% relative gyratory wet density after 180 minutes.

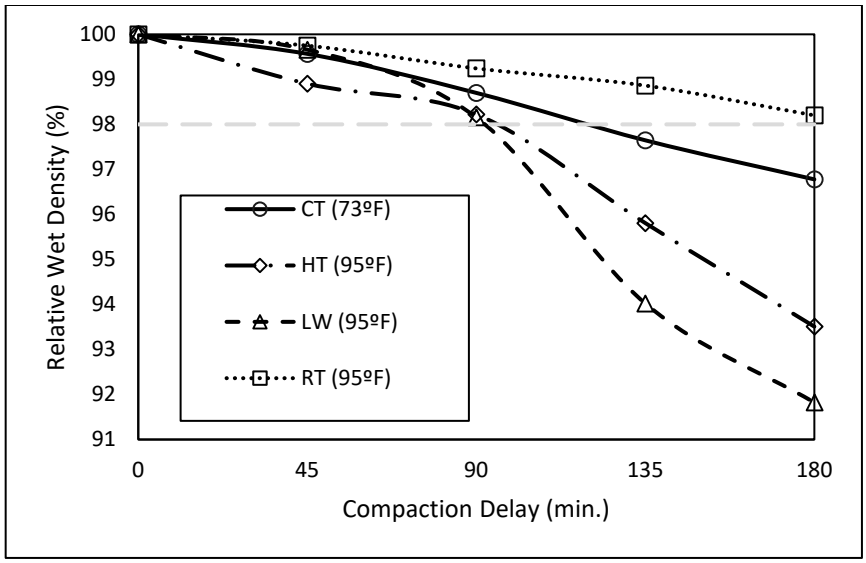

Figure M5. Impact of Compaction Delay on Relative Gyratory Wet Density.

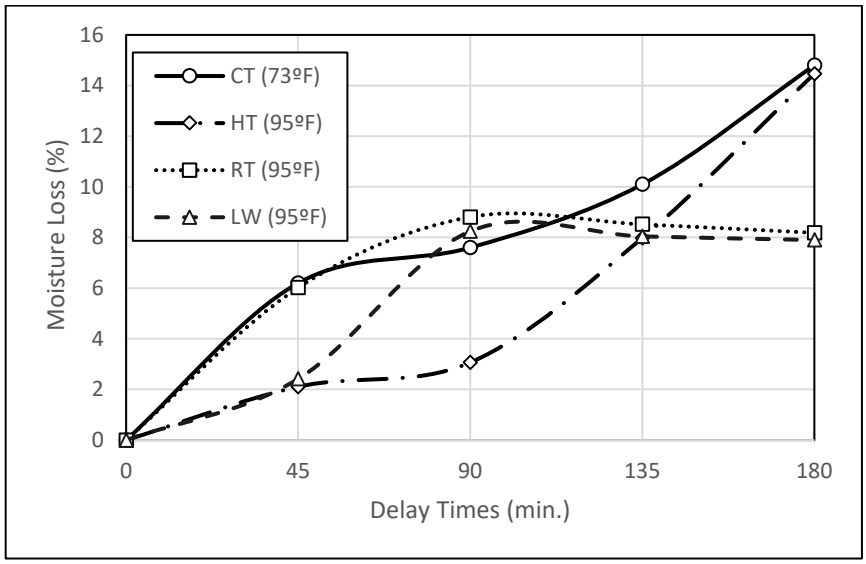

Figure M6. Compaction delay effect on RCC mix moisture loss.

M.4.3 Compressive Strength

The average 7-day compressive strengths of samples prepared with the gyratory compactor (2 samples) and the vibrating hammer (3 samples) are shown in Figure M7. All mixes maintained or decreased in compressive strength as the compaction delay time increased. Mix RT had the highest initial compressive strength (49 MPa or 7.11 ksi) with the gyratory compaction method, and after 180 minutes of compaction delay, mix RT had the highest compressive strength (40 MPa or 5.8 ksi) while mix HT had the lowest compressive strength of 18 MPa (2.6 ksi). For mixes CT, HT, and LW significant strength losses of the gyratory-compacted samples occurred at 135 minutes of compaction delay.

This is consistent with the literature on compaction delay of cement treated materials (Guthrie et al 2009, Senol et al 2004, Arman 1972) where there is general agreement that if compaction is not performed within 120 minutes of initial mixing, reduced strengths are observed.

The current RCC guide specifications call for the preparation of compressive strength samples with the use of the vibratory hammer (American Concrete Pavement Assocation 2014, Portland Cement Association 2004). Even though the use of the vibratory hammer to compact RCC cylinders is a standard method (ASTM C1435, 2014), it is user dependent and does not result in a constant compactive effort. Clearly, strengths obtained from the vibratory hammer and gyratory samples don't have the same magnitude nor follow the same trends versus compaction delay times.

Additionally, some unexpected observations in the compressive strength data indicate that the gyratory compactor results are more reliable. For the CT mix after 135 minutes of compaction delay, the vibratory hammer compacted specimens had their maximum strength while the gyratory compacted specimens had a significantly lower strength. This discrepancy was most likely due to a disproportionately large user pressure and/or compaction time when using the vibratory hammer for compaction. For the RT mix, while the gyratory compacted specimens showed a decrease in strength over the compaction delay times, the vibratory hammer compacted specimens had nearly constant strength over the delay times tested. This result demonstrates that the gyratory compactor is more sensitive to changes than the vibratory hammer. Thus, for both the CT and RT mix the gyratory compactor yielded more reliable and consistent results. While the vibratory hammer compaction method is satisfactory to use as a regular quality control measure, it is not sensitive enough, especially between users, to observe the effects of varying delay time.

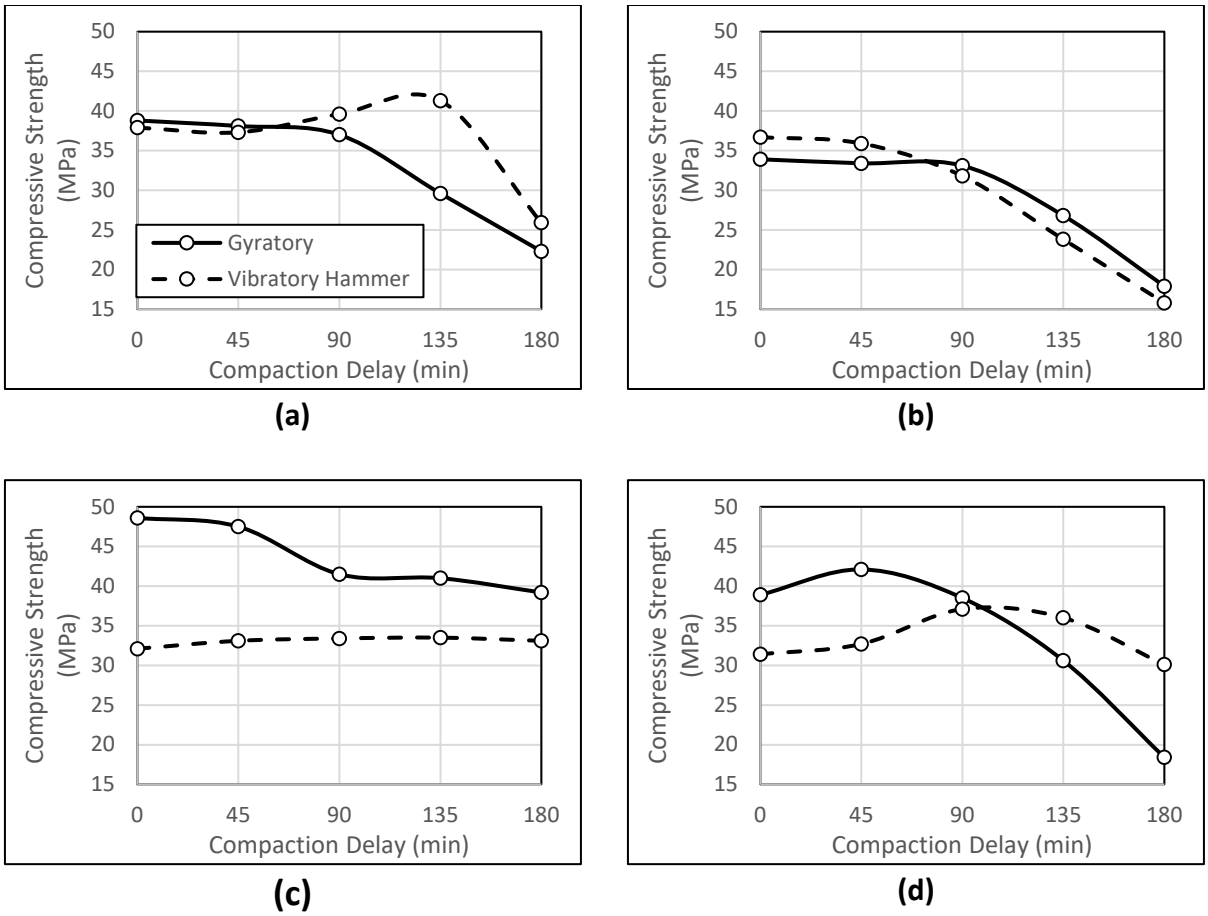

Figure M7. Comparison of the 7-day compressive strength between gyratory compactor (solid line) and vibratory hammer (dashed line) at multiple delay times for mixes (a) CT, (b) HT, (c) RT, and (d) LW. (1 ksi = 6.89 MPa)

M.4.4 RCC Fracture Properties

The materials' fracture properties provide indicators of its resistance to crack initiation and growth and can be related to the concrete slab capacity (Ferrebee et al. 2014, Gaedicke et al. 2012). The 7-day DCT fracture properties of RCC including fracture toughness (KIC), crack tip opening displacement (CTODc), and total fracture energy (GF) are listed in Table M4. The fracture properties for each delay time are an average of multiple samples, with the number of samples varying from 2 to 5. The results showed stable fracture properties for all mixes until a large deviation at 180 minutes of compaction delay for all mixes except the RT mix. Compared with the strength specimens from the gyratory compactor, which showed reductions at 135 minutes, the RCC fracture properties were less sensitive to compaction delay time. In a previous paper with recycled aggregates in RCC, LaHucik and Roesler (2016) reported that RCC compressive strength was, in general, the most sensitive to changes in the mix relative to the fracture properties derived from the DCT.

Table M4. Fracture Testing Results from Gyratory Compacted Specimens (COV, % in brackets)
(1 MPa-$m^{1/2}$ = 0.910 ksi-$in^{1/2}$; 1 GPa = 145 ksi; 1 in = 25.4 mm; 1 lb/in = 175 N/m)

Mixture ID	Compaction Delay (minutes)	K_{IC} (MPa-$m^{1/2}$)	CTODc (mm)	G_F (N/m)
CT	0	1.03 (6.57)	0.0168 (12.8)	118.91 (6.49)
	45	1.00 (7.46)	0.0160 (12.0)	115.60 (13.10)
	90	1.10 (8.86)	0.0174 (24.8)	131.47 (11.55)
	135	1.01 (12.52)	0.0200 (18.3)	119.81 (14.38)
	180	0.68 (15.25)	0.0160 (20.7)	99.94 (19.05)
HT	0	0.92 (7.11)	0.0161 (13.1)	163.79 (25.50)
	45	0.86 (5.23)	0.0164 (13.5)	125.74 (26.42)
	90	0.79 (9.46)	0.0137 (30.0)	117.79 (13.01)
	135	0.71 (10.13)	0.0149 (12.7)	101.92 (12.29)
	180	0.55 (13.57)	0.0162 (11.2)	77.22 (30.82)
RT	0	1.12 (3.06)	0.0193 (8.7)	148.39 (2.81)
	45	1.06 (3.41)	0.0189 (8.7)	127.70 (6.12)
	90	0.98 (1.56)	0.0160 (15.0)	142.71 (19.18)
	135	1.00 (11.32)	0.0172 (19.5)	144.17 (23.38
	180	0.97 (6.81)	0.0154 (12.1)	154.66 (16.53
LW	0	1.00 (10.18)	0.0181 (24.6)	133.70 (11.66)
	45	0.88 (6.26)	0.0179 (5.6)	143.46 (17.87)
	90	0.95 (10.98)	0.0202 (19.7)	123.33 (18.41)
	135	0.81 (10.69)	0.0198 (19.1)	125.68 (19.88)
	180	0.55 (20.71)	0.0172 (15.3)	101.18 (19.05)

M.5 CONCLUSIONS

An RCC mixing and test methodology was developed to evaluate the impact of delaying compaction, higher mix temperatures, and admixtures on RCC fresh and hardened properties. For this study, three mixes were maintained at an elevated temperature 35°C (95°F) and compared to a control mix at an average room temperature of 22.8°C (73°F). In addition to the control mixes at the room and elevated temperature, one mix (RT) included a retarding and rheology-modifying admixture, and the fourth mix (LW) included FLWA. The compaction delay times tested ranged from 0 to 180 minutes.

For all mixes except mix RT, lower strengths were obtained at compaction delay times greater than 90 minutes, and these lower strengths coincided with a decrease in wet density below 98% of the gyratory density with no compaction delay. While both mix RT and mix LW limited the amount of moisture loss by maintaining the internal moisture of the sample, only mix RT had relative gyratory wet density above 98% after 180 minutes of compaction delay. Additionally, mix RT had the largest gyratory compressive strength at all compaction delay times, with the strength after 180 minutes of compaction delay maintaining 80.7% of the immediately-compacted strength. Thus, the retarding and rheology-modifying admixture used in the RT mix was determined to be an adequate method to mitigate the effect of compaction delay. For projects where early opening to traffic is a design requirement, further work is necessary to determine if the addition of the retarding admixture will significantly affect the 1-day strength of RCC.

The gyratory compactor was shown to be a useful tool to assess the effect of compaction delay on RCC properties. In this investigation, the Vebe consistency test was used to assess the workability of the mixes, but Vebe consistency times past the industry standard (40 seconds) did not show any connection to a significant decrease in strength or density. It was concluded that Vebe times were too subjective to be able to capture the effect of compaction delay on RCC. An alternative measure of workability to the Vebe test could be some measure of workability based on density versus number of gyration data, which would lead to more consistent results due to the more consistent nature of gyratory compactor data. With respect to compressive strength, strength data from both the gyratory and vibratory hammer compaction methods also indicated that the gyratory compactor was a more sensitive test yielding more consistent results in this investigation. While the gyratory always applies a consistent compactive effort, the vibratory hammer compactive effort is subject to variations in applied pressure and compaction time (operator error). Finally, fracture properties were not significantly affected by compaction delays. In general, the gyratory compactor results, as compared to other results in this investigation, were more consistent and more sensitive to small changes in mix properties due to compaction delay.

APPENDIX N: SUMMARY OF RCC CONSTITUENTS AND THEIR IMPACT ON RCC MECHANICAL PROPERTIES

Appendix N summarizes the pertinent results found throughout this research investigation related to mix design development. The following sections correspond to the constituents found in typical RCC mixtures: aggregates, cementitious (cement & fly ash), and water.

N1. AGGREGATES

The aggregate content of RCC is the greatest by volume of the various constituents. Unlike other concrete materials, RCC derives its primary strength from a dense packing of aggregates. This packing requires that the gradation be carefully controlled, and tests have been run throughout this investigation to determine which gradation parameters are key to controlling the mechanical behavior of RCC.

N1.1 Mix Design and Workability

The appropriate water content for a given mix in this report has been determined by moisture-density testing using the modified Proctor test or proposed gyratory compaction method. From results in both Chapter 2 and Chapter 4 of this report, the sand content was the most significant parameter effecting the moisture-density results. Both Chapters 2 and 4 conclude that increasing sand content results in a higher optimum moisture content (OMC) given the modified Proctor testing. Additionally, chapter 4 concludes that maximum dry density (MDD) decreases with increasing sand content. Chapter 2 noted for the mixes tested that the nominal maximum aggregate size (NMAS) and fines content (passing the 0.075 mm (#200) sieve) didn't produce predictable trends in the MDD and OMC from modified Proctor testing.

Workability was measured throughout this report by use of the Vebe consistency test. The Vebe test gives both a Vebe time and density. Of the three parameters tested in Chapter 4 (sand content, fly ash content, and cementitious content), none had a statistically significant effect on the Vebe time. However, it was found that an increase in sand yields a decrease in Vebe density. Chapter 2 tested the effect of fines (passing the 0.075 mm (#200) sieve) on the Vebe time, which found that an increase in aggregate fines content resulted in a higher Vebe time. Finally, in Appendix F aggregate shape was found to impact Vebe time. Addition of river gravel (with a more rounded shape) resulted in lower Vebe times, while addition of manufactured sand (as opposed to natural sand with a more rounded shape) resulted in higher Vebe times.

N1.2 Compressive Strength

The effect of aggregates on compressive strength of RCC samples has been analyzed in Chapters 2 and 4, and Appendix F. In Chapter 2, regression equations were developed to determine relationships between gradation parameters and compressive strengths for certain group of constituent materials. The regression equation for predicting 14-day compressive strength (measured in psi) is shown in Equation N1 with parameter definitions in Table N1 (LaHucik and Roesler, 2015). Additionally, chapter 4 concluded that an increase in sand content resulted in a

decrease in compressive strength which is expressed in the predictive equation for 28-day compressive strength (measured in MPa) shown below in Equation N2 with parameter defined in Table N2. This result is consistent with previous findings by both Qasrawi et al. (2005) and LaHucik and Roelser (2015), which both conclude that strength is positively correlated with coarse-to-fine aggregate ratio.

$$\sigma_{c,14} = 6002(FAc) + 1535\left(\frac{CA}{FA}\right) + 195(1/2") - 148(\#8) \quad \text{(Eq. N1)}$$

Table N1: Compressive Strength Regression Parameters (LaHucik and Roesler, 2015)
(1 in = 25.4 mm)

Variable	Definition
FAc	$\frac{\text{cum. \% passing \#16}}{\text{cum. \% passing \#4}}$
1/2"	individual % retained on ½"
#8	individual % retained on #8
CA/FA	$\frac{\text{100 - cum. \% passing \#4}}{\text{cum. \% passing \#4}}$

$$\sigma_{c,28} = 57.9 + 4.39\alpha_c - 3.21\alpha_s \quad \text{(Eq. N2)}$$

Table N2: Compressive Strength Predictive Equation Parameters

Variable	Definiton
α_c	$\frac{Cementitious\ Content\ \left(\frac{kg}{m^3}\right) - 281.7}{26.5}$
α_s	$\frac{Sand\ Percentage\ (\%) - 50}{5.95}$

Appendix F tested various mixes with different types of aggregates (for example, river gravel, dolomite, and trap rock). Compressive strengths from river gravel and control samples were compared to determine if aggregate shape had an effect on compressive strength. In normal

concrete, a rounded aggregate with similar mixture proportions would be expected to yield lower strength. However, at both 1 day and 28 days, the river gravel and control mixes had statistically similar compressive strengths. A mix incorporating trap rock, also tested in Appendix F, resulted in lower compressive strengths than the control mix because it resisted compaction due to its higher angularity, surface texture, and material strength. Ultimately, compressive strength of RCC incorporating different types of aggregates was most related to aggregate properties through the compactibility of the mix.

N1.3 Split Tensile and Flexural Strengths

Split tensile and flexural strengths were consistently less sensitive to changes in the aggregate properties of the mix. As seen in Chapter 2, and LaHucik and Roesler (2015), there was no statistically significant relation between split tensile strength and gradation parameters. Appendix F, which tested mixes incorporating different types of aggregates, resulted in statistically similar flexural and split tensile strengths for all mixtures, with the exception of the mix incorporating manufactured sand. Finally, Chapter 4 concluded that an increase in percent sand yields a decrease in split tensile strength, especially at later ages. In the same chapter, an increase in sand content also resulted in a decrease in 28-day flexural strength.

N1.4 Fracture Properties

Compared to strength properties, less conclusions on the relationship between aggregate constituents and fracture properties have been made in this report. In Chapter 2, it was shown that NMAS did not have a significant effect on fracture properties of RCC. Additionally, in Appendix F which tested mixes incorporating different types of aggregate, the trap rock and river gravel mixes had lower critical stress intensity factors.

N1.5 Drying Shrinkage

Generally, aggregate gradations were not shown to directly affect RCC drying shrinkage amounts. Chapter 2 supports this conclusion, where a lack of strong trends was explained by the fact that drying shrinkage is more controlled by cement and water contents, which were similar for all the mixes tested in Chapter 2. Chapter 4 also concluded that percent sand did not affect drying shrinkage. However, the river gravel and trap rock mixes from Appendix F did have lower drying shrinkage than the control mixes tested (dolomite and manufactured sand).

N1.6 Other Findings

In addition to virgin aggregates tested throughout the report, Appendix G compared RCC mixes incorporating virgin and recycled aggregates. The relative effect of various types of recycled aggregates on strength properties is shown in Table N3. With respect to fracture properties, the 28-day critical stress intensity factor and total fracture energy for the mixes incorporating recycled aggregates were statistically similar or greater than the control mix (virgin dolomite). Because previous literature shows flexural slab capacity is related to fracture properties for concrete with recycled aggregates, it was hypothesized that RCC slab capacity with recycled aggregates is similar to RCC slabs with virgin aggregates.

Table N3: RCC Strength Trends from Recycled Aggregate Relative to Virgin Aggregate Mixture

Recycled Aggregate	Compressive Strength	Split Tensile Strength	Flexural Strength
RCA	Lower – Similar	Similar	Lower
RAP	Lower	Similar	Lower
SFSFRAP	Lower	Similar	Lower
EAF	Similar – Greater	Similar	Similar

Additionally, some general conclusions regarding aggregates to be used for RCC are made. There are a range of aggregate types, gradations, and proportions that can achieve acceptable RCC properties but testing must be done to verify the desired properties for a project are achieved. In Chapter 2, the amount of aggregates fines (passing the 0.075 mm or #200 sieve) can affect RCC properties and thus should be thoroughly analyzed in the laboratory, e.g., moisture density relationship, workability, finishability, and strength. The cementitious materials may also be plotted as part of the gradation to determine its affect on the overall packing density of the constituent materials.

N2. CEMENTITIOUS MATERIAL

N2.1 Mix Design and Workability

As seen in Chapter 4 of this report, the OMC and MDD from modified Proctor compaction procedure was controlled primarily by sand content. There also seems to be an optimum point for MDD in the fly ash-cementitious content space as shown in Figure N1. This combination of fly ash and cement could indicate a best combination of fly ash and cement based on their particle packing characteristics and relative specific gravities. Because the mixes don't include aggregate fines (passing 0.075 mm or #200 sieve), the cement and fly ash act as these fine particles for RCC mixes.

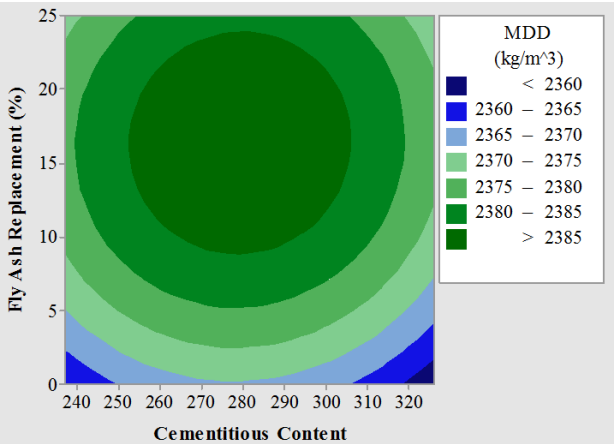

Figure N1: Contour Plot for MDD (Chapter 4). (1 kg/m^3 = 1.686 lb/yd^3)

With respect to workability, Vebe times have been shown to be unaffected by cementitious material. Appendix J concluded that Vebe time does not vary significantly with the addition of silica fume, fly ash, or ground granulated blast furnace slag (GGBFS). Additionally, Chapter 4 concluded that neither total cementitious content nor fly ash replacement level had a significant effect on Vebe time.

N2.2 Compressive Strength

Compressive strength has been shown to be directly related to cementitious content, with a decrease in early-age strength with the addition of less reactive pozzolans. Chapter 4 showed an increase in cementitious content resulted in a higher compressive strength for all ages. Additionally, Chapter 4 demonstrated that an increase in fly ash replacement level resulted in a decrease in 1-day compressive strength but no significant decrease in compressive strength at later ages (7 and 28 days). This result is consistent with the result from Appendix J where all mixes that included pozzolans, with the exception of the silica fume mix, had statistically lower 1-day compressive strengths when compared to a control mix without pozzolans. However, only the mix with 40% GGBFS replacement had a statistically lower 28-day compressive strength when compared to the control mix. Because only the silica fume and control mixes met the strength requirement for opening to traffic at 1 day (as per Appendix J), it was concluded that addition of other supplementary cementitious materials (SCMs) to an RCC pavement may require a slightly longer time before opening to traffic.

N2.3 Split Tensile and Flexural Strengths

Similar to compressive strength results, Appendix J concluded that the silica fume and control mixes had statistically greater 1-day compressive strength over the fly ash and GGBFS mixes. However, 28-day split tensile strength was greater for the control mix than all other mixes, which is somewhat unexpected given other results. Looking at the flexural strength results also from Appendix J, all mixes has statistically similar 28-day flexural strength with the exception of the 8% silica fume mix which had greater strength. From Chapter 4, it is shown that while cement content controls early (1-day) split tensile strength, sand content controls later strength (28-day). This is also consistent with the flexural strength results from Chapter 4, where fly ash replacement level and total cementitious content had less of an effect on flexural strength than the sand content. Also, Chapter 4 demonstrated that fly ash addition has a less significant effect on split tensile strength than on compressive strength. Finally, an optimum cementitious content seems to be identified in Chapter 4 based on the flexural strength results, as shown in Figure N2.

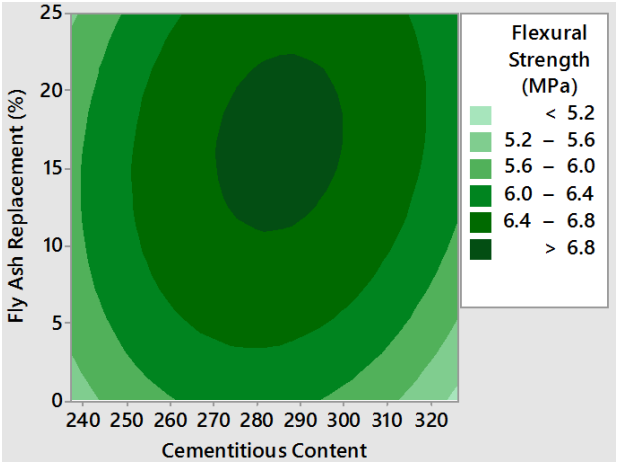

Figure N2: Contour Plot for 28-Day Flexural Strength, from Chapter 4. (1 kg/m^3 = 1.686 lb/yd^3; 1 ksi = 6.89 MPa)

N2.4 Fracture and Elastic Modulus Properties

Appendix J demonstrated that among mixes prepared with the same total cementitious content, cement replacement with fly ash or GGBFS resulted in similar fracture properties to the control mix (without SCMs). With respect to elastic modulus, Chapter 4 demonstrated that and increase in total cementitious content resulted in a higher elastic modulus.

N2.5 Drying Shrinkage and Freeze-Thaw Resistance

With respect to drying shrinkage, Appendix J evaluated the effect of different SCMs on the total drying shrinkage strain at a constant cementitious content. It was concluded that large SCM replacement levels yield decreased drying shrinkage strain, while the mixes with silica fume and the mix with 12.5% fly ash replacement resulted in similar drying shrinkage strain when compared to the control. Chapter 4 evaluated the effect of both total cementitious content and fly ash replacement level on the drying shrinkage strain. In general, a decrease in cementitious content resulted in a decrease in drying shrinkage strain. The interaction between cement content and fly ash replacement level on drying shrinkage strain is shown in the predictive equation, shown again here as Equation N3.

$$28 - Day\ Drying\ Shrinkage\ Strain\ (\mu\epsilon) = 312.3 - 39.2\alpha_C\alpha_F \qquad \text{(Eq. N3)}$$

Freeze-thaw resistance was evaluated in Chapter 4. An RCC mix prepared with a lower cementitious content had a lower relative dynamic modulus (a measure of freeze-thaw resistance). This result is indirectly related to the fact that a lower cementitious content results in a higher water-to-cement ratio for the RCC paste. Water-to-cement ratio is not a parameter directly considered in the RCC mix design methodology, however this result indicates that RCC durability issues arising from a paste microstructure with too large a water-to-cement ratio can be controlled by maintaining some

minimum cementitious content. As expected, drying shrinkage and freeze-thaw durability properties are related to the paste properties of the RCC mix.

N3. WATER

The influence of water as a constituent has not been studied directly in this report. Water content of mixes has mostly been determined by optimum moisture content from moisture-density testing using the modified Proctor compaction procedure. The modified Proctor procedure tests a certain combination of solid constituents prepared at various water contents to determine which water content results in the greatest dry density. An example moisture-density plot, from Appendix M, is shown in Figure N3. Because RCC mechanical properties are related to density, achieving the maximum density is the design goal that moisture-density testing aims to achieve.

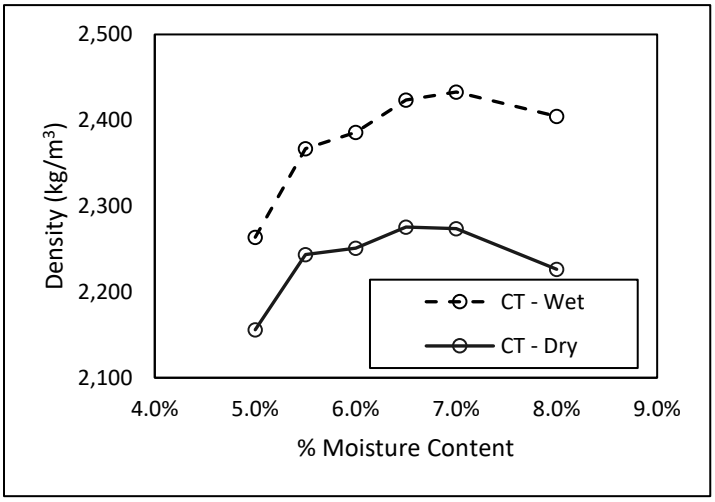

Figure N3: Example of Moisture-Density Plot from Appendix M. (1 kg/m^3 = 1.686 lb/yd^3)

Some factors that impact the optimum moisture content at which an RCC mix is prepared have been discussed previously in these appendices. Firstly, as demonstrated in Appendices F and G, the absorption capacity of the aggregates was shown to be directly related to the optimum moisture content. Secondly, sand content was also shown to be directly related to optimum moisture content. Finally, Appendix E discussed application of the gyratory compactor as an alternative to modified Proctor compaction for moisture-density testing. Compaction method was also shown to have an impact on the optimum moisture content.


Illinois Department
of Transportation


ILLINOIS